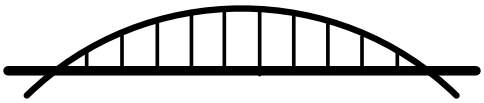

ASR/DEF-DAMAGED BENT CAPS:
SHEAR TESTS AND FIELD IMPLICATIONS

by

DEAN J. DESCHENES, OGUZHAN BAYRAK, AND KEVIN J. FOLLIARD

Technical Report No. 12-8XXIA006
summarizing work conducted for the
Texas Department of Transportation

at

FERGUSON STRUCTURAL ENGINEERING LABORATORY
THE UNIVERSITY OF TEXAS AT AUSTIN

August 2009

Investigation performed in cooperation with the Texas Department of Transportation.

Acknowledgments

We greatly appreciate the financial support from the Texas Department of Transportation that made this project possible. The support of the project monitoring committee, John Vogel and Kenny Ozuna, is also very much appreciated.

Disclaimer

The contents of this report reflect the views of the authors, who are responsible for the facts and the accuracy of the data presented herein. The contents do not necessarily reflect the view of the Federal Highway Administration or the Texas Department of Transportation. This report does not constitute a standard, specification, or regulation.

Not Intended for Construction,
Permit, or Bidding Purposes

ASR/DEF-Damaged Bent Caps:
Shear Tests and Field Implications

Over the last decade, a number of reinforced concrete bent caps within Houston, Texas have exhibited premature concrete damage (cracking, spalling and a loss of material strength) due to alkali-silica reaction (ASR) and/or delayed ettringite formation (DEF). The alarming nature of the severe surface cracking prompted the Houston District of the Texas Department of Transportation to initiate an investigation into the structural implications of the premature concrete damage. Specifically, an interagency contract with the University of Texas at Austin charged engineers at Ferguson Structural Engineering Laboratory to:

1. Establish the time-dependent relationship between ASR/DEF deterioration and the shear capacity of affected bridge bent caps.
2. Develop practical recommendations for structural evaluation of in-service bridge bent caps affected by ASR and/or DEF.

To accomplish these objectives, six large-scale bent cap specimens were fabricated within the laboratory. Four of the specimens (containing *reactive* concrete exposed to high curing temperatures) represented the most severe circumstances of deterioration found in the field. The remaining two specimens (*non-reactive*) provided a basis for the comparison of long-term structural performance. All of the specimens were subjected to a conditioning regimen meant to foster the development of realistic ASR/DEF-related damage. Resulting expansions were characterized over the course of the study through a carefully-planned monitoring program. Following a prolonged exposure period, three of the six bent cap specimens (representing undamaged, mild, and moderate levels of deterioration) were tested in shear. Observations made over the course of each test captured the service and ultimate load effects of ASR/DEF-induced deterioration. Six shear-critical spans were tested prior to this publication: three deep beam and three sectional shear tests. The remaining six shear spans (contained within the remaining three specimens) were retained to establish the effects of severe deterioration through future shear testing.

Subsequent analysis of the expansion monitoring and shear testing data provided much needed insight into the performance and evaluation of ASR/DEF damaged bent structures. The results ultimately formed a strong technical basis for the preliminary assessment of a damaged bent structure within Houston, Texas.

Table of Contents

List of Tables

List of Figures

CHAPTER 1
Introduction

1.1 MOTIVATION

The rapid pace of recent infrastructure growth in the State of Texas has come at the expense of the long-term durability commonly associated with concrete construction. Unrestrained use of *high-sack* concrete mixtures accelerated the construction of concrete bridge elements, but also resulted in elevated alkali loadings, high curing temperatures, and substantially increased chances for alkali-silica reaction (ASR) and delayed ettringite formation (DEF).

Figure 1-1: US 59 and I-10 Interchange - Houston, Texas

The consequences of accelerated construction practices are no more apparent than in the Houston District (HOU) of the Texas Department of Transportation (TxDOT). A number of reinforced concrete bent caps, constructed within the last ten to fifteen years, have developed map cracking and spalls characteristic of ASR and DEF (Figure 1-1). In total, it is estimated that the Houston District has more than one billion dollars worth of prematurely damaged infrastructure within its own jurisdiction (Vogel 2008). Numerous other cases have been identified elsewhere in the state and more are likely to be discovered. Outdated material specifications were only recently updated to address the responsible deficiencies. The cost of inspection, maintenance and replacement for these

structures is expected to become a substantial burden for Houston District and the Texas Department of Transportation in the future.

As a matter of public safety, Houston District engineers recognized that the potential structural implications of the deterioration needed to be established without delay. The commonly observed material strength loss due to ASR/DEF could have led district engineers to explore any number of structural consequences. However, concurrent discovery of severe diagonal cracking within several other Houston District bent caps led them to question the impact of the deterioration on the long-term shear performance (in terms of strength and serviceability) of the affected structures. The selected focus of the assessment was substantiated by the serious consequences of shear capacity reduction; a potential for brittle failure with little warning. Similar logic prevailed after the late twentieth century discovery of ASR in international bridge structures. Testing programs within South Africa, Japan, and the United Kingdom sought to establish the shear capacity reduction due to ASR. While test specimens with minimum shear reinforcement did not exhibit a loss of shear strength, the small scale of the specimens (beam depth of twenty inches or less) provided a poor representation of the commonly affected highway structures (Chapter 2). Due to the poor scaling effects of shear behavior and complex nature of ASR/DEF deterioration, it was realized that proper consideration of the problem could only be accomplished through large-scale testing.

1.2 OBJECTIVES AND SCOPE

The Houston District of the Texas Department of Transportation established an interagency contract (IAC) with the University of Texas at Austin to conduct a large-scale testing program at Ferguson Structural Engineering Laboratory. The primary objectives of the testing program were to (1) establish the time-dependent relationship between in-situ deterioration and nominal shear capacity, and (2) develop practical recommendations for the evaluation of in-service bridge bent caps affected by ASR and/or DEF.

A comprehensive literature review and experimental testing program were conducted to address the immediate needs of the Houston District. Review of the previous research provided background information essential to the development of the testing program and interpretation of the results. Particular emphasis was placed on the review of microstructural damage imposed by the deterioration and its historical impact on the structural performance of both plain concrete materials and reinforced concrete members. In response to the small scale of the specimens referenced within the literature, six near

full-scale bent cap specimens were designed and fabricated at Ferguson Structural Engineering Laboratory. Each specimen weighed nearly thirteen tons and accommodated two tests at different shear span-to-depth ratios (i.e. sectional and deep beam shear). Experimental testing of the bent cap specimens was conducted in three phases which collectively addressed the need for information regarding the structural performance and assessment of ASR/DEF-affected bent caps. Following fabrication, a conditioning regime was used to foster the development of realistic ASR/DEF-related damage. The deterioration of each bent cap specimen was recorded through the use of unique instrumentation (Phase I: Specimen Conditioning and Expansion Monitoring). Upon attainment of the desired levels of deterioration (undamaged, mild and moderate), three of the six bent caps were tested in shear. A total of six shear-critical spans were tested: three deep beam and three sectional shear tests. The most severe deterioration included ASR/DEF-related expansions well-in-excess of the reinforcement yield strain. Future testing (not reported here) of the remaining three bent cap specimens will establish the effects of severe deterioration (Phase II: Shear Testing). Implementation of the shear testing results ultimately relied on the ability to estimate the expansions within field structures. A number of forensic analysis techniques were therefore evaluated within the context of the current study (Phase III: Forensic Analysis). Results from all three phases of the experimental program were collectively used to conduct the preliminary assessment of a damaged bent structure within Houston, Texas.

1.3 REPORT ORGANIZATION

Work conducted over the course of the three-year study is reviewed within the following six chapters: (Chapter 2) background, (Chapter 3) test specimens, (Chapter 4) experimental program, (Chapter 5) experimental results, (Chapter 6) field assessment, and (Chapter 7) conclusions. A brief outline of each chapter is provided below.

All relevant background information pertaining to the objectives of the current study is presented within *Chapter 2*. To begin, the premature concrete deterioration (PCD) mechanisms of ASR and DEF are briefly introduced. The physical symptoms of the mechanisms are outlined and their role in the loss of plain concrete strength and stiffness is examined. Development of the deterioration within the restraints of a loaded, reinforced structure is subsequently considered. Sensitive structural details are identified and applicable structural testing results are presented. The potential for correlation between the structural testing results and measured material properties is thoroughly explored afterward. Finally, international experience regarding the management and

long-term performance of PCD-affected structures is examined to provide a practical perspective on the task at hand.

The design and fabrication of six large-scale bent cap specimens (which formed the basis for the experimental operations) are outlined within *Chapter 3*. Initial review of the specimen geometry, reinforcement configuration, and concrete mixture reflects the two underlying design criteria. Specifically, the final specimen design had to achieve: (1) general representation of the damaged structures within the TxDOT inventory, and (2) unmistakable shear failure at each end of the specimen. Discussion of the fabrication process then demonstrates the unprecedented nature of the current study. The implementation of unique concrete materials and construction techniques is presented, and subsequent examination of the fabrication results provides an indication of the future deterioration potential.

Procedures and techniques used over the course of the three-phase experimental program are outlined within *Chapter 4*. A description of Phase I (Specimen Conditioning and Expansion Monitoring) details efforts to trigger field representative ASR/DEF deterioration and monitor subsequent expansions within each of the bent cap specimens. The unique facilities and methods used during the Phase II (Shear Testing) testing of six individual shear spans are then presented. Finally, the Phase III (Forensic Analysis) examination of structural evaluation techniques (reported within the literature and/or commonly recommended in assessment guidelines) is reviewed.

Measurements and observations made during the course of the three-phase experimental program are discussed within *Chapter 5*. To begin, the development of ASR/DEF deterioration is presented through an examination of the expansion measurements and documented cracking patterns. Impacts of the deterioration on the serviceability and strength of sectional and deep beam shear spans are then explored through the consideration of eight individual shear tests. Finally, the ability of the various forensic techniques to successfully establish the cause, extent and future potential of the deterioration is evaluated. As demonstrated over the course of the chapter, particular emphasis was placed on examining the relationship between the measured in-situ damage and the results from structural testing and forensic analyses.

The preliminary assessment of a damaged bent structure within Houston, Texas is presented within *Chapter 6*. A discussion of the structure location, geometry, and visual appearance provides a suitable introduction to the assessment process. General implementation of the experimental results is then reviewed during a description of the

bent inspection. Consequences of the measured deterioration are explored and recommendations for the maintenance of the structure are made.

The experimental work completed during the study is briefly summarized within *Chapter 7*. Conclusions regarding the structural performance of ASR/DEF-affected bridge bent caps are presented and recommendations for the assessment of field structures are made. Additional work is suggested to address additional gaps which exist within the relevant technical literature.

CHAPTER 2
Background

2.1 OVERVIEW

A critical review of the previous research on alkali-silica reaction (ASR) and delayed ettringite formation (DEF) is presented within this chapter. The topics were chosen and organized to give the practicing engineer insight into the behavior and management of prematurely deteriorated structures. Details provided throughout this review also form the basis for the laboratory construction and assessment of the ASR/DEF affected bent cap specimens (Chapters 3 and 4).

The first two topics included in this chapter form a summary of the laboratory research completed within the last three decades. The premature concrete deterioration (PCD) mechanisms of ASR and DEF are briefly reviewed (Sections 2.2.1 and 2.2.2, respectively). A study of relevant materials and environmental factors can be used to identify sources of variability in affected concrete properties. Expansion and cracking are identified as the primary symptoms of PCD in plain concrete and their role in the loss of strength and stiffness is examined (Section 2.3.1). The performance of affected concrete is then considered within the physical restraints of a loaded, reinforced structure. The inability to generalize the effects of PCD on the engineering properties of concrete justifies the need for structural testing of reinforced elements. Sensitive structural details are identified and applicable structural testing results are presented (Section 2.3.2).

The final topic reviews the discovery, management, and long-term performance of PCD affected structures worldwide (Section 2.4). Parallels drawn between the international experiences help to explain the current *outbreak* of ASR and DEF within the State of Texas and also identify substantial challenges that lie ahead.

2.2 PREMATURE CONCRETE DETERIORATION MECHANISMS

The mechanisms of alkali-silica reaction (ASR) and delayed ettringite formation (DEF) subject concrete to expansive forces, causing premature distress and the loss of serviceability in affected structures. Alkali-silica reactivity has been recognized as a potential source for premature distress since the late 1930's (Stanton 1940). A considerable amount of research has been conducted since the discovery, yet ASR

continues to be a significant durability issue worldwide. In 1982, researchers reported the development of a second distress mechanism, referred to as delayed ettringite formation. Although a number of theories exist regarding the recent development of DEF, a great number of researchers suspect that the mechanism may have been previously misdiagnosed as ASR (Hime 1996).

From a structural engineer's perspective, the two mechanisms cause internal expansion and indistinguishable cracking at the concrete surface. As such, following a brief discussion of the chemical and physical processes of each mechanism, no distinction will be made between their deleterious effects. Although the descriptions provided below are greatly simplified (see technical report for TxDOT Project 0-4085 for further detail), they will be sufficient in establishing the complexity and inherent variability of ASR/DEF distress.

2.2.1 (ASR) Alkali-Silica Reaction

Alkali-silica reaction occurs between alkali hydroxides in the concrete pore solution and reactive minerals within the aggregates. The development of destructive ASR may be visualized as a two step process, shown in Figure 2-1.

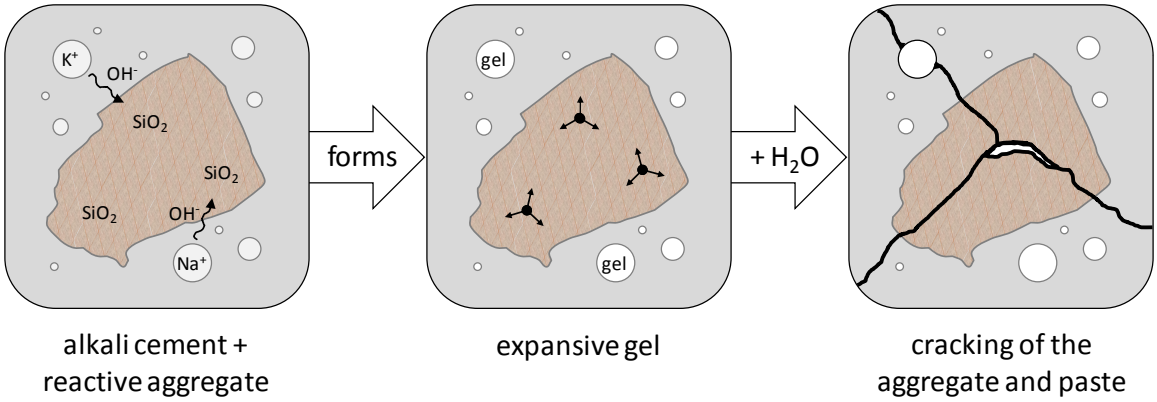

Figure 2-1: Alkali-Silica Reaction

Reactive silica phases within the coarse and/or fine aggregates are chemically unstable in the presence of the highly basic fluid (pH $\geq$ 12.5) of dissolved alkali hydroxides. The silica (SiO_2) rapidly dissolves and reacts with the alkalis (Na+, K+) to form a viscous gel. The gel readily absorbs water and swells, generating pressure within the aggregate particles and hardened cement paste. In the presence of sufficient moisture, the pressure has been shown to exceed 1500 psi (Rigden et al. 1995). Such pressure easily exceeds the

tensile strength of conventional concrete, creating microcracks and causing volumetric expansion.

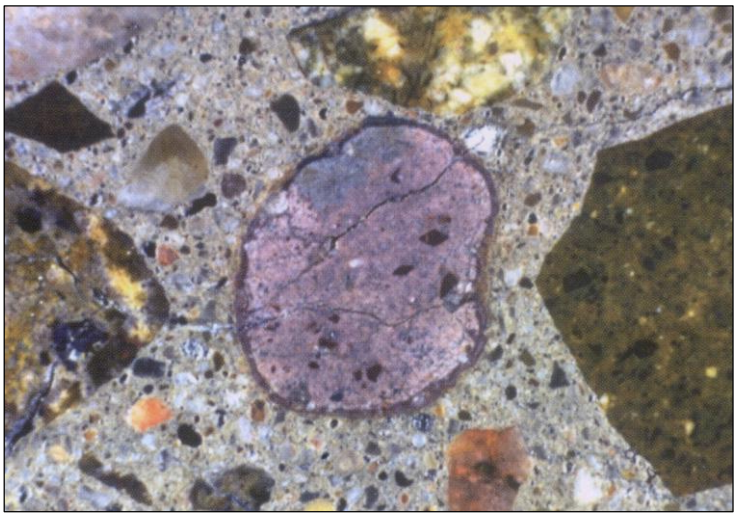

Figure 2-2: Petrographic Features of ASR (Farny and Kerkhoff 2007)

It is important to note that the presence of viscous gel does not necessarily indicate destructive ASR. Swelling characteristics of the gel are influenced by a number of factors (briefly discussed below) and the resulting pressures may be accommodated without deleterious cracking. As a result, care must be taken when evaluating deteriorated concrete as the presence of innocuous ASR gel can lead to misdiagnosis (Figg 1987). Physical deterioration is only attributed to ASR when it clearly originates from the reactive aggregate. Several petrographic features are commonly found within the aggregate and surrounding concrete matrix: microcracks, reaction rims, cement paste debonding, and alkali-silica gel (Figure 2-2). The most severe cases of ASR produce a damaging network of microcracks, resulting in bulk expansion of the concrete and severe deterioration of its mechanical properties (refer to Section 2.3.1).

The potential for physical distress due to alkali-silica reaction is dependent on three conditions: (1) a reactive aggregate, (2) a high concentration of alkalis within the pore solution, and (3) the presence of sufficient moisture.

`

Table 2-1: Three Necessities of ASR and Related Sources of Variability

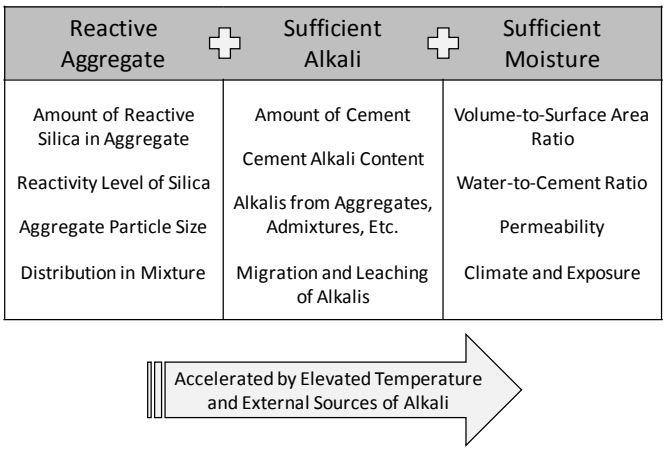

Once initiated, the reaction is highly sensitive to any preexisting or transient conditions that may alter the availability of any one of the three necessities (as shown in Table 2-1). The wide range of materials, mixture characteristics and exposure conditions found within in a single concrete element leads to significant variation of the associated deterioration over the structure's geometry and service life (within a well-controlled laboratory setting as well as in the field).

2.2.2 (DEF) Delayed Ettringite Formation

Delayed ettringite formation, occasionally referred to as *late ettringite formation*, is a form of sulfate attack that occurs when concrete is subjected to high temperatures early in the curing process. The development of destructive DEF may be visualized as a two step process, shown in Figure 2-3.

`

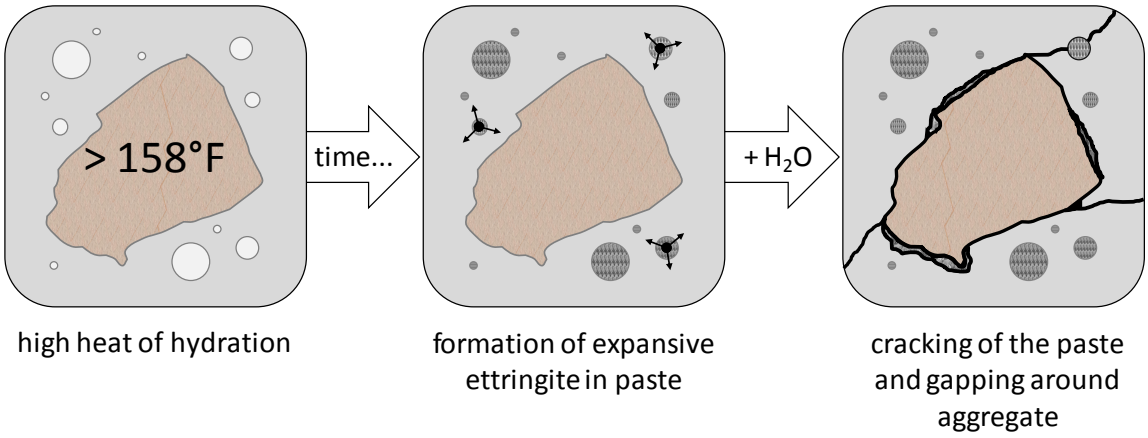

Figure 2-3: Delayed Ettringite Formation

The natural formation of ettringite occurs during the early hydration process of cement (prior to hardening) and does not pose a risk to concrete durability. However, when fresh concrete is exposed to temperatures in excess of 158°F (70°C), the ettringite decomposes and the component phases (sulfates and aluminates) become trapped within the early cement hydration products (Bauer et al. 2001). Over a period of time, the sulfates and aluminates diffuse out of the hydration products to react and form ettringite. As with classic sulfate attack, the reformation of ettringite produces expansive forces and microcracking of the hardened cement paste.

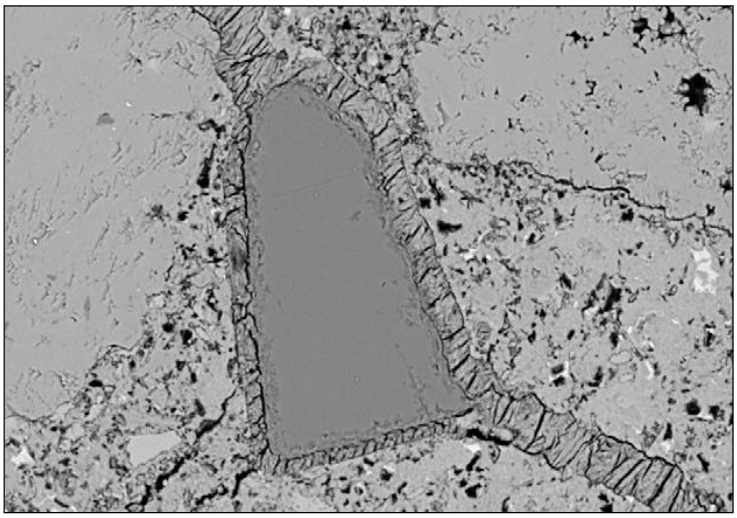

Figure 2-4: Back-Scattered Electron Image of DEF (Thomas et al. 2007)

`

The formation of large amounts of ettringite within the hardened cement paste can potentially cause expansions of magnitudes well in excess of those found due to ASR (as observed in TxDOT Project 0-4085). The growth of ettringite nests leads to bulk expansion of the cement paste and the development of cracks and gaps around the aggregates (which do not expand). Once cracking is significant, the ettringite fills the rims surrounding the aggregates, furthering overall expansion and crack development (as seen in Figure 2-4). To the naked eye, "the resulting damage is very similar to that caused by ASR, as would be expected for any internal expansive type reactions within a non-ductile material" (Lawrence et al. 1999).

The potential for physical distress due to delayed ettringite formation is dependent on two conditions: (1) concrete curing temperatures in excess of 158°F (70°C) and (2) sufficient moisture to allow for the formation of ettringite. Although these two conditions are sufficient to produce DEF, the rate and magnitude of the deterioration are subject to a number of other factors. As with alkali-silica reaction, wide variations in cement composition (sulfate content), mixture characteristics (porosity), and exposure conditions (moisture availability) will lead to an equivalent variation of the deterioration within a highway structure.

2.3 EFFECTS OF ALKALI-SILICA REACTION AND DELAYED ETTRINGITE FORMATION

The deterioration mechanisms of ASR and DEF lead to microcracking of the concrete microstructure and subsequent expansion of the body of the concrete. Over time, the deterioration process manifests itself as map (or pattern) cracking at the surface of the member (Figure 2-5). The appearance of the cracking has often been the source of much concern to practicing engineers as cracks typically indicate structural distress. In fact, it has been commonly assumed that the growth of PCD-related expansion (and cracking) is closely related to a loss of structural capacity.

`

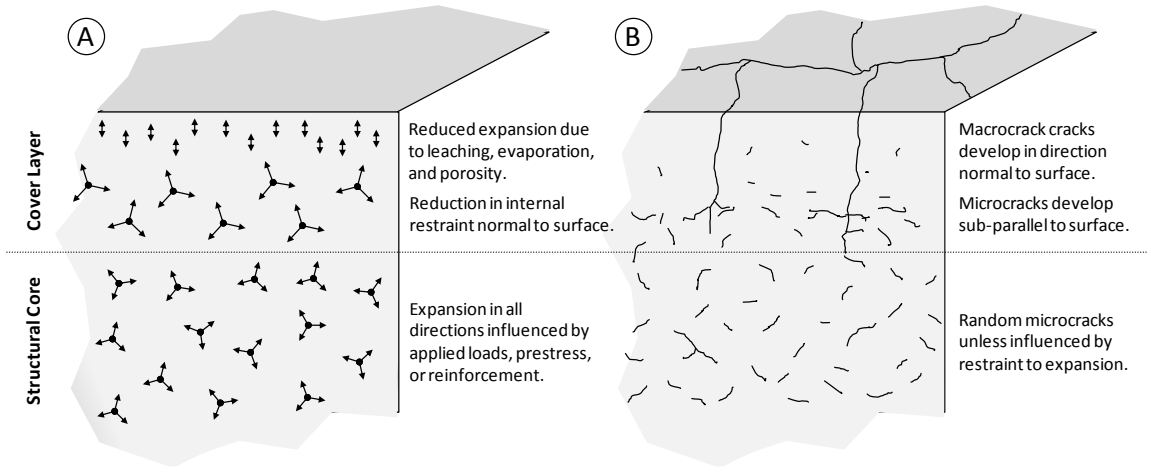

Figure 2-5: (A) Expansion and (B) Cracking due to ASR (Adapted from Courtier 1990)

A number of studies have been conducted in an attempt to characterize the relationship between expansion and strength loss. In Sections 2.3.1 and 2.3.2, the results of those studies will be reviewed and the correlation of expansion with the loss of concrete material strength and structural performance will be evaluated. Please note that many of the results referenced here were obtained for ASR testing only. As mentioned earlier, the similarities of the physical distress allow a direct application of the results to DEF affected structures.

2.3.1 Strength and Stiffness of Concrete Materials

The internal expansion and microcracking due to ASR/DEF can reduce concrete strength gain over time, and in some circumstances, lead to a true loss of ultimate strength; the presence of surface cracks only enhances these effects. To illustrate the loss of strength and stiffness with increasing expansion, nearly three hundred material test results were gathered from five distinct references published between 1988 and 2006. The results were normalized by their corresponding twenty-eight day values and plotted in Figure 2-6. A majority of the data points (number of data points, N = 252) were obtained from studies conducted in the United Kingdom (UK) during an intense period of ASR research; referred to as *Results from Literature*. To bridge the gap between practices in the UK and Texas, a number of tests (N = 36) conducted on concrete materials from El Paso are also included (Smaoui et al. 2006). The results are accompanied by strength reduction guidelines (developed by the Institution of Structural Engineers, ISE) to provide insight into current strength evaluation practices. A listing of the references for the data can be found in Table 2-2.

`

Table 2-2: References for ASR/DEF Material Testing Data

Reference	Number of Mechanical Tests, N			
	f_{cu}	f'_c	f'_t	E_c
	cube compressive strength	cylinder compressive strength	splitting tensile strength	modulus of elasticity
1992 Ng and Clark	56	56	56	0
1988 Swamy and Al-Asali	12	0	9	0
2006 Smaoui et al.	0	12	12	12
2003 Ahmed et al.	9	0	9	9
Total	77	68	86	21

While all of the engineering properties displayed in Figure 2-6 are influenced by exceedingly high levels of PCD-related expansion, only the splitting tensile strength and elastic modulus are sensitive to the levels of expansion commonly observed in the field (up to two percent). In fact, the loss of splitting tensile strength and elastic modulus is commonly attributed to the development of microcracking, which may occur well before significant expansion is measured. The relationship between concrete expansion and microcracking is different for each combination of materials, mixture characteristics and environment. While testing a combination of Texas concrete materials, Smaoui recorded a thirty-four percent loss of elastic modulus at 0.04 percent expansion. It should be noted that testing results from the El Paso aggregate frequently exceeded the lower bound losses recommended by ISE. Quarries within the El Paso area have been identified as sources of *extremely reactive* aggregates in the literature.

`

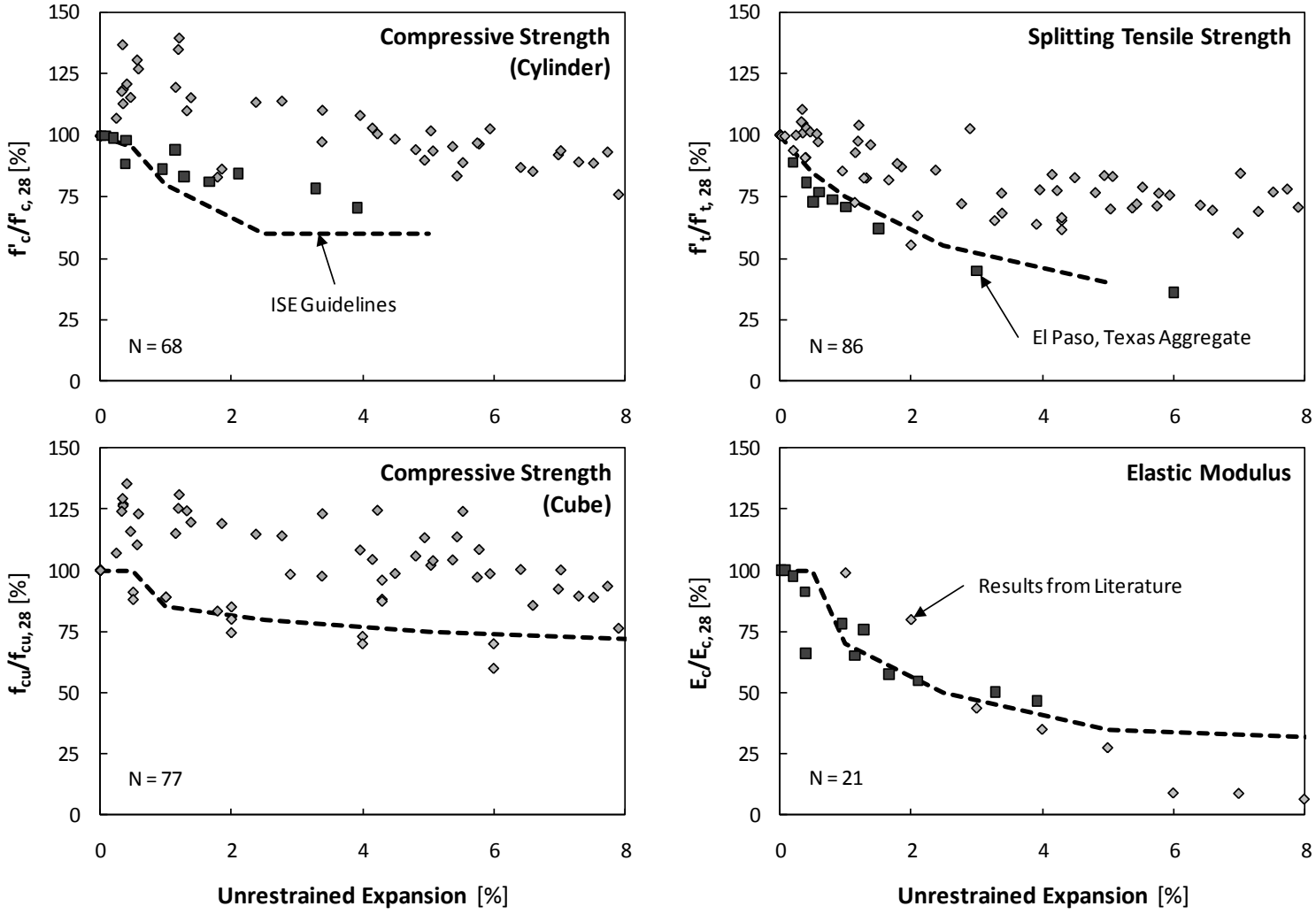

Figure 2-6: Impact of ASR on the Engineering Properties of Concrete

In most cases, the effect of ASR/DEF on engineering properties of concrete cannot be generalized in terms of expansion due to the dependency on a set of highly variable factors (particularly environmental factors). This assertion is supported by the large variation of strength/stiffness loss found for any given level of expansion in Figure 2-6. Furthermore, the testing of ASR/DEF affected samples has limited applicability to the behavior of a reinforced concrete element.

> *It has to be realized that any strength test conducted on a specimen quantifies the performance of the material in relation to that method of test only and does not necessarily reflect the performance of the material in its structural context. The significance of this for the assessment of structures [subject to ASR] is that no reliance should be placed on the values obtained from any one test and that commonly accepted procedures, such as the cube crushing test, may not indicate the value to be used in a normal design check (Clayton et al. 1990).*

Due to the complex interplay between the expansive structural core and surrounding reinforcement in concrete elements, Clayton suggested that only full-scale testing should be used to evaluate the effects of ASR on structural performance.

2.3.2 Strength and Stiffness of Reinforced Concrete Beams

Early discoveries of map cracking in highway structures led engineers to investigate the impact of the unidentified deterioration on the concrete properties. The results of core tests typically revealed a severe deterioration of the concrete modulus and tensile strength; thereby prompting further investigation of the structure's flexural stiffness and load-carrying (shear) capacity. During the 1980's, Japanese researchers conducted a large number of small-scale laboratory studies to supplement the results from ongoing load tests of in-service structures affected by ASR (refer to Section 2.4.2 for more detail). At the end of the decade, Clark summarized the Japanese research program in support of efforts to create assessment guidelines for affected structures within the United Kingdom. The following is largely an overview of the observations made during Clark's desk study. A number of recent references are also included to provide the most recent knowledge on the behavior of reinforced concrete beams affected by ASR/DEF.

A summary of the various parameters studied over the last three decades is included in Table 2-3. Simple beams up to thirteen feet in length were generally fabricated using reactive and non-reactive aggregates (to provide a basis for strength and stiffness

comparison). The growth of expansions and/or crack widths was then closely monitored as various techniques (outdoor exposure, heated water baths, etc.) were used to accelerate the deterioration. Upon achieving the desired level of distress, the beams were typically tested under symmetric two point loading with supports forming identical shear spans to each side of a constant moment region. The flexural mode of failure was generally induced by providing a sufficient number of stirrups ($0.0 \leq \rho_v \leq 1.3$) along each shear span. Shear failure, though not the subject of many tests included here, was accomplished through the manipulation of the longitudinal reinforcement ($0.2 \leq \rho \leq 2.7$) and shear span-to-depth ratio ($1.5 \leq a/d \leq 5.6$). A great number of unreinforced shear tests were conducted and reviewed by Clark, but are omitted here as current practice does not encourage the use of such details. Furthermore, the effects of ASR/DEF on reinforcement anchorage and bearing capacity are beyond the scope of this document.

Table 2-3: Studies of Reinforced Concrete Beams Affected by ASR

Reference		Number of Tests	Specimen Details					Failure Mode
			h	b	ρ	ρ_v	a/d	
Clark 1989	Kyoto University, Japan	11	8 in	8 in	0.8-1.8 %	0.2-0.3 %	2.5	Flexure
	Ritsumeikan University, Japan	16	8	8	1.2	0.2	2.5	Flexure
	Giffu Univerisity, Japan	18	7	4	1.7	*	2.8	Flexure
	Kobe Univeristy, Japan	20	8	8	0.8-1.2	0.0-0.3	1.5-2.5	Flexure/Shear
	Konoike Construction Co., Japan	8	20	20	0.5	*	2.5	Flexure
	Takenaka Research Laboratory, Japan	3	20	10	0.9	*	3.3	Flexure
	Public Works Research Institute, Japan	27	20	20	0.2-1.4	0.0-0.4	-	Flexure
	Swamy and Al-Asali	3	4	3	1.8	1.3	3.1	Flexure
Chana and Korobokis, 1991		24	8	4	2.3	0.2	5.6	Shear
Ahmed, Burley and Rigden, 1998		8	5	3	2.7	0.4	3.6	Shear
Fan and Hanson, 1998		6	10	6	0.4-1.0	0.3	2.2	Flexure
Total/Range		144	4-20	3-20	0.2-2.7	0.0-1.3	1.5-5.6	

* *shear reinforcement provided throughout the length* - unspecified

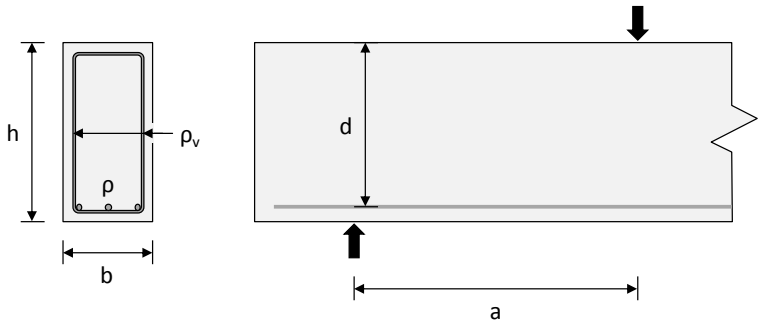

Over a wide range of structural parameters, concrete mixtures, and conditioning techniques, a number of common observations were made and are noted here. As deterioration progressed, the development of surface cracks was strongly influenced by the application of conditioning loads and the presence of reinforcement. Very few cracks formed perpendicular to the primary tension reinforcement in most of the referenced exposure tests, with a significant amount of the deterioration and expansion occurring at the compression side of singly reinforced specimens. This phenomenon frequently led to significant camber (upward deflection) of the specimens over time. During the static tests, many of the researchers failed to observe a measureable difference between the reactive and non-reactive specimen stiffness; despite the noticeable camber and loss of

elastic modulus (up to seventy percent in some cases). Researchers also noted a significant delay in the formation of flexure and shear cracks within the deteriorated specimens and some even commented on a complete absence of cracking at the nominal capacity (Figure 2-7). Very few signs of ductility were observed prior to both flexural and shear failures.

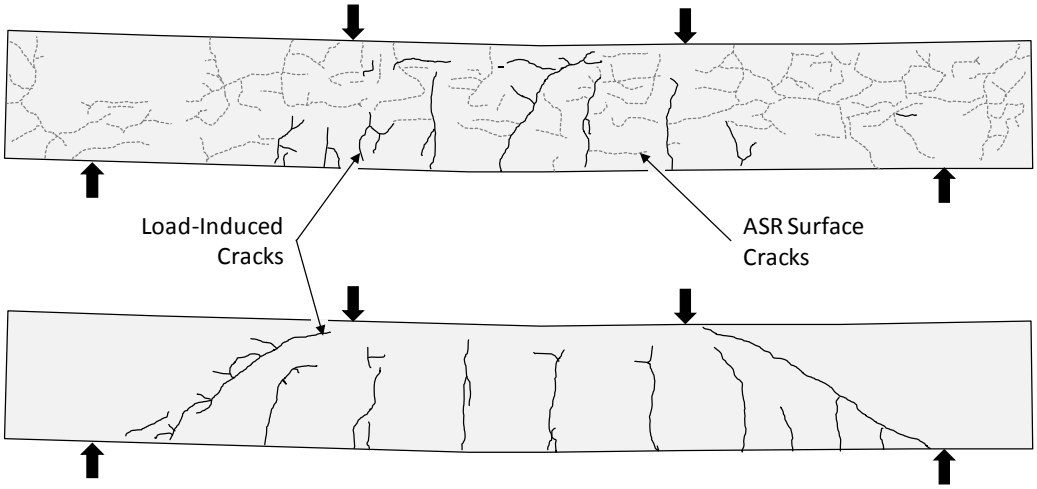

Figure 2-7: Effect of ASR on Load-Induced Cracking in Nominally Identical Beams (Adapted from Clark 1989)

The range of ASR-related expansions evaluated during each study is not presented within Table 2-3 as researchers used a number of measurements to track the progress of the deterioration (crack widths, compressive stresses, etc.). However, the ability of PCD to yield the shear reinforcement was mentioned on a frequent basis and a number of specimens were subjected to expansive strains in excess of 0.2 percent (typical yield strain for grade 60 reinforcing bars). The high strains and stresses experienced by the reinforcement did not result in a noteworthy loss of structural capacity. Static failure loads of the deteriorated beams were 0.93 to 1.47 times the measured capacities of comparable undamaged beams. In particular reference to shear failures, poor anchorage of the primary tension reinforcement in a number of specimens did not even lead to premature failures. None of the tests showed any distress in bond or bearing. It was commonly suggested that the loss of material strength and reinforcement elasticity is compensated by the compressive stress induced as ASR expansion is restrained by the reinforcement. Not surprisingly, the use of cylinders and cores to predict the loss or gain of strength was not successful (due to a lack of structural context). Both methods provided different (Figure 2-8), yet equally poor indications of the impact of PCD-related

distress on structural behavior. Researchers regularly concluded that ASR deterioration did not have a detrimental effect on the stiffness or strength of a beam. However, Chana, Korobokis (1992) and McLeish (1990) commented on the large scatter of the test results and urged the use of conservative methods when evaluating deteriorated structures.

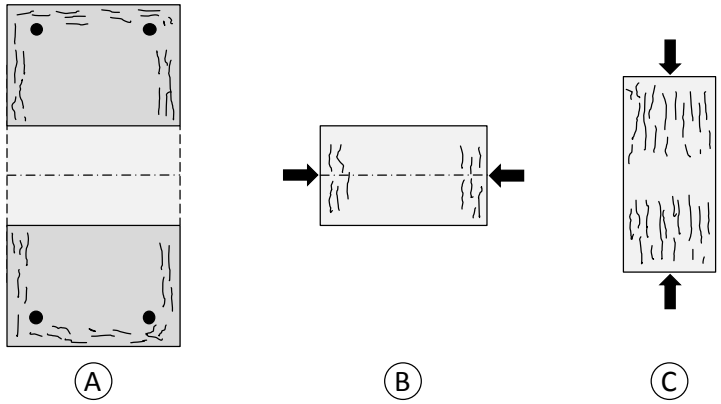

Figure 2-8: Relation Between (A & B) Core and (C) Cylinder Tests (Adapted from Clark 1989)

The promising results of the 144 tests reviewed here are overshadowed by a few substantial concerns. Very few of the specimens included in the review are over ten inches in height and therefore do not provide a reliable representation of the large highway structures being considered in this study. The use of various conditioning regimes to accelerate premature concrete deterioration in the small-scale specimens further discounts the applicability of the results presented here. Questions regarding the development and permanence of the compressive stresses induced during the accelerated conditioning period were raised during Clark's review and have yet to be resolved. If the compressive stresses are not as large or are lost to creep in field structures, the enhancement of structural capacity may not be applicable. Lastly, very few of the elements tested here were designed with the expressed purpose to evaluate the impact of ASR/DEF on the brittle failure mode of shear. A series of tests conducted on shear-critical beams with representative amounts of shear reinforcement would lend more insight into the impacts of ASR/DEF on the sectional and deep beam shear transfer models.

2.4 PERFORMANCE OF IN-SERVICE STRUCTURES AFFECTED BY ASR/DEF

Despite the promising results of laboratory tests, researchers recognized the limitations of their studies and typically prescribed precautionary measures (generally coating treatments to mitigate further deterioration) to maintain structural safety. The effects of ASR/DEF deterioration had only been evaluated at discrete levels of deterioration which were believed to be representative of the condition of in-service structures. Unknown consequences, including the loss of structural safety, were feared to lie outside the bounds of the experimental results.

A review of the international discovery and management of PCD affected structures will provide insight into the long-term nature of ASR and DEF deterioration. Parallels drawn between the international experiences will help to explain the current *outbreak* of ASR and DEF within the State of Texas and also identify the substantial challenges that lie ahead.

2.4.1 Experience in South Africa (Blight et al. 1983 to 2000)

In 1977, undeniable evidence of ASR was found in a number of South African highway structures. The discovery was unexpected; domestic aggregates did not fit the characteristics of reactive aggregates found internationally. Furthermore, severe cracking had developed over a relatively short period of time, leading engineers to question structural safety. A general lack of expertise emphasized the need for a comprehensive research program and spurred cooperation between government, industry and research entities. Work conducted over the following years included the first formal study of ASR affected structures. It provided the basis for a great number of field and laboratory tests conducted internationally.

2.4.1.1 Load Testing and Maintenance of Johannesburg Portal Frame

A portal frame supporting a major Johannesburg motorway (Figure 2-9) was diagnosed with alkali-silica reaction in 1978. An analysis of cored samples from the structure revealed that the concrete contained silica-rich quartzite and cement with an exceedingly high alkali content (equivalent alkali loading of about 14 lb/yd^3). Fifteen years into service (completed in 1963) the exposed portions of the frame had deteriorated to an extent that was “visually alarming.” The long-term performance of the deteriorated structure was subsequently evaluated through continuous monitoring and two full-scale load tests (1982 and 1988).

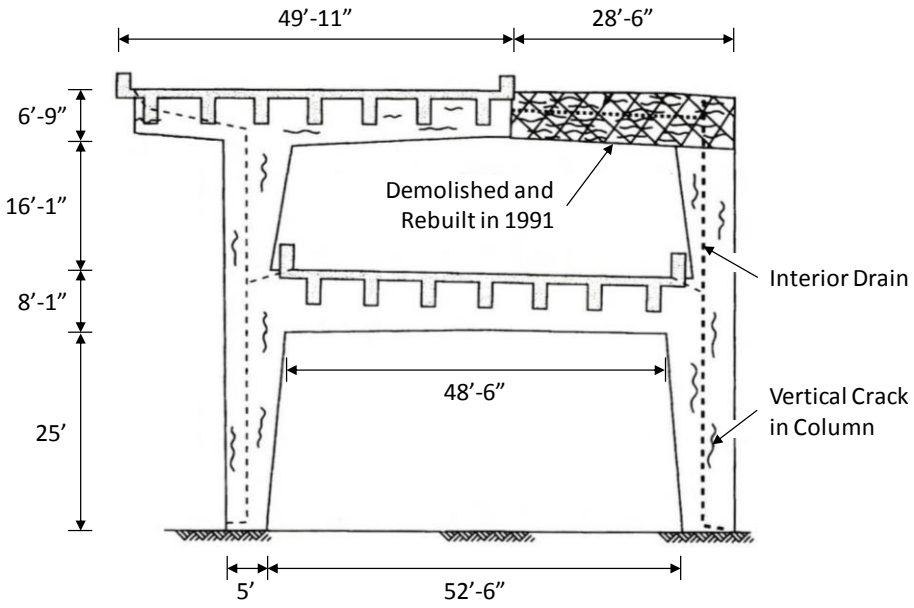

Figure 2-9: Two-Level Portal Frame in Johannesburg (Adapted from Blight 2000)

The full-scale testing was designed to assess the serviceability and strength of the deteriorated portal frame. Displacement, rotation and strain of the structure were monitored under the application of a design load. An elastic finite element analysis provided a point of reference for the performance of the structure. Concrete properties used in the model were established via mechanical testing of cores from various parts of the frame. The expansive strains induced by ASR were recognized, but no attempts were made to characterize the state of stress prior to the analysis or load testing.

During the first load test (Figure 2-10B), the frame was subjected to nearly eighty-five percent of the design load over the course of five hours. The application of the first load increment led to large concrete compressive strains that were attributed to the closure of surface cracks. Subsequent changes in compressive strain as well as measured displacements, rotations and reinforcement tensile strains correlated well with predicted values. No creep was observed over the test period and eighty to eighty-five percent of the frame displacement was recovered when unloaded. The portal frame was deemed structurally adequate and it was recommended that sources of water ingress be eliminated.

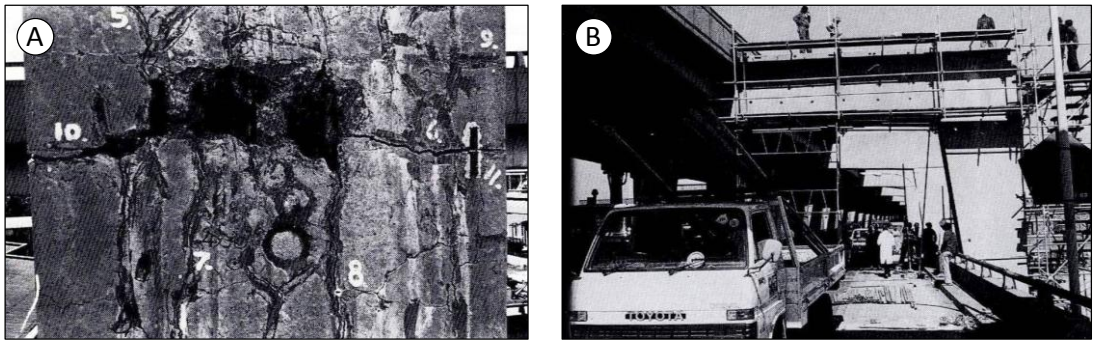

Figure 2-10: Two-Level Portal Frame (A) Surface Cracking at Beam-to-Column Joint (B) View of Site During Load Test (Blight 1989)

The accelerated growth of a number of cracks (up to sixth-tenths of an inch wide, Figure 2-10A) led to a second load test in 1988. The response of the structure was nearly identical with very little indication of the deterioration accumulated since 1982. Observations made during the initial load test were confirmed and similar recommendations made. Two years later, the ill-timed application of a waterproof coating trapped seasonal moisture in the concrete frame. Expansion accelerated and the coating cracked extensively within seven months of the application. In 1991, the deteriorated upper beam was demolished and rebuilt in an attempt to eliminate maintenance related costs (Figure 2-9). Blight last reported in 2000 that continued expansion of the original concrete was threatening to damage the repaired beam segment.

The South African load tests produced consistent results and demonstrated that adequate structural safety and serviceability were preserved over the six year period. The researchers concluded that the unsightly cracking was not necessarily indicative of structural adequacy. This conclusion was reaffirmed by lack of visible deterioration outside the cover length of extracted cores. Load testing was recommended as the "ultimate criterion" of the safety and serviceability of ASR affected structures. However, no consideration was given to brittle modes of failure (i.e. shear) that may occur with overloads.

Almost four decades after the completion of the portal frame, ASR induced expansion continued to be a maintenance concern. The long-term nature of the reaction demonstrated the need for effective mitigation methods.

2.4.2 Experience in Japan

During the 1970's, several Japanese rail transit structures developed large width cracks early in their service lives. Subsequent investigations were inconclusive, but strengthening measures were commonly taken to compensate for "inadequate construction." In 1982, similar cracks in nearly one-hundred bridge piers of the Hanshin Expressway were studied and attributed to alkali-silica reaction. The magnitude of the discovery led to an ensuing nationwide survey that revealed ASR damage in additional bridge (including the aforementioned rail structures) and protective structures (levees, sea walls, etc.). Following the lead of South African colleagues (Section 2.4.1), a comprehensive research program focused on the development of countermeasures for alkali-silica reaction and management strategies for affected concrete structures (Kojima 2000).

2.4.2.1 Loading Testing and Maintenance of Hanshin Expressway Piers

The Hanshin Expressway, constructed between 1969 and 1979, is a major Japanese viaduct supported on over five-hundred reinforced and prestressed concrete piers (similar to that shown in Figure 2-11). Routine inspections revealed the formation of small cracks within four years of construction. The cracking progressed and was considered severe (up to two-tenths of an inch wide and the depth of the cover) in nearly one-hundred bridge piers by 1982. An analysis of cored samples from the affected structures revealed a volcanic coarse aggregate (reactive andesite) and an equivalent alkali loading up to 12 lb/yd^3 (derived from high alkali cement and unwashed sea-dredged sand, West 1996). It was determined that alkali-silica reaction was responsible for the visible deterioration and significant loss of concrete mechanical properties. The long-term performance of the deteriorated viaduct was subsequently evaluated through continuous monitoring and a full-scale load test in 1984.

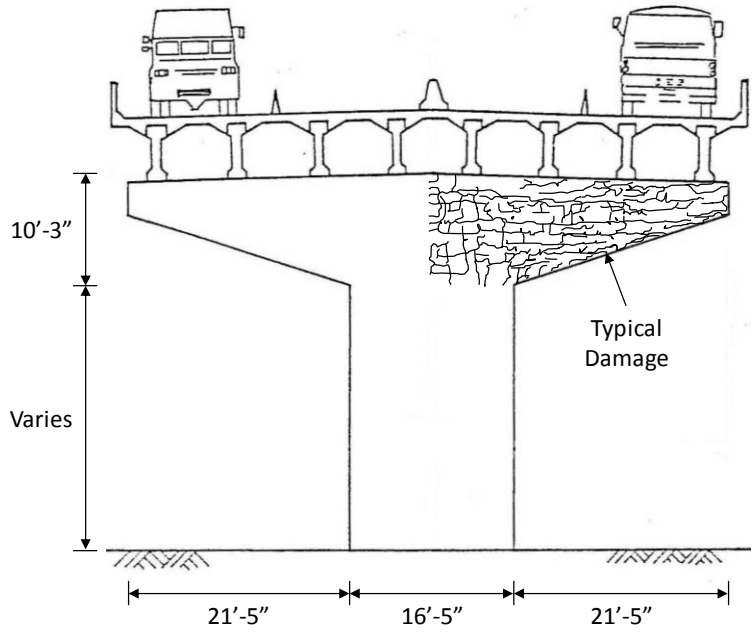

Figure 2-11: Hanshin Expressway Pier in Osaka, Japan (Adapted from Clark 1989)

In accordance with the South African load tests (Section 2.4.1.1), Japanese researchers assumed that service load behavior was indicative of the structural adequacy of the bridge piers. No consideration was given to ultimate strength. Tests were performed on four bridge piers (two damaged and two undamaged) and an elastic finite element analysis provided a point of reference. Placement of the design trucks on the outer lanes of the pier, in symmetric and non-symmetric fashion, took into account the most severe loading scenarios. Displacement of the structure was monitored under the application of up to eighty percent of design load.

ASR-induced damage did not significantly influence the performance of the damaged bridge piers; only minimal increases in displacement were noted. Further comparison of the measurements led researchers to conclude that the in-situ elastic modulus of the damaged concrete was approximately ninety percent of the undamaged value. In contrast, an eighty percent loss of elastic modulus was measured through the mechanical testing of cores. The loss was not representative of the overall structural performance and therefore led to overestimation of the displacements by the finite element model. Researchers concluded that the stiffness and load carrying capacity of the structure had not been significantly affected (Imai et al. 1983).

A number of complementary studies (Section 2.3.2) reinforced the Japanese argument that alkali-silica reaction did not pose a significant threat to the safety and serviceability of concrete structures (Ono 2000). Following the successful implementation of control measures for new construction, efforts shifted to the long-term maintenance of damaged structures. Maintenance strategies commonly relied on the exclusion of moisture to mitigate future expansion and prevent corrosion of the reinforcement. Laboratory trials of various waterproofing techniques led the Hanshin Expressway Corporation to recommend a two stage repair consisting of epoxy resin injection (large cracks) and silane impregnation (surface). Three years after the initial application, Imai reported that the coating technique effectively controlled reinforcement corrosion and expansion of the piers.

Many deteriorated concrete structures were actively treated with waterproof coatings throughout the 1980's and 1990's. In some structures, persistent expansion cracked the waterproof coating and prompted re-application within as little as three years. Poor performance of the coating was initially attributed to inadequate application, but subsequent repairs also failed to arrest the ASR-related expansion.

2.4.2.2 Discovery of Fractured Reinforcement in Highway Structures

In the late 1990's, fractured reinforcement was found in a bridge pier with nearly twenty years of cumulative ASR damage. The pier (shown in Figure 2-12) was built in 1979 and developed visible signs of ASR in the 1980's. Severe cracks prompted the application of a waterproof coating in 1989 and 1992. During an investigation of the structure in 1999, the accelerated growth of a crack along the main reinforcement was found to coincide with a considerable loss of concrete compressive strength and elastic modulus. Removal of the concrete cover along the crack exposed fractures of the stirrup corners.

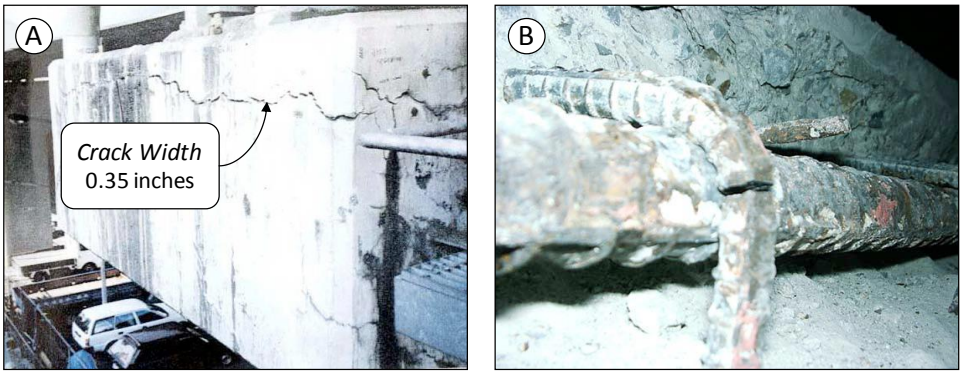

Figure 2-12: (A) Typical Pier Damage (B) Associated Reinforcement Fracture (Miyagawa 2006)

A subsequent survey of ASR affected structures revealed thirty additional cases of fractured reinforcement. The discovery led Japanese researchers to reassess the impact of ASR on structural safety and serviceability.

> *As long as reinforcing steels are not broken due to ASR-caused expansion, the safety of a structure is considered not to be seriously compromised. However, the safety of a structure becomes questionable when the confinement of the concrete becomes degraded due to fracture of reinforcing steel bars* (Miyagawa 2006).

Research directed by the Japan Society of Civil Engineers sought to clarify the mechanisms of the reinforcement fractures.

ASR-induced fractures were brittle failures (no signs of cross-section reduction) occurring within bent sections of the reinforcement. Fractures were typically concentrated in lightly reinforced and unsheltered regions of the structure (most susceptible to severe ASR expansion). To investigate the cause of the fractures, researchers carried out a series of material tests on reinforcement samples. The impact of bending radius, strain aging, and delayed deterioration (due to stress-corrosion cracking and hydrogen embrittlement) on the initial cracking and fracture sensitivity of the reinforcement was considered. A number of samples were bent to various interior radii (1 to 2.5 times the bar diameter) and then subjected to environmental treatments to simulate the effects of strain aging and/or delayed deterioration. The interior of the bend was examined for cracks prior to tensile testing (Figure 2-13). Results of the bent samples were compared with similarly conditioned straight samples.

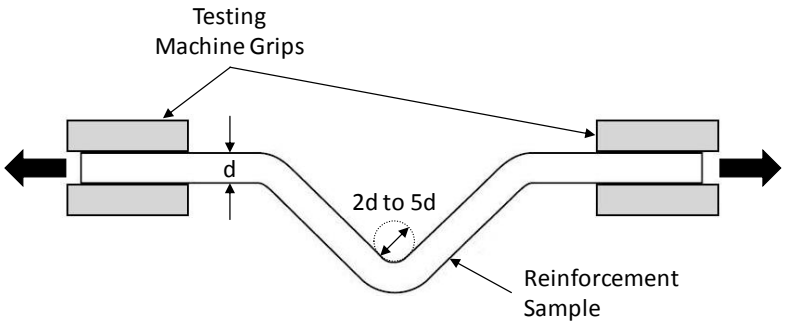

Figure 2-13: Tensile Testing of Bent Reinforcement (Adapted from Miyagawa 2006)

Although strain aging and delayed deterioration of the reinforcement had adverse effects on the fracture resistance of the samples, the effect of small bending radii was most significant. Visual inspection of the smallest bend radius (equal to the bar diameter) revealed initial cracking that reduced the tensile strength by sixty percent. Furthermore, brittle fracture only occurred in the smallest bend diameter samples. Loss of the cross-section occurred in all other bend radii, regardless of the test conducted. The typical bend diameters of field fractured reinforcement were not reported, so valid comparisons cannot be made. Nevertheless, the mechanism shown in Figure 2-14 was adopted by the researchers to explain the ASR-induced fractures.

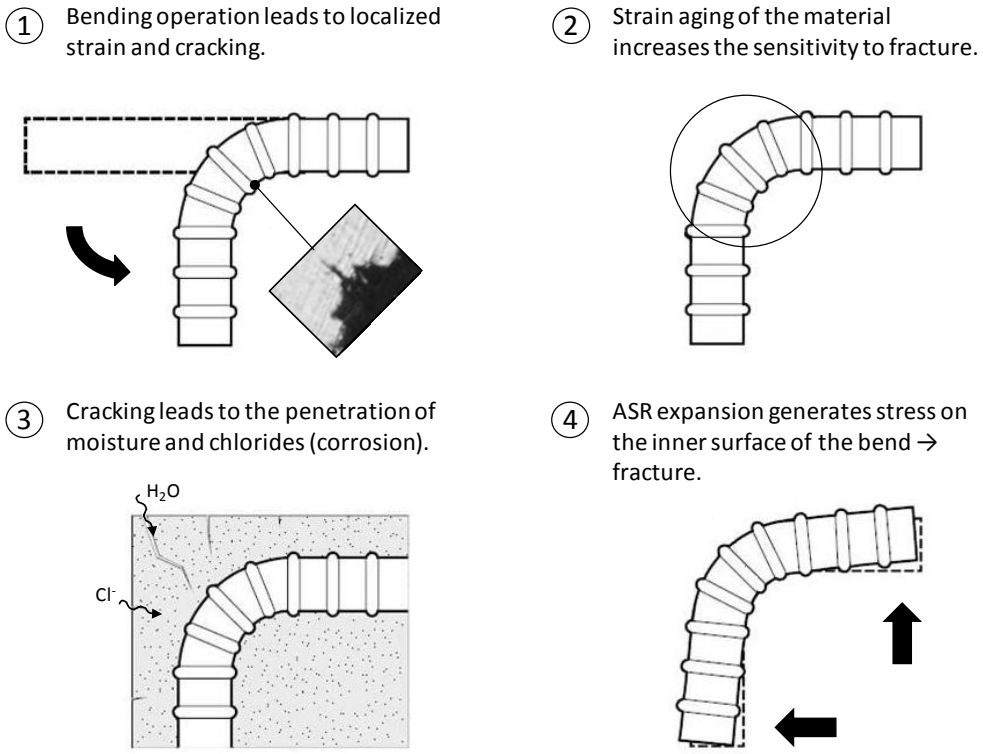

Figure 2-14: Presumed Mechanism of Reinforcement Fracture (Adapted from Miyagawa 2006)

Historically, laboratory and field studies (Section 2.4.2.1) failed to demonstrate an ASR-related loss of strength and the deterioration was therefore categorized as a serviceability issue. Perception of ASR as structurally harmless deterioration persisted until the recent discovery of fractured reinforcement in the deteriorated structures of Japan. It was immediately recognized that the ASR-induced fracture of reinforcement would lead to a sudden loss of structural capacity. In fact, tests of structural members subjected to shear have shown that the inability to develop the full capacity of the fractured stirrups leads to the loss of overall strength (Mikata 2008). Presently, many Japanese studies are focused on the development of assessment tools and strengthening methods for bridge elements with fractured stirrups.

It is difficult to comment on the potential for reinforcement fractures in ASR-affected structures found within the United States. The results of Miyagawa's study on fracture mechanisms suggest that reinforcement is only subject to brittle failure when significant damage exists at the interior of the bend. During the tests, damaging cracks only formed when bend radii were exceedingly small or subject to stress-corrosion cracking.

American practice dictates the use of large radius bends: two times the bar diameter for the reinforcement used within the Japanese study. Stress-corrosion cracking did lead to fracture of the large diameter bends, but the observed loss of cross-section was not characteristic of fractures found in the field. Despite this observation, the lower ductility standards used in the manufacture of American reinforcement may offset the benefits of larger bend radii. Standards (ASTM A615) currently require a minimum elongation of twelve percent, whereas the Japanese reinforcement exhibited elongations over twenty percent.

It should be noted that Miyagawa did not present a rationale for the study of such small bend radii. Due to the structural ductility required to withstand the high seismicity of Japan, it is unlikely that such bend details were employed in the design of the stirrups found within the damaged pier structures (Figure 2-12, above). In fact, implementation of bend details similar to those found within American practice would be necessary to achieve sufficient ductility. A more definitive assessment clearly requires further investigation of the circumstances leading to the fracture of Japanese reinforcement. The typical bend diameters and distribution of the fractured reinforcement are among the details necessary to make a valid comparison.

2.4.3 Experience in Texas

In the decades following the discovery of alkali-silica reaction, a few isolated cases of the deterioration led the Texas Department of Transportation to restrict the combined use of reactive aggregate sources and high-alkali cements (greater than 0.6% equivalent alkali content). Similar measures, adopted by transportation authorities throughout the United States, had successfully prevented ASR in new concrete structures. However, late twentieth century discoveries of premature concrete distress in a number of Texas highway structures raised significant concerns regarding the long-term effectiveness of the specifications. Preliminary investigations documented TxDOT's first experience with delayed ettringite formation and revealed a general lack of technical knowledge regarding the distress mechanisms of ASR and DEF. A comprehensive research campaign was launched to develop practical tools and techniques for the mitigation of ASR/DEF and the evaluation of affected concrete structures.

2.4.3.1 Modern Discovery of Premature Concrete Deterioration

In 1997, fifty-six precast concrete box beams were deemed unsuitable for use due to the severity of ongoing deterioration within the end regions. The box beams were fabricated

in 1991 as part of a total of sixty-nine required for a future TxDOT project. While maintained in approved storage, the beams were subject to routine inspections that identified hairline cracking of the end regions within one year of fabrication. The application of crack sealants in 1993 did not slow the progression of the cracking and much of the repair work failed prior to the final inspection in 1995. Crack widths within four years of fabrication were as large as one-quarter of an inch. The results of a preliminary study attributed the damage to internal expansion of the concrete, but did not conclusively implicate a particular mechanism. Structural studies were not carried out on the deteriorated beams prior to the recommendation for disposal (Lawrence et al. 1999).

The unprecedented rate of deterioration led to significant concern; all of the materials used within the concrete had demonstrated excellent long-term performance in Texas concrete infrastructure. A limited survey of in-service bridge structures was conducted to establish the extent of the problem. Visually distressed precast and cast-in-place elements, all under twenty years of age and in some cases only a few years old, were identified throughout the state (Figure 2-15).

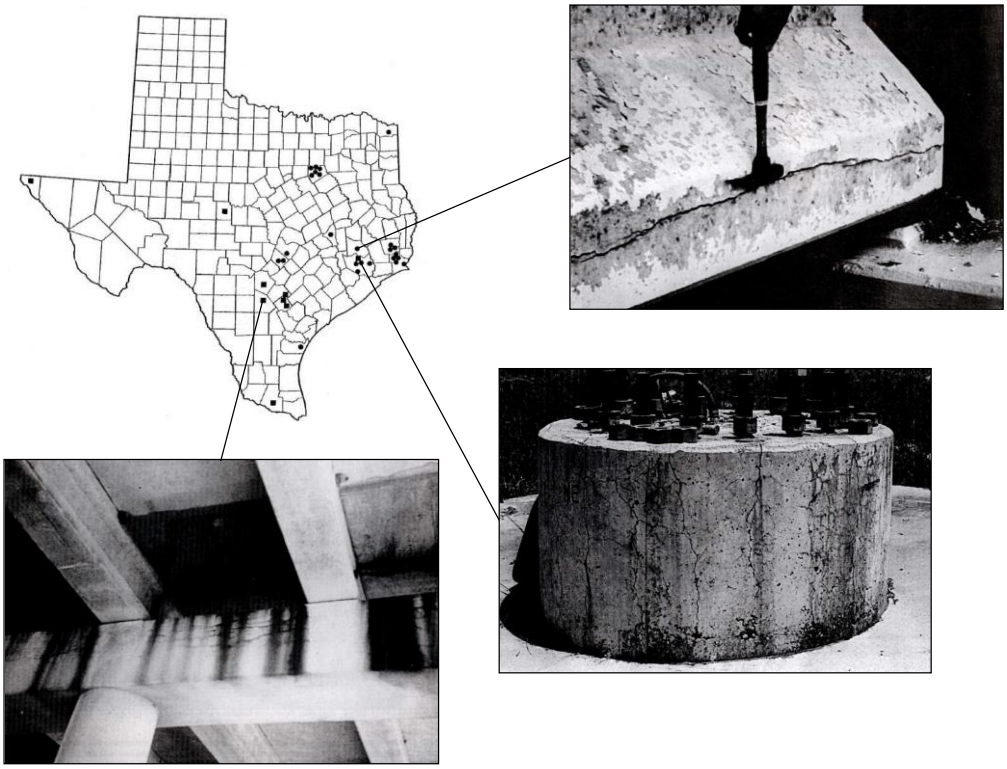

Figure 2-15: Texas Structures with PCD as of September 1999 (Adapted from Lawrence et al. 1999 and Boenig 2000)

Although the severity of the damage varied, similarities could be drawn between the affected structures. Damaged elements were generally classified as mass concrete. Large cast-in-place bent caps, columns, and piers were commonly affected when exposed to moisture from roadway runoff or nearby bodies of water (and even when sheltered, see the Atascosa County bent cap in Figure 2-15). The large bottom flange and/or end block portions of precast girders also developed significant deterioration. Furthermore, construction of the affected elements was occasionally accelerated through the use of *high-sack* concrete mixtures. Generally reserved for precast construction, the practice was also used in cast-in-place substructures to expedite the placement of connecting elements (precast girders, high mast illumination poles, etc.).

Petrographic analysis of concrete materials sampled from the fifty-six precast concrete box beams and a number of the in-service structures identified dense ettringite nests within the voids, cracks, and gaps of the cement matrix. After reviewing the findings with an independent consultant, TxDOT engineers concluded that delayed ettringite formation was partially responsible for the widespread deterioration (refer to Hime 1996 for further detail). It was the state's first encounter with DEF - a distress mechanism only recognized within the last two decades. Based on the results of the survey, it was clear that the uninhibited use of high-early strength concrete (without regard to elevated alkali loadings or curing temperatures) was triggering the development of both ASR and DEF in new concrete construction.

The loss of concrete durability can primarily be attributed to a general lack of expertise regarding premature concrete deterioration (PCD – a term developed by TxDOT to encompass the damage done by ASR or DEF; often indistinguishable). Historical performance of the materials was satisfactory, and as a result, construction specifications were not updated to reflect the most recent knowledge regarding the distress mechanisms. However, the situation was further exacerbated by unrecognized changes in the cement and aggregates industries. Cement chemistry was rapidly changing to meet environmental regulations and quality aggregate was quickly becoming a rare commodity. Both developments contributed to the late twentieth century *outbreak* of premature concrete deterioration and would persist as long-term challenges to the production of durable concrete.

From the outset, the long-term safety of the affected structures was a primary concern of TxDOT engineers. However, as initial assessments progressed it became clear that very few methods to quantify the structural impacts of the distress existed. Furthermore, the ongoing deterioration threatened to burden TxDOT with significant maintenance and

repair costs in the near future. A quotation from an early study (TxDOT Project 0-1857, 1999 to 2002) reveals the department's perspective at the time:

> *In past instances, structures have been removed from service or repaired after only several years of service. As statewide inspection of in-service concrete structures progresses, more structures with this problem are being identified. The cost for replacing and repairing these structures is already significant, and will continue to increase.*

The considerable size and growing nature of the problem led the Texas Department of Transportation to pursue simple assessment and mitigation technologies. A series of studies were conducted at the University of Texas through the turn of the millennium; subsequent recommendations relevant to the current study are summarized in Table 2-4.

Table 2-4: Studies of PCD at the University of Texas at Austin

TxDOT Project	Title	Primary Recommendation(s) and/or Product(s)
0-1857	Structural Assessment of In-Service Bridges with PCD	· The growth of PCD-related cracks (as measured through a *Damage Index*) should be used to estimate the residual material strength and corresponding loss of flexure and/or shear strength.
0-4069	Mitigation Techniques for In-Service Structures with PCD	· An application of silane and TxDOT appearance coat paint is the most effective mitigation treatment for affected structures; extending life of treated structures by a factor of 1.3 to 1.5.
0-4085	Preventing ASR and DEF in New Concrete	· The TxDOT maximum alkali loading requirement of 4 lbs/yd^3 should be lowered due to highly reactive aggregates within the State of Texas. · Maximum curing temperatures should be limited to 150°F for precast girders and 160°F for mass concrete placements.
0-5218	Extending Service Life of Large or Unusual Structures Affected by PCD	· A protocol was developed for evaluating the cause and extent of deterioration due to ASR and DEF and for predicting future expansion. · The use of sealants is recommended for ASR/DEF suppression; pressures required to confine the expansion are impractically high – around 600 psi.
IAC 88-5DDIA004	Anchor Bolt Behavior in ASR/DEF-Damaged Drilled Shafts	· As a precautionary measure, damaged drilled shaft structures should be protected from further deterioration and corrosion (no significant strength loss was observed in current state). · No correlation between the *Damage Index* from TxDOT Project 0-1857 and the damaged drilled shaft behavior was found.
IAC 88-8XXIA007	Shear Loading and Autopsies of ASR/DEF Damaged Trapezoidal Box Beams	Testing in progress.

The testing of salvaged structural elements (Project 0-1857 and IAC 88-5DDIA004) has eased concerns regarding the safety of affected structures. However, these studies only cover the behavior of two distinct types of infrastructure components and do not

represent the wide range of deterioration found within the State of Texas. Furthermore, the implementation of assessment techniques developed during these studies (including Project 0-5218) was unsuccessful; TxDOT engineers still lack practical tools that are universally applicable to all component types. While advances in mitigation technologies have been made and implemented (through specification changes and coating technologies), deterioration continues to develop in new structures as well as those previously repaired (see Section 2.4.3.2 below). A truly effective PCD mitigation technique has proved to be an elusive target.

2.4.3.2 Maintenance of the US 183 and IH 35 Interchange, Austin, Texas

Following four years of construction, the elevated section of US Highway 183 was completed in 1998 at a cost of seventy-three million dollars. Ten nearly-identical straddle bents were used to support new mainline and exit ramp structures (precast concrete segmental bridges) above Interstate Highway 35. To form each straddle bent, a post-tensioned precast concrete cap was set on a pair of cast-in-place columns at a simple span of sixty-nine to eighty feet. The massive post-tensioned caps were nearly ten feet deep, eight feet wide, and weighed over four hundred tons each when placed.

"Early signs" of premature concrete deterioration were recognized in the precast caps within the first decade of service; far short of its expected design life. Due to the significance of the interchange, a special waterproofing specification was developed for the treatment of the affected interchange structures. TxDOT officials hoped to slow the deterioration before it could cause considerable damage to the structure (Pruski 2005). Over two months, the concrete end caps (concealing the post-tensioning grout pockets) of each straddle bent were replaced, all surfaces were blasted with an abrasive medium, and a series of waterproofing agents were applied: (1) silane, (2) opaque sealer, and (3) cementitious coating. All of the waterproofing materials were deemed watertight, but breathable; thereby allowing moisture to escape over time. The application of the treatment required a complex series of overhead operations, causing extensive lane closures and traffic delays. The formal cost of the repair was nearly sixty thousand dollars per cap or six hundred thousand dollars for the interchange; as detailed in Figure 2-16.

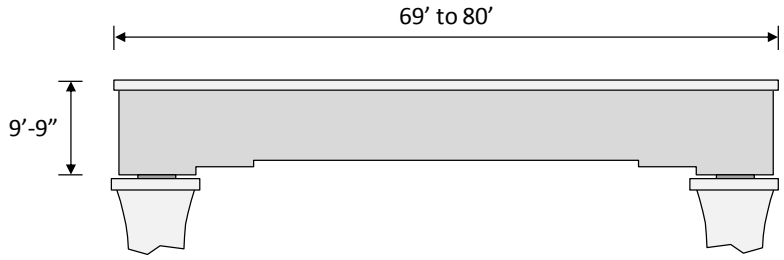

Repair Item	Average Cost
1. Remove and Replace Concrete End Caps.	$ 6,586
2. Abrasive Blast All Surfaces to Remove Contaminants.	$34,412
3. Apply Penetrating Silane Treatment and Breathable Cementitious Coatings.	$3,990
4. Provide Barricades, Signs, and Traffic Control.	$14,926
Total Cost per Bent	$ 59,914

Figure 2-16: Costs Associated with Straddle Cap Repair

Although the repair was recently completed in 2006, signs of persistent deterioration have already emerged. A brief visual survey of the structures in the summer of 2008 identified new damage in all but two of the repaired straddle bents. Map cracking patterns (visible to a passing motorist, Figure 2-17) were commonly found in the new cast-in-place end caps, suggesting that the waterproofing treatment has failed to arrest the internal expansion due to ASR and/or DEF. As previously suggested, field implementation of such techniques (in Texas and elsewhere, refer to Sections 2.4.1 and 2.4.2) successfully slows the progress of the mechanisms, but ultimately fails to arrest future crack development; thereby allowing further moisture ingression and the acceleration of deterioration. It should be noted that no definitive assessment of the repair technique can be made without a comprehensive study of the time-dependent deterioration.

Figure 2-17: Condition of Straddle Caps within Three Years of Repair

Without a reliable treatment, the relatively young concrete structures may continue to experience ASR/DEF related expansions for an extended period of time. Experiences in South Africa and Japan have shown that periods of active expansion may last several decades in select structures and have serious structural consequences. Uninhibited long-term expansion of may ultimately lead to the fracture of reinforcement and the need for major structural retrofit in a period of time that is well short of the structure's intended service life.

2.5 SUMMARY

The most current knowledge regarding the time-dependent deterioration, laboratory behavior and in-service performance of concrete structures subject to ASR/DEF was reviewed to provide practicing engineers with a fundamental basis for the assessment and management of affected structures. The current study was subsequently designed to further explore and expand upon each of these topics, as will be reviewed in the remainder of this document.

While the deterioration processes of ASR and DEF were recognized as distinct chemical reactions, it was concluded that the physical manifestation of the deterioration is nearly indistinguishable. Internal expansion of the concrete microstructure leads to a well-distributed network of microcracks and bulk expansion of the concrete. Further development of ASR/DEF reaction products leads to the common appearance of map cracking at the concrete surface. Both mechanisms were found to be highly dependent on a set of variable factors including cement composition, mixture characteristics and exposure conditions. Consequential deterioration of in-service structures was noted to be highly variable through both space and time.

The deterioration of the engineering properties of concrete materials affected by ASR/DEF was reviewed in the context of corresponding expansive strains. The common assumption that the loss of strength and stiffness is directly related to expansion was challenged. It was noted that only splitting tensile strengths and elastic moduli were sensitive to increasing expansion and more specifically, the degree of microcracking. The use of in-situ expansions to estimate the engineering properties of the in-service concrete was dismissed due to the high variability of the results and the lack of structural context (a deteriorated sample is not subjected to the same restraints found in a structural member).

Nevertheless, the considerable loss of elastic modulus and tensile strength have historically led to concern regarding the flexural stiffness and shear strength of concrete structures. A summary of simple beam tests conducted over the last three decades revealed a number of common behavioral consequences of ASR/DEF (reinforcement aligned surface cracking, camber, delay of load-induced cracking, etc.). However, the deterioration and large reinforcement strains/stresses induced did not lead to a measureable loss of strength or stiffness; although results were highly variable. The applicability of the testing was questioned due to unrepresentative specimen sizes and the use of techniques to accelerate deterioration. Furthermore, a majority of the testing programs only evaluated flexural behavior and left a considerable gap in knowledge regarding the behavior of shear dominated members.

A presentation of the discovery and management of structures in South Africa and Japan revealed a number of commonalities. The appearance of ASR/DEF deterioration was often unexpected and led to a considerable amount of field and laboratory research. Predictable behavior of affected structures during short-term load tests did much to alleviate the concerns of supervising engineers, but did not give any indication of the reserve strength or future impacts of deterioration. Attempts to mitigate persistent deterioration through the use of waterproofing treatments consistently failed and eventually led to the discovery of fractured reinforcement within Japanese structures. All available details regarding the fractures were reviewed in an attempt to assess the risk to structures which contain reinforcement bends meeting the AASHTO LRFD Bridge Design Specifications. A lack of critical information prevented a decisive assessment and further research was recommended.

The discovery and management of prematurely damaged concrete structures in the State of Texas paralleled the experiences in South Africa and Japan. Rapidly changing characteristics of well used and highly regarded materials led to an increased risk for

ASR and DEF. Common use of accelerated construction methods in mass concrete structures further heightened the potential for premature deterioration. Surveys identifying deteriorated structures throughout the state prompted the introduction of new construction specifications and further research into management strategies. Despite a considerable amount of investment in assessment and mitigation technologies, the Texas Department of Transportation is still challenged by a lack of practical assessment tools and an inability to eliminate deterioration in new structures to a great level of certainty. Recent evidence suggests that uncontrolled deterioration may lead to significant structural consequences and retrofit expenditures.

CHAPTER 3
Test Specimens

3.1 OVERVIEW

Despite decades of research, the structural consequences of premature concrete deterioration are still not fully understood. To address the shortcomings identified within the literature review of Chapter 2, a comprehensive study of the physical deterioration due to ASR/DEF and its consequential impact on structural performance was conducted at the University of Texas at Austin. Six large-scale bent cap specimens, representative of the most severe circumstances of deterioration found in the field, were produced using the select materials and techniques presented within this chapter. These bent caps formed the basis for the expansion monitoring, shear testing, and forensic analyses presented within Chapter 4.

The design of the bent cap specimens was firmly rooted in the need to explore the effects of premature concrete deterioration in shear dominated concrete bent caps (as discussed in Chapter 1 and reinforced by the results reviewed within Chapter 2). Due to wide variety of boundary conditions, reinforcement schemes, and deterioration found within the Texas Department of Transportation's inventory, laboratory replication of a damaged structure was not desirable. As demonstrated throughout this chapter, the final specimen design was carefully chosen to ensure general applicability of the experimental results. A review of the specimen geometry and load configuration reflects the consideration given to the size and layout of commonly affected field structures (Section 3.2.1). Focused study of the effects of ASR/DEF on shear strength was then accomplished through careful detailing of the specimen reinforcement (Section 3.2.2) and selection of concrete mixture components (Section 3.2.3). A pilot test (presented within Section 3.3) was used to eliminate questions regarding the shear criticality of the specimen design.

The production of the six bent cap specimens (four reactive and two non-reactive) was critical to the success of the project. Implementation of unique concrete materials and fabrication techniques was the result of significant forethought and planning (Section 3.4). Fabrication results, presented at the end of this chapter, reveal the potential for deleterious expansion in each reactive specimen and give a preliminary indication of future structural performance.

3.2 DESIGN OF BENT CAP SPECIMENS

The rising concerns of TxDOT engineers were rapidly addressed with a simple, yet carefully crafted, strategy: structural testing of the most vulnerable (i.e. least conservative) shear details found in practice would definitively expose any potential threats to the safety of damaged bent cap structures. A thorough review of the literature and relevant design specifications (Interim 2008 AASHTO LRFD Bridge Design Specifications and 2006 TxDOT LRFD Bridge Design Manual) provided a basis for the lower bound design outlined below.

Each bent cap specimen was large enough to conclusively eliminate scaling effects related to premature concrete deterioration and/or shear transfer mechanisms. Shear spans of 1.85 and 3 times the effective depth were incorporated at opposite ends of the beam to evaluate the impact of ASR/DEF on deep beam and sectional shear behavior, respectively. The overall test program therefore accommodated twelve shear tests, two non-reactive and four reactive regions per shear span type (Section 3.2.1). It should be noted that only half of the shear tests were conducted prior to the publication of this report. The purpose and most recent condition of the remaining six shear spans will be reviewed within Chapters 4 and 5, respectively. Each shear span was sufficiently reinforced in flexure and limited to the minimum transverse reinforcement to ensure a lower-bound shear failure. All six of the bent cap specimens were structurally identical (Section 3.2.2). Careful control of the concrete mixture reactivity then allowed an individual specimen to represent an independent stage of deterioration (ranging from mild to severe). The final collection of test results would thereby clarify the time-dependent effects of premature concrete deterioration and provide an indication of challenges to come (Section 3.2.3).

3.2.1 Overall Specimen Geometry

Premature concrete deterioration found in a large number of TxDOT bent caps served as the primary motivation for the current project. The description of the US 59 and I-10 Interchange bent structure given in Chapter 1 exemplifies the general state of deterioration being investigated here. In order to accurately model the effects of such deterioration within the laboratory, the size of the bent cap specimen was maximized (with consideration given to laboratory limitations, discussed below) to obtain a sufficient representation of existing full-scale TxDOT bent caps. Future implementation of the project results would not require size-related extrapolation.

The cross-section design is compared to three bent caps currently in use by TxDOT within Figure 3-1. The one-of-a-kind US 59 and I-10 bent cap is an unusually large structure in comparison to the standard bent caps (for Type C and Type IV prestressed concrete girders) routinely used in highway structures. While the specimen cross-section may be substantially smaller than the largest bent caps affected by ASR/DEF, it is nearly as large as the majority of bent caps currently in use (and occasionally subjected to PCD) throughout the State of Texas.

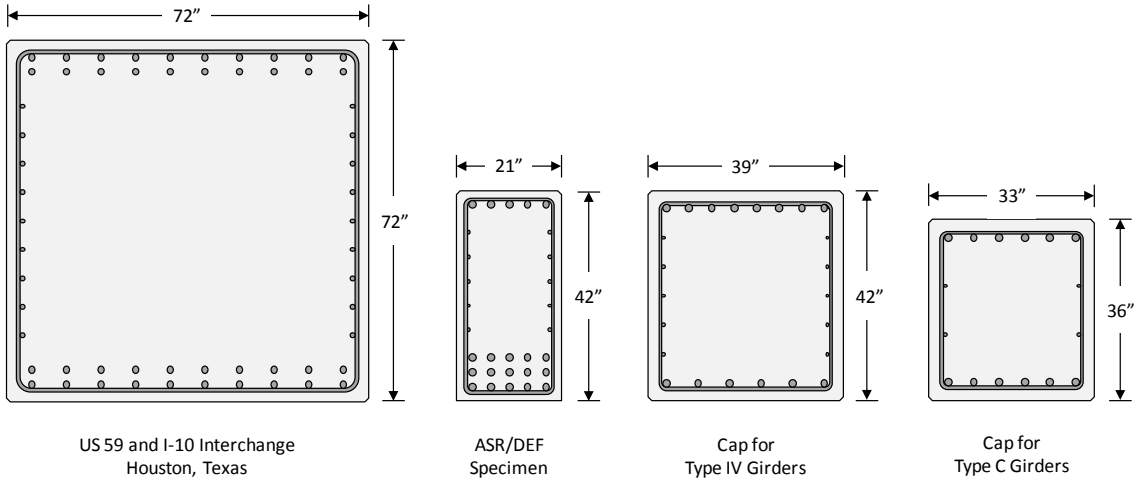

Figure 3-1: ASR/DEF Specimen and Texas Bent Caps

The final size (and corresponding weight) of the ASR/DEF specimen was controlled by limitations of laboratory facilities and equipment. To avoid conflicts with the high-strength threaded rods found at either end of the Large-Scale Beam Test Facility (shown in Figure 3-9 and described in Chapter 4), the cross-sectional width of the specimen was limited to twenty-one inches (b = 21”). The specimen height of forty-two inches (h = 42”) was then selected to obtain an aspect ratio of two to one; a common characteristic of the largest in-service bent caps. The span length of the test specimen was controlled by the distance between the reaction points of the large-scale beam test facility (L_{span} = 21’-4”). Additional length was then added to accommodate hooked anchorage of the primary flexural reinforcement at either end. However, the anchorage length was limited to ensure that each of the completed bent cap specimens could be transported outside with the fifteen ton forklift. The overall length of the specimen was over twenty-seven feet (L = 27’-8”) resulting in a total weight of nearly thirteen tons. Within the laboratory, the specimen was easily handled by a twenty-five ton overhead crane. An elevation view of the specimen can be found in Figure 3-3B.

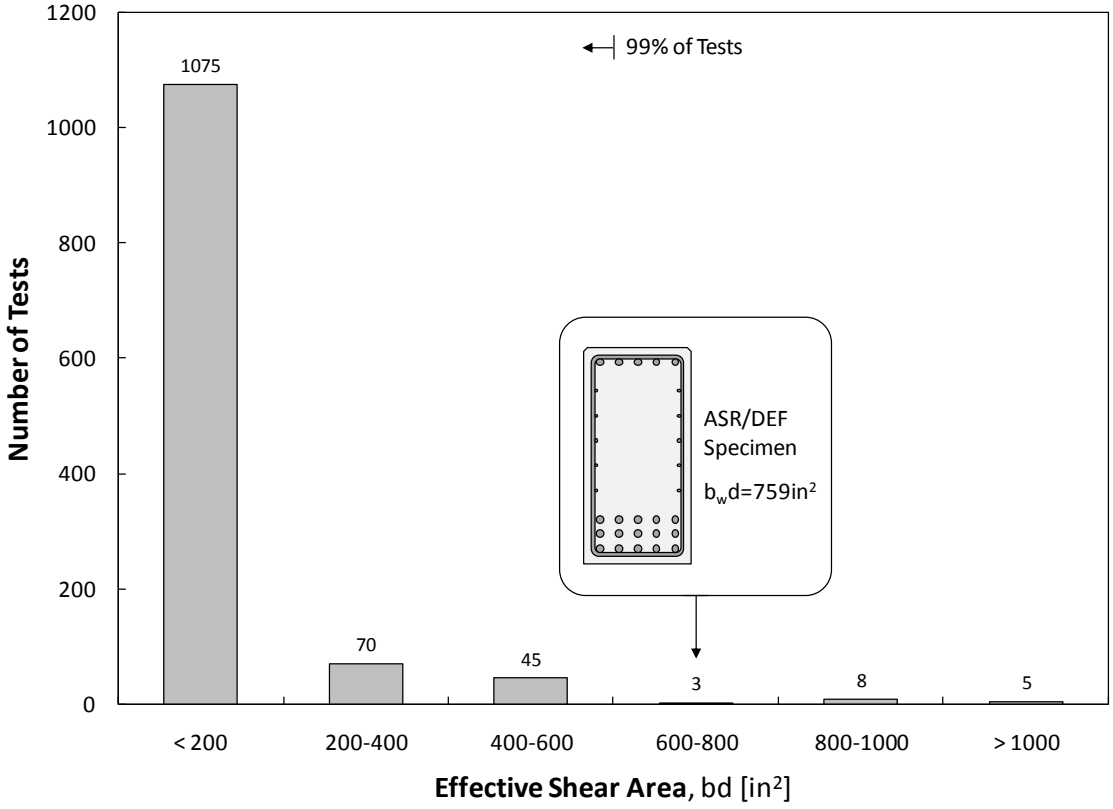

Figure 3-2: TxDOT Project 0-4371 Shear Database – Effective Shear Area

The resulting bent cap specimens are some of the largest *reactive* concrete elements ever produced within a laboratory setting. Moreover, the specimens are among the largest shear-critical beams ever tested (see Figure 3-2). At a shear area of 759 in^2, the ASR/DEF specimens were larger than ninety-nine percent of the historical shear tests compiled by TxDOT Project 0-4371. To add perspective, a majority of the ASR/DEF specimens indentified within Chapter 2 reside below the fortieth percentile of the shear database.

The clear span of the specimen was long enough to include two *independent* shear tests (testing procedures are briefly described in Section 3.3.2), one at each end as shown in Figure 3-3B. The load and support bearing plates which designate each span are included in all subsequent diagrams of the specimen; thereby providing a point of reference for the design. The final configuration resulted from thoughtful consideration of the shear span-to-depth ratios commonly found in practice. The bearing plate configuration of the US 59 and I-10 bent cap is shown in Figure 3-3A to illustrate the range of shear spans found in a given structure. It is important to note that most TxDOT bent caps are analyzed and designed as simply supported members; reactions are assumed to be located at the center

of each column. For the ASR/DEF specimen, the most demanding conditions were chosen for the shear transfer mechanisms of compressive strutting and diagonal tension. This translated to separate shear spans of 1.85 and 3 times the effective depth of the bent cap specimen, respectively. Following structural testing of each shear span, the impact of ASR/DEF on capacity was evaluated using traditional strut-and-tie ($a/d < 2$) and sectional ($a/d > 2$) design models.

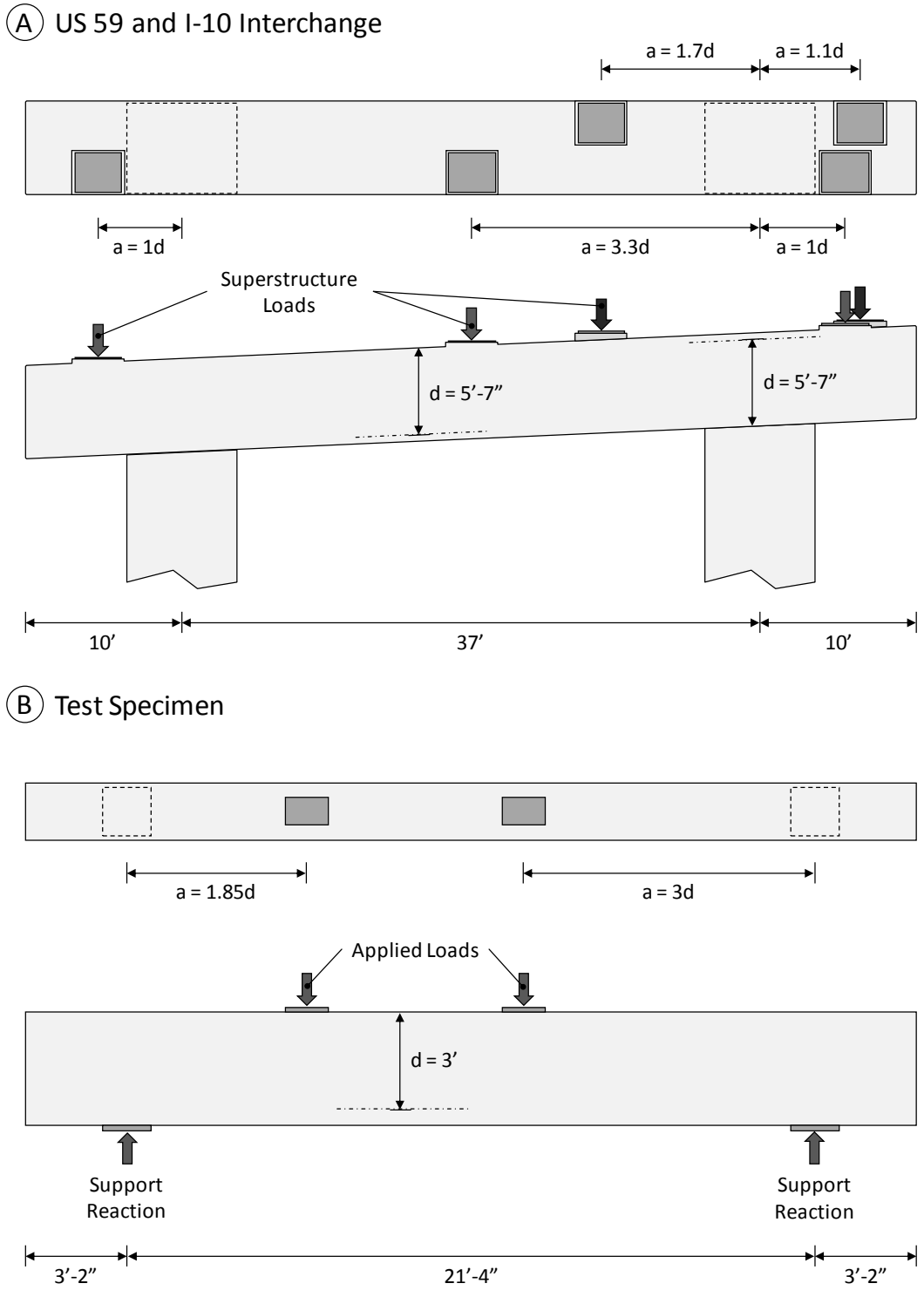

Figure 3-3: Shear Span-to-Depth Ratios (A) US 59 and I-10 Interchange (B) Specimen

3.2.2 Reinforcement Layout

The current test program was designed to be an explicit study of the potential PCD-related loss of *shear* strength. A preliminary review of historical shear testing results suggested that substantial longitudinal reinforcement was necessary to successfully avoid flexural failure and thereby ensure a shear critical test. As such, each bent cap specimen was to be flexurally reinforced with fifteen well-anchored No. 11 bars. The resulting (longitudinal) tensile reinforcement ratio (ρ) of about three percent was higher than typically found in practice. A review of several TxDOT bent cap designs showed that severe flexural demands required a tensile reinforcement ratio of two percent at most. The implications of the high reinforcement ratio were subsequently investigated to ensure the validity of future experimental results. As detailed below, the shear critical design did not compromise the practicality of the testing program.

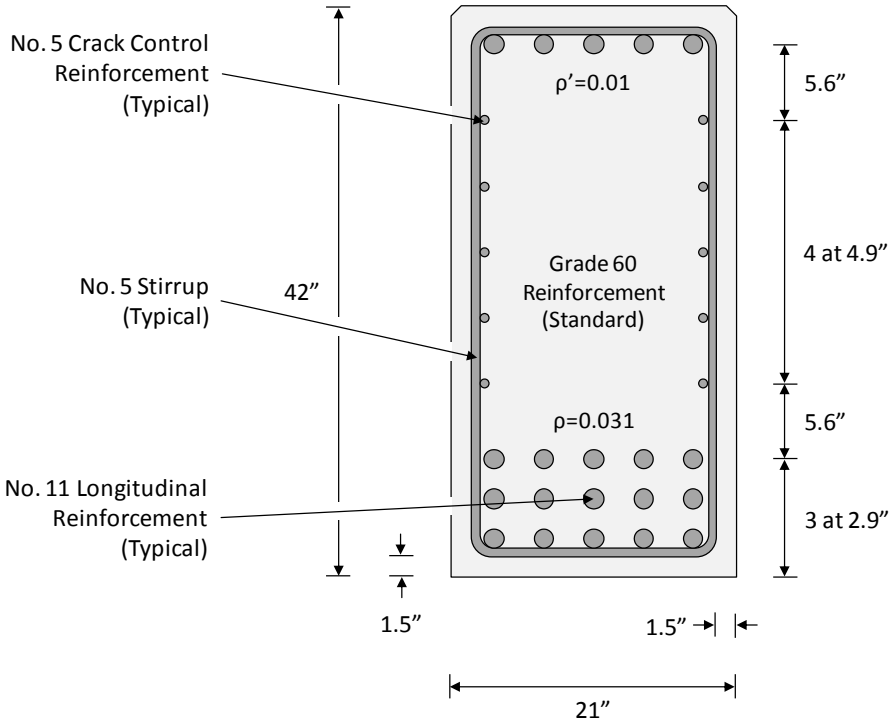

Figure 3-4: Specimen Reinforcement – Cross-Section

The flexural design (shown in Figure 3-4) met all the code requirements for classification as a tension-controlled member; a common design constraint. The effective reinforcement ratio (ρ-ρ′) of two percent resulted in an extreme tensile steel strain of 0.006 in/in at a nominal moment capacity of approximately 44,500 k·in. Flexural failure

corresponded to the application of $12.5\sqrt{f_c'}b_w d$ normalized shear during the deep beam test and nearly $8\sqrt{f_c'}b_w d$ shear during the sectional shear test. A final concrete strength of 5 ksi is assumed for the calculation of flexural capacity and normalized shear forces.

To examine the potential for flexural failure, the shear induced at the flexural capacity of the specimen was compared to the normalized shear required (as reported in the literature) to cause compression strut (at a/d = 1.85) or diagonal tension (at a/d = 3) failure. The comparisons were expedited through the use of a shear test database compiled by the researchers of TxDOT Project 0-4371. Selection of results within a narrow range of the selected shear span-to-depth ratios provided an adequate number of tests for assessment. A graphical summary of the results can be found in Figure 3-5.

As noted, flexural failure of the deep beam shear span (a/d = 1.85) was estimated to occur at an applied shear of $12.5\sqrt{f_c'}b_w d$. For shear spans ranging from 1.8 to 2 times the depth, over eighty percent of the tests reported within the literature failed at shear stress levels lower than that required to fail the current specimen in flexure. The results therefore suggested that the likelihood of a flexural failure was about twenty percent. It should be noted that the shear reinforcement ratio was disregarded when the historical test results were compiled. The shear capacities summarized within Figure 3-5A may have been obtained from test specimens with more shear reinforcement than considered here (and detailed below). A study of similar sectional shear spans resulted in even greater confidence (see Figure 3-5B). Likelihood of a flexural failure during the sectional shear test was estimated to be about five percent.

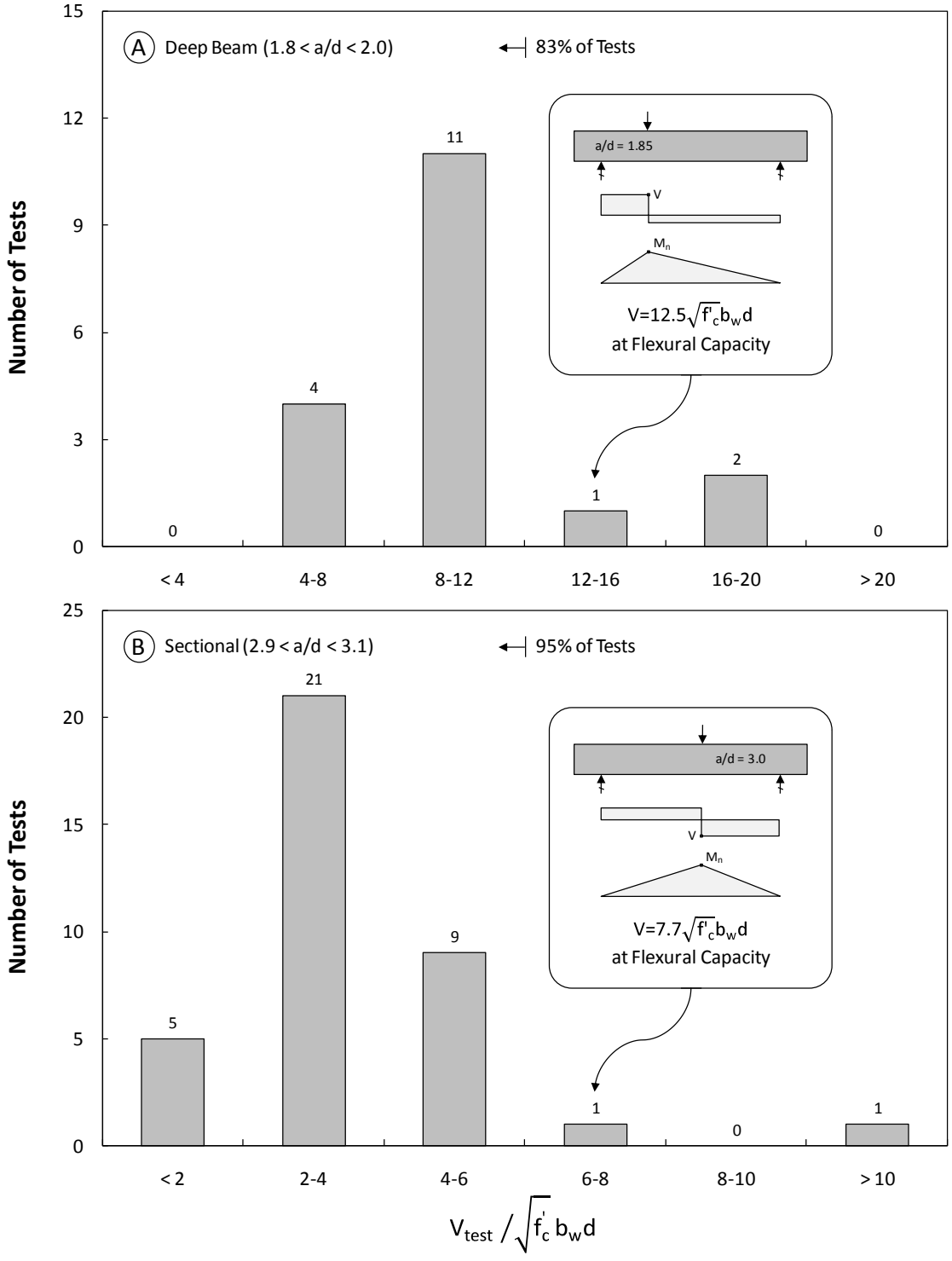

Figure 3-5: TxDOT Project 0-4371 Shear Database – Shear Capacity

The review of historical test data made it clear that the heavy longitudinal reinforcement was *necessary* to meet the project objectives; unintended flexural failures would result in the loss of substantial investments in the fabrication and conditioning of each specimen. However, the use of three percent longitudinal reinforcement was inconsistent with common practice and therefore may cast doubt on future implementation of the project results. From a practical standpoint, the shear critical design had two potential implications: (1) the development of uncharacteristic ASR/DEF expansions and (2) an unconservative increase of shear strength.

While the reactions of ASR and DEF are commonly assumed to result in uniform volume expansion (and surface map crack patterns), there are a number of external parameters which may lead to directionality of the damage. To begin with, ASR-induced expansions are highly sensitive to the application of compressive stress. Compression developed along the axis of a reinforcing bar can effectively restrain expansions in that direction. The overall expansion potential is not reduced; rather the expansion in a less-restrained direction is amplified (Multon et al. 2005). In the case of a reinforced concrete bent cap, the longitudinal reinforcement ratio is always a number of magnitudes greater than the transverse reinforcement ratio. As a result, the expansion is characteristically anisotropic and primarily oriented in the transverse direction. The anisotropic expansion may also be derived from the characteristics of the concrete placement (i.e. mixture characteristics and consolidation method). Plain concrete test samples of various shapes, sizes, and reactive aggregate compositions have consistently exhibited a *natural* tendency for expansion in the vertical (perpendicular to the casting plane) direction (Smaoui et al. 2004).

ASR/DEF deterioration *in reinforced concrete bent caps* is clearly characterized by principal expansion in the transverse direction; irrespective of the longitudinal reinforcement ratio. Therefore, the shear critical design was *not* expected to impact the nature of the deterioration; additional reinforcement in the longitudinal direction would not substantially alter the predisposed development of transverse expansion. Regardless of the assertions made above, it is important to recognize that singular comparison of longitudinal reinforcement ratios between field and laboratory structures is an inappropriate approach to ensure future relevance. The specimens included within this test program were conditioned and tested under simple boundary conditions. Affected bent caps in the field are likely integral members of continuous frames and are thereby subject to unknown (and perhaps more severe) restraint conditions.

To address alternate concerns regarding the impact of heavy longitudinal reinforcement on ultimate shear strength, historical test data was again examined within the context of the current study. Please note that the following discussion only applies to sectional shear failure; deep beam *failure* is generally not influenced by the primary longitudinal reinforcement. Figure 3-6 was obtained from MacGregor and Wight's *Reinforced Concrete: Mechanics and Design* to show the relationship between the concrete contribution to shear strength and the longitudinal reinforcement ratio.

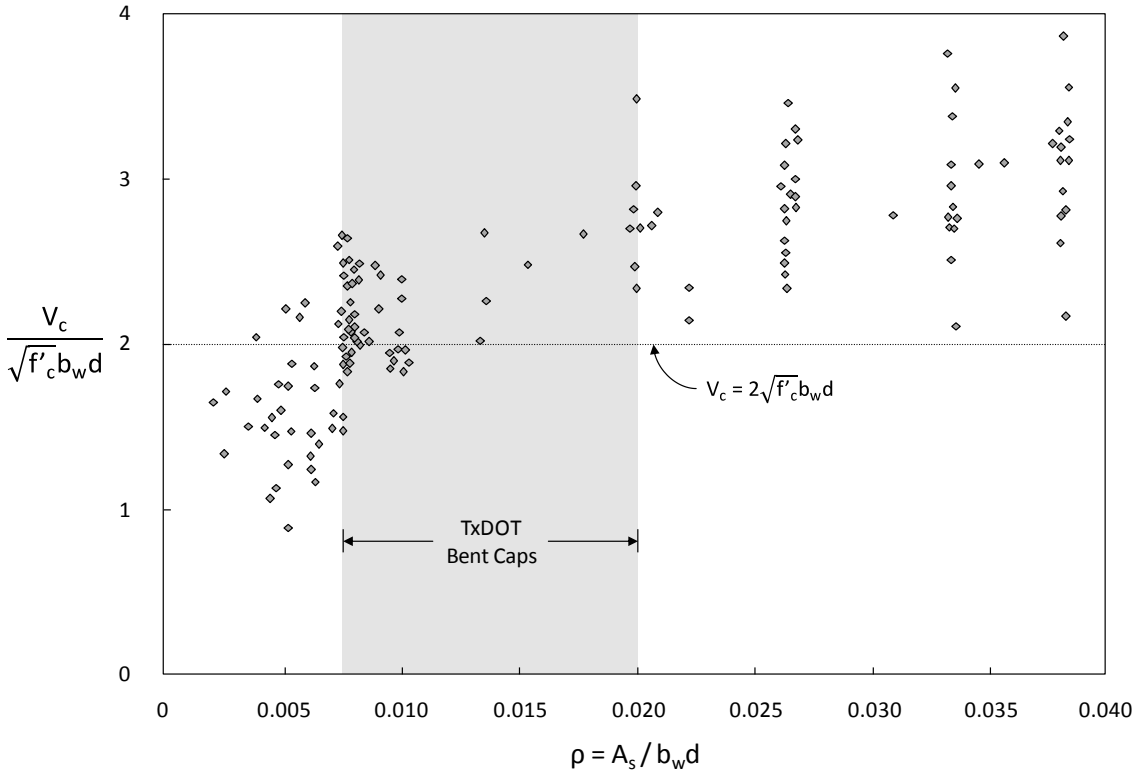

Figure 3-6: Effect of Longitudinal Reinforcement Ratio on Concrete Shear Capacity (Adapted from MacGregor and Wight 2005)

Within the range of reinforcement ratios commonly found in TxDOT bent caps, the addition of longitudinal steel has little to no effect on the lower bound concrete shear strength. In fact, it seems that the benefits of longitudinal reinforcement are only truly realized at *low* (in the context of large bridge structures) reinforcement ratios ($\rho < 0.01$). From an ultimate strength perspective, the proposed use of three percent longitudinal tension reinforcement was no less representative than the use of one percent reinforcement; both are subject to the same lower bound shear failures.

Lastly, a minimum amount of transverse reinforcement was used in each shear span to ensure that the design represented the least conservative shear details. Minimum transverse reinforcement ratios were determined using the sectional and strut-and-tie design models (AASHTO LRFD Bridge Design Specifications - Interim 2007, Sections 5.8.3 and 5.6.3). The required reinforcement was provided at the maximum allowable spacing. No. 5 stirrups, spaced at 9 ½ inches within the deep beam shear span, were placed at 20 inch intervals within the sectional shear span; corresponding transverse reinforcement ratios were 0.31 and 0.15 percent, respectively. The stirrup spacing within the sectional shear span, though uncommonly large, satisfies the AASHTO maximum spacing limits for lightly stressed sections (Article 5.8.2.7-1). Closely spaced stirrups prevented premature failure of the specimen outside the two test regions. Finally, longitudinal skin reinforcement was provided per Article 5.7.3.4-4 of the AASHTO LRFD Bridge Design Specifications. A final elevation of the reinforcement cage is shown in Figure 3-7.

The structural design outlined above became the basis for the fabrication of the six bent cap specimens included in the test program. A complementary concrete mixture (detailed within the next section) was then tailored for rapid ASR/DEF expansion. True lower bound evaluation of the shear-critical bent cap specimens came with the most severe deterioration developed over the course of the study.

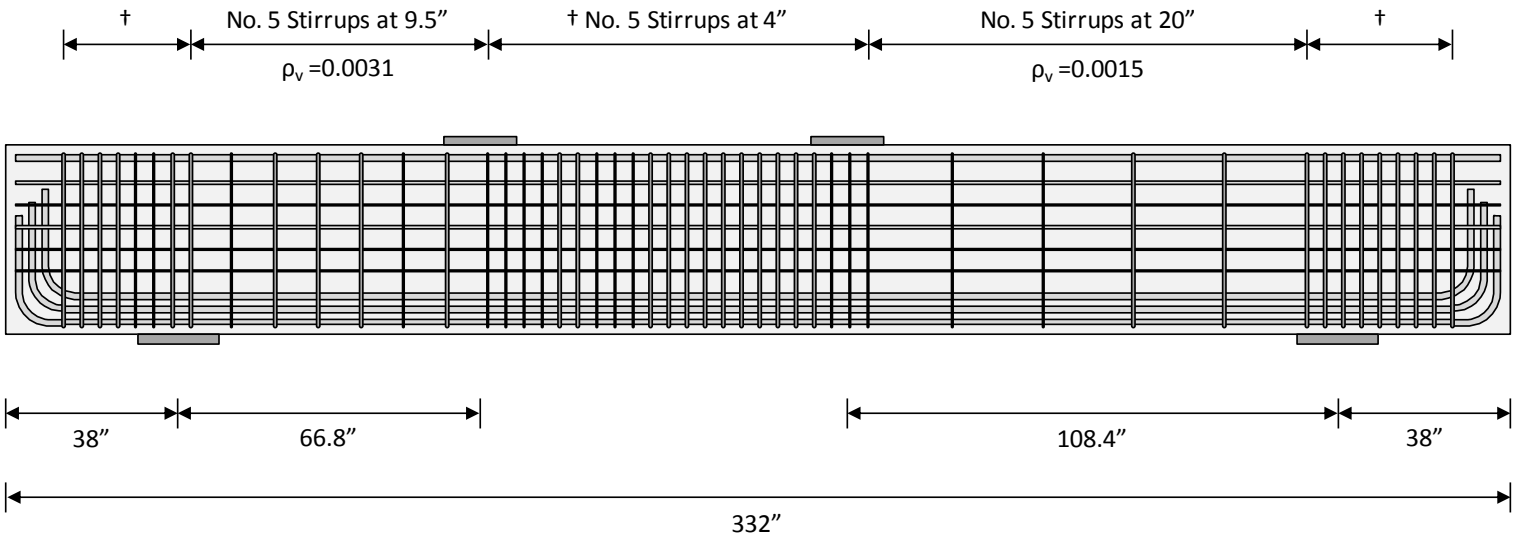

Figure 3-7: Specimen Reinforcement - Elevation

3.2.3 Concrete Mixture Design

The concrete materials and mixture proportions were carefully chosen with two objectives in mind: (1) maximize the deleterious expansion achievable within the timeline of the current study, while (2) maintaining an accurate representation of current engineering practice. Over the course of the mixture design process, the expertise of researchers at the Concrete Durability Center (CDC) of the University of Texas at Austin was solicited frequently. Consequently, the results presented within this section rely heavily on precedents set during ASR/DEF research studies conducted at the CDC. It is important to note that the details presented here are primarily concerned with maximizing the potential expansion due to ASR. While certain materials and mixtures will enhance the magnitude of DEF-related expansion, only the use of high temperature curing (as discussed in Section 3.4.3) was necessary to guarantee future development of DEF.

Efforts at the CDC are presently focused on characterizing the susceptibility of Texas concrete materials to ASR/DEF with the ultimate goal of developing successful mitigation techniques. As part of work recently completed for TxDOT Project 0-4085, researchers conducted a substantial amount of expansion testing using a number of aggregates sourced from locations throughout Texas. Each reactive aggregate was incorporated into a concrete mixture designed according to ASTM C1293 (see Section 3.4.4.2 for a description of the test method). The mixtures were then placed in a number of plain concrete prisms and blocks for long-term exposure and ASR expansion monitoring. Free expansion results of the most reactive aggregates are compared within Table 3-1. The reactive sand from El Paso, Texas produced large expansions in both controlled laboratory and uncontrolled outdoor exposure conditions. Researchers noted the “extremely high level of expansion due to ASR” (Folliard et al. 2006). The aggregate, commonly referred to as *Jobe-Newman sand*, was sourced from the same quarry identified as *extremely reactive* by Smaoui in Chapter 2 of this report.

Table 3-1: TxDOT Project 0-4085 – Free Expansion Potential of Reactive Aggregates

Texas Aggregate Source	Prism Expansions		Block Expansions	
	Plain Concrete Prisms (3" x 3" x 11¼") Stored at 100°F and near 100% RH		Plain Concrete Blocks (15" x 15" x 28") Stored Outdoors in Austin, TX	
El Paso	*0.59 %*	at 1 year	*1.01 %*	at ages over 3 years
Mission	0.12		0.80	
Cleveland	0.06		0.37	
Austin	0.06		0.39	
Amarillo	0.2		0.10	
Robstown	0.11		0.91	

Based on these results, Jobe-Newman sand was selected for the production of each reactive bent cap specimen. To determine the applicability of the ASTM C1293 standard mixture design, trial batching was conducted. Initial batches were stiff, hard-to-place, and resulted in exceedingly high compressive strength. Standard mixtures produced nearly 8000 psi of compressive strength within twenty-eight days (Table 3-2). In contrast, Class C concrete with a minimum twenty-eight day strength of 3600 psi is commonly required for the construction of TxDOT substructure components. TxDOT field engineers noted that actual concrete strengths were typically in the range of 5000 to 6000 psi, so a conservative lower bound twenty-eight day strength of 5000 psi was targeted. Further trial batching established the mixture proportions (also summarized within Table 3-2) necessary to obtain the appropriate strength characteristics.

Table 3-2: Concrete Mixture Design

	ASTM C 1293	ASR/DEF Specimen
Type III Cement	708 lb/yd^3	700 lb/yd^3
Water	297 lb/yd^3	400 lb/yd^3
Fine Aggregate	855 lb/yd^3	1110 lb/yd^3
Coarse Aggregate	1790 lb/yd^3	1475 lb/yd^3
Water-to-Cement Ratio	0.42	0.57
Theoretical Unit Weight	135 lb/ft^3	136 lb/ft^3
28-Day Strength Estimate	8000 psi	5000 psi

Reduction of the coarse aggregate fraction was offset by supplemental additions of water and fine aggregate. Though the final water-to-cement ratio was quite high, the mixture was workable and consistently produced the desired twenty-eight day strength. Furthermore, the development of a porous (water permeable) microstructure would enhance the growth and development of ASR and DEF within the bent cap specimens. Following trial batching of the reactive mixture, it was decided that simple material replacements would be used to eliminate durability concerns from the non-reactive concrete mixture. The rationale for the selection/use of both reactive and non-reactive materials is discussed within the following sections.

3.2.3.1 Reactive Concrete Mixture

While the use of Jobe-Newman sand would likely lead to deleterious ASR in the high sack concrete mixture detailed in Table 3-2, expansions (in excess of 1%) may take more than a decade to develop. The discussion below identifies a solution commonly used within laboratories to accelerate the development of ASR.

As discussed within Chapter 2, deleterious ASR will not develop unless the reactive aggregate is incorporated into a highly basic concrete mixture, pH $\geq$ 12.5. The pH is controlled by alkalis present in the various mixture components: cement, aggregate, admixtures, etc. In field structures, as little as 3 ½ pounds of alkalis (per cubic yard of concrete) have produced ASR-related distress; albeit over several years of exposure. Higher alkali contents generally lead to an increase in pH and greater reactivity. In fact, laboratory tests are frequently accelerated by *boosting* the alkali content of the mixture to more than 8 lb/yd^3 of concrete. In order to meet the first objective of the mixture design (maximize the achievable expansion), a boosted mixture was therefore selected.

High-alkali portland cement was to be dosed at a rate of seven hundred pounds per cubic yard. At an alkali content of about 0.9 percent (by weight), the cement would contribute approximately six pounds of alkalis to each cubic yard of concrete (0.9% x 700 lb/yd^3 = 6.3 lb/yd^3). A final concrete alkali content of 8.85 lb/yd^3 (as specified in ASTM C1293) would be achieved through the addition of sodium hydroxide solution.

Table 3-3: Reactive Beam Material Details

Material	Description	Source
Cement	Type III High-Alkali Cement	Lehigh Cement Company Fleetwood, PA
Water	Hot Tap Water (about 130°F)	Municipal Water Supply Austin, TX
Fine Aggregate	Jobe-Newman Sand	Cemex El Paso, TX
Coarse Aggregate	¾" Crushed Limestone	Texas Crushed Stone Company Georgetown, TX
Sodium Hydroxide	50% NaOH Solution	Fisher Scientific Company Pittsburgh, PA

Sources of all the mixture components are identified in Table 3-3. It is important to note that the use of hot mixing water (at approximately 130°F) was only intended to boost the initial temperature of the concrete mixture. The application of external heat would be necessary to obtain temperatures in excess of 158°F and thereby guarantee the future development of DEF.

3.2.3.2 Non-Reactive Concrete Mixture

Material and environmental sources of premature concrete deterioration would be eliminated to ensure the long-term durability of the non-reactive specimens. Mixture substitutions are identified in Table 3-4.

Table 3-4: Non-Reactive Beam Material Details

Material	Description	Source
Cement	Type III Low-Alkali Cement	Alamo Cement Company San Antonio, TX
Water	Cold Tap Water	Municipal Water Supply Austin, TX
Fine Aggregate	Local River Sand	Texas Concrete Materials, Ltd. Del Valle, TX
Coarse Aggregate	¾" Crushed Limestone	Texas Crushed Stone Company Georgetown, TX

The production of non-reactive concrete would require the substitution of low-alkali type III cement and local river sand. The use of sodium hydroxide and hot mixing water would be excluded and curing temperatures held below 158°F to prohibit the development of DEF. The coarse aggregate fraction of *all* concrete produced would be obtained from a limestone quarry with no history of deleterious behavior.

3.3 DESIGN VALIDATION

As discussed in Section 3.2.2, the design of each shear span (deep beam and sectional) was substantiated through a review of historic testing data. A very small percentage of tests were shown to sustain loads in excess of the chosen flexural capacity. However, the uncertainty associated with shear testing (highly variable results) ultimately prompted the development of a pilot test to physically validate the performance of the structural design. Failure to produce shear-critical specimens would result in the loss of substantial investments in fabrication materials and conditioning time.

A brief description of characteristic deep beam and sectional shear failures sets the standard for desirable shear behavior in this study (Section 3.3.1). It is then followed by a review of the pilot testing details, with particular emphasis on the ultimate load performance (Section 3.3.2). Please note that fabrication, conditioning and testing operations of all specimens were conducted in an inverted fashion. To eliminate confusion, all figures and photos are presented *as tested* through the remainder of the document.

3.3.1 Definition of Shear Failure (Ferguson 1981)

Although a member under high loads may show significant shear distress, failure may be controlled by a mode unrelated to shear transfer. A number of precautions were taken during the design process (as described in Section 3.2) to eliminate these alternate modes of failure (anchorage, bearing, flexure) and thereby force a *pure* shear failure. The following descriptions of characteristic deep beam and sectional shear failures provide a basis for the comparison of testing results presented within this document.

Where the shear span is less than twice the effective beam depth ($a < 2d$ or deep beam), a large portion of the shear is carried by an inclined strut between the load and support. Application of high loads results in a distribution of inclined cracks between the two bearing plates. The inclined cracks may be initiated by early flexural cracks, but are more likely the result of principal tension found perpendicular to the concrete strut. Final failure, as shown in Figure 3-8A, occurs suddenly when the reinforcement crossing the primary crack can no longer equilibrate the tension and the strut splits. The loss of equilibrium due to strut splitting is followed by significant displacements and crushing along the length of the failure crack.

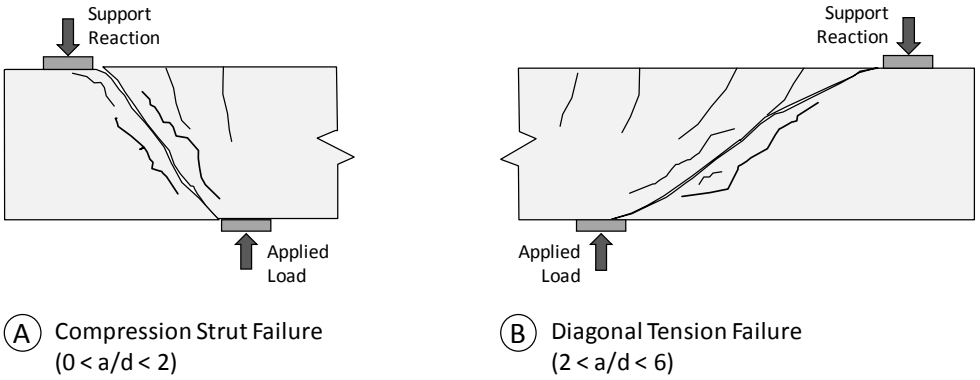

Figure 3-8: Shear Failure Modes (Adapted from ACI-ASCE Committee 426-1973)

For shear spans in excess of two times the effective depth (a > 2d or sectional), the ultimate load behavior tends to be relatively ductile in comparison to the deep beam failure mode described above. A diagonal shear crack typically propagates from the flexural crack located closest to the support. With further loading, the diagonal crack progresses toward the applied load at increasingly shallow inclinations and is eventually arrested by the high stresses at the compression side of the beam. Failure occurs suddenly when very shallow cracks extend to both the support and applied loading points (shown in Figure 3-8B).

3.3.2 Pilot Test

A pilot beam was fabricated using the structural details presented in Sections 3.2.1 and 3.2.2. The beam was cast using conventional ready-mix concrete designed to achieve a compressive strength of 5000 psi within twenty-eight days. Mixture proportions were determined by the supplier, but included the use of the fine and coarse aggregates identified in Table 3-4. Careful attention to such detail ensured the pilot tests would appropriately represent the future series of reactive and non-reactive bent cap specimens. When the compressive strength reached 5060 psi at thirty days, the beam was moved into the Large-Scale Beam Test Facility (Figure 3-9) for shear testing.

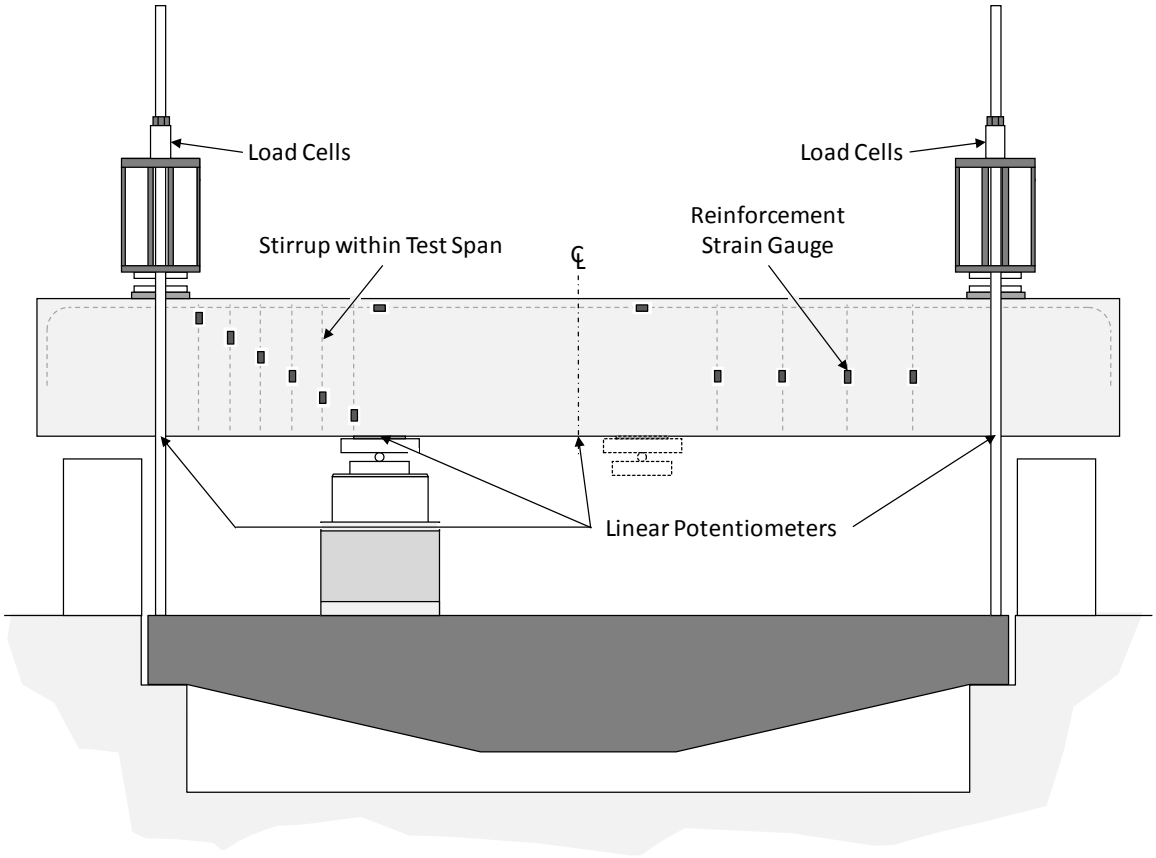

Figure 3-9: Large-Scale Beam Test Facility with Instrumentation Layout for Pilot Test

Static loading of both the deep beam and sectional shear spans was conducted within three days of beam placement in the testing facility. A double-acting hydraulic ram was supported on a strong floor and exerted an upward force at the desired shear span location. Simple supports were provided at the two large steel-plate girders and high strength threaded rods transferred load back to the floor. Displacements were continuously monitored as the load was applied monotonically up to failure. At each load increment, reinforcement strains were measured and the formation of additional cracks was noted. The deep beam shear span was tested and then repaired with external clamps to accommodate the sectional shear test. General descriptions of both tests are provided below. Further detail regarding the structural testing facility and related procedures can be found in Chapter 4.

3.3.2.1 Deep Beam Shear Test

The deep beam shear span was loaded to failure in increments of seventy-five kips (55 kips of applied shear, V) over the course of a few hours. Load cells were located at each reaction point to monitor the total load and shear in each span. All values have been adjusted for the effect of self-weight. The first diagonal cracks formed as extensions of deep flexural cracks at twenty-five to thirty percent of the ultimate shear, V_{test} (as indicated by visual observations and stirrups strains). A single web-shear crack then formed and grew towards the points of load application between forty to eighty percent of V_{test}. At this stage, cracks began to distribute over the width of the compression strut signaling significant distress. The deep beam shear span suddenly failed through splitting of the strut between the inside edges of the support and load bearing plates; a significant drop in load was recorded. Continued load application resulted in significant deflection and crushing along the edges of the splitting crack, but no increase in load resistance.

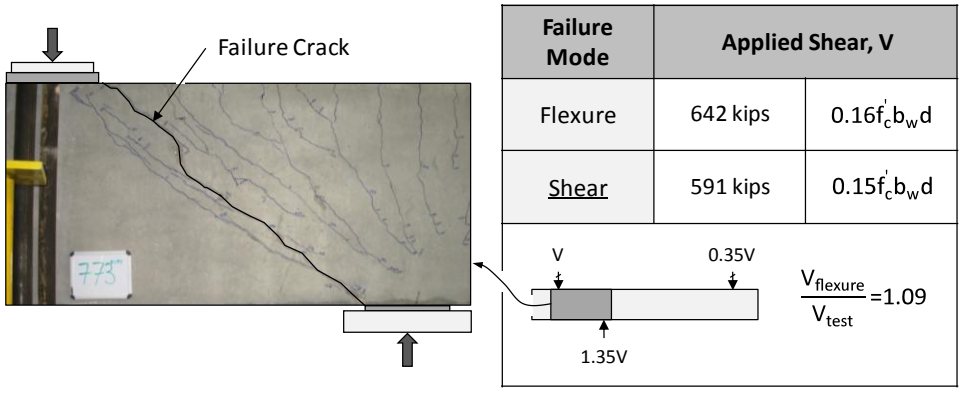

Figure 3-10: Deep Beam Shear Failure (a/d = 1.85)

The pilot test of the deep beam shear span was a satisfactory demonstration of the characteristic behavior described by Ferguson. Although strain gauges indicated yielding of the outermost layer of flexural reinforcement, the beam clearly failed in shear prior to developing the full flexural capacity (see Figure 3-10 for a comparison). Furthermore, no signs of anchorage or bearing distress were observed.

3.3.2.2 Sectional Shear Test

Following the repair of the deep beam shear span, the sectional span was loaded to failure in increments of fifty kips (30 kips of applied shear, V) over the course of a few hours. The initial development of flexural-shear cracking along the length of the span was followed by the formation of a diagonal web-shear crack at about forty percent of the

ultimate shear, V_{test}. All diagonal cracks then continued to grow within several inches of the applied load bearing plate without penetrating the compression zone. At shears in excess of seventy percent of V_{test}, shallow cracks began to extend toward the support reaction. The applied shear dropped rapidly when a crack extending between the inside edges of the bearing plates suddenly grew wider. Attempts to apply additional load were met by increasing deflections and the rapid growth of the failure crack at the compression side of the beam (due to hinging about the inside edge of the support bearing plate).

Sectional shear failure occurred well before the flexural capacity of the section was developed. In fact, strains in the outermost layer of flexural reinforcement failed to exceed the yield point. The margin between the two failure modes is shown below.

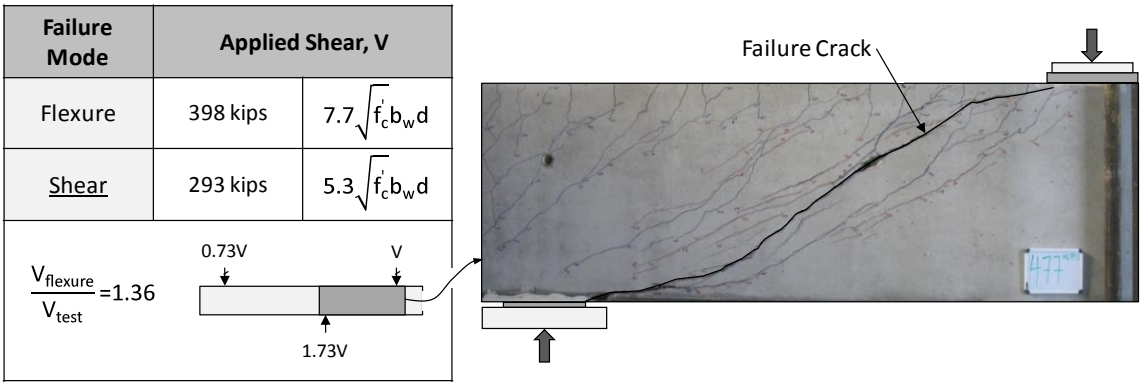

Figure 3-11: Sectional Shear Failure (a/d = 3.00)

The behavior of both shear spans was well within the expectations established prior to the pilot test. As discussed in the following section (3.4), the validated design was used to fabricate all six bent cap specimens. Further discussion of all the structural testing results, including those presented here, are included in Chapter 5.

3.4 FABRICATION OF BENT CAP SPECIMENS

The six large-scale bent cap specimens (four reactive and two non-reactive) were fabricated at Ferguson Structural Engineering Laboratory (FSEL) over a seven month period from June to December of 2007. The scale of the fabrication effort was unprecedented in the realm of ASR/DEF structural testing. Each specimen required over eight cubic yards of laboratory-batched concrete and weighed over twenty-five thousand pounds when completed. An overview of the reactive and non-reactive bent cap specimen fabrication is shown in Figure 3-12, parts (A) and (B) respectively.

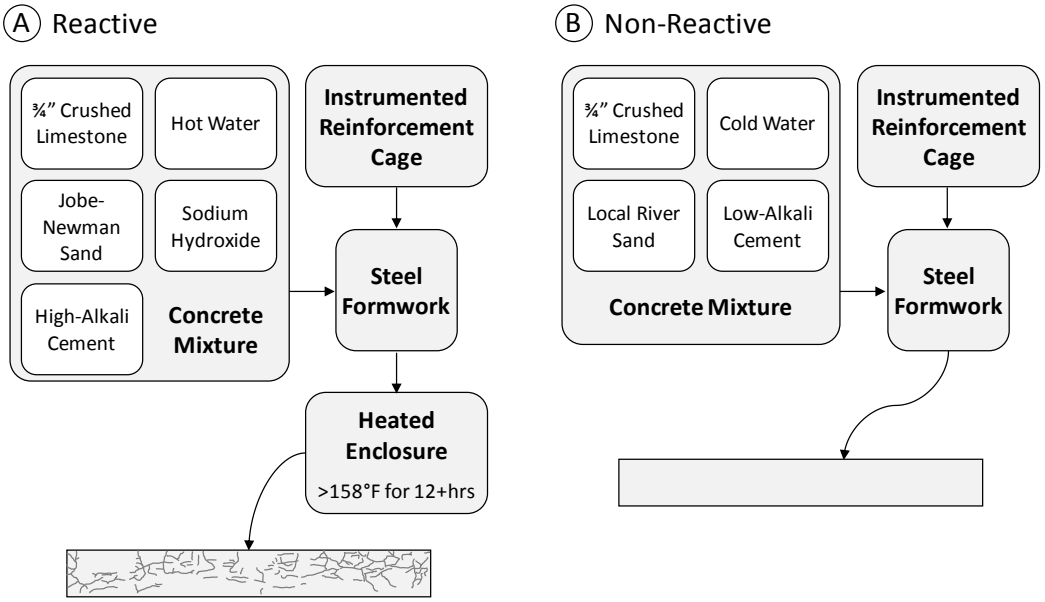

Figure 3-12: Reactive and Non-Reactive Specimen Fabrication

As described in Chapter 4, each completed beam was moved outdoors and placed under conditions favorable to the development of deleterious ASR/DEF expansion. The ultimate success of the conditioning phase (please see Chapter 5) was largely attributable to a number of unique methods implemented during the fabrication process. Following a brief description of the reinforcement cage in Section 3.4.1, techniques used in the production, placement and curing of the non-reactive and reactive concrete mixtures are detailed (Section 3.4.2). A review of the resulting hydration temperature curves then establishes the potential reactivity of each bent cap specimen (Section 3.4.3). Finally, the production of ASR/DEF-susceptible material samples for the long-term evaluation of expansion and strength loss is described in Section 3.4.4.

3.4.1 Reinforcement Cage

Each of the six identical reinforcement cages was fabricated in an inverted orientation within the laboratory. Careful placement of the reinforcement ensured uniformity across the series of bent cap specimens and facilitated the placement of instrumentation. The development and installation of the unique hardware for long-term expansion monitoring is described at length in Chapter 4. When completed, the reinforcement cage was enclosed within steel formwork, as shown in Figure 3-13. Please refer to Figure 3-4 and Figure 3-7 for fully dimensioned reinforcement layouts.

Figure 3-13: Instrumented Reinforcement Cage on Form Soffit

The reinforcement used in the bent cap specimens had a nominal yield strength of 60 ksi and conformed to ASTM A615. Two samples of each bar size (No. 5 and No.11) from all of the specimens were tested in tension (according to ASTM A370 guidelines) using a 600 kip universal testing machine at FSEL. The stress-strain response of each reinforcement sample was recorded via the testing machine load cells and an axial extensometer. The results were very consistent over the series of bent cap specimens; each stress-strain response was virtually identical to that of the paired sample. The yield strain indicated during each test was used in conjunction with experimental strain data (during both the condition and shear testing phases, see Chapter 4) to determine the point at which the transverse and longitudinal reinforcement yielded. A summary of the reinforcement yield strains per specimen is provided in Appendix A.

3.4.2 Concrete Batching and Placement

The success of the current study depended on the production of a highly-expansive ASR/DEF concrete mixture. As described in Section 3.2.3, an extensive trial-batching program was used to establish the necessary mixture proportions and components. However, completion of the trial-batching program was a small step toward large-scale fabrication. Laboratory production of eight cubic yards of reactive concrete was unprecedented. In fact, the logistical challenges of such a task had limited the size of the reactive specimens studied in the past (refer to Chapter 2). The following description of the reactive concrete batching process is the result of considerable troubleshooting conducted over the course of the fabrication period.

Prior to concrete placement, reactive aggregate and cement were obtained from sources located up to 1,400 miles away (Figure 3-14). Eleven ton loads of Jobe-Newman sand were transported from El Paso, Texas to Austin, Texas on at least four occasions. The sand was stockpiled at FSEL under a heavy tarp to limit exposure to the weather and wind-driven debris. Within a few days of each concrete placement, a skid steer loader was used to blend the sand and place it in fifty-five gallon barrels. In addition, ninety-four pound bags of type III cement were shipped via pallet from the Lehigh Cement Company (Evansville Plant) located in Fleetwood, Pennsylvania. Upon arrival, the cement was placed alongside a dehumidifier and covered with plastic sheeting to prevent exposure to moisture.

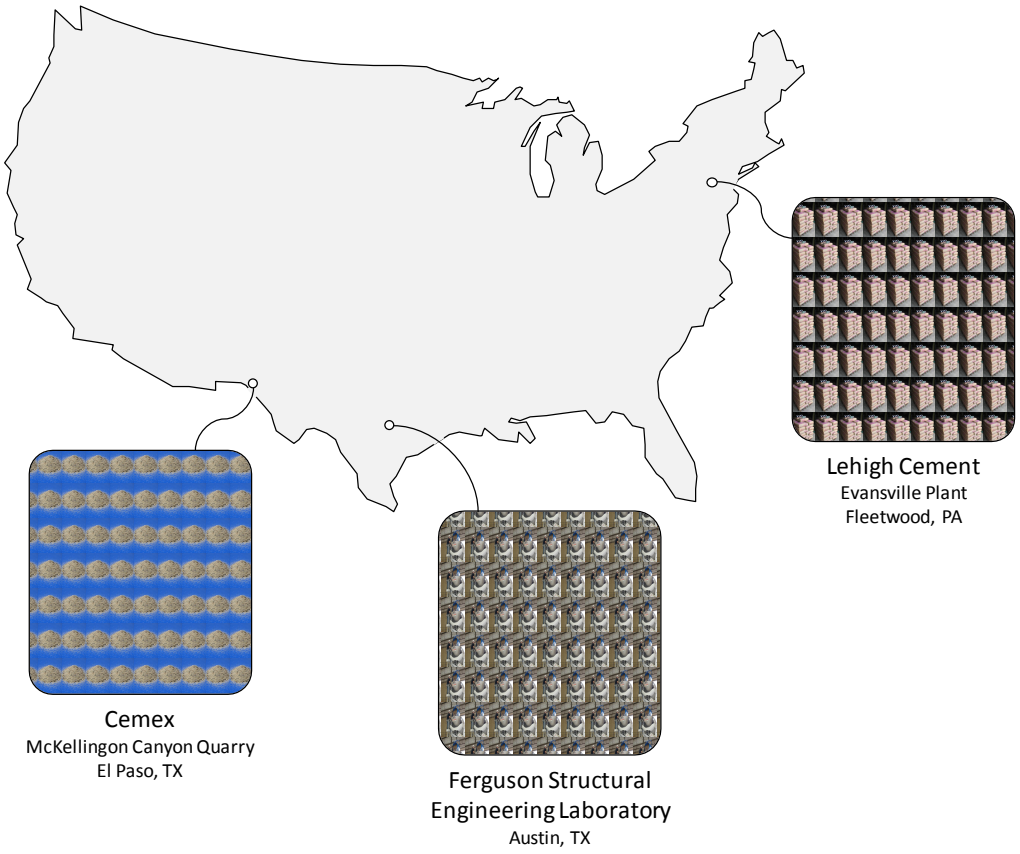

Figure 3-14: Sources of Concrete Materials

An eleven cubic yard concrete mixer truck (supplied by a local ready-mix company) was used to produce the reactive concrete for the bent cap specimens. On the morning of each concrete placement, the truck was charged with the coarse aggregate at the ready-mix

facility. The truck was then driven into the laboratory and an overhead crane allowed the remainder of the materials to be loaded into the concrete mixer. A geared drum turner attached to the crane was used to place the pre-weighed barrels of Jobe-Newman sand in a controlled manner (Figure 3-15A). Samples were taken from several barrels of sand to estimate of the moisture content and allow adjustment of the mixing water. The ready mix supplier did not track the moisture content of the coarse aggregate, so a similar adjustment could not be made for that material. Twelve to fourteen barrels of Jobe-Newman sand were placed into the mixer for each batch of reactive concrete.

Figure 3-15: Concrete Materials Batching
(A) Reactive Sand (B) Sodium Hydroxide (C) High-Alkali Type III Cement (D) Hot Water

Based on the results of cement alkalinity tests conducted at a commercial laboratory (please see Table 3-5 for the results), up to seventeen pounds of sodium hydroxide was diluted in two fifty-five gallon drums of water. The solution was then poured into the concrete mixer; operator safety was addressed through the use of eye protection and a

splash jacket (Figure 3-15B). As hot water was added to the mixture, the high-alkali cement was quickly batched into the ready-mix truck via a one cubic yard concrete bucket (Figure 3-15C). The total water addition was controlled through the use of a volumetric flow-meter plumbed into the hot water outlet. Four eighty-gallon water heaters (specifically installed for the study discussed here) supplied the mixing water at temperature in excess of 120°F (Figure 3-15D).

Following the addition of all the concrete materials, the mixer was turned a minimum of two hundred revolutions to ensure uniformity. The mixture was then checked for consistency and additional revolutions and/or mixing water were added as necessary. Slump of the mixture ranged from eight to eleven inches and was easily placed using conventional and side form vibration as shown in Figure 3-16.

Figure 3-16: Concrete Placement and Form Vibration

The reactive mixture design (as set in Section 3.2.3) is compared to the *as-placed* mixture quantities within Table 3-5. Due to higher than expected cement alkalinity, each mixture

easily met the threshold alkali loading and thereby enhanced the potential for deleterious alkali-silica reactivity. However, errors made during the concrete batching process did lead to small unintended variations between the final concrete mixtures. In particular, an excess amount of coarse aggregate was charged into the concrete mixer for two of the bent cap specimens, R3 and R4. The presence of the aggregate in combination with conservative water addition led to lower slumps and somewhat higher concrete strengths (as discussed in Chapter 5). Nevertheless, the concrete mixtures were still well within conventional proportions and the impact on future structural testing was deemed negligible.

Table 3-5: Reactive Concrete Mixture As-Placed

	Mixture Design	Specimen Mixture As-Placed			
		R1	R2	R3	R4
Type III Cement	700 lb/yd^3	708	711	669	668
Water	400 lb/yd^3	399	394	346	352
Fine Aggregate	1110 lb/yd^3	1178	1182	1112	1110
Coarse Aggregate	1475 lb/yd^3	1479	1485	1704	1693
Sodium Hydroxide	≥ 4.0 lb/yd^3	3.8	3.9	3.6	3.6
Water-to-Cement Ratio	0.57	0.56	0.55	0.52	0.53
Cement Alkali Content	0.9 ± 0.1 %	0.82	0.86	0.92	0.95
Mixture Alkali Content	≥ 1.25 %	1.25	1.28	1.34	1.37

The production of the concrete mixture for the non-reactive bent cap specimens (nR1 and nR2) was analogous to the process discussed above. Crushed limestone and sand were preloaded into the concrete mixer. Cold mixing water and low-alkali cement were batched at the laboratory and the mixer was turned until an adequate consistency was achieved. The non-reactive mixture design is compared to the *as-placed* mixture quantities within the table below.

Table 3-6: Non-Reactive Concrete Mixture As-Placed

	Mixture Design	Specimen Mixture As-Placed	
		nR1	nR2
Type III Cement	700 lb/yd^3	720	717
Water	400 lb/yd^3	361	367
Fine Aggregate	1110 lb/yd^3	1252	1233
Coarse Aggregate	1475 lb/yd^3	1502	1506
Water-to-Cement Ratio	0.57	0.50	0.51

Due to the complexity and scale of the task described above, ready-mix suppliers were reluctant to produce the concrete mixture at their facilities. Many did not have the ability to batch high early strength (type III) concrete and/or were unwilling to stockpile the highly reactive aggregate used within this study. Despite these logistical challenges, over thirty cubic yards of the reactive concrete mixture were successfully produced and placed within Ferguson Structural Engineering Laboratory.

3.4.3 High Temperature Curing

In order to ensure future development of DEF, it was necessary to subject each reactive bent cap specimen to a high temperature curing cycle. Please recall that curing temperatures in excess of 158°F (70°C) are necessary to trigger the deleterious reaction (see Chapter 2 for further information regarding DEF). Concrete durability researchers commonly subject a number of concrete samples to a *curing temperature cycle* in order to determine the mixture's susceptibility to delayed ettringite formation. For example, the Fu Test Method subjects a mortar bar to a temperature of 203°F (95°C) within two hours of initial hydration. The temperature is then held for a minimum of twelve hours in an attempt to "mimic the typical precast concrete curing regime" (Folliard 2006). Subsequent length expansion of the mortar bar is recorded and analyzed to determine the onset and progression of the deterioration. While the large mass of each bent cap specimen would generate a substantial amount of heat, it would not be sufficient to sustain temperatures in excess of 158°F for an extended period of time. As described below and shown in Figure 3-17, a make-shift *oven* provided the additional heat necessary to sustain temperatures in excess of 158°F for a minimum of ten hours.

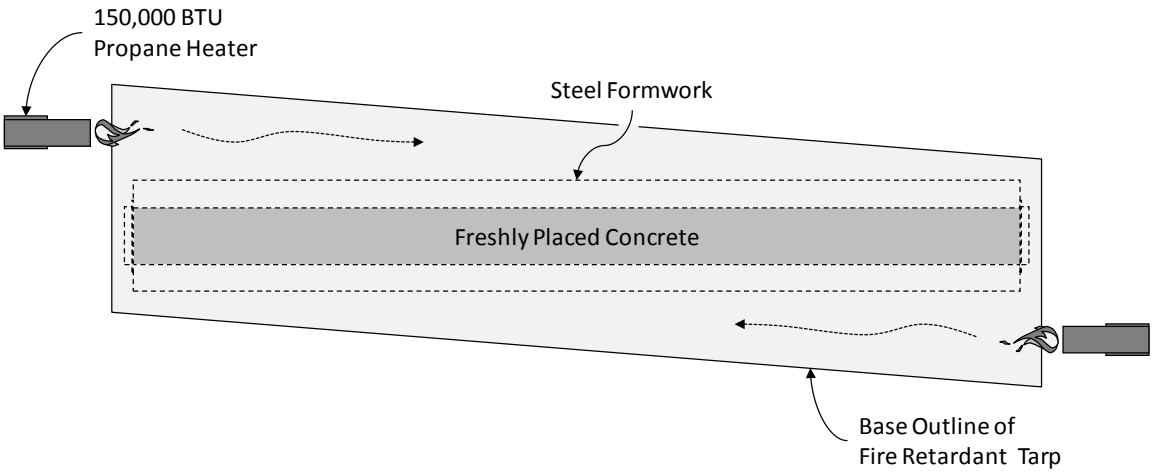

Figure 3-17: Plan View of High Temperature Curing Setup

When the finishing operations were complete, plastic sheeting was applied directly to the top surface of the beam to prevent the formation of plastic shrinkage cracks. A heavy fire retardant tarp was then used to enclose the entire length of the steel formwork (Figure 3-18B). Two portable propane heaters were positioned at opposite corners (Figure 3-18A) and adjusted to promote a circulatory current within the tarp *oven*. Temperatures at the nozzle of each propane heater easily exceeded 300°F when measured by infrared thermometer. Supplemental heat was applied for the duration of the ten hour curing period and occasionally longer. Shortly after the heaters ran out of fuel, ends of the tarp were sealed to eliminate rapid cooling of the specimen.

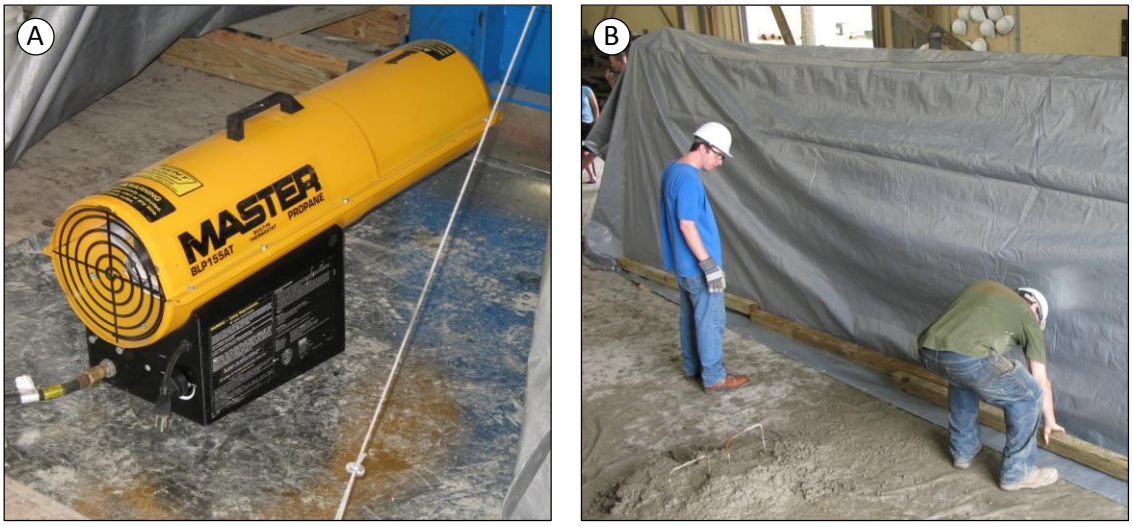

Figure 3-18: High Temperature Curing Setup (A) Propane Heater (B) Heavy Tarp

It is important to note that only the reactive specimens were subjected to high temperature curing. In fact, non-reactive specimens cured without cover and were cooled by large industrial fans to ensure that hydration temperatures did not exceed the DEF threshold. To definitively establish the potential for DEF in each of the bent cap specimens, several thermocouples were embedded within each specimen (Figure 3-19).

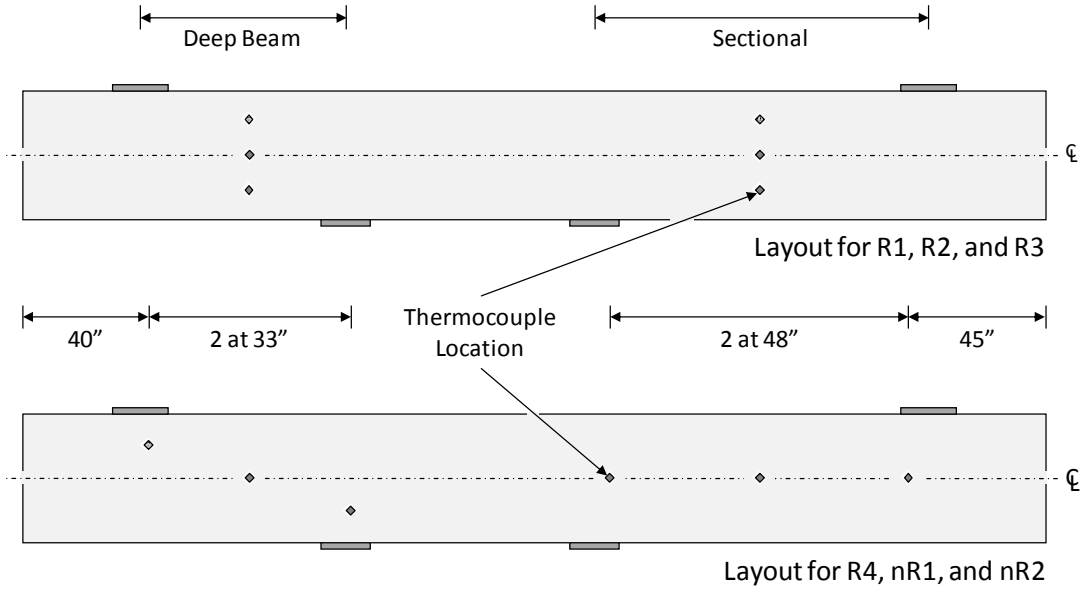

Figure 3-19: Thermocouple Layout

The two thermocouple arrangements shown in Figure 3-19 were used to establish the magnitude as well as variation of hydration temperatures over the depth and length of the bent cap specimens. The thermocouples were continuously monitored (see Section 3.4.4.1 for detail) for the duration of the curing period and were only disconnected when the beam had sufficiently cooled (to about 100°F). At this point the steel side forms and bulkheads were removed without fear of thermal shock and cracking. Select temperature hydration curves for both reactive and non-reactive specimens are shown on the following two pages and discussed below.

The typical hydration temperature curve for a reactive specimen (R3) can be found in Figure 3-20A. Shortly after mixing was completed (here defined as the initial hydration point) and the concrete was placed within the formwork, hydration temperatures began to rise rapidly. Within four to six hours, the temperature in each reactive beam exceeded the DEF threshold of 158°F. Peak temperatures were achieved about twelve hours after initial hydration and the beam began to slowly cool over a period of up to three days. As

indicated by the overall minimum and maximum curves, temperature variation through the length (between the deep beam and sectional shear spans) and through the depth was under 10°F at any point in time. Corresponding potential for DEF was therefore uniform over the volume of concrete.

The results for all of the reactive specimens are compared within Figure 3-21A. Heat provided by ongoing cement hydration and the propane heaters maintained temperatures in excess of 158°F for a minimum of ten hours and a maximum of twenty-seven hours. Corresponding peak hydration temperatures ranged from 163°F to 192°F. The duration and magnitude of the curing temperatures was known to have a significant effect on the ultimate expansion potential of the concrete (Folliard 2006). A preliminary review of the fabrication results presented here suggested that specimen R1 would exhibit the least deterioration in the future (R3 would therefore exhibit the most). Expansion monitoring results are compared within Chapter 5.

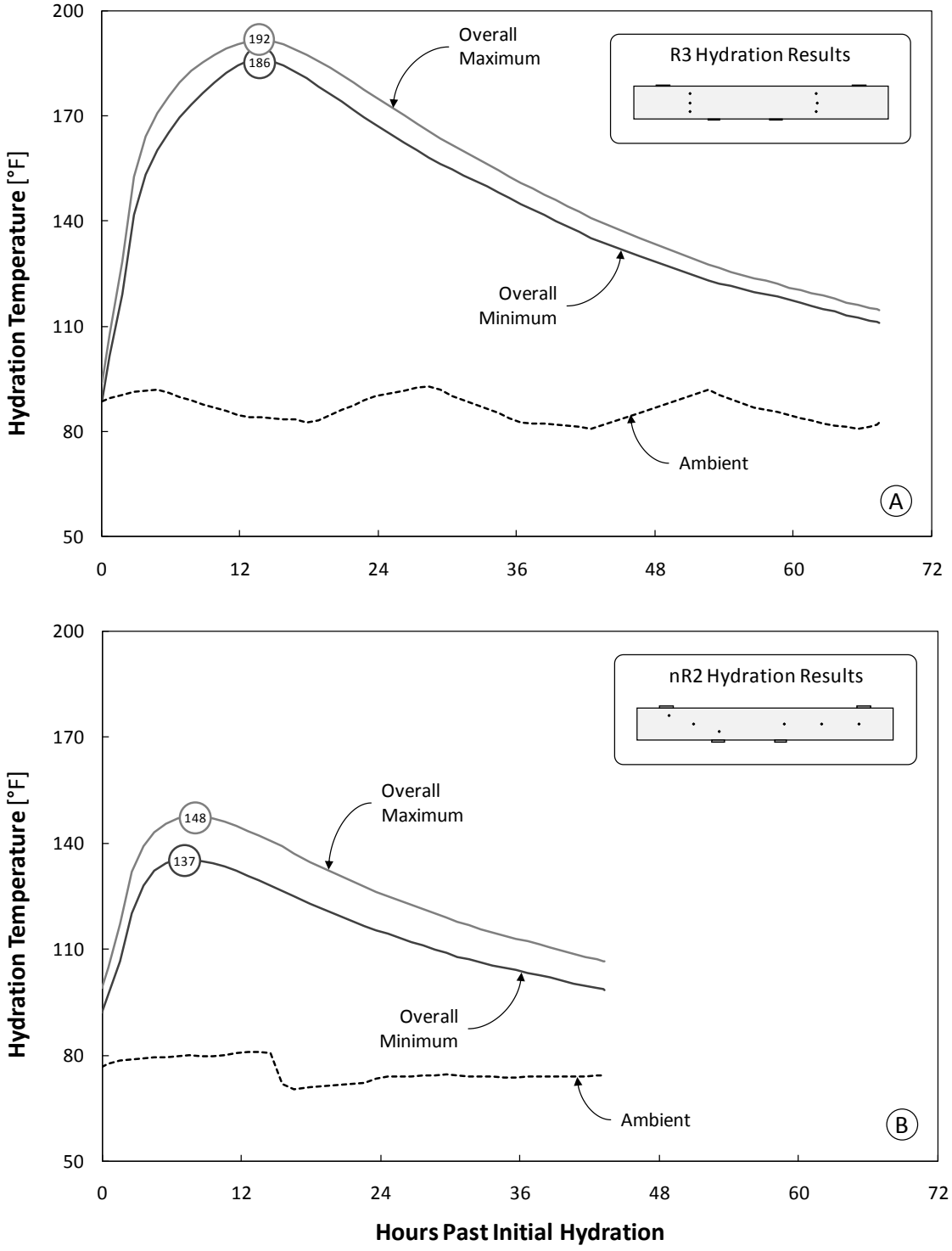

Figure 3-20: Typical Hydration Temperature Curves (A) Reactive (B) Non-Reactive

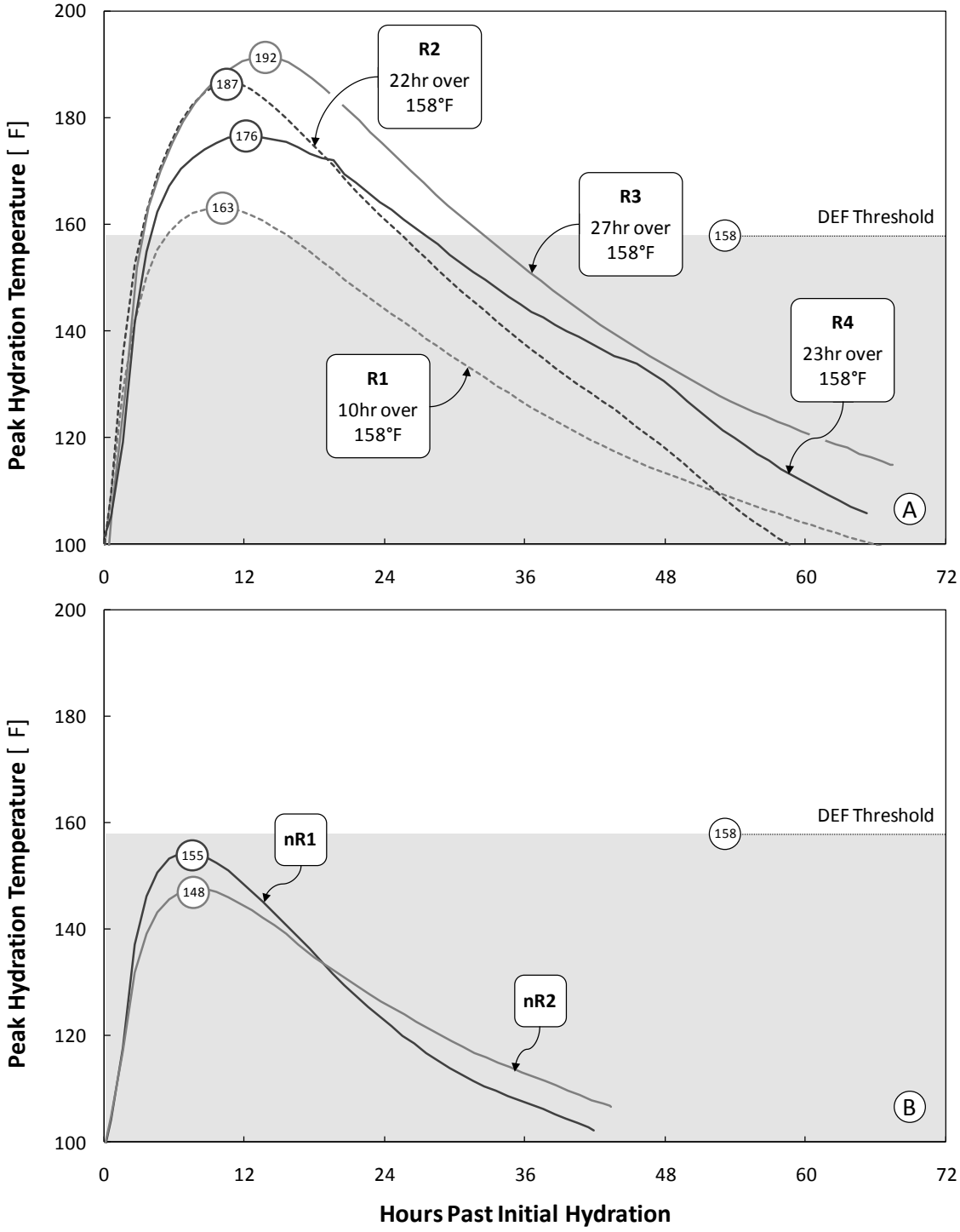

Figure 3-21: Peak Hydration Temperature Curves (A) Reactive (B) Non-Reactive

Hydration temperatures for both non-reactive specimens are summarized within Figure 3-20B and Figure 3-21B. Peak temperatures were successfully held below the DEF threshold in both cases. Temperature variation through the specimen depth and length were slightly higher, but did not bear any consequence on the long-term durability of the specimen. Above all, the non-reactive hydration temperature curves demonstrate the need for external heating methods in the production of reactive specimens.

Examination of the temperature hydration curves provided excellent insight into the potential for and variation of damage due to delayed ettringite formation. However, long-term impacts of the deterioration due to ASR and DEF would be quantified through the use of expansion monitoring techniques (as discussed in Chapter 4) and standard materials tests.

3.4.4 Concrete Material Testing

A poor correlation between concrete material tests and structural performance was identified in the literature reviewed within Chapter 2. To further evaluate this conclusion a series of concrete samples were produced alongside each bent cap specimen. Every opportunity was taken to ensure the potential for ASR/DEF was consistent between the specimen and each paired sample (while following the relevant ASTM guidelines). When subjected to similar conditioning environments, the specimen and samples would develop similar deterioration and therefore allow valid comparisons to be made. Unique measures taken during the fabrication of standard concrete cylinders (for strength development) and plain concrete prisms (for free expansion measurement) are discussed below. The same procedures were used for both reactive and non-reactive samples.

3.4.4.1 Cylinders for Long-Term Strength Assessment

Standard concrete cylinders (4” diameter) were fabricated according to ASTM C192. To ensure the cylinder strength accurately represented the curing conditions and future deterioration found within each bent cap specimen, temperature match curing technology was used.

Temperature match curing was originally developed for the precast concrete industry. It is based upon the simple observation that the maturity (and strength) of a concrete element is controlled by the temperature history. The mass of an individual cylinder is incomparable to that of a precast concrete member and will therefore fail to generate the heat and temperatures necessary to mature at the same rate. The resulting cylinder

strength will be unrepresentative of the precast concrete member. To obtain consistent maturity and strength, temperature match curing techniques use external sources of heat (i.e. generated by the mass concrete placement or an electrical source) to match the cylinder temperature to that of the precast member. When implemented during the current study, temperature match curing provided an additional benefit: cylinders simultaneously cast with each specimen possessed nearly identical expansion characteristics.

Figure 3-22: FSEL Sure Cure System – Controller and Molds

An in-house temperature match curing system (*Sure Cure*) was used to fabricate all of the cylinders in this study (Figure 3-22). The six thermocouples identified in the previous section (3.4.3) were connected to a wireless transmitter as shown in Figure 3-23. At six minute intervals, temperatures were relayed to a wireless receiver located at the opposite end of the laboratory. The match cure controller than conducted a comparison between the specimen and cylinder temperatures; electrical output to the heated mold was then adjusted as necessary. A time-temperature history was also logged by the match cure system and used to produce the hydration temperature curves discussed above.

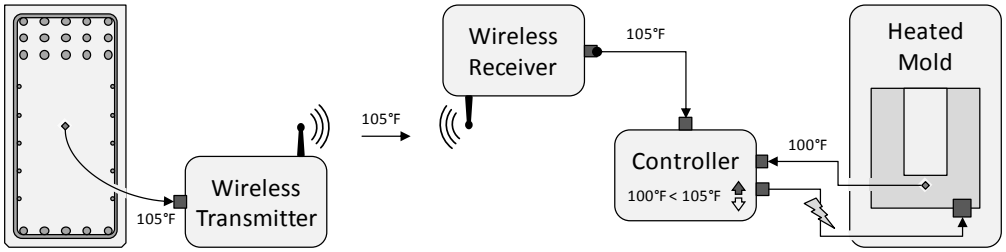

Figure 3-23: Wireless Match Cure System

A total of thirty to forty-eight match cured cylinders were fabricated with each bent cap specimen. In preparation for potentially high temperature variation over the beam length, each shear span was paired with a representative set of match cured cylinders. Half of the cylinder molds were controlled by the temperature at the center of the deep beam shear span. The remaining cylinder molds were controlled by the sectional shear span temperature as shown in Figure 3-24. Match curing did not end until the thermocouples were disconnected for side form removal; only after the specimen had sufficiently cooled. Cylinders were then unmolded and exposed to the same conditioning regimen experienced by the bent cap specimens (Chapter 4).

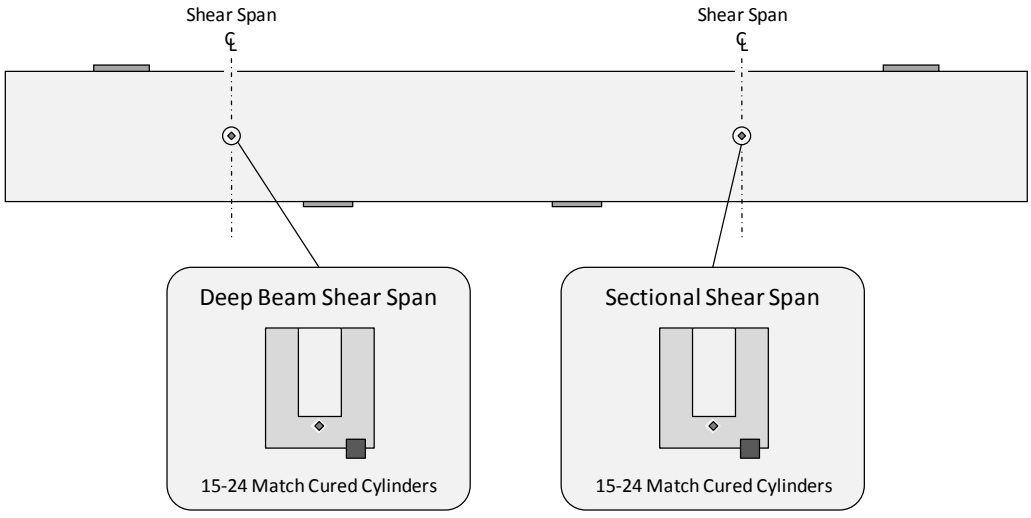

Figure 3-24: Match Cured Cylinders for Each Shear Span

Periodically a number of match cured cylinders from each shear span were subjected to compression (ASTM C39) and/or splitting tensile tests (ASTM C496). Results are discussed within Chapter 5.

3.4.4.2 Prisms for Free Expansion Potential

The bent cap specimens were each paired with four plain concrete prisms (3" x 3" x 11¼"). Each prism was individually cast at various stages of the beam placement to ensure that any variability of the mixture would be represented within the set. In contrast to the concrete cylinders, no special considerations were made for the effects of hydration temperatures. All of the concrete prisms produced within this study conformed to ASTM C157 and were tested according to ASTM C1293, "Test Method for Concrete Aggregates by Determination of Length Change of Concrete Due to Alkali-Silica Reaction."

ASTM C1293 is intended to evaluate the potential of a concrete mixture to expand deleteriously through alkali-silica reactivity. Concrete prisms containing potentially expansive coarse or fine aggregates are subjected to controlled laboratory curing conditions. Following twenty-four hours of in a moist room, each prism is measured and then placed within a sealed storage container above water (Figure 3-25A). The container of prisms is stored within an environmental chamber calibrated to 100°F (38°C). Subsequent length change of each prism is periodically measured with a comparator (Figure 3-25B) over a period of one to two years. Pre-established criteria are then used to determine the severity of the resulting expansions. If the average expansion of the prisms exceeds 0.04 percent in one year, the concrete mixture (and constituent aggregate) will be classified as deleteriously reactive.

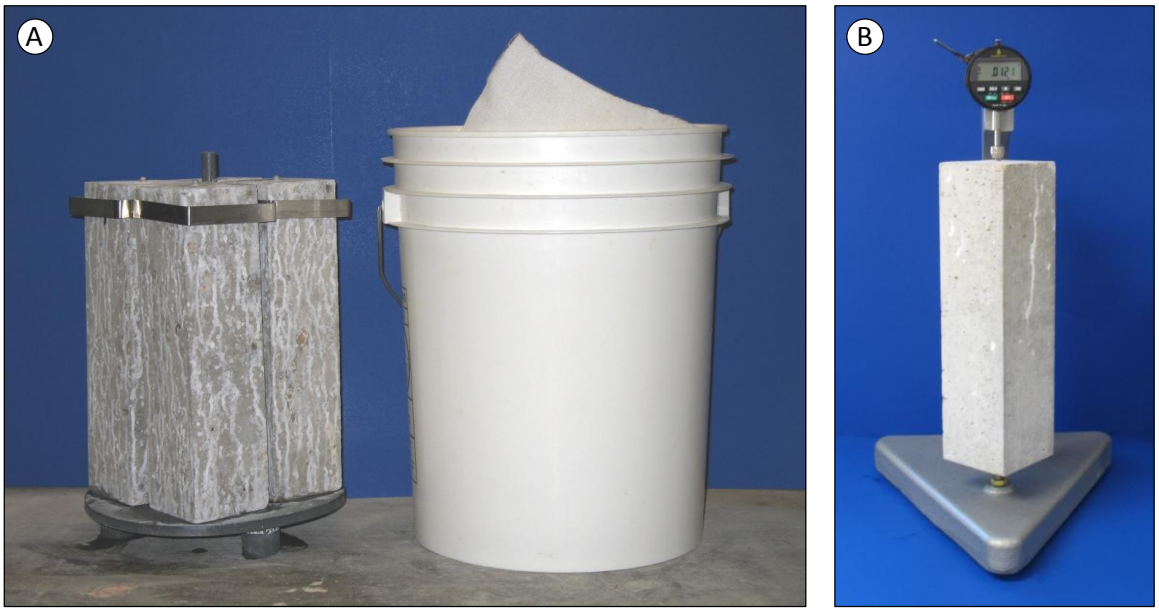

Figure 3-25: Free Expansion Potential (A) Elevated Prisms Set in Felt-Lined Bucket (B) Periodic Measurement of Length Change with Digital Comparator

The concrete durability research community has commonly accepted ASTM C1293 to be the best predictor of field performance. In fact, the expansion limit of 0.04 percent was selected due to good correlation with "cracking of test prisms, as well as field structures suffering from ASR" (Folliard 2006). The method has been recently adopted by the Texas Department of Transportation for the testing of aggregates statewide. However, doubt has been cast on the method due to a number of discrepancies between the curing regimen used within ASTM C1293 and conditions commonly found in the field. In particular, no consideration is made for high initial curing temperatures that may accelerate the process of ASR and potentially trigger DEF. As a result, it is unclear whether or not the test is truly representative of the damaged in-service structures. Further evaluation of the method within the context of the current study was therefore desirable.

Additional methods of expansion testing will be reviewed in Chapter 4 and compared to ASTM C1293 within Chapter 5. Expansion histories of all the prisms may be found within Appendix A.

3.5 SUMMARY

The design and production of the near full-scale bent cap specimens was unprecedented in the realm of ASR/DEF testing. Six shear-critical bent cap specimens, weighing nearly thirteen tons each, were produced over the course of a seven month period. Each completed beam was moved outdoors and placed under conditions favorable to the development of realistic ASR and DEF damage. Subsequent expansion monitoring and shear testing of each specimen (presented within Chapters 4 and 5) form the basis for the recommendations made at the end of this report.

Structural design of the bent cap specimen was conducted with one goal in mind: to subject the most vulnerable shear details found in practice to severe ASR/DEF deterioration. To begin, the geometry of the bent cap specimen was maximized to accurately model the effects of premature concrete deterioration. The resulting cross-section was of nearly the same scale as the commonly affected bent caps and of sufficient size to be classified as one of the largest beams ever tested in shear. The clear span of the specimen was sufficiently long for the inclusion of two independent tests: one deep beam ($a/d = 1.85$) and one sectional ($a/d = 3$) shear test at opposite ends of the beam. As a result, a total of twelve test regions were accommodated within the six specimens produced for the testing program. Lower bound shear failure of each test region was guaranteed by a substantial amount of longitudinal reinforcement and the minimum

allowable quantity of transverse reinforcement. All reinforcement was detailed according to the AASHTO LRFD Bridge Design Specifications – Interim 2007.

To complement the lower bound philosophy of the structural design, the concrete mixture was adjusted to provide the maximum amount of expansion within the time constraints of the study. With respect to ASR-related deterioration, the well-recognized destructive effect of highly reactive sand from El Paso, Texas was augmented through the addition of high-alkali cement and sodium hydroxide. Although not explicitly addressed within the composition of the concrete mixture, DEF was triggered by the use of high temperature curing. Ultimate expansions of similar mixtures had exceeded one percent of expansion within three years of outdoor exposure. The selected mixture proportions also delivered strength gains consistent with in-service structures.

Prior to full-scale production of the six bent cap specimens, the final design was validated via a pilot test. The pilot beam was fabricated using the selected reinforcement details and conventional ready-mix concrete. Behavior of both the sectional and deep beam shear spans was well within the expectations established by prior shear researchers. No flexural failures were observed and the design was classified as shear-critical.

Fabrication of the six large-scale bent cap specimens concluded in December of 2007. All aspects of the specimen production, including concrete batching and placement, were handled by the researchers, technicians and students at Ferguson Structural Engineering Laboratory. The reactive concrete mixture was assembled from a number of unique components. To ensure alkali silica reactivity, Jobe-Newman Sand and Lehigh Cement were transported significant distances (up to 1, 400 miles) prior to the concrete placement. While hot mixing water and the Type III cement boosted early hydration temperatures, portable propane heaters provided the additional energy needed to raise temperatures above 158° F for several hours. Time-temperature histories, as recorded by several thermocouples embedded throughout the specimen, were used to provide a preliminary indication of the DEF expansion potential. All of the reactive specimens met pre-established requirements and substantial expansion was expected.

Fabrication and testing of complementary concrete material samples was outlined. Periodic testing of match-cured cylinders and the measurement of standard prisms would reveal the time-dependent progress of the ASR/DEF deterioration within each specimen.

CHAPTER 4
Experimental Program

4.1 OVERVIEW

In-house fabrication of the near full-scale bent caps (described in Chapter 3) presented the unique opportunity to thoroughly document the time-dependent effects of ASR/DEF on both service load and ultimate strength behavior. The experimental work was divided into a three-phase study, outlined in Figure 4-1 and detailed below. The results from each phase (presented in Chapter 5) provided much needed insight into the performance and evaluation of ASR/DEF damaged bent structures.

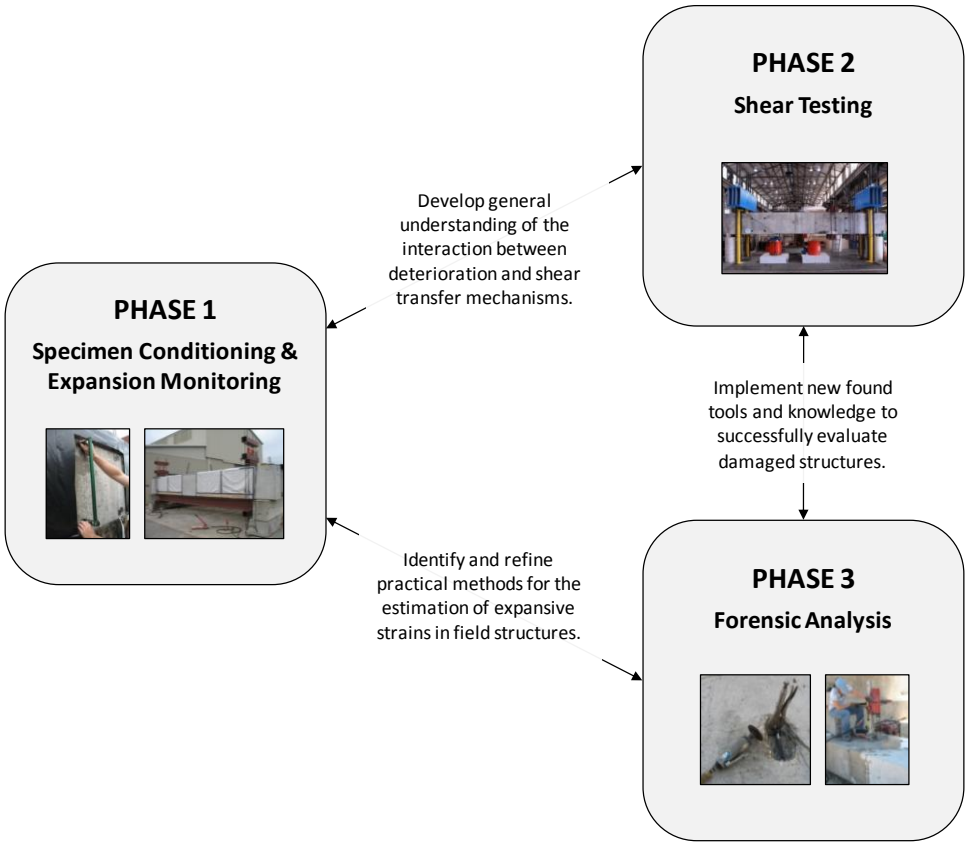

Figure 4-1: Three-Phase Experimental Program

Following fabrication, all six of the bent cap specimens were moved to an exposure site outside of Ferguson Structural Engineering Laboratory. At this point, the experimental study formally commenced. Phase I (*Specimen Conditioning and Expansion Monitoring*) details efforts to trigger field representative ASR/DEF deterioration and monitor subsequent expansions (Section 4.2). Particular emphasis is placed on the long-term instrumentation due to the critical nature of the expansion data. Phase II (*Shear Testing*) features the unique facilities and methods used to test three of the six large-scale bent caps (Section 4.3). Well-defined boundary conditions and carefully placed instrumentation allowed each test to be characterized. Phase III (*Forensic Analysis*) is an examination of structural evaluation techniques, reported within the literature and/or commonly recommended in assessment guidelines. The techniques described within Section 4.4 were collectively selected to determine the cause, extent, and future potential of the expansive mechanisms.

4.2 PHASE I: SPECIMEN CONDITIONING & EXPANSION MONITORING

The reactive specimens were primed for rapid deterioration: each batch of highly reactive concrete (basis for ASR) had been subjected to extraordinarily high curing temperatures (DEF). Shortly after fabrication, a conditioning program was developed to exploit the large expansion potential of each bent cap. The growth of realistic ASR/DEF damage depended on a number of external (climate, exposure conditions, and structural boundaries) and internal factors (reinforcement configuration, see Chapter 3). Deliberate consideration of these factors led to the rapid development of the most severe, yet field-representative, premature concrete deterioration.

Prolonged exposure to heat and moisture was critical to the progression of the ASR/DEF deterioration. Each bent cap was moved outside Ferguson Structural Engineering Laboratory (FSEL) to maximize exposure to Austin's mild climate (Section 4.2.1). To keep the reactive concrete moist, a timed watering system subjected the specimens to frequent wet-dry cycles (Section 4.2.2). Application of a constant-magnitude service load then provided an appropriate structural context for the deterioration (Section 4.2.3). Subsequent concrete expansions and steel strains were measured by using a well-crafted, robust set of instrumentation (Section 4.2.4). Please note that the following discussion applies to all of the specimens, reactive and non-reactive. Every shear span (including the non-reactive pairs) was subjected to the same conditioning and monitoring routines, thereby enabling the valid comparison of results.

4.2.1 Exposure Site

Shortly after removal of the formwork, each beam was moved outside. A fifteen-ton forklift and set of rollers were used to maneuver the near full-scale specimens out of the laboratory doors. Careful planning and extreme care minimized spalling and cracks due to transport. The test regions did not incur any damage. Concrete dunnage placed at the north end of the laboratory supported the beams and all future conditioning operations (see Figure 4-2). It is worth noting that the Concrete Durability Center (UT Austin) has conducted a large number of long-term ASR/DEF studies at their own outdoor exposure site, located less than two hundred feet from Ferguson Structural Engineering Laboratory.

Figure 4-2: Exposure Site at Ferguson Structural Engineering Laboratory

It was recognized that the rate and severity of ASR/DEF deterioration would ultimately depend on a number of local environmental factors (especially exposure to heat and moisture). Variation in temperature directly impacts the rate at which alkali-silica gel is formed. Higher temperatures generally result in more rapid formation of the gel. Researchers commonly exploit this characteristic when testing samples for ASR-susceptibility; sustained conditioning temperatures at or above 100°F are typical.

Expansive pressures subsequently developed by the growth of gel (ASR) and ettringite crystals (DEF) are controlled by the availability of moisture. Internal relative humidity in excess of eighty percent will generally sustain ASR expansion. Although the interior portions of a large concrete element generally contain sufficient moisture, long periods of severe drying may ultimately slow the deterioration (Stark 2006). The influence of these particular factors on the long-term performance of the ASR/DEF specimens was evaluated through a brief review of the local climate conditions.

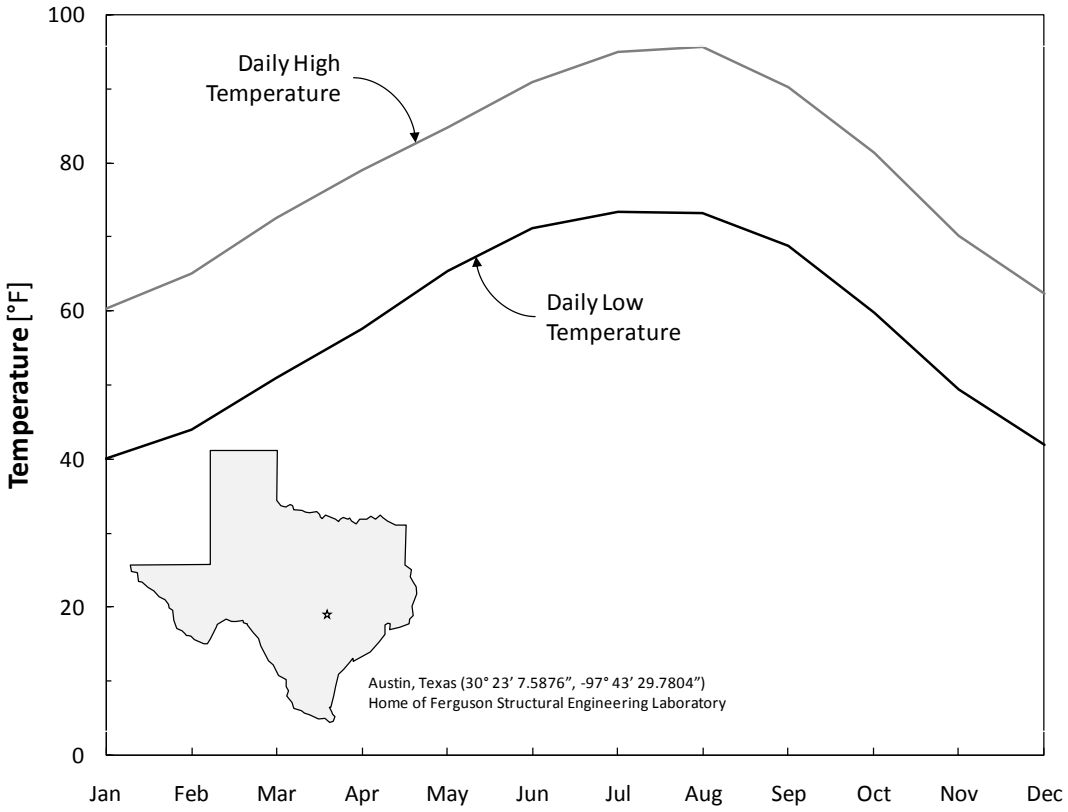

Figure 4-3: Average Monthly Temperatures in Austin, Texas (NOAA 2009)

Austin, Texas has a *subtropical subhumid* climate that is noted for hot summers and dry winters (Larkin and Bomar 1983). Although the average high temperature is 79°F, it is not uncommon to see temperatures exceed 100°F during the summer months. A thirty-year average of the monthly temperatures is plotted in Figure 4-3. Eighty days (again, on average) of the year are subject to some form of precipitation, amounting to an annual rainfall of about thirty-four inches. Relative humidity ranges between fifty-eight and eighty-six percent over the course of the year. Context for this discussion is provided

through a comparison between the climates of Austin and Houston, Texas (identified earlier as the nucleus of the ASR/DEF outbreak within the state) in Table 4-1.

Table 4-1: Annual Weather Conditions in Austin and Houston, Texas (NOAA 2009)

	Austin, Texas	Houston, Texas
Temperature	High: 96°F Low: 40°F	High: 94°F Low: 41°F
Relative Humidity	High: 86% Low: 58%	High: 91% Low: 65%
Days of Precipitation	78 days	100 days
Annual Rainfall	34 inches	48 inches

Houston is located on the Gulf Coast of Texas, nearly two hundred miles east of Austin. The climate is categorized as *subtropical humid* and is most noted for warm summers (Larkin and Bomar 1983). As reflected in the climatic label change, the relative humidity within Houston is five to seven percentage points higher than that within Austin. The additional moisture in Houston's atmosphere may be attributed to damp ocean winds and an additional fourteen inches of rainfall each year.

Based on the results, the most active periods of expansion were expected to occur during the warm summer months. Simple measures were taken to maximize the natural heat gain during daylight hours. Each specimen was wrapped in black plastic and all sources of shade/cover were eliminated. No attempts were made to provide artificial heat. Local temperature variation would be comparable to that found in the field. Natural sources of moisture, on the other hand, could not be relied upon. The average annual rainfall gives no indication of the potential for drought. At the time of this study, Texas was experiencing abnormally dry conditions with rainfall totals well below normal levels. A watering system (described below) provided the moisture necessary to sustain continuous expansion.

4.2.2 Moisture Conditioning

Expansion and cracking due to ASR/DEF is generally most severe in structures exposed to a renewable source of moisture. It is not uncommon to see heavy deterioration on a substructure element located directly below an open expansion joint or supporting a drainage pipe (see Figure 4-4 for examples from the Houston area). One poor (and unfortunately common) detail was used in the construction of the US 59 and I-10

interchange substructures (introduced in Chapter 1 and closely examined in Chapter 6). The drainage piping was concealed within the concrete caps and columns of all the bents. While more aesthetically pleasing, poorly maintained interior drains frequently clog, leading to backup of rainwater within the concrete section. The interior drain then effectively becomes a well from which the expansive processes of ASR and DEF can draw an unlimited supply of water.

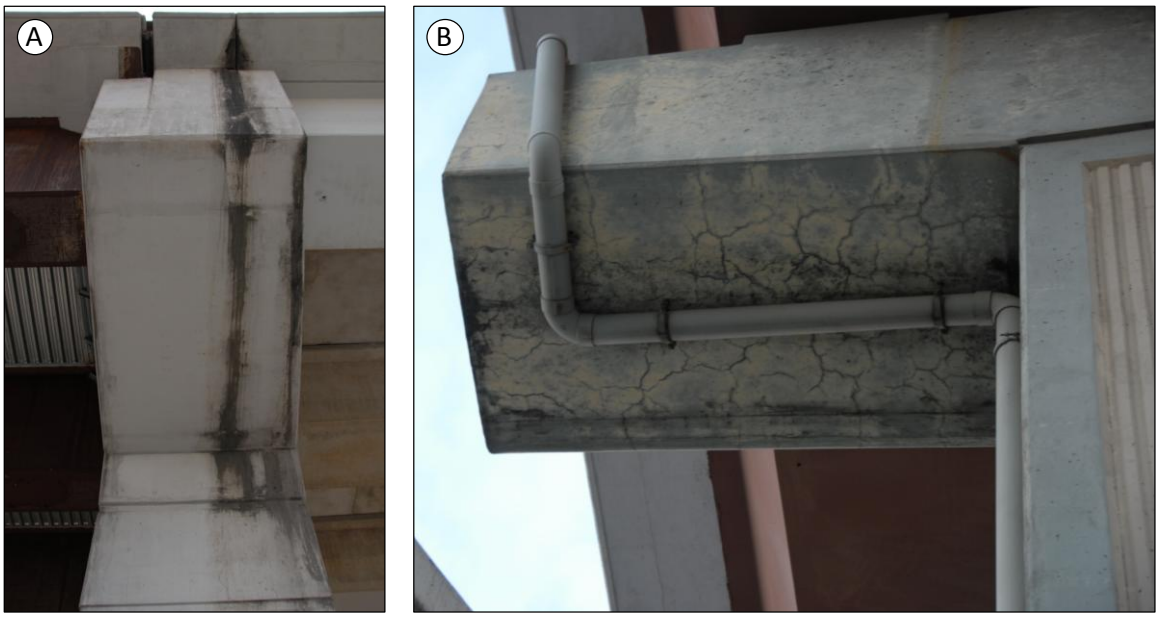

Figure 4-4: Sources of Renewable Moisture (A) Expansion Joint (B) Drainage Pipe

To replicate the severe conditions described above, a watering system was installed at the exposure site. Three irrigation lines ran the length of each beam. Regularly spaced emitters ensured even water coverage over the top and sides of each shear span (see Figure 4-5). Moisture conditioning of the end regions was not necessary and the irrigation lines were therefore terminated to maximize efficiency. Poly-coated burlap was eventually applied to trap water at the end of each cycle; rapid drying of the specimen was thereby limited.

Figure 4-5: Demonstration of Watering System

Each specimen was plumbed in a parallel system with two companions. As a result, two individual watering zones were formed. The first zone contained specimens selected for short-term conditioning (R1, R2 and nR1), while the second zone contained those intended for further long-term study (R3, R4 and nR2); please see Section 4.3 for further explanation. Each zone was controlled by a commercial timer and sprinkler valve. Watering cycles were programmed to occur after dusk at an interval of twelve minutes. To maintain adequate pressure, the supply of water was diverted to one individual zone at any given time. A schematic of the completed watering system is shown in Figure 4-6. All of the plumbing fixtures used within the system were obtained from a local supplier of landscape irrigation products.

Figure 4-6: Alternating Two-Zone Watering System

The moisture conditioning techniques used within this study were quite different from those encountered during the literature review. Small-scale specimens were frequently submerged in hot water baths charged with alkali salts. The technique successfully accelerated the conditioning process, but was extraordinarily aggressive and unrepresentative of field deterioration processes. Efforts to accelerate the deterioration process within the current study were tamed by a desire to maintain field representation. External watering of the specimens was not unlike the field exposure conditions described above.

4.2.3 Load Conditioning

The influence of compressive stress on the directionality of ASR/DEF expansion and cracking was explored in Chapter 3. Although the discussion was limited to internal restraints (i.e. reinforcement), the same concepts are valid for externally applied loads. Compressive stresses developed as a result of load application may force expansion to occur in a less-restrained direction. When the influence of reinforcement is temporarily disregarded, it is conceivable that heavy shear could lead to the development of diagonal cracks between the load and support (parallel to the direction of principal compression). Nevertheless, application of a service level load was not expected to substantially alter the anisotropic, predominantly transverse nature of the deterioration (refer to Chapter 3 for details). Load conditioning was conducted as part of the broad effort to maintain field representation in all aspects of the testing program.

Transient live loads would not have an effect on the long-term development of ASR/DEF deterioration. Consequently, the magnitude of the conditioning load was to be determined by service checks relating to the application of dead load only. Bent cap design guidelines presented within the 2006 *TxDOT LRFD Bridge Design Manual* were reviewed for applicable provisions. To minimize flexural cracking, the performance criteria for reinforced concrete bent caps included a 22 ksi limit on the reinforcement stress under dead load. The stress limit ultimately controlled the design of the load conditioning program.

Due to the high longitudinal reinforcement ratio ($\rho = 3.1\%$) of the ASR/DEF specimen, a disproportionate amount of force would be required to produce 22 ksi of stress in the outermost layer of reinforcement. At the stress limit, a typical field structure (conservatively reinforced with $\rho = 1.3\%$) would be subjected to less than fifty percent of the shear required for the current specimen. To ensure that the conditioning load was equivalent to dead load forces found in the field, the reinforcement stress requirement was factored. A ratio of 1.3 : 3.1 ($\rho_{specimen} : \rho_{typical}$) produced an effective stress limit of about 9 ksi. The targeted twenty-eight day concrete strength of 5 ksi was then used to calculate the necessary moment and shear for each test region. The respective shear stress levels were fourteen and eighteen percent of the deep beam and sectional capacities measured during the pilot tests (see Chapter 3, Section 3). The desired superimposed shear force diagram is shown alongside the conditioning load setup in Figure 4-7.

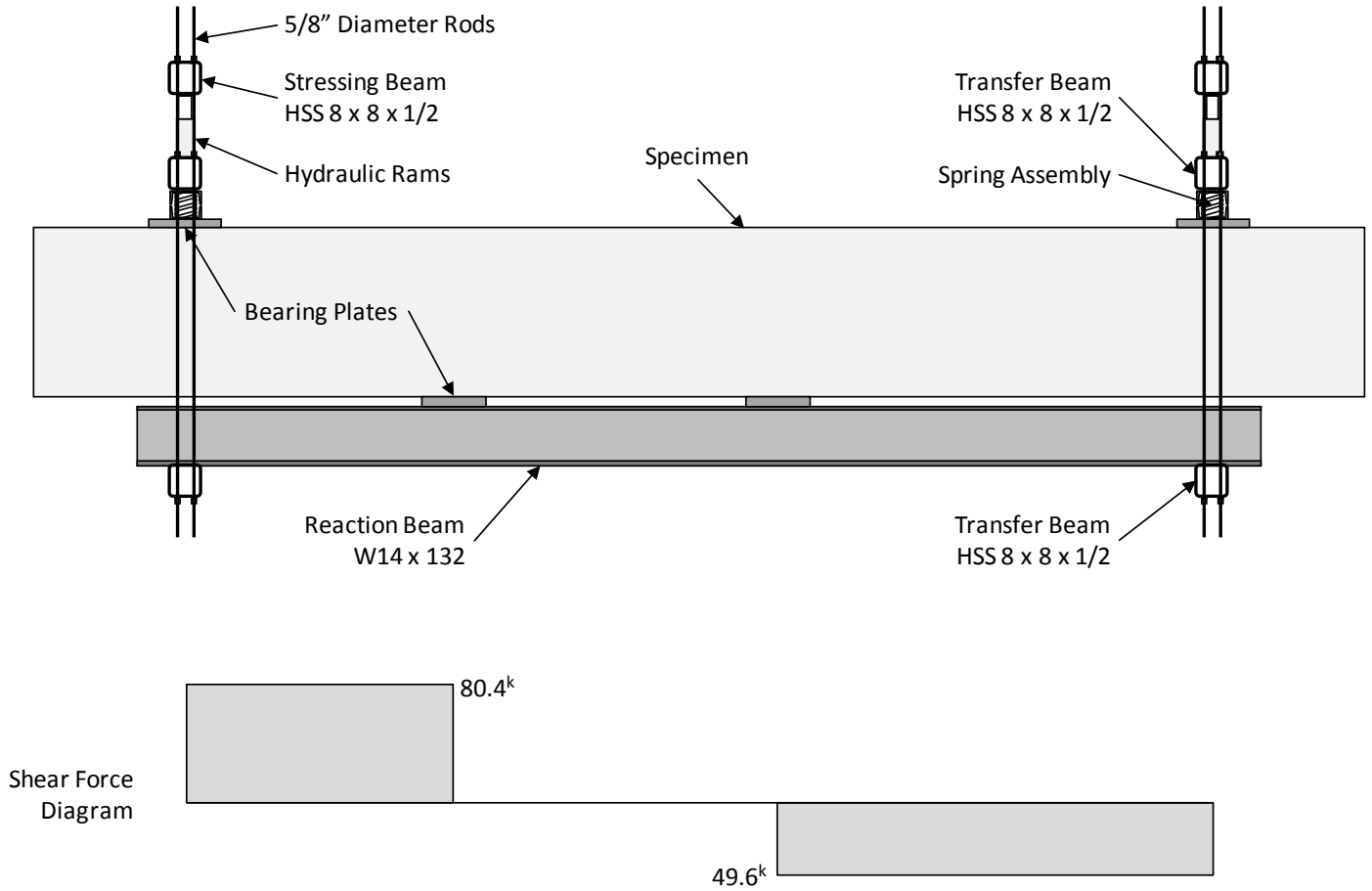

Figure 4-7: Sustained Loading Setup with Superimposed Shear Force

The conditioning load was applied after all bent caps were transferred to the exposure site. A photo of the loading setup is including in Figure 4-8. To begin, bearing plates (please see Section 4.3.1 for dimensions) were carefully positioned on a heavy steel beam. Hollow steel sections, paired at opposite ends of the specimen, were then coupled via high strength post-tensioning bars. Finally, four thirty-ton hydraulic jacks provided the force necessary to lift the reaction beam into place and apply the desired shear. Large railroad springs mounted above each support plate limited the loss of post-tensioning force. Although variation in the concrete strength may have caused deviation from the targeted reinforcement stress, the desired magnitude of shear was achieved.

Figure 4-8: Load Conditioning Setup

It should be noted that the specimens were loaded at different stages of deterioration. A comprehensive timeline, presented in Chapter 5, will place the loading operations within the context of all other critical tasks conducted during the study. Consequences of time, loading, and various other operations/factors will then be thoroughly examined.

4.2.4 Restrained Expansion Monitoring

Expansion data gathered over the course of the conditioning period were expected to provide critical insights into the behavior of the affected bent caps. For that reason, the selection of instrumentation was not taken lightly. Accuracy and repeatability of the measurements were two of several qualities desired. The hardware/electronics also needed to be sufficiently robust to survive a long tenure within the harsh (highly basic) conditions of the reactive concrete. Ideally the technique would effectively characterize the global behavior of the locally-variable expansions with as few measurements as possible. After considering a number of options, a non-traditional implementation of mechanical strain measurement (similar to DEMEC) was selected. Much needed redundancy was achieved through the installation of traditional reinforcement strain gages. Ultimately, careful selection of the instrumentation ensured that the results would be unquestionable.

4.2.4.1 Mechanical Strain Measurements

Traditional mechanical strain measurements are frequently referenced within ASR/DEF-related literature. The versatility and economy of the technique has proven to be popular among many ASR/DEF researchers and consulting engineers. A brief description of its implementation will reveal the advantages (and disadvantages) of the approach, as well as provide a basis for the development of instrumentation within the current study.

Typical implementation of the technique includes the use stainless steel targets and a mechanical strain gage. To begin, a pair of small targets is positioned to form a gage length over which the expansion measurements can be taken. The targets are typically attached to the surface of the structure using a two-part epoxy or similar adhesive. The mechanical strain gage which interfaces the targets typically consists of a dial gage attached to an invar reference bar. A fixed conical point mounted at one end of the bar is complemented by a pivoting conical point at the other end. When a measurement is taken, the operator inserts both points into the fixed targets. Length extension indicated by movement of the pivoting conical point is measured by the dial gage. When a consistent gage length is used for all measurements of a structure, only one mechanical strain gage is necessary. Furthermore, measurements can be taken as frequently of infrequently as desired once the targets have been placed. There is no need for a multi-channel data acquisition system to provide continuous monitoring of the instruments.

Traditional mechanical strain measurement does not come without disadvantages. In particular, there are a number of inaccuracies associated with the use of surface-mountable targets. The loss of data is not uncommon. Adhesive binding the targets to the concrete surface frequently fails during the unattended periods between measurements. Dependent on the frequency of the measurements, weeks or even months of expansion may go unrecorded. Furthermore, laboratory use of surface expansion data as a benchmark for structural performance is less than desirable. As noted within Section 4.4.2.1, expansive strains *imposed* on the cover layer are much different than those *developed* within the concrete member. Furthermore, it can be expected that direct environmental exposure alone will lead to a significantly larger variation of strains measured via the concrete surface. The use of surface-mounted targets may thereby yield expansions with less than sufficient accuracy for the purposes of a laboratory study.

To eliminate the abovementioned problems, use of surface targets was abandoned. In fact, the influence of cover expansions was eliminated from the measurement process altogether. A unique approach to mechanical strain measurement allowed expansions of the concrete core and strains in the confining reinforcement to be measured directly. Following a discussion of the instrumentation layout (shown in Figure 4-9), production and installation of the targets will be discussed. Hardware and electronics used to measure the time-dependent expansions will then be revealed.

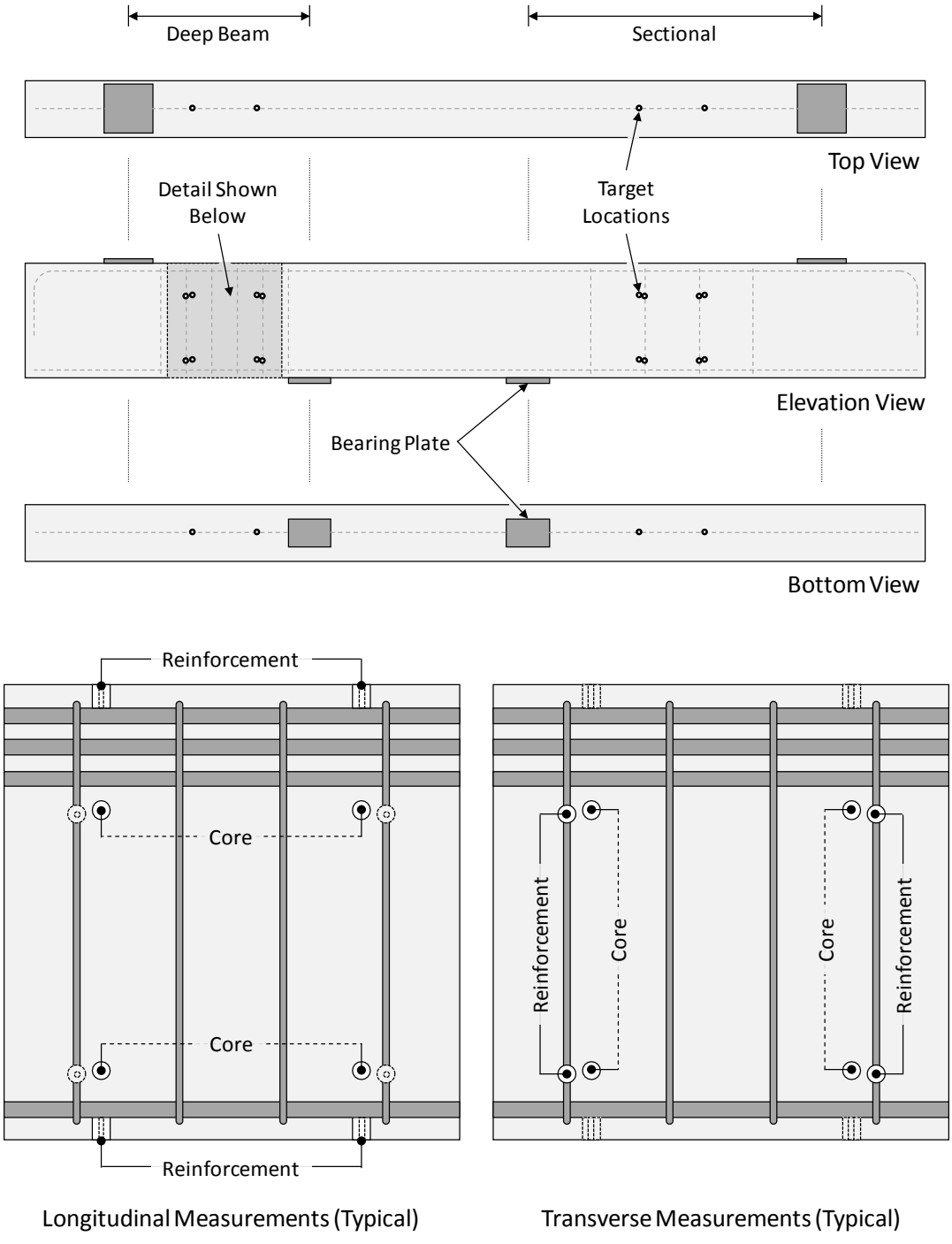

Figure 4-9: Layout of Targets for Expansion Measurement

The results of past research (see Chapter 2) suggested that the interplay between the expansive concrete core and surrounding reinforcement is critical to the behavior of an ASR/DEF affected concrete member. As a result, instrumentation was placed to efficiently quantify both concrete and steel strains at a number of sections (horizontal and vertical) throughout each bent cap specimen. Figure 4-9 (previous page) serves as an excellent reference for the discussion which follows. Longitudinal (horizontal) and transverse (vertical) concrete core expansions were measured via a twenty-four inch grid of targets placed at the center of the test regions. Each target was machined into the square face of a stainless steel rod. The finished rods were then *suspended* within the concrete core. The position of the rods within the cross-section can be seen in Figure 4-10 (Section A-A). The grid of targets resulted in eight individual measurements of the concrete core expansion (two longitudinal and two transverse per test region elevation). Complementary strains in the longitudinal and transverse reinforcement were measured in a similar manner. Matching targets were first machined into short stainless steel studs. Pairs of studs were then welded to the desired segment of reinforcement at the common spacing (gage length) of twenty-four inches. Figure 4-10 shows the location of longitudinal steel (Section A-A) and transverse steel (Section B-B) stud pairs. In the end, twenty-eight gage lengths (individual measurements) were formed by the strategic placement of only forty targets. Efficiency of the layout should not be undervalued. The design, production, and installation of the instrumentation were highly demanding tasks.

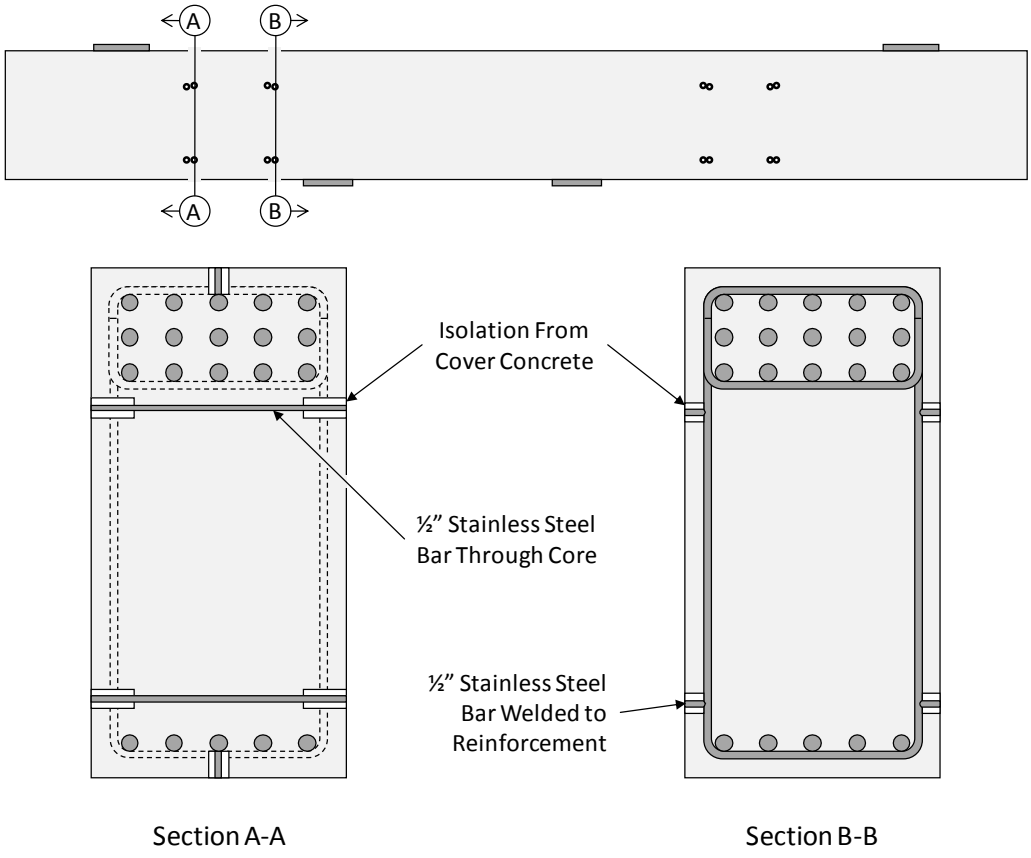

Figure 4-10: Concrete Core and Mild Reinforcement Measurements

The final design of the target was largely attributable to the advice of Dr. Karl Frank (UT Austin). Based on his personal experience with mechanical strain measurement, he recommended the incorporation of a small chamfer at the outside edge of the target hole. It was suggested that the chamfer, ten to fifteen degrees shallower than the conical point of the mechanical strain gage, would produce the most repeatable measurements. If nothing else, the bevel at the leading edge of the hole helped the operator to center the points of the mechanical strain gage. The detail is shown as designed within Figure 4-11 and as implemented within Figure 4-12B.

All of the instrumentation components were fabricated in-house. Production of the stainless steel rods and studs required a series of operations on a metal lathe and computer controlled milling machine. Nearly two-hundred stainless steel (ASTM A303) components were fabricated over the course of the study. Close tolerances ensured that all of the targets were virtually identical. While the effort required an extraordinary

investment of man-hours, resulting familiarity with the instrumentation led to high confidence in the monitoring results.

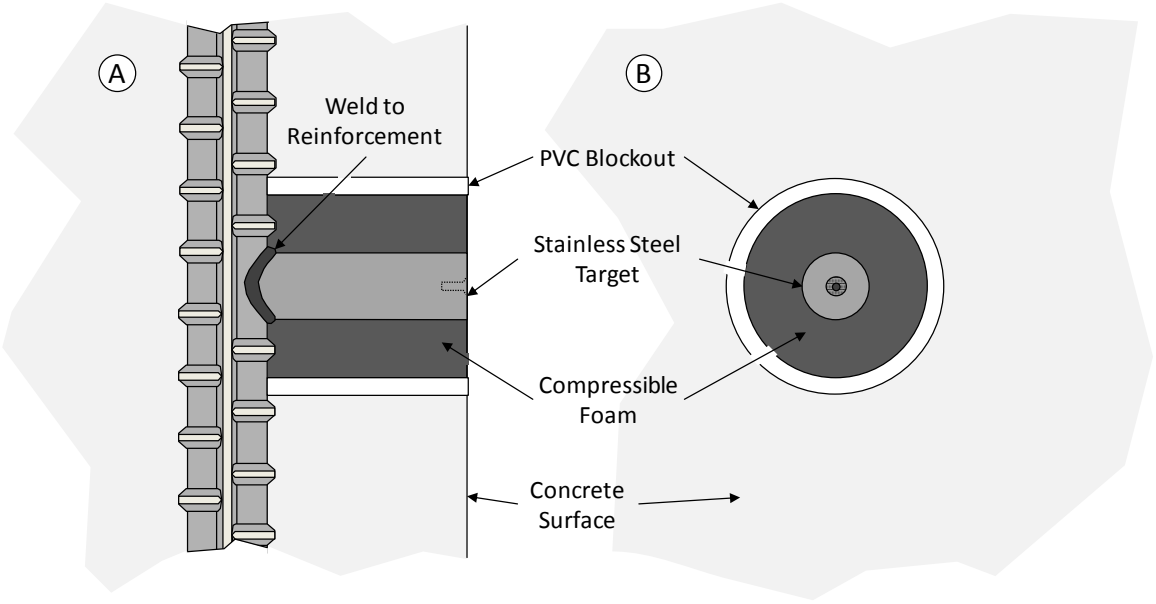

Figure 4-11: Measurement Target Detail (A) Section View (B) External View

Installation of the targets was no less demanding. To accurately place the concrete core instrumentation within each shear span, an aluminum template was fabricated. The template temporarily held the stainless steel rods at the desired gage length of twenty-four inches. Mild steel wire was then used to permanently secure each rod within the reinforcement cage. As intended, the final grid of targets was *suspended* within the concrete core; no direct contact with the reinforcement was made. The same aluminum template was used to place the reinforcement instrumentation. After marking the final location of the studs on the reinforcing bar, mill scale and deformations were removed using an air-powered die grinder. Extreme care was exercised to limit removal of the cross-section. After thoroughly cleaning the bare steel and positioning the targets, the base of each stud was attached to the reinforcement using metal inert gas (MIG) welding (shown in Figure 4-11). Restricted application of the weld metal helped to limit toughening of the steel reinforcement.

The instrumentation of each beam was completed by the installation of the target blockouts. The standard blockout detail, applicable to both concrete core and reinforcement instrumentation, is shown in Figure 4-11. The detail can also be seen within the context of the specimen cross-section in Figure 4-10. To form the blockout, a

segment of 1½-inch diameter pipe was centered on each target via an intermediate layer of foam. The stainless steel target face and porous foam were then sealed against concrete paste infiltration. Following concrete placement, the seal was removed to allow access to each of the targets. Due to the compressible nature of the foam, a one half inch *void* was effectively created around the circumference of each target. The blockouts allowed unimpeded length expansion of up to one inch over the gage length; equivalent to an expansive strain of about four percent. This limit was more than adequate for the core expansions and reinforcement strains expected to develop over the course of the study. As a result, the influence of irrelevant concrete cover expansions was not a concern.

Consistent production and placement of the targets ensured that the same instrument could be used for all measurements. A long gage length extensometer with an achievable accuracy of 0.0025 percent was chosen to serve the function of a traditional mechanical strain gage. Originally intended for reinforcement coupon testing, the extensometer required slight modifications for use in the current study. Following the changes, the device was well-suited to interface each of the twenty-four inch gage lengths. Two small aluminum brackets replaced the original knife edges at either end of the extensometer. Each bracket was drilled and tapped to accept a common dial indicator point, as shown in Figure 4-12C. The carbide indicator points were selected for their exceptional hardness and durability. A demonstration of the completed device can be seen in Figure 4-12A.

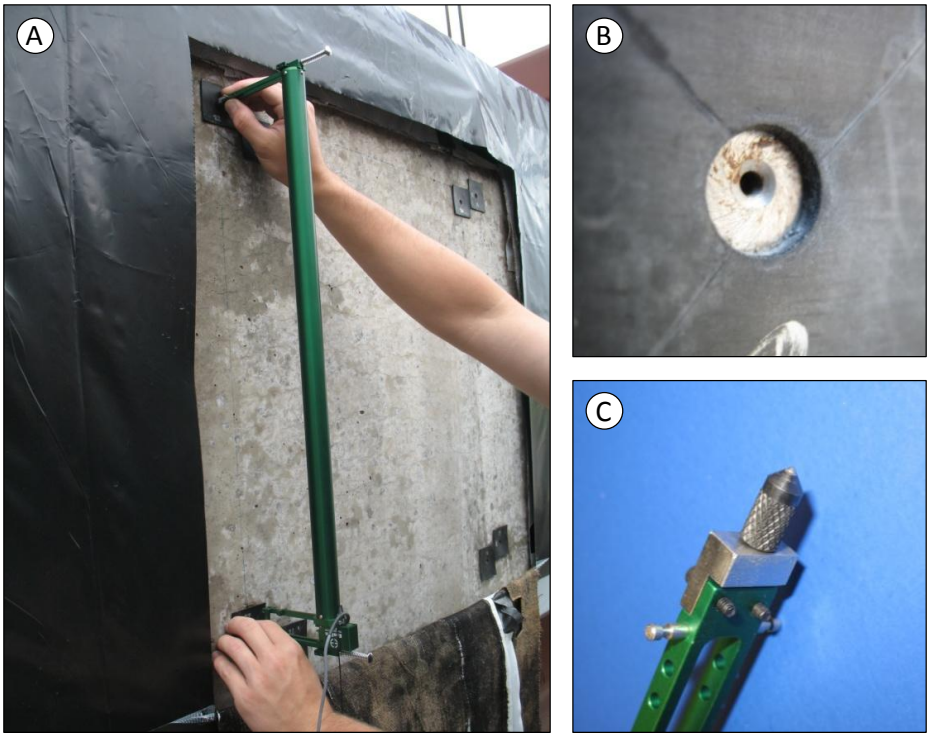

Figure 4-12: Long Gage Length Measurements (A) Demonstration of Measurement (B) Measurement Target (C) Extensometer Modification

In contrast to the traditional methods described above, routine expansion measurements required the use of a sophisticated data acquisition system. While more complicated, the approach had a number of benefits; foremost being the electronic retrieval and storage of data. Expansions (or contractions) were registered by movement of the extensometer's active arm. The position of the active arm (in reference to the standard gage length) controlled the linear output of a full bridge circuit powered by ten volts of direct current. Output of the circuit was recorded via a cart-mounted National Instruments data acquisition system. A calibrated scaling factor allowed the electrical output to be converted to strain.

Standard measurement techniques were developed and implemented to minimize the influence of the environment and operator. Weather conditions were examined and noted before each measurement cycle. Expansions were preferentially recorded on calm, partly cloudy days to eliminate the influence of local temperature variation. This effectively dictated the frequency of the records; measurements were taken every one to six weeks. The effects of any large deviations from the baseline temperature of 70°F were later

corrected using a well-accepted coefficient of thermal expansion ($\alpha = 5.5 \cdot 10^{-6}$ in/in·°F). Although the extensometer was never operated by another individual, it was handled and positioned by the author in a consistent manner; a precaution taken in response to the sensitivity of the instrument. As a result, the measurement technique demonstrated excellent accuracy and repeatability throughout the tenure of the study. It should be recognized that minor variability potentially introduced by these factors became increasingly small in relation to the magnitude of the expansions developed over time.

4.2.4.2 Electrical Strain Measurements

Due to the atypical nature of the mechanical strain measurements, researchers felt it was prudent to install a number of foil strain gages on the reinforcement. Output from the gages was used to further substantiate the mechanical strain results, but did not serve as the primary source of expansion data. This was a deliberate decision based on the inherent limitations of foil strain measurements. Foil strain gages are exceptionally short and can only capture local variation in strain. To capture the average state of deterioration within each of the shear spans would have required an inordinate number of gages. Furthermore, foil strain gages performed poorly in a number of former ASR/DEF studies at the University of Texas at Austin. The strain gage adhesives and protective coatings routinely used within the laboratory rapidly failed when placed in reactive concrete. Expectations for the performance of the foil gage instrumentation were correspondingly low. Layout of the instrumentation is shown in Figure 4-13. The location of each measurement target is included to provide context for the placement of the foil strain gages.

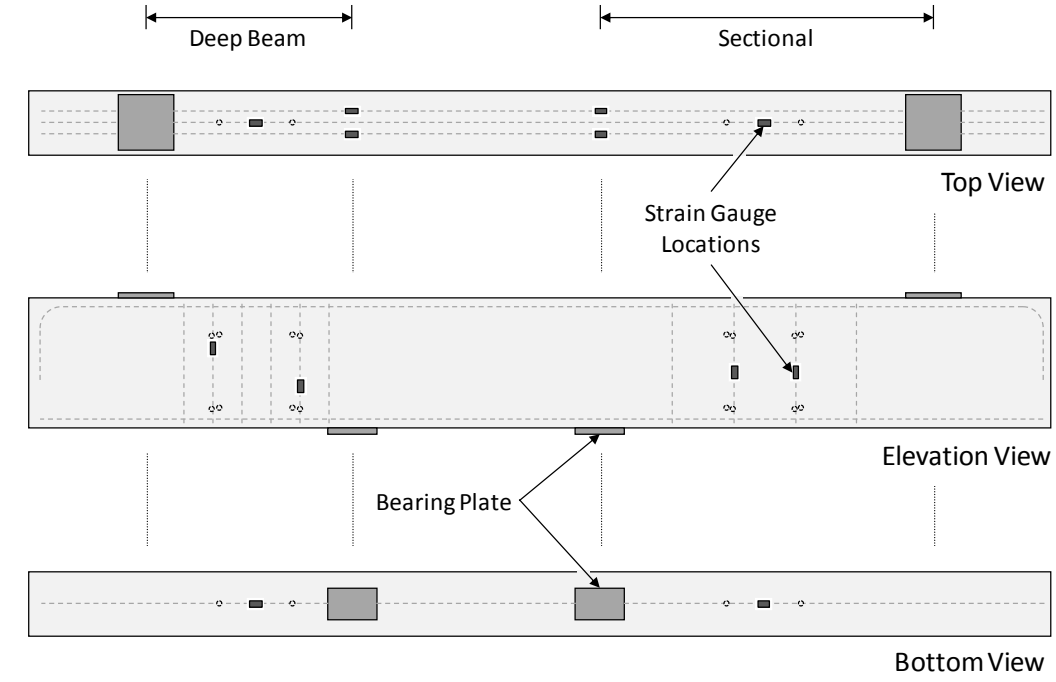

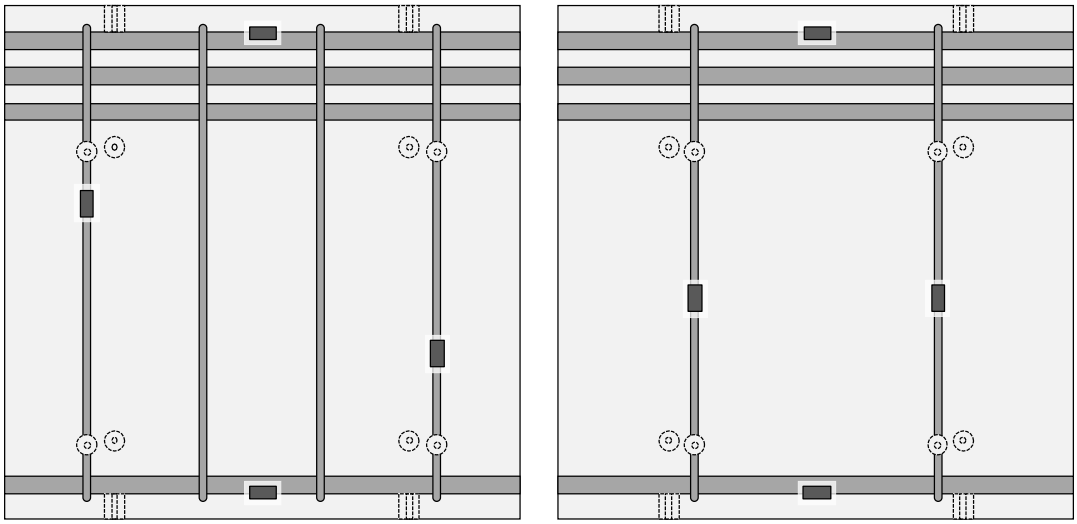

Figure 4-13: Layout of Reinforcement Strain Gauges

The foil strain gages were typically applied to the reinforcement at the center of each mechanical strain gage length. However, to allow the instrumentation to better serve the needs of the structural testing phase, a couple of exceptions were made. Within the deep beam shear span, the transverse reinforcement strain gages were aligned with the assumed axis of the inclined compression strut. Close proximity to primary diagonal splitting crack allowed the strain gages to capture the behavior of the stirrups near ultimate load. Additionally, two gages were placed on the outermost layer of longitudinal tension reinforcement, directly above the loading point. These gages were to provide an early indication of longitudinal yielding during each of the shear tests.

The foil strain gages were applied to the reinforcement with conventional techniques. Using an air-powered die grinder, the mill scale and deformations were removed from a small area of the bar. Care was exercised to limit removal of the cross-section. A series of increasingly fine polishing wheels then achieved a near mirror finish of the steel. Sequential application of acid and base solutions etched and cleaned the surface. Tokyo Sokki Kenkyujo Co. strain gages (Model No. FLA-3-11-5LT) were then attached with a cyanacrolate adhesive. Acrylic coating, a neoprene pad and aluminum foil tape (applied in that order) formed a barrier against moisture and electrical noise.

Following transfer of the beams to the exposure site, a data acquisition system was assembled to periodically record the foil strain gage output. Sixteen channel multiplexers, mounted to each of the specimens, relayed the electrical output of each gage to a central datalogger. The only available model of datalogger (Campbell Scientific 21X Micrologger) recorded up to forty-eight channels of data. As a result, two separate zones containing three specimens each (analogous to those formed for moisture conditioning purposes) were monitored via separate 21X Microloggers. A wiring diagram of each zone each shown in Figure 4-14. Also included is an example of the weather proof enclosures used to protect all of the data acquisition components.

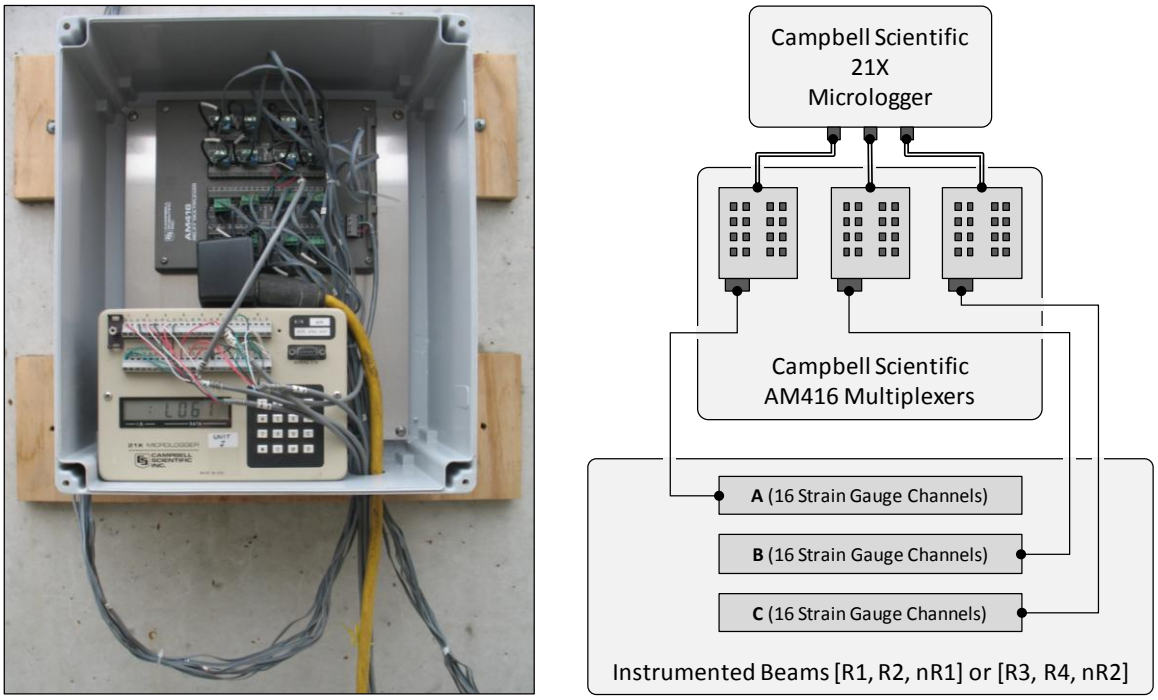

Figure 4-14: Long-Term Data Acquisition for Strain Gauges

Reinforcement strains were recorded shortly after midnight each day. A rotating yearlong history of the measurements was permanently stored on each datalogger. To eliminate the risk of data loss due to battery failure, the data acquisition system was connected to the domestic power supply. The measurement histories were retrieved periodically via serial port transfer to a laptop computer. Each record was stamped with the respective time and temperature. These values were then used to correct the strains for thermal effects (as described above) and conduct a time-dependent comparison with the mechanical strain results. Expansion monitoring results are examined and summarized in Chapter 5.

4.3 PHASE II: SHEAR TESTING

Up to this point, the fabrication and conditioning of the six bent cap specimens have been described in detail. Treatment of the two series of specimens, (R1, R2, nR1) and (R3, R4, nR2), has been identical. However, *Phase II* represents the divergence of both their treatment and purpose. The following discussion presents the underlying rationale for the creation of two separate bent cap specimen series.

Per the original project scope, only three shear spans were to be subjected to structural testing during the tenure of this study. Each one of the spans was to represent a distinct level of damage; i.e. undamaged, moderately damaged, and extensively damaged. Results from the three shear tests would then support the development of a generalized relationship between the level of damage and shear capacity. It was soon realized (following the thorough literature review) that such an objective was overly ambitious. Three test regions could not adequately represent the range of significant variables (i.e. level of deterioration, shear span-to-depth ratio, and length of exposure) found in practice. For this reason, the test program was expanded to include six bent cap specimens with a total of twelve test regions (one deep beam and one sectional shear span per beam).

To accomplish the immediate goals of the project, three of the six specimens were conditioned and then selected for structural testing within one year of fabrication (as discussed within this section). These specimens (R1, R2, nR1) were instrumental in collecting strength and serviceability data in the short-term. In fact, the expansion monitoring and shear testing results from the six shear spans form the basis for many of the observations and conclusions drawn in later chapters. The remaining three specimens (R3, R4, nR2) were left to condition under load and moisture for an extended (and undefined) period of time. It is hoped that data collected from these test regions will help to answer questions related to the long-term effects (i.e. reinforcement fracture, see Chapter 2) of ASR/DEF deterioration. Expansions are being closely monitored and structural testing may be conducted at a later date.

The first series of bent cap specimens was tested in the summer of 2008. A wide range of ASR/DEF-related damage had developed during the course of the previous eight to twelve months. While the most severe deterioration produced expansions well in excess of the reinforcement yield strain, the non-reactive control specimen remained undamaged. Following selection, the bent cap specimens were prepared for structural testing. ASR/DEF-related cracking was documented. The beams were then unloaded and brought into the laboratory. The Large-Scale Beam Testing Facility at FSEL easily accommodated the loads necessary to test each span in shear (Section 4.3.1). Instrumentation (described in Section 4.3.2) captured all the forces, deformations and strains necessary to characterize each test. Careful planning and unique repair techniques (Section 4.3.3) ultimately made all six of the shear tests possible.

4.3.1 Test Setup (Large-Scale Beam Testing Facility)

Static loading of each bent cap specimen was conducted within the Large-Scale Beam Testing Facility. The large test frame was conceived and built under the auspices of TxDOT Project 0-5253 to accommodate the high loads required to fail large-scale deep beams. Since completion in 2006, the facility has been used to test reinforced concrete beams deeper than six feet and capable of resisting more than one million pounds of shear (Birrcher et al. 2008). The author of this report assisted in a number of the aforementioned deep beam tests. Collaboration with the researchers of Project 0-5253 greatly facilitated the development and testing of the ASR/DEF bent cap specimens.

The centerpiece of the new facility was a 96,000 pound cast-steel platen; donated to FSEL after a six million pound universal test machine was decommissioned by the U.S. Navy. The steel platen or *strong floor* provided the test frame with the *backbone* resistance necessary to test the bent cap specimens in shear. A two million pound capacity, double-acting hydraulic ram was supported by the strong floor and exerted an upward force at the desired shear span location. Simple supports were provided at the two large steel plate girders (i.e. transfer beams) and high strength threaded rods transferred the load back to the floor. Configuration of the test frame for the current study is illustrated in Figure 4-15, Figure 4-16, and Figure 4-17. The extraordinary scale of the facility is demonstrated in a photograph (Figure 4-18) taken at the conclusion of deep beam shear testing.

A well-defined, simply-supported testing condition was created by the installation of roller and pin assemblies at the load and support points, respectively. To permit free rotation and translation at the applied load, a three-inch diameter steel bar was allowed to roll freely between a pair of four-inch thick steel plates. Rotations were similarly released at each support through the use of a two-inch diameter steel bar and two-inch thick steel plates. In contrast to the roller assembly, horizontal movement at each support was restricted by welding the round bar to the bottom plate. Considerable flexibility of the threaded rods eliminated the potential for axial restraint of the specimen.

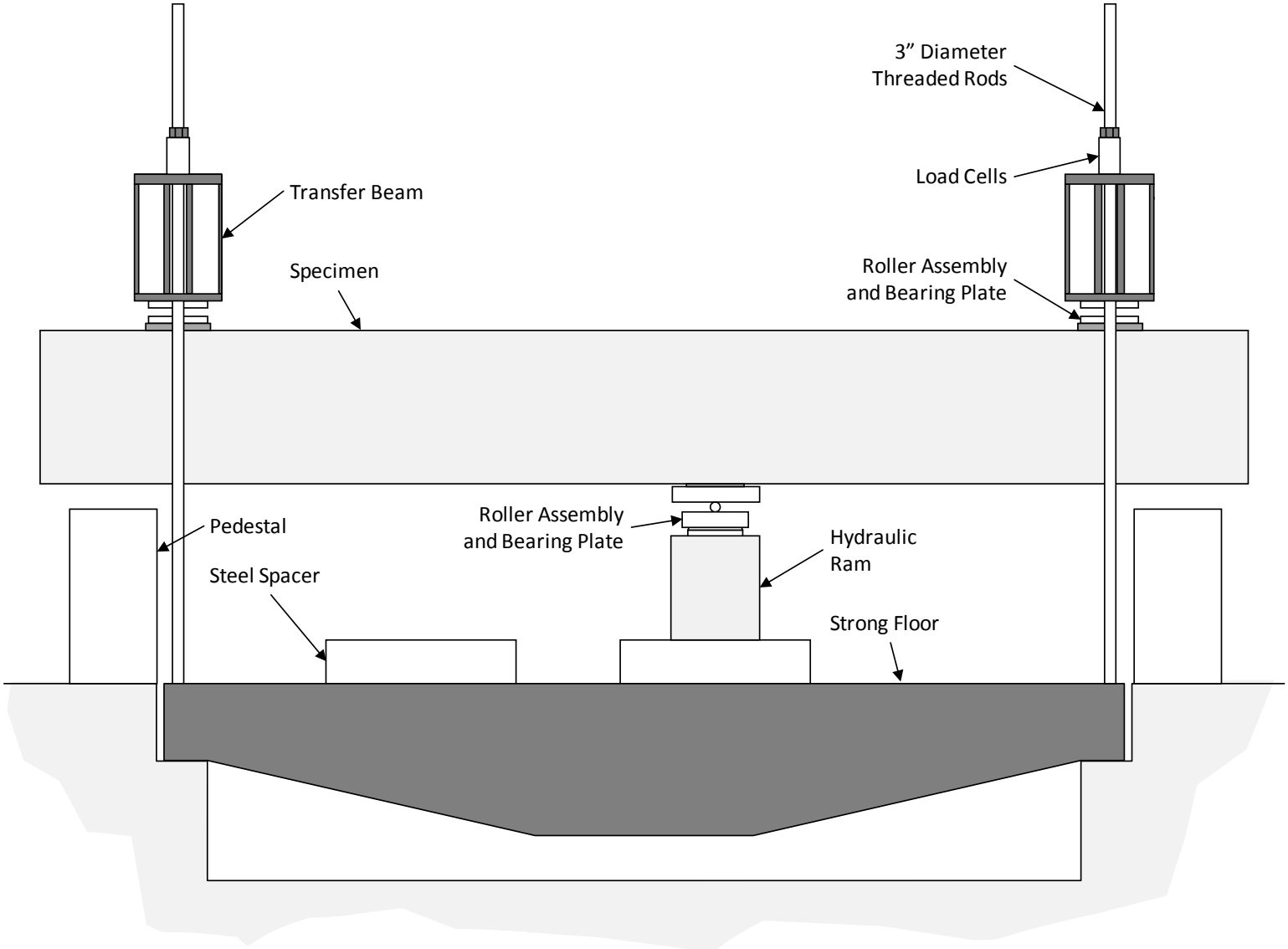

Figure 4-15: Large-Scale Beam Test Facility, Elevation View

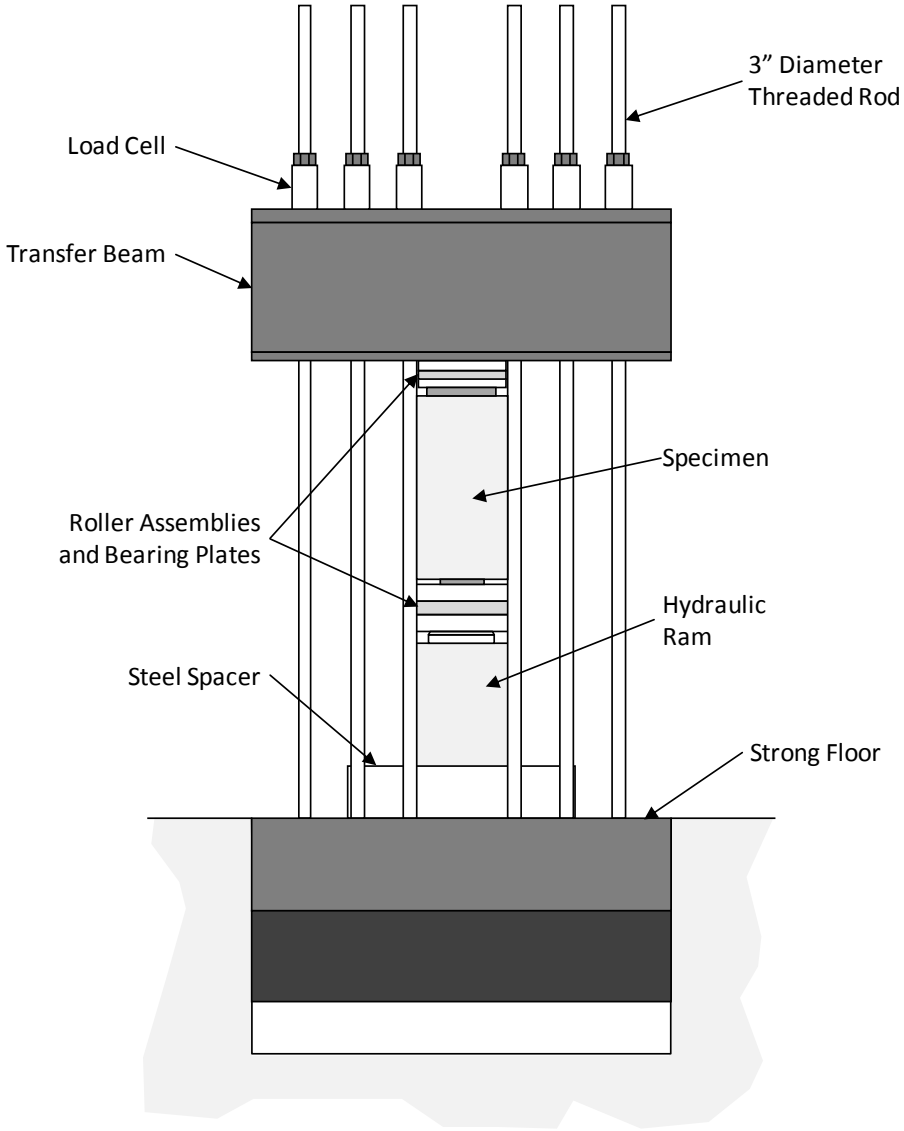

Figure 4-16: Large-Scale Beam Test Facility, End View

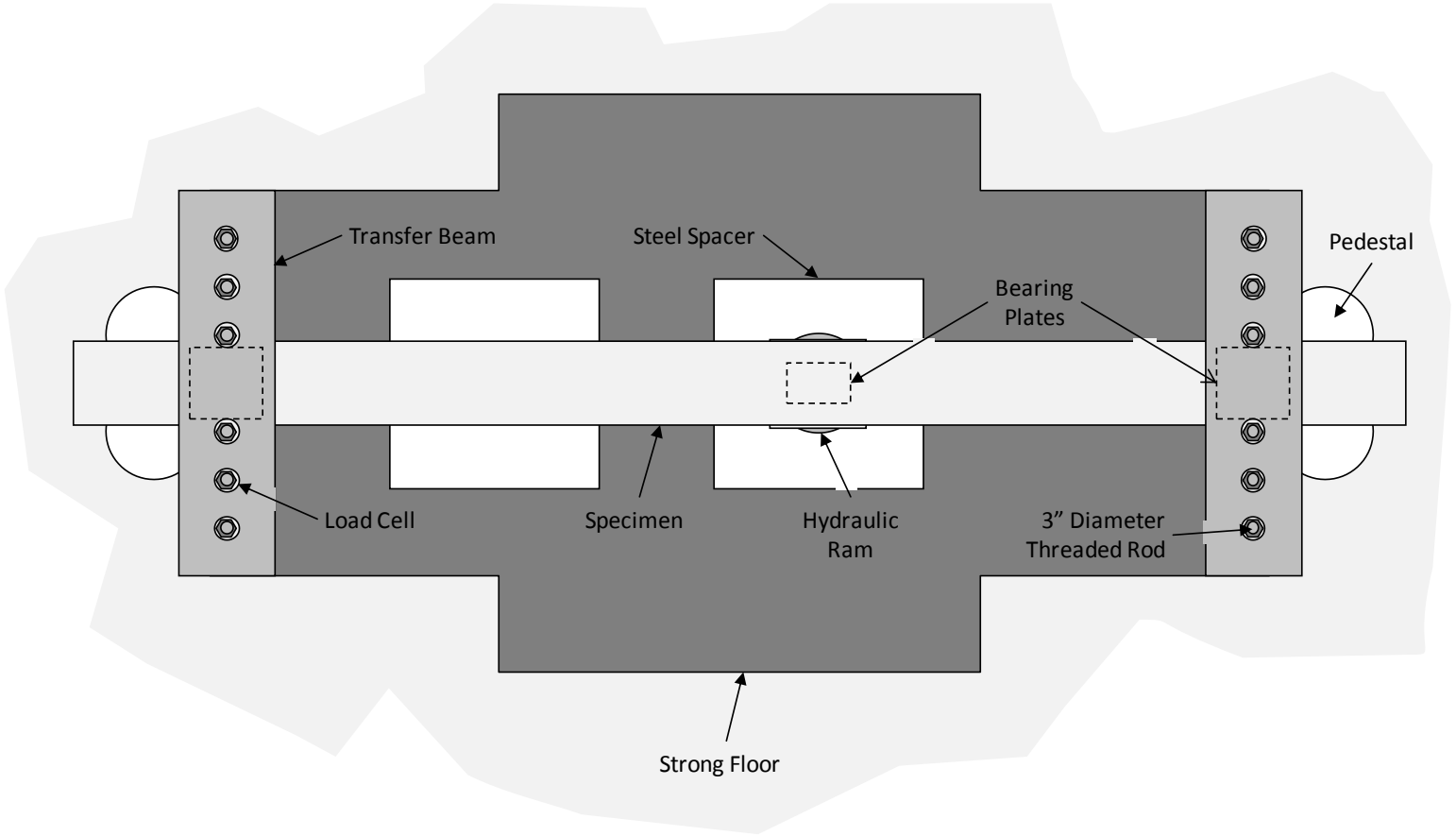

Figure 4-17: Large-Scale Beam Test Facility, Plan View

Figure 4-18: Large-Scale Beam Test Facility

To obtain a planar loading surface, steel bearing plates were set in *hydrostone* (gypsum cement) prior to the placement of the roller/pin assemblies. Selection of the bearing plate geometry is briefly reviewed here and the results are summarized within Figure 4-19. All underlying assumptions resulted in conservatively large bearing plates; thereby eliminating the potential for bearing distress. To begin, support bearing plates were proportioned according to column design guidelines. Recommendations within the recently-retired TxDOT *Bridge Design Manual* (2001), suggested that the column width should be a minimum of three inches narrower than the attached bent cap. Assuming a square *column*, an eighteen-inch square plate was selected (Figure 4-19A). Next, the loading plate was proportioned to simulate two girders framing into a bent cap at a common point. TxDOT standards for elastomeric bearing pads served as the primary reference for the design. Assuming the use of Type IV girders, a total bearing area of 308 in^2 is required for standard bent cap applications ($b_{standard}$ = 39"). Accounting for the difference in scale ($b_w/b_{standard}$ = 0.54), a loading plate area of 166 in^2 was targeted. Final dimensions of the plate (Figure 4-19B) were based on common bearing pad proportions.

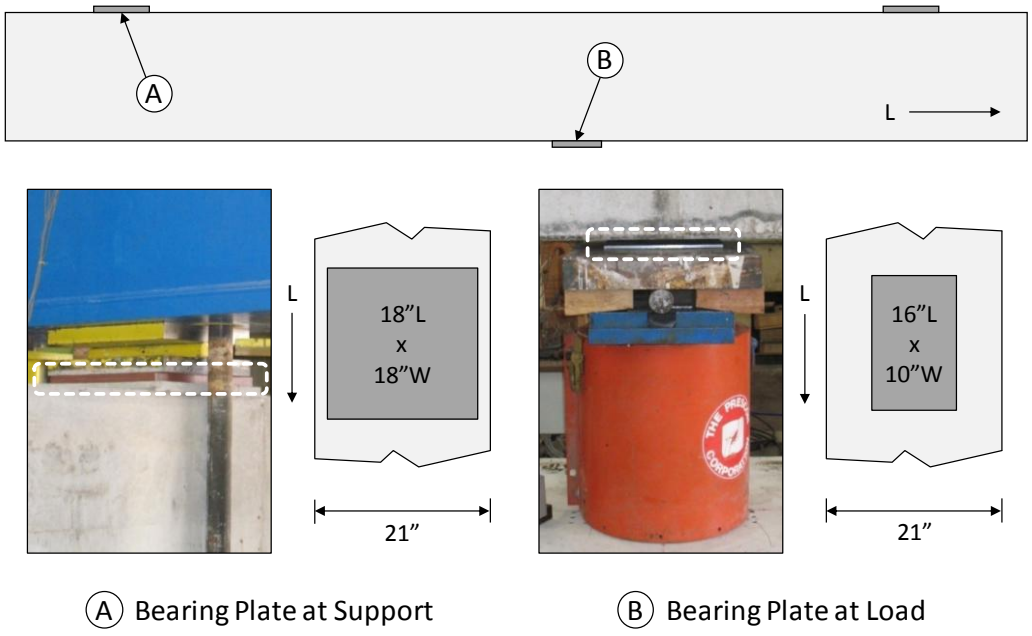

Figure 4-19: Bearing Plate Details

4.3.2 Instrumentation and Data Acquisition

A comprehensive set of instrumentation captured the data necessary to uniquely characterize the behavior of each shear span. Comparison of the measurements and

observations made during the non-reactive and reactive bent cap tests was vital to establishing the effects of ASR/DEF on live load performance (see Chapter 5). This section details the instruments and techniques used to measure load, displacement and strain during each of the shear tests. A general layout the instrumentation is shown in Figure 4-20.

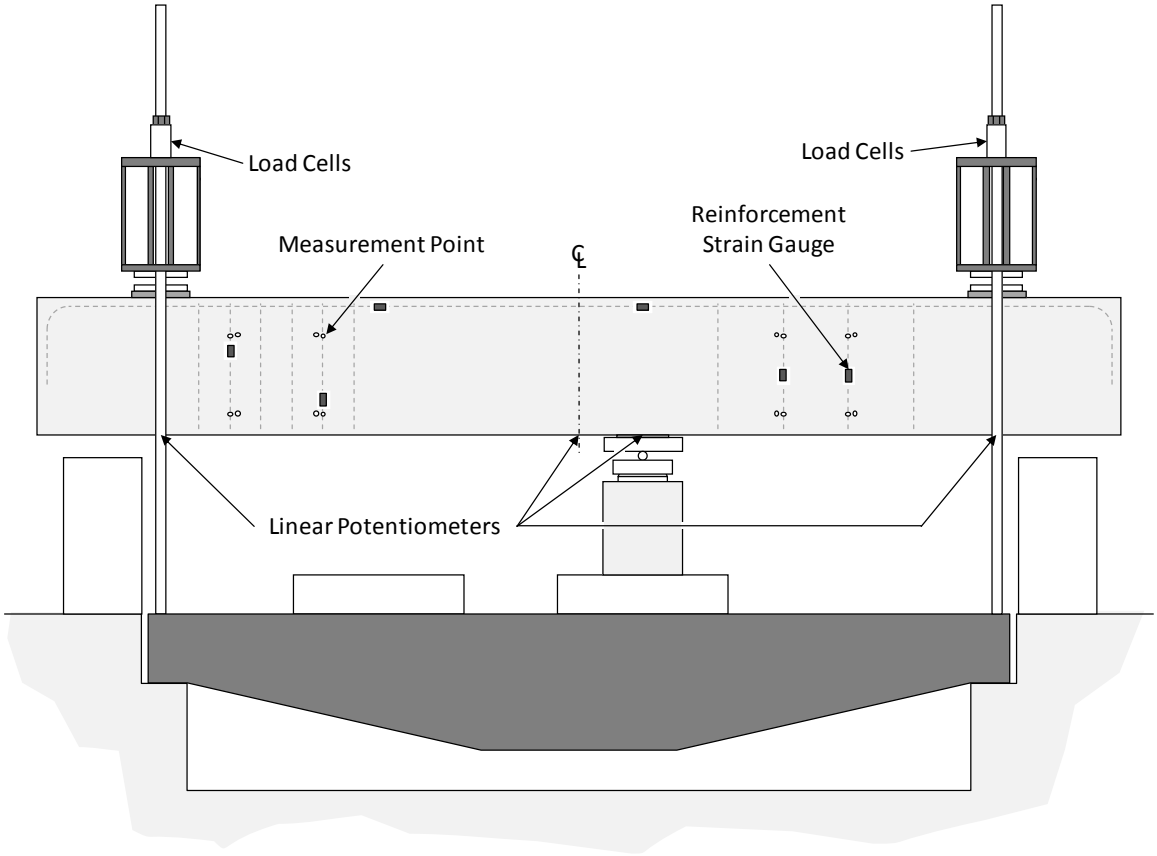

Figure 4-20: General Instrumentation Layout

The reaction at each support was measured by a set of six load cells. As shown in Figure 4-16 and Figure 4-22A, the five hundred kip capacity, center-hole load cells were individually placed over each high-strength rod. Once all of the load cells were set on the topside of the transfer beam, the reaction nuts were leveled. Maintenance of a consistent gap between the load cells and reaction nuts ensured an even distribution of the load among the rods (and corresponding transducers).

Due to the position of the load cells, components of the shear force were not recorded by the data acquisition system. Specifically, the self-weight of the specimen and load

imposed by both transfer girders were not measured by the load cells mounted atop each transfer beam. That said, the weight of the transfer beams and test specimen were accounted for during data analysis of each test record (results are presented within Chapter 5). Figure 4-21 includes the free-body diagram and equations used to calculate the full shear force at the critical section. For the purposes of this study, the critical section was defined at the center of the test region under consideration. It should be noted that the near reaction (R_A) was taken as the sum of the load cells at that support. All future plots and figures reflect implementation of the procedures discussed here.

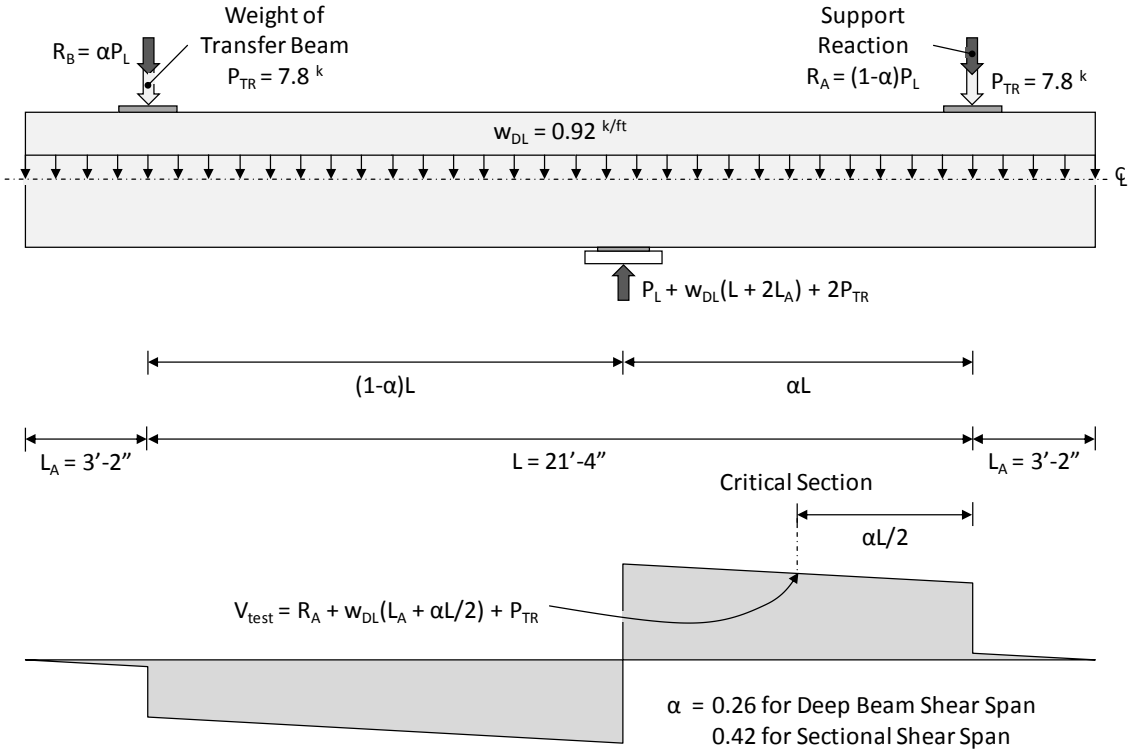

Figure 4-21: Shear Force Diagram for a Typical Beam Test

To monitor the displacements, four six-inch linear potentiometers were positioned along the bottom side of each specimen. Displacements measured at the centerline, load point, and each support were used to isolate the live load deflection of the bent cap. The location of each linear potentiometer is illustrated within Figure 4-20. A photograph of the centerline potentiometer is included within Figure 4-22B.

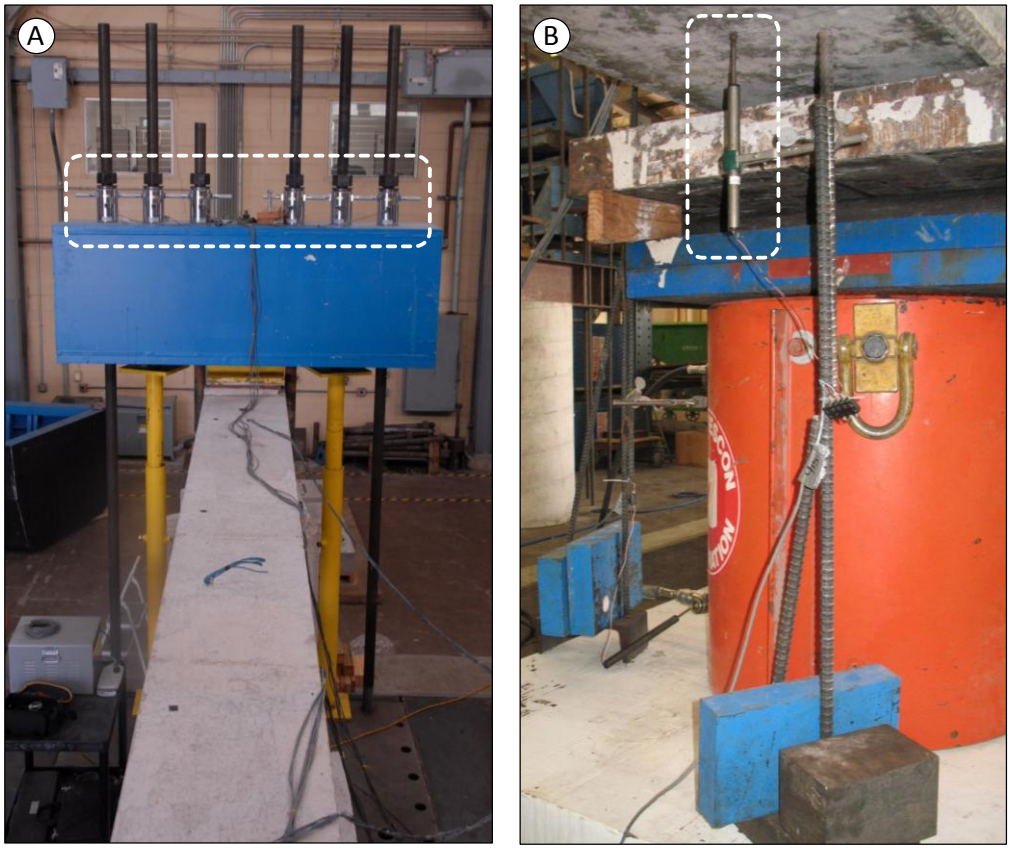

Figure 4-22: Instrumentation (A) 500 Kip Load Cells (B) 6-Inch Linear Potentiometer

The linear potentiometers were active throughout the shear test. Displacements were first recorded when the hydraulic ram lifted each end of the specimen off the temporary supports (or pedestals, refer to Figure 4-15). Reaction nuts and high-strength rods closest to the applied load were activated first; additional ram extension caused the beam to pivot toward the far support. An illustration of the rigid body motion and beam deformation at this point of the test is shown in Figure 4-23A. Once the far support was activated (Figure 4-23B), the additional displacement was attributable to further extension of the support rods and deflection of the specimen. Calculation of the beam deformation (Δ_{BEAM}) during each separate stage is summarized within Figure 4-23.

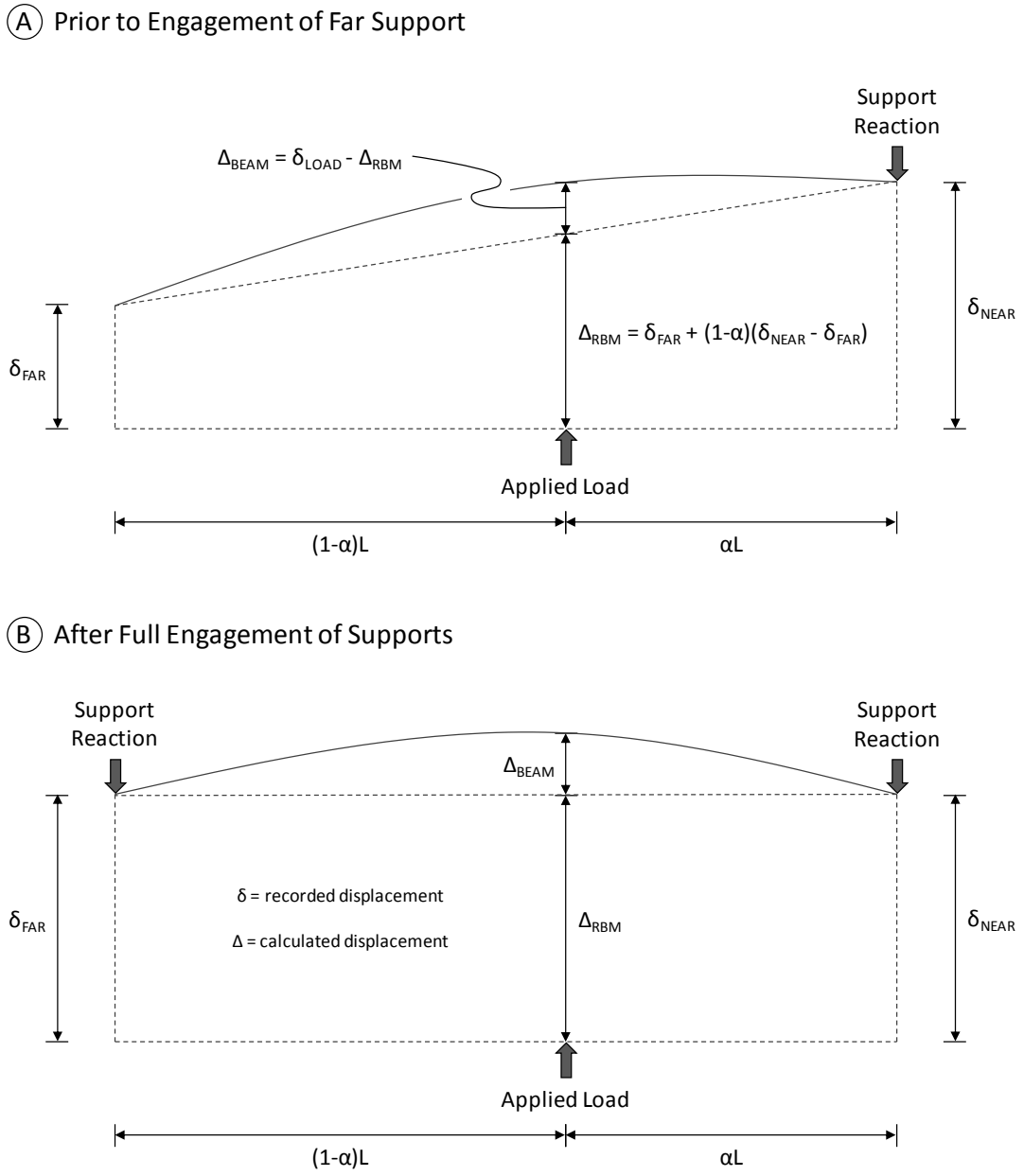

Figure 4-23: Calculation of Specimen Displacements and Deformations

The concrete and steel strains resulting from live load application were recorded via the mechanical and electrical methods described in Section 4.2.4. No additional strain instrumentation was necessary. Pre-existing gages adequately captured the live load behavior of the damaged shear spans. In particular, the strain data was used to identify the formation of diagonal cracks and the development of plasticity within the longitudinal

and transverse reinforcement. Figure 4-9, Figure 4-13 and Figure 4-20 illustrate the layout of both mechanical strain targets and foil strain gages.

Prior to the application of any load, all twenty-eight of the mechanical strain gage lengths were measured. This created a final record of the deterioration for use during data analysis. Load was then applied to the specimen and mechanical strains were recorded at the end of each load step (see the next section for details). To ensure that all of the strains would correspond to their respective load, hydraulic ram pressure was maintained as well as possible during the course of the measurements. The nearly instantaneous acquisition of foil strain gage output would have been preferable in this situation. However, very few of the supplementary foil strain gages survived the conditioning period. As designed, the foil gages were only meant to provide confirmation of the earliest expansions measured via alternate methods. That said, functioning foil gages were interrogated over the course of the test, but did not serve as the basis for the observations and conclusions presented within Chapter 5.

Each of the transducers (load cells, linear potentiometers, and strain gages) were wired to bridge completion modules and then interrogated via a 120-channel scanner. The voltage output was converted into valid engineering data via predetermined calibration factors. A computer with National Instruments LabVIEW software stored the data and allowed it to be visually monitored in real-time.

4.3.3 Test Procedure

Each of the six shear spans were monotonically loaded to failure in increments of fifty to one hundred kips (dependent of the shear span-to-depth ratio and concrete strength). The increment was generally small enough to accommodate a minimum of eight load steps to failure. Between each of the load steps, mechanical expansions were measured, cracks were marked, and the width of the largest diagonal crack (if present). was recorded. Photographs of the test region were used to document the propogation of cracks and the final failure was documented on a video camera.

Each bent cap specimen was designed to yield two separate tests at shear span-to-depth ratios of 3.00 (sectional shear) and 1.85 (deep beam shear). For the current series of specimens (R1, R2, and nR1), the sectional shear span was always tested prior to the deep beam shear span. Each test was conducted as described above. Careful observations and continuous monitoring continued until a defintive shear failure occurred. Following failure of the sectional shear span, external post-tensioned clamps strengthened the

sheared portion of the beam. The hydraulic ram was then moved to the opposite end of the specimen and positioned for the deep beam shear test. When both ends were sheared, the beam was tranferred to the storage yard for further forensic testing (described in Section 4.4). The complete testing sequence is depicted in Figure 4-24.

Practical considerations excluded the alternate testing sequence. The loads required to fail the deep beam span would have caused heavy cracking within the untested sectional span. Such a precondition may have skewed the sectional test results in an unrepresentative manner. These concerns were not unfounded. Similar difficulties were encountered during the pilot test (refer to Chapter 3). As the deep beam shear span approached failure, large cracks appeared on the untested alternate span (subjected to sixty-five percent of its ultimate capacity). The beam was immediately unloaded. External post-tensioned clamps were then used to reinforce the sectional span while the remainder of the deep beam test was completed. In contrast, leadoff testing of sectional shear span only subjected the deep beam test region to a maximum of forty-five percent of its ultimate capacity. Diagonal cracks were observed in one test, but were not of sufficient width to cause concern.

The structural testing results are examined within the context of the specimen deterioration in Chapter 5. Photographs relevant to each shear span test may be found in Appendix B.

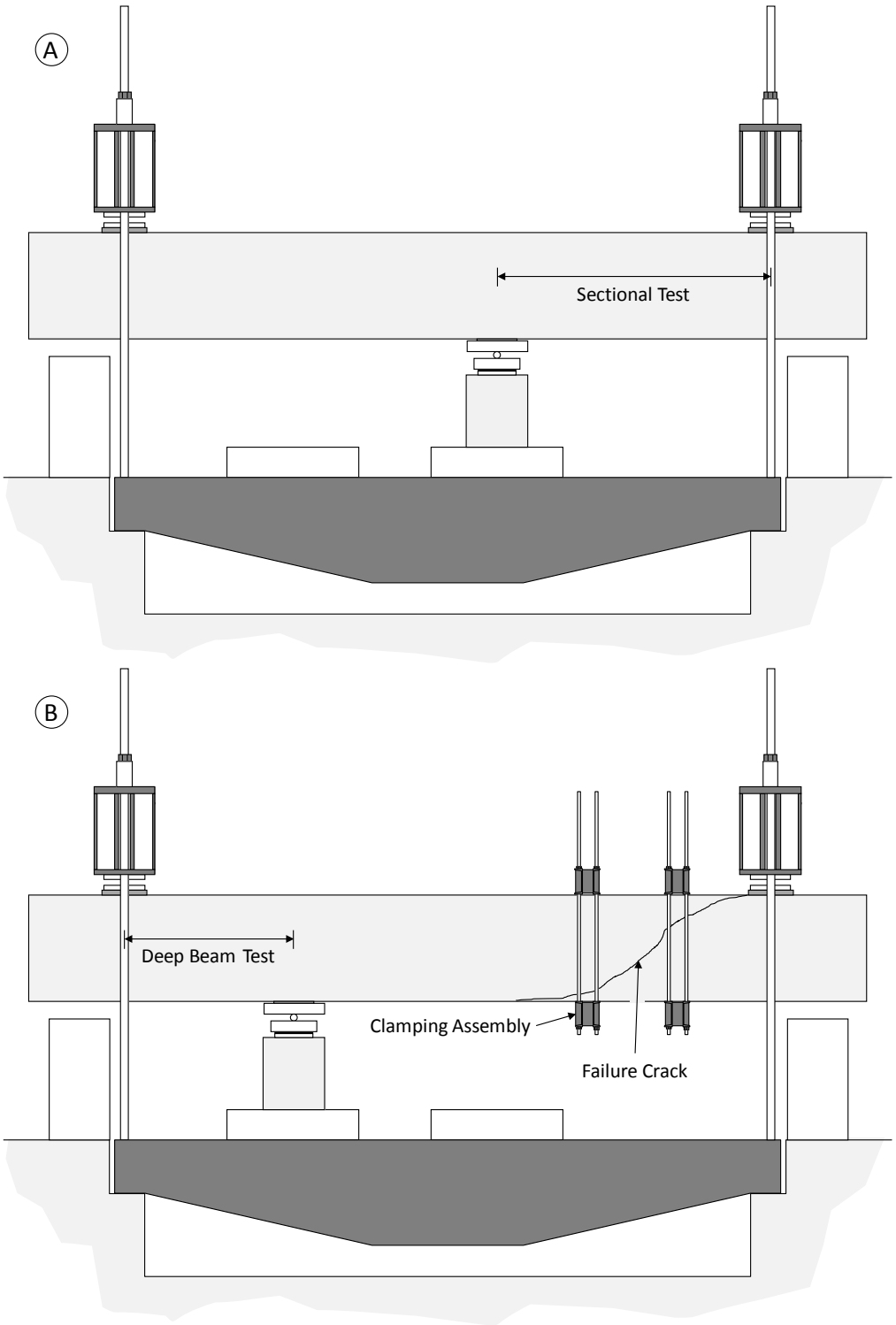

Figure 4-24: Testing Sequence (A) Sectional Test (B) Deep Beam Test

4.4 PHASE III: FORENSIC ANALYSIS

Current assessment guidelines (e.g. Fournier et al. 2004, Folliard et al. 2007) call for a myriad of laboratory tests and field inspections to establish the cause, extent and future potential of the premature concrete damage. The recommended methods are often geared toward evaluating the performance of the concrete material and not the structure as a whole. In fact, language regarding structural assessment is decidedly vague in most documents. Consulting engineers are therefore left to interpret the results of tests which may not even have relevance to the immediate task of assessing structural safety. This discussion is not meant to disparage the use of these guidelines. They are excellent references for the diagnosis and mitigation of ASR/DEF-related *durability* concerns. However, it is recognized that significant work is left to be accomplished in the realm of ASR/DEF-related *structural* concerns.

A number of forensic techniques were therefore selected for implementation during the current study. Collectively the techniques accomplish all three goals of the aforementioned assessment guidelines; i.e. establish the (1) cause, (2) extent and (3) future potential of the deterioration. To first identify the nature of the bent cap deterioration, a number of concrete samples were sent out for petrographic evaluation (Section 4.4.1). The extent of the damage was then quantified through the estimation of expansive strain (Section 4.4.2) and measurement of material strength loss (Section 4.4.3). Finally, residual expansion tests were used to estimate the future deterioration potential (Section 4.4.4). Data gathered during Phases I and II formed a basis on which to assess the accuracy and relevance of each technique. Furthermore, the direct *assessment* of near full-scale structures provided insight into the potential for future field implementation of the methods. First-hand impressions and final recommendations are presented within Chapter 5.

4.4.1 Diagnosis of ASR/DEF Deterioration

Due to the preconceived nature of the current study, the petrographic evaluation did not serve its traditional role. The evaluation was instead tailored to provide insights into the *character* (and not necessarily the *cause*) of the deterioration. The following paragraph provides a description of, and underlying motivation for, each task performed during the petrographic evaluation.

First, a written description of the microstructural damage due to ASR and DEF was requested. Common features were to be illustrated by visual documentation (photographs,

scanning electron imagery, etc.). The final document would provide third-party validation of the deterioration and ultimately allow the relative contributions of ASR and DEF to be qualified. Second, the predominant orientation of ASR/DEF-related microcracks was to be documented at a number of sections along each core length. Characterization of the crack network would clarify the role of restraint in the development of microstructural damage within both core and cover concrete. Finally, a qualitative ranking of the cores by the damage severity was desired. A total of six cores, one from each shear span of the first series (R1, R2, nR1), were submitted for evaluation. Correlation between the qualitative ranking and the documented expansions would be studied. Results would be used in a preliminary assessment of petrographic *damage rating* techniques.

The cores were extracted, stored, and transported shortly after the conclusion of Phase II. A detailed description of the coring procedures, along with an illustration of common extraction points, is provided within Section 4.4.3. Evaluation of the cores was performed by petrographers at the Texas Department of Transportation Concrete Laboratory. Information regarding the origin of the cores and the general purpose of the petrographic evaluation was not disclosed to the TxDOT personnel. This ensured that the evaluation would not be subject to any external bias. Petrographers completed all of the tasks described above using procedures recommended within *Petrographic Methods of Examining Hardened Concrete*; a petrographic manual published the Federal Highway Administration. Results of the final report are summarized within Chapter 5.

4.4.2 Estimation of Current Expansive Strains

Determination of the current expansive strains within an affected concrete structure is difficult, but ultimately necessary. In the absence of a suitable datum, engineers are faced with the challenging task of estimating expansion via indirect measurements. Knowledge gained through these measurements is potentially invaluable. An accurate estimate of the current expansive strains would allow an engineer to confidently explore the consequences of ASR/DEF deterioration in quantifiable structural terms. Unfortunately, currently available estimation methods are frequently dismissed by researchers and practitioners alike as overly cumbersome, inaccurate, or a combination of the two. Resolution of this long-standing deficiency would substantially improve the validity of future assessment efforts.

The estimation techniques studied here were limited to those which promised fast, *sufficiently* accurate results. This limitation was a direct result of the sponsor's expressed need for rapid assessment techniques (Vogel 2006). Repair or replacement of each

structure within TxDOT's damaged inventory needed to be quickly prioritized to ensure that future budget outlays could accommodate such costs. Following the literature review, two simple methods were selected for implementation: (1) surface crack width summation and (2) in-situ reinforcement testing. Both methods were to be used in the field and would not require cores to be taken for laboratory testing. Each method employed measurements of ASR/DEF-related structural phenomena. As a result, the structural context of the deterioration was not lost and dependency on highly-variable material factors was eliminated.

4.4.2.1 Surface Crack Width Summation

Surface cracking is the result of differential expansion which occurs between the cover layer and core of an affected concrete member. The phenomenon, as related to ASR, was first explained by Hobbs in 1988. Initial exposure of the concrete surface to wetting-and-drying cycles results in leaching of the alkalis necessary for cover layer expansion. The unaffected concrete core soon begins to expand, causing the non-reactive cover layer to go into tension. If sufficient expansion occurs, visible cracks are formed within the cover concrete. The surface cracks are a therefore a singular manifestation of the core expansion. In fact, the sum of the crack widths divided by the length over which they were measured should equate to the total core expansion minus the initial cracking strain of the concrete.

The use of surface crack width summation for the estimation of in-situ expansions was first recommended by the Institution of Structural Engineers (ISE) in 1992. The proposed method required the consulting engineer to measure the width of all surface cracks intersecting a parallel set of five one-meter long reference lines. The total deformation due to deterioration was then assumed to be equal to the sum of all the cracks widths divided by the total length of the reference lines. The practicality of the method was undeniable. It was non-destructive, inexpensive, and easy to implement. It was also recognized that results from the method did not *perfectly* correlate with laboratory expansions (Chana and Korobokis 1992). Despite this fact, it was held in sufficient regard to be used extensively within a late twentieth century survey of damaged highway structures in the United Kingdom (ISE 1992).

Following the ISE recommendation, the estimation method was subjected to further scrutiny. In 1994, Jones and Clark published a document examining the *practicalities* of crack width summation. In addition to providing a summary of earlier works, they reported results obtained from the expansion monitoring of seventy-two cylinders and

eight small-scale beams. Based on the data gathered, the researchers highlighted a number of factors (size and shape of member, restraint present, depth of cover, etc.) leading to *poor* correlation between the crack width summation technique and measured expansions. In 2004, a similar assessment was made by Smaoui following the study of fifty-one blocks and fourteen slabs (both of small-scale). Field application of the technique by Berube in 2005 ultimately led to a strikingly different judgment.

> *The measurement of crack widths at the surface of the concrete members under investigation appeared to be a rather reliable method for estimating the expansion to date as long as the measurements were made on the most severely exposed sections of the members investigated (Berube et al. 2005).*

Furthermore, it was suggested that earlier results yielded poor correlations due to their limited size relative to commonly affected field structures. The current study therefore provided the perfect opportunity to successfully validate the method's application to full-scale structures.

The surface cracks were measured on two separate occasions during the course of the study. The first crack survey was completed shortly before the first series specimens were transferred to the laboratory floor. To begin, all twenty-eight of the mechanical gage lengths (shown in Figure 4-9) were traced on the surface of each reactive beam. A crack comparator card was then used to measure the width of all cracks intersecting the marked reference line (Figure 4-25). The sum of the widths was then divided by the initial gage length (as measured by the extensometer at the beginning of the Phase I) to obtain an estimate of the in-situ expansion. The second survey was completed approximately six months afterward and only included reactive specimens R3 and R4. A total of 168 expansion estimates were obtained during the two crack surveys. Placement of the reference lines along each of the established gage lengths allowed direct comparison between the estimates and Phase I monitoring results.

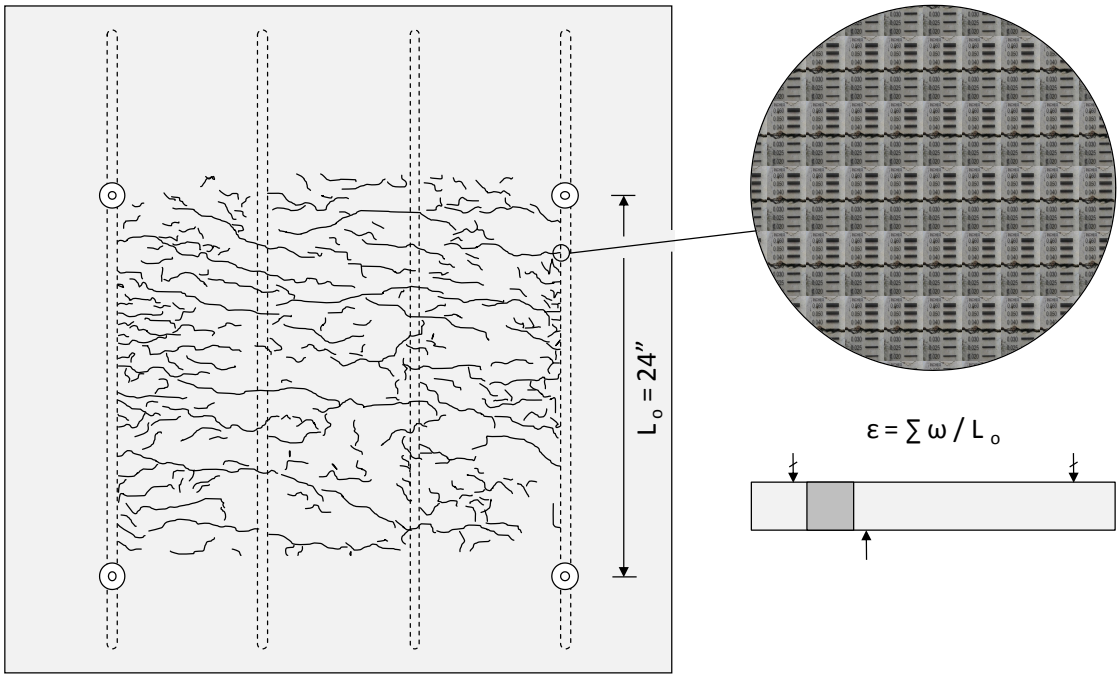

Figure 4-25: Summation of Crack Widths over Established Gage Lengths

To avoid potential confusion, a short note on the applicability of cover expansions is necessary. The measurement of cover expansions was dismissed in Section 4.2.4.1 for several reasons, but most importantly for potentially inaccurate results. It must be recognized that *accuracy* is a relative term. In laboratory applications, measurements frequently serve as standards for the comparison of results and the development of general models. A high level of accuracy is therefore necessary. However, in the current context of structural evaluation, measurements are not held to such a high standard. The ultimate goal is not to obtain a perfectly accurate measurement. Rather, it is to ensure a *sufficiently* (as determined by the user) accurate and more importantly, *conservative* estimate. The accuracy and conservatism of the techniques discussed here will be examined in the following chapter.

4.4.2.2 In-Situ Reinforcement Testing

Assuming the maintenance of perfect bond, expansive strains within the affected concrete and confining reinforcement should be equivalent. The previous statement implies that evaluation of the reinforcement could serve as an alternate means for the estimation of expansions. The time-dependent development of expansions within a reinforced concrete member is reviewed below. Based on the review, the feasibility of an in-situ

reinforcement test is examined and the implicit limitations of such an approach are identified. Finally, a testing procedure outlined within the literature is adapted for the purposes of this study.

At the outset of ASR/DEF deterioration, the reinforcement and concrete are only subject to stresses resulting from the application of external loads. In a large reinforced concrete bent cap, stresses due to superimposed dead loads and traffic will amount to a small fraction of the elastic limit for both steel and concrete. Over time, the growth of concrete expansions will lead to the development of significant tensile strains within the reinforcement. The resulting tensile stress within each reinforcing bar is accommodated by an equivalent amount of compression within the concrete; effectively acting as a self-equilibrating system. It should be noted that the reinforcement induced-compression generally reduces the rate and magnitude of the concrete expansions, but never restricts them completely. Reinforcement yield is therefore unavoidable when expansions are sustained for long periods. Furthermore, reinforcement fracture may be a possibility in certain circumstances (please refer to Chapter 2).

The only apparent method for obtaining the reinforcement strain is to expose, cut, and measure the shortening of a *highly-stressed* reinforcing bar (shown in Figure 4-26). *Highly-stressed* is emphasized for good reason; such a test is not appropriate for the evaluation of a structure which only exhibits the earliest signs of deterioration. In that case, ASR/DEF-induced strains would not be sufficiently distinguishable from those due to routine traffic loads. This approach does have one other limitation: strains in excess of the reinforcement yield will not be detectable. As a result of the cut, *elastic* unloading of the reinforcement will occur and the measurable rebound will never exceed the reinforcement yield strain. Despite these limitations, the technique could be of substantial value to consulting engineers who only wish to identify ASR/DEF-induced yielding. A number of researchers (Berube et al. 2005, Fournier et al. 2004) have suggested an expansion threshold corresponding to the reinforcement yield strain. As recommended, exceedance of the threshold would alert the engineer to the need for a more detailed investigation of the structural safety (Folliard et al. 2007).

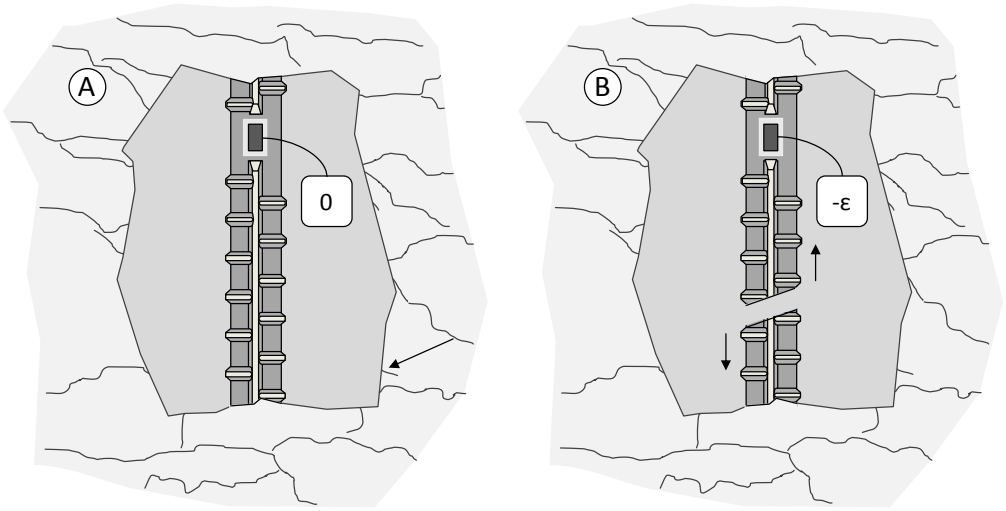

Figure 4-26: Elastic Rebound Test (A) Exposed Reinforcement with Strain Gauge (B) Cut to Relieve Tension and Measure Elastic Rebound

In 1994, Danay took a structural mechanics approach (similar to the current strategy) to the diagnosis and assessment of an ASR-affected concrete dam. In an effort to establish the state of stress within the structure, Danay implemented the abovementioned technique. First, a short length of a reinforcing bar was exposed and instrumented with a standard foil strain gage. An electric saw was then used to sever the exposed reinforcing bar. Contraction of the bar (initially in tension) was recorded via the strain gage. The in-situ stress of the reinforcement was subsequently obtained through application of the elastic modulus for the steel. Although significant scatter was noted, strain results obtained from several reinforcement tests were in general agreement with the range of expansions estimated via alternate means (crack analysis, overcoring, etc.).

Application of the elastic rebound test (shown in Figure 4-27) was limited to the transverse reinforcement in the current study. Testing of the longitudinal reinforcement was not considered due to poor prospects for future field implementation. While it may be feasible to select and test a lightly loaded (perhaps nonessential) stirrup, it is unlikely that an engineer will consent to the destructive testing of flexural reinforcement. In any case, stirrups strains will most likely be the subject of deepest scrutiny due to the predisposition for transverse expansion in bent caps.

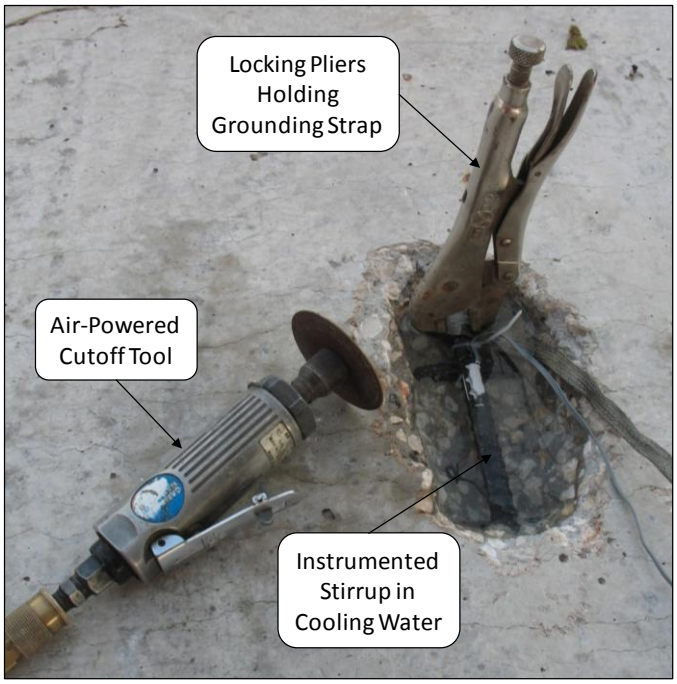

Figure 4-27: Elastic Rebound Test

Shortly after the conclusion of Phase II, a total of six elastic rebound tests were conducted on the first series specimens. Each individual test was carefully positioned within one of the sheared deep beam spans. Regions of little to no load-induced cracking were selected to ensure the most representative estimates of expansion. Typical test locations can be seen in Figure 4-29. Similar diagrams for all of the forensic tests can be found within Appendix C. The abovementioned test procedure served as a model for the current implementation. A small segment of the reinforcement (approximately six inches in length) was first exposed using an electric jackhammer. The task was approached delicately to minimize prying or impacts that would disturb the in-situ state of stress. The reinforcement was then cleaned and instrumented using the methods described in Section 4.2.4.2. When the electrical strain gage adhesive had adequately cured, a portable data acquisition unit was connected. The grounding strap shown in Figure 4-27 was necessary to eliminate electrical interference during the test. The hole was then filled with water to control the temperature of the electrical strain gage during the cutting process; each specimen had been previously laid on its side to facilitate the forensic tests. Compressive strain was continuously monitored as an air-powered cutoff tool was used to sever the reinforcement. Final values reported within Chapter 5 were recorded after all dynamic effects of the reinforcement release had dissipated.

4.4.3 Determination of In-Situ Concrete Properties

Mechanical testing of concrete cores has historically served as the primary basis for the structural retrofit of ASR/DEF-affected structures. While the caution exercised by the consulting engineers cannot be questioned, the loss of safety inferred from such testing is generally not supported by structural test data (as presented within Chapter 2). In spite of this assertion, a number of mechanical tests were included within the current study. Testing of the near full-scale specimens provided a fresh opportunity to examine the applicability of strength predictions obtained via in-situ mechanical properties (and concurrent consideration of existing strains/stresses). Mechanical testing of the cores from the first series specimens will be discussed following the development and implementation of a coring methodology.

Due to the anisotropic nature of the deterioration within each shear span, the concrete sampling process required an unusual amount of forethought and planning. Two important criteria guided the extraction of samples for mechanical testing. First, the samples were to be representative of the concrete components (i.e. struts in compression or webs in tension) controlling behavior of the individual shear spans. Second, deterioration within each sample had to produce conservative estimates of material strength and stiffness. To illustrate the subsequent thought process, the criteria are examined within the context of the deep beam shear span (shown in Figure 4-28). Ideally, the most representative sample would be extracted from the axis of the strut and subsequently tested in compression. However, extraction through the heavy longitudinal reinforcement was not feasible within the laboratory study nor (more importantly) future field evaluations. Samples would simply have to be taken within the vicinity of the test region. Therein two options existed; cores could be extracted through the width or length of the bent cap. An overall greater level of deterioration within the sample would lead to more conservative test results. Accordingly, cores were taken through the width of the section (transverse as noted in Figure 4-28A) as it was subject to the least restraint, and theoretically, the most severe deterioration.

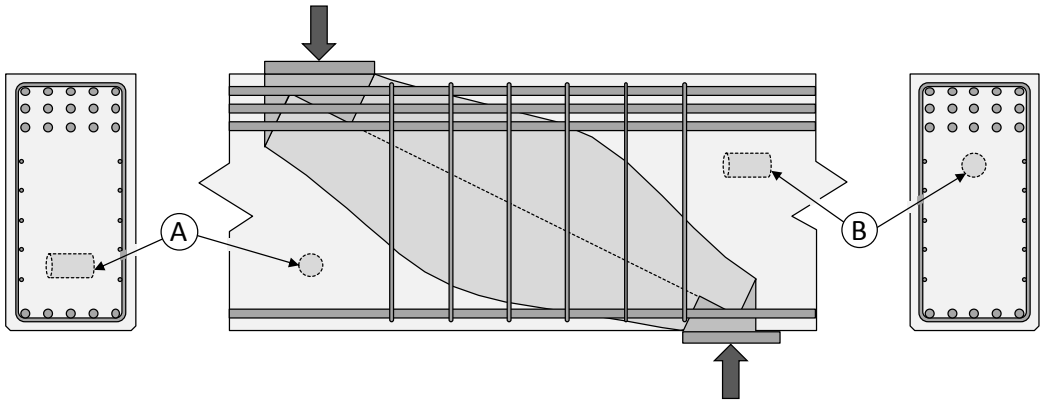

Figure 4-28: Potential Core Orientations in Relation to Reinforcement Restraint and Ultimate Load Path (A) Transverse (B) Longitudinal

Typical core extraction locations for the first series specimens are illustrated in Figure 4-29. Analogous diagrams for each beam can be found within Appendix C. Sampling was conducted at the conclusion of Phase II as a matter of simplicity. Following shear testing, each specimen was transferred to the storage yard and laid on its side. Cores were then taken within the vicinity of the test region, but outside the influence of load-induced cracking. A total of thirty-eight cores were ultimately extracted from the six test regions sheared during Phase II. As mentioned earlier, a fraction of the cores (six to be exact) were reserved for petrographic evaluation (Section 4.4.1). All others were subjected to compression or splitting tension tests (as described below).

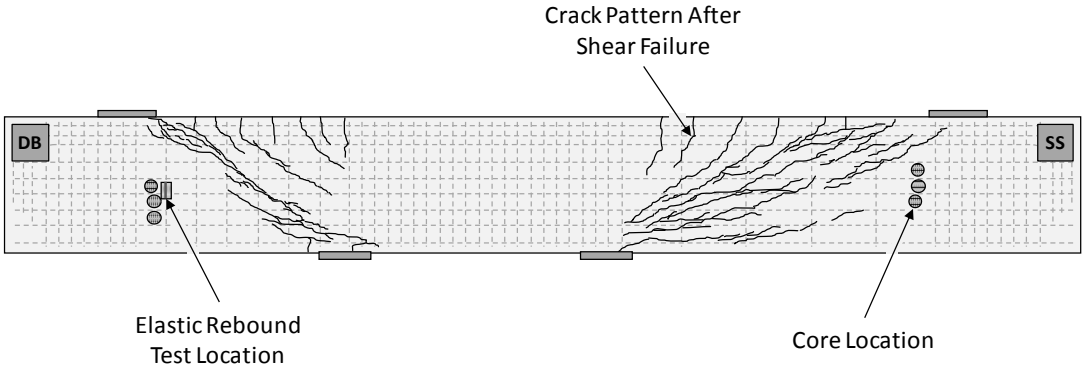

Figure 4-29: First Series Specimens - Forensic Test Locations

All of the samples were extracted using a coring system outfitted with a four-inch diameter diamond core bit and powered by a 5000 watt generator (shown in Figure 4-30). Prior to installation of the coring system, the location of the reinforcement was marked

on the concrete surface. The bit was then aligned and advanced halfway through the section. Following the removal of the first segment, an extension was placed on the core bit to allow removal of the remaining cross-section width. Each sample was towel dried immediately after extraction and then allowed to air dry for a maximum of one hour. Plastic wrap and a plastic bag were used to seal each core against further moisture loss during the interim period between extraction and testing. All relevant procedures found within ASTM C42 were implemented during the sampling process.

Figure 4-30: First Series Specimens - Extraction of Cores

Prior to mechanical testing, the cores were prepared as required by ASTM C42, ASTM C39 (Compressive Strength), and ASTM C496 (Splitting Tensile Strength). A concrete saw was used to trim the rough cores to the appropriate length and aspect ratio. All core dimensions (length, diameter and respective variations) were then measured before the application of sulfur caps and/or load. Records of these measurements can be found within Appendix C. Subsequent compressive and splitting tensile strength tests were conducted according to the guidelines set within the aforementioned ASTM documents. Load was applied at the recommended rate via a 400-kip compression machine dedicated to material testing. The machine configuration for both tests is shown below in Figure 4-31. In addition to noting the failure stress, qualitative observations were made regarding the relative performance of the reactive and non-reactive samples under load. It

should be noted that all preparation tasks and mechanical tests described above were conducted soon after the original core extraction date; moisture loss and potential relaxation of the damaged samples were thereby minimized.

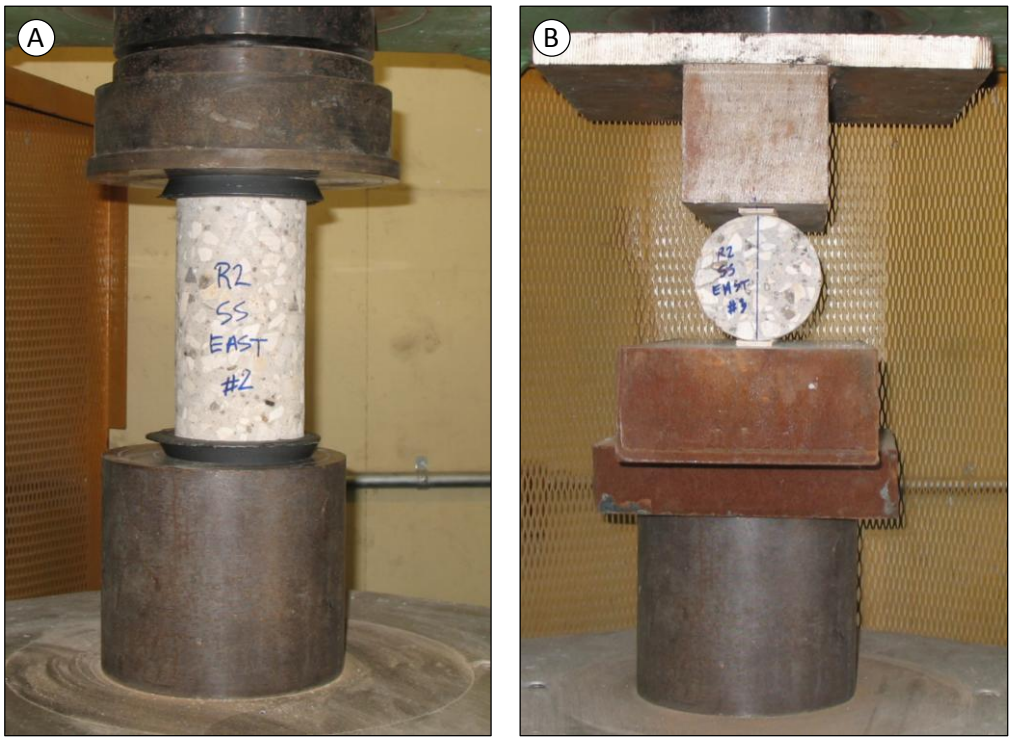

Figure 4-31: Mechanical Tests on Extracted Cores
(A) Compressive Strength (B) Splitting Tensile Strength

Concrete properties obtained from both cores and conventional cylinders (introduced at the end of Chapter 3) are compared within the following chapter. Recommendations for the use of core-based strength predictions are made.

4.4.4 Estimation of Future Expansion Potential

A number of assessment guidelines recommend the use of expansion testing on cored samples. As described by those authoring the guidelines, the tests typically serve two purposes: (1) to evaluate the future expansion potential of the affected concrete, and more generally, (2) to establish if the concrete is susceptible to further ASR or DEF. It has been suggested that this information can be used to successfully plan the future maintenance of a damaged structure. While this is certainly true for the application of mitigating (durability-related) treatments, the information may have limited value in the structural

evaluation process. Researchers, including Fournier (2004), have questioned the suitability of expansion testing due to the "unknown true correlation between *free expansion* of cores and the actual expansion in reinforced concrete members." To further investigate these claims, expansion testing procedures outlined within Folliard's *Protocol for the Diagnosis and Prognosis of Concrete Structures Affected by ASR and/or DEF* (2007, referred to as the *Protocol* from herein) were implemented within the current study.

In contrast to the conservative approach advocated above, the *Protocol* recommended the extraction of several cores that would collectively represent the full spectrum of damage found with a given structure. Cores were to be selected from "good, bad, and indifferent" regions of the affected concrete member. In reference to the condition of the cores upon extraction, "good" cores would be relatively undamaged, while "bad" cores would be subject to the heaviest deterioration. "Indifferent" cores would fall somewhere in between. Rather than relying on subjective visual assessment of the specimens, selection of the three sampling regions was completed via a rational consideration of the reinforcement restraint. "Good" cores were therefore extracted from the region of highest restraint (end blocks), while "bad" cores were extracted from region of least restraint (sectional shear span). A typical layout of the sampling locations within a second series specimen is shown in Figure 4-32. Please note that future interference with structural tests was minimized by sampling outside the expected failure load paths (as observed during Phase II).

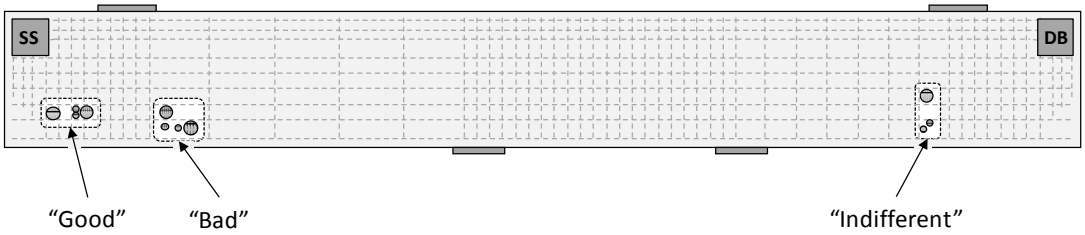

Figure 4-32: Second Series Specimens - Forensic Test Locations

All of the cores were extracted while the second series specimens continued to condition at the FSEL exposure site. A fair amount of additional labor was required to setup the coring system for the horizontal extraction of cores (shown in Figure 4-33). Aside from difficulties related to the upright orientation of the specimens, the sampling process was straightforward. Coring procedures detailed with Section 4.4.3 were implemented in the same manner as before.

Figure 4-33: Second Series Specimens - Extraction of Cores

A minimum of nine cores (three per sampling region) were extracted from each second series specimen for the expressed purpose of conducting residual expansion tests. Additional samples (outlined in Appendix C) were taken for future petrographic evaluation and water-soluble alkalis tests, but the results are not reported within this document. One sample from each region ("good" G, "bad" B, and "indifferent" I) was included in each of the expansion tests recommended by the *Protocol*. The overall testing program is outlined in Figure 4-34 and detailed below.

- *ASR Expansion Potential* - Test A (as designated in the *Protocol*) was designed to rapidly evaluate the maximum potential of future ASR-induced expansions. Two-inch diameter samples were subjected to high temperatures (176°F) and an infinite supply of alkalis to isolate ASR deterioration and suppress DEF. It should be noted that the test provides an upper bound limit for ASR-related expansion; an adequate supply of alkalis may not exist within the concrete structure in question.

- *DEF Expansion Potential* - Test B was designed to assess the potential of future DEF-induced expansions. Two-inch diameter samples were submersed in lime water at room temperature (73°F). The storage

conditions promoted the leaching of alkalis, which suppressed the development of ASR and triggered DEF. Theoretically, only samples taken from structures exposed to curing temperatures in excess of 158°F should exhibit DEF-related expansion during this test.

- *PCD Expansion Potential* - Test C was designed to provide realistic estimates of expansion due to either of the premature concrete deterioration mechanisms. Four-inch samples were subjected to elevated temperatures (100°F) and close to one hundred percent relative humidity. The storage conditions led to the concurrent development of ASR and DEF. While the temperatures were sufficiently high to accelerate ASR, the moist environment also allowed adequate leaching of alkalis to trigger DEF.

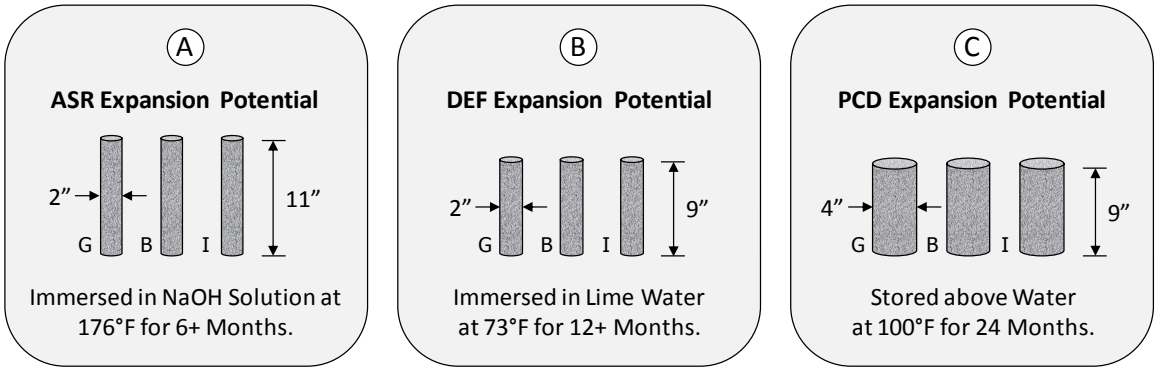

Figure 4-34: Residual Expansion Testing Per Specimen

Following extraction of all the necessary cores, each sample was trimmed to length and outfitted with gauge studs (Figure 4-35B). The completed specimens were then allowed to acclimate (over a one day period) in their respective conditioning environments prior to initial length measurements. Subsequent length change of the samples was measured weekly (via comparator, Figure 4-35A) for a minimum of five months. Residual expansion tests, A and B, could not be sustained for the recommended durations due to manpower restrictions. Nonetheless, preliminary data gathered from all three tests provided insight into the applicability of residual expansion testing.

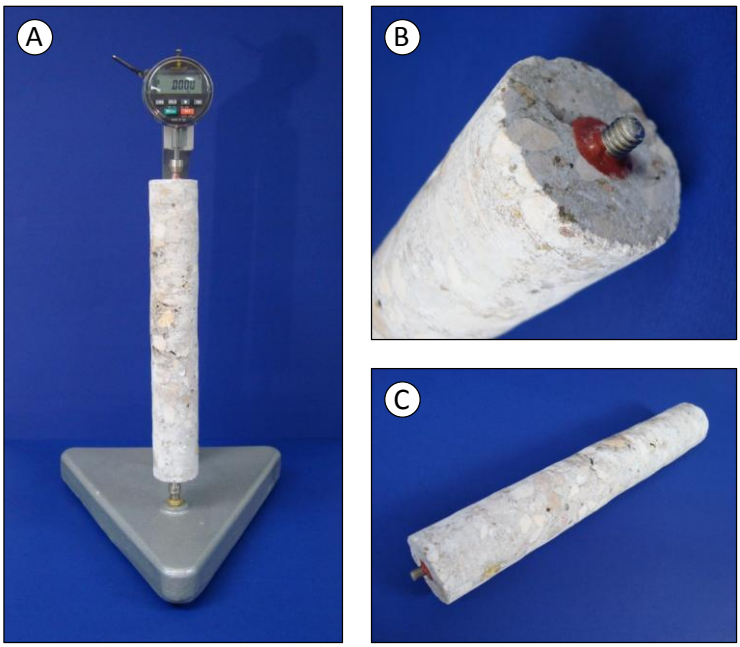

Figure 4-35: Residual Expansion Testing
(A) Digital Comparator (B) Gauge Stud Set in Epoxy (C) Completed Core Specimen

The measured expansion of the second series specimens (R3, R4, nR2) serve as the basis for comparisons made within Chapter 5. A subsequent discussion regarding the utility and expense of such testing will ultimately allow the practicing engineer to form his/her own opinion of the method.

4.5 SUMMARY

Following fabrication, all six of the bent cap specimens were moved to an exposure site outside of Ferguson Structural Engineering Laboratory. The three-phase experimental study reviewed within this chapter formally commenced at that point. Ensuing results from each phase provided much needed insight into the performance and evaluation of ASR/DEF damaged bent structures. General observations, recommendations and conclusions are presented within Chapter 5.

Phase I (Specimen Conditioning and Expansion Monitoring) detailed efforts to trigger field representative ASR/DEF deterioration and monitor subsequent expansions. Prolonged exposure to heat and moisture was critical to the progression of the ASR/DEF deterioration. Each bent cap was moved outside Ferguson Structural Engineering Laboratory (FSEL) to maximize exposure to Austin's mild climate. To keep the reactive

concrete moist, a timed watering system subjected the specimens to frequent wet-dry cycles. Application of a constant-magnitude service load then provided an appropriate structural context for the deterioration. Subsequent concrete expansions and steel strains were measured by using a well-crafted, robust set of instrumentation.

Phase II (Shear Testing) featured the unique facilities and methods used to test three of the six large-scale bent caps. The first series bent cap specimens (R1, R2, nR1) were tested in the summer of 2008. A wide range of ASR/DEF-related damage had developed during the course of the previous eight to twelve months. While the most severe deterioration produced expansions well in excess of the reinforcement yield strain, the non-reactive control specimen remained undamaged. Following selection, the bent cap specimens were prepared for structural testing. ASR/DEF-related cracking was documented. The beams were then unloaded and brought into the laboratory. The Large-Scale Beam Testing Facility at FSEL easily accommodated the loads necessary to test each span in shear. Instrumentation captured all the forces, deformations and strains necessary to characterize each test. Careful planning and unique repair techniques ultimately made all six of the shear tests possible. The remaining three second series specimens (R3, R4, nR2) were left to condition under load and moisture for an extended (and undefined) period of time. It was noted that data collected from those test regions would help to answer questions related to the long-term effects of ASR/DEF deterioration.

Phase III (Forensic Analysis) was an examination of structural evaluation techniques, reported within the literature and/or commonly recommended in assessment guidelines. The techniques were collectively selected to determine the cause, extent, and future potential of the expansive mechanisms. To first identify the cause of the bent cap deterioration, a number of concrete samples were evaluated via traditional petrographic techniques. Particular instructions to the TxDOT personnel conducting the evaluation were outlined. The extent of the damage was then quantified through the estimation of expansive strain. Specifically, implementation of the crack width summation technique and in-situ reinforcement test was described in detail. Following the development and implementation of a coring methodology, in-situ concrete properties were established via mechanical testing. Finally, residual expansion tests were used to estimate the future deterioration potential due to ASR and/or DEF. The purpose and procedures for three distinct expansion tests were reviewed. It was noted that the data gathered during Phases I and II formed the basis for the assessment of each technique. The direct application to the bent cap specimens also provided insight into the potential for future field implementation of the methods.

CHAPTER 5
Experimental Results

5.1 OVERVIEW

Measurements and observations made during the course of the three-phase experimental program (Phase I: Specimen Conditioning and Expansion Monitoring, II: Shear Testing, and III: Forensic Analysis) are reviewed within this chapter. Particular emphasis is placed on examining the relationship between the measured in-situ damage and the results from structural testing and forensic analyses. Conclusions drawn and recommendations made within this chapter are used to conduct the preliminary field assessment of an ASR/DEF-affected bent cap; presented in Chapter 6.

The development of ASR/DEF deterioration is presented through an examination of the expansion measurements and documented cracking patterns. Throughout Section 5.2, special attention is paid to the time-dependent influence of the various experimental operations (summarized in Figure 5-1). Impacts of the deterioration on the serviceability and strength of sectional and deep beam shear spans are then explored through the consideration of eight individual shear tests (six from the first series specimens and two from the pilot beam, Section 5.3). The second series specimens are excluded from this discussion; structural tests had not been completed before the publication of this report. Finally, the ability of the various forensic techniques to successfully establish the cause, extent and future potential of the deterioration is evaluated (Section 5.4).

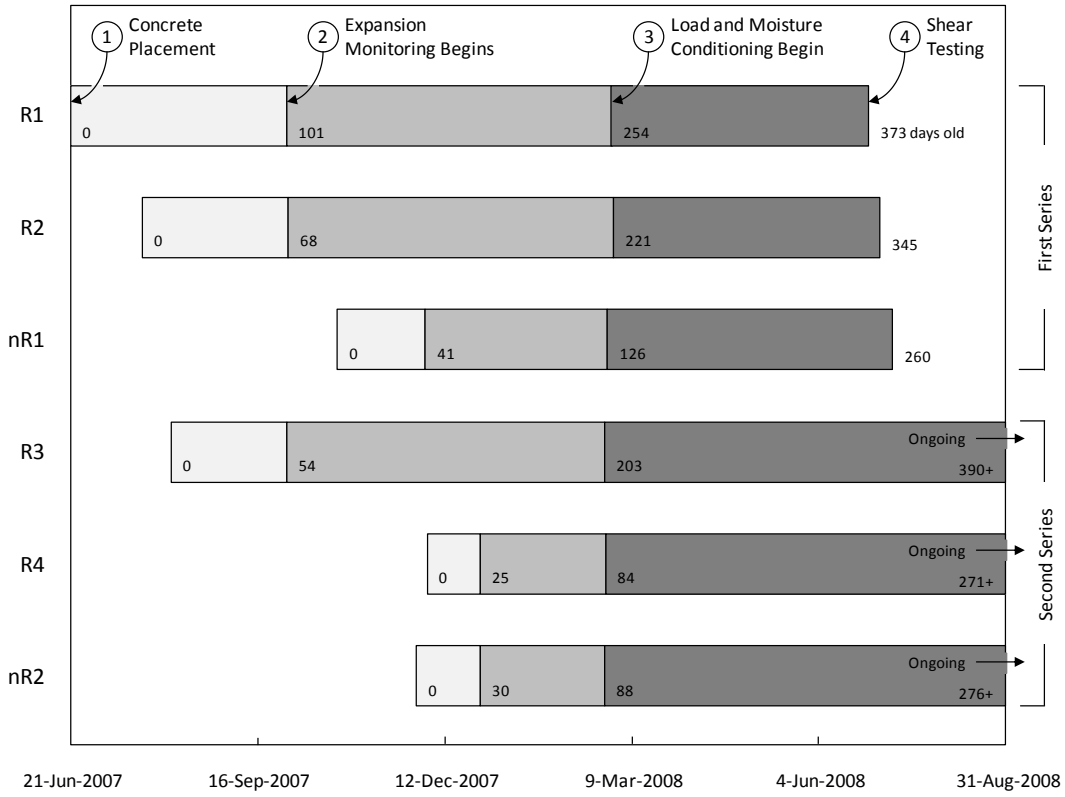

Figure 5-1: Timeline of Experimental Operations for First and Second Series Specimens

5.2 DEVELOPMENT OF ASR/DEF DETERIORATION

Sustained deterioration due to alkali-silica reaction and delayed ettringite formation leads to expansion and cracking of concrete members. In the current study, a carefully planned conditioning and monitoring program was implemented to investigate the structural impact of these phenomena on reinforced concrete bent caps (Phase I as described in Chapter 4). Measurements and observations made during the course of Phase I are reported herein. The tables and figures incorporated within this section collectively summarize the condition of each bent cap specimen and thereby serve as the basis for comparisons made within Section 5.3 (Live Load Behavior) and Section 5.4 (Forensic Analysis).

The following review of the specimen deterioration begins with a detailed exploration of the mechanical strain measurements. For each specimen, the time-dependent development of structural core expansion is examined within the context of the reinforced concrete section. The structure of the discussion facilitates a clear understanding of the

interaction between the expansive concrete and confining reinforcement (Section 5.2.1). Attention is then diverted to the external manifestation of ASR/DEF deterioration: surface cracking. Discussion of the test region cracking explores the influence of the reinforcement configuration and externally applied loads on the development of pattern damage (map and/or diagonal cracking). Photographs provided throughout the section will place the observed deterioration within the context of commonly noted field damage (Section 5.2.2). Please note that unless otherwise stated, the condition of the specimens is in reference to the pre-test (first series specimens – R1, R2 and nR1) or most recent (second series specimens – R3, R4 and nR2) measurements and observations.

5.2.1 Measured Expansions

The expansion histories for each of the ASR/DEF-affected bent caps are presented in a manner which reflects the interaction between the expansive concrete core and the confining reinforcement. The growth and variation of the structural core expansions within the reactive and non-reactive specimens are first examined with respect to time. Strains consequentially developed within the longitudinal and transverse reinforcement are then reviewed. Finally, compressive stresses imposed by the strained reinforcement are calculated and their subsequent impact on the development of the structural core expansions is evaluated.

To facilitate the following presentation of results, a consistent set of notation was developed. Examples of the notation as implemented during the discussion of measured expansions are presented below in Table 5-1. In general, the first subscript denotes the material being considered: "c" for concrete and "s" for steel. This provides a quick indication of whether core or reinforcement strains are being considered. The second subscript then denotes the direction of the measurement: "t" for transverse and "l" for longitudinal. As referenced throughout this document, longitudinal and transverse measurements are taken along the length and depth of the specimen, respectively.

Table 5-1: Notation for the Discussion of Measured Expansions

Term	Description
ε_{ct}	**c**oncrete core expansion in the **t**ransverse direction
ε_{cl}	**c**oncrete core expansion in the **l**ongitudinal direction
ε_{st}	**s**teel strain in the **t**ransverse reinforcement
ε_{sl}	**s**teel strain in the **l**ongitudinal reinforcement

5.2.1.1 Structural Core Expansions

Experimentally-significant core expansions (greater than 0.01%) were generally recorded within three to five months of the concrete placement. In virtually all of the reactive test regions, a short period of slow growth was followed by rapid and seemingly unrelenting expansion in the transverse direction (ε_{ct}). The structural core expansion history for specimen R2 is summarized in Figure 5-2. During the peak expansion period, the sectional shear span of R2 was expanding in the transverse direction by one tenth of a percentage point (0.1%) every thirty days. To put the expansion rate into perspective, one should consider that the yield point of grade 60 reinforcement corresponds to a strain of about two tenths of a percentage point (0.2%). It should also be noted that this observation is only presented to demonstrate the powerful nature of the deterioration encountered within this study. Such a high rate of expansion is unlikely to be encountered within practice, but herein essential to produce much needed experiment results in a timely manner.

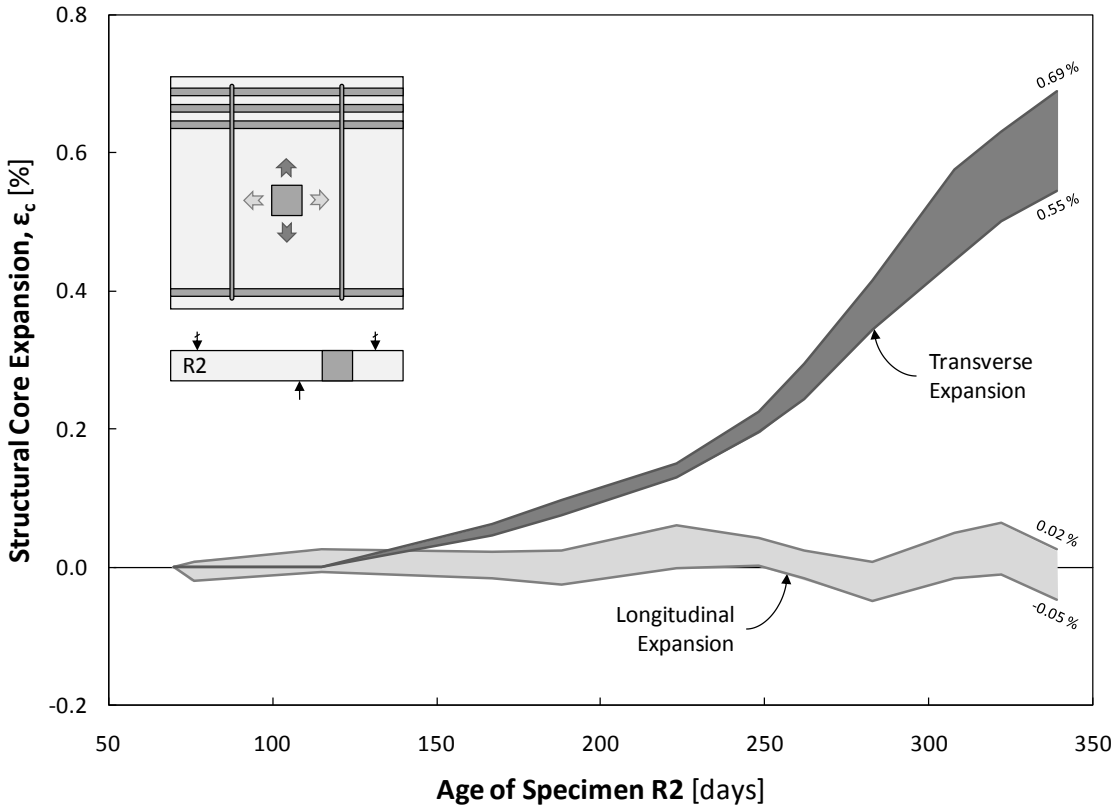

Figure 5-2: Typical Range of Structural Core Expansions for a Reactive Specimen

The longitudinal core expansions (ε_{cl}) of each test region were generally insignificant (less than 0.1%) when compared to the long-term transverse expansions. For the duration of the exposure period, the longitudinal expansion of specimen R2 fluctuated between a maximum expansion of 0.06 percent and a maximum contraction of 0.05 percent. Virtually no net longitudinal expansion was measured at the time of structural testing; as was the case with nearly all of the specimens. The aforementioned behavior was not unexpected. Based on literary evidence summarized within Chapter 3, anisotropic (predominantly transverse) expansion was found to be characteristic of ASR deterioration occurring within reinforced concrete bent caps. The behavior was speculated to be the result of two circumstances: (1) there is an inherent (overwhelming) disparity in the restraint capacity of the transverse and longitudinal reinforcement found within a typical bent cap, and (2) ASR-affected concrete has a natural tendency to expand in the direction perpendicular to the casting plane (vertically). To further substantiate the broad assertion made within Chapter 3 and thereby validate the field-representative nature of the measured deterioration, key experimental evidence (reinforcement strains and imposed stresses) is examined later within this chapter.

Structural core measurements from the non-reactive specimens simply provide a point of reference for the aforementioned reactive behavior. The core expansion history for the sectional test region of specimen nR1 is presented in Figure 5-3. While the structural core appears to undergo cycles of slight expansion and contraction, the behavior is most likely attributable to the effects of climatic variation (for which the thermal expansion coefficient could not compensate). Additionally, one must consider that these measurements do not take into account the appreciable shrinkage which occurred between the concrete placement and the start of expansion monitoring (please refer back to Figure 5-1 for the sequence of experimental operations). The time-dependent variations seen in Figure 5-3 were therefore dismissed from further consideration and the efforts to control the deleterious expansion were deemed successful. Since noteworthy expansion was not observed within the four non-reactive test regions, discussion regarding their long-term performance is limited to the information above. Please refer to Table 5-4 at the end of this section for a summary of all relevant expansion monitoring results.

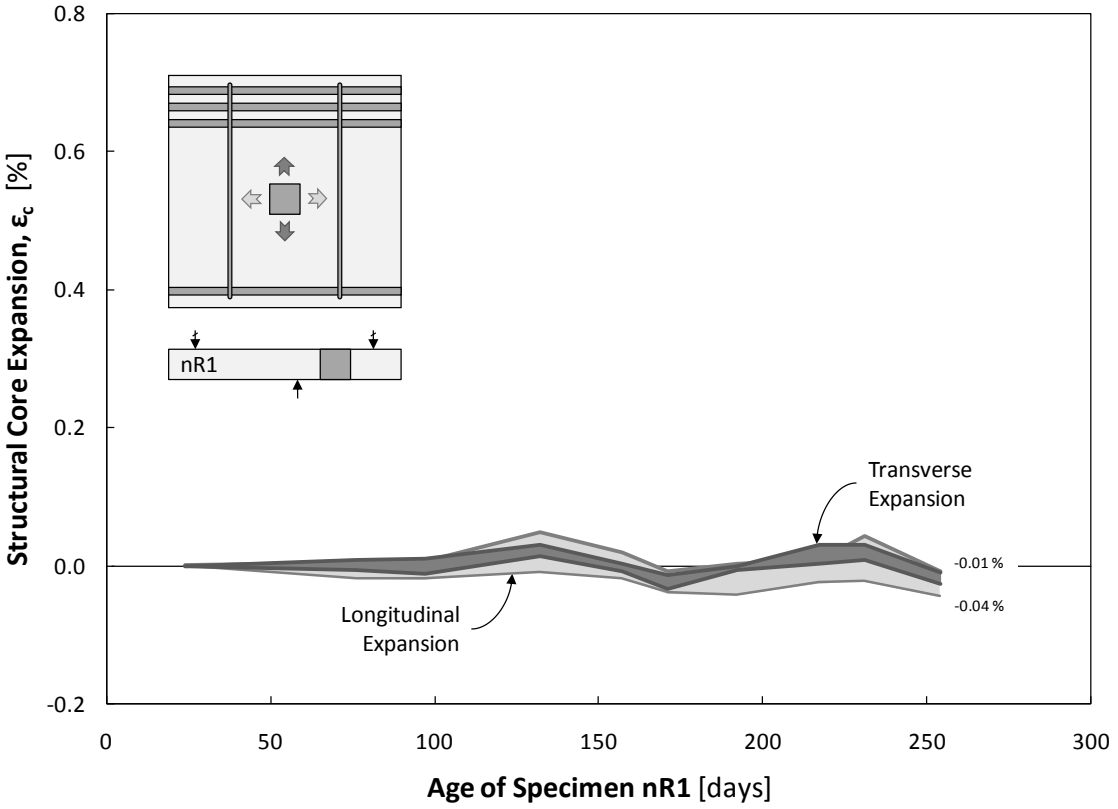

Figure 5-3: Typical Range of Structural Core Expansions for a Non-Reactive Specimen

A few additional observations regarding the role of certain external factors (reinforcement configuration, spatial variability of the deterioration, and initial curing temperatures) will complete the discussion on the structural core expansions. First, it is important to recognize that the time-dependent variation of longitudinal expansions within the reactive and non-reactive specimens was virtually identical. When plotted on a calendar basis, the measured longitudinal expansions are of similar magnitude and time-dependent profile; absolute high and low values correspond to the same point in time. This similarity suggests that the slight longitudinal expansions reported for the reactive specimens are not attributable to ASR or DEF. As indicated earlier, the measured values are more likely the result of external factors for which no compensation could be made. This evidence ultimately raises doubt on the role of the reinforcement in the development of the anisotropic expansion.

Secondly, the relatively small variation of measured core expansions over a given test region should be noted. Variation, as discussed here, is defined as the individual measurement deviation from the average expansion calculated for a particular set of

measurements (i.e. longitudinal and transverse) at a particular point in time. In the transverse direction, individual measurements rarely deviated more than ten percent (plus or minus) from the calculated average for the corresponding test region. Moreover, each set of longitudinal measurements was consistently bounded by a range of expansions no larger than 0.05 percent (i.e. $\varepsilon_{cl,max}$ - $\varepsilon_{cl,min}$ = 0.05%). The small magnitude of these disparities should be appreciated in light of the variability found within the constituent deterioration processes, exposure conditions, concrete mixtures, etc. Please consider that the unreinforced concrete blocks (refer to Folliard 2006 for further detail) commonly used for free expansion testing have historically exhibited expansions ranging over a full percentage point within an individual specimen.

Finally, the development rate and ultimate magnitude of the structural core expansions should be reviewed within the context of the initial hydration temperatures. To eliminate the influence of season-to-season climatic variation, specimen R4 is excluded. It was fabricated during the relatively cool month of December and is therefore differentiated as a *winter* beam. The alternate three specimens (R1, R2, and R3) were fabricated from June to August and are correspondingly referred to as *summer* beams. The summer beams were fabricated in rapid succession and were therefore subjected to similar (initial) curing temperatures and (long-term) exposure conditions. Placement of the reactive concrete materials (cement, sodium hydroxide, and Jobe-Newman sand) was also consistent between these three bent cap specimens (as summarized in Chapter 3). With everything else held virtually constant, the only factor left to contribute to the variation of expansion rate and ultimate magnitude is the initial curing temperature. The peak hydration temperature ranged from 163°F to 192°F. These temperatures were sufficient to trigger the development of DEF. However, results obtained from petrographic analyses (conducted during the time period under consideration and reviewed within Section 5.4.1) attributed the accumulated damage to the effects of ASR; evidence for DEF was minor and dismissible. The peak transverse expansion at three hundred days is plotted against the peak curing temperature in Figure 5-4. The equation defining the best fit line through the data is not meant for design or analysis purposes. Rather it is included to illustrate the remarkable correlation between the structural core expansions (due to ASR) and peak curing temperatures.

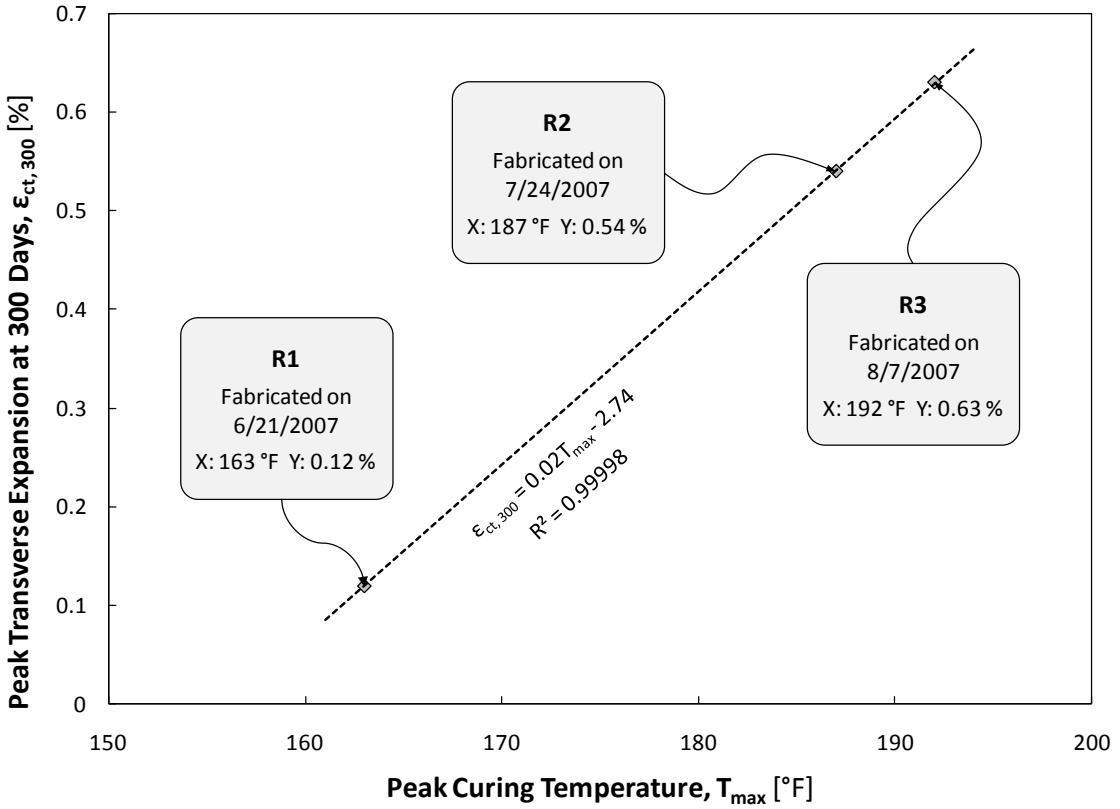

Figure 5-4: Correlation between Peak Curing Temperature and ASR-Induced Expansion

While further test results would substantiate the observation made within this study, it is clear that the severity of ASR-related expansion (rate and magnitude) is greatly influenced by the initial curing temperatures. The use of supplementary cementitious materials and admixtures may limit ASR, but additional measures to control curing temperatures may still be advisable. Conclusive recommendations can only be obtained through a comprehensive materials testing program.

5.2.1.2 Reinforcement Strains and Confining Stresses

Now that the time and spatial variations of the structural core expansions have been established, the resulting reinforcement strains may be compared. Presentation of the strains and expansions was facilitated by the calculation of average values. Figure 5-5 illustrates the individual measurements used to calculate the average transverse reinforcement strain (ε_{st}) and concrete expansion (ε_{ct}) at a given bent cap cross-section. An analogous approach was taken for the calculation of longitudinal deformations. The design of a reinforced concrete bent cap is typically conducted without consideration to

the width of the element (i.e. treated as a planar problem). The use of averaged expansions is therefore in agreement with the former practice and also provides the most fair representation of the measurements taken throughout each test region. Nevertheless, it is important to recognize that most strained and most distressed regions of a specimen may control the shear failure. Shear testing results presented within Section 5.3 are consistently compared to the peak strain and expansion values.

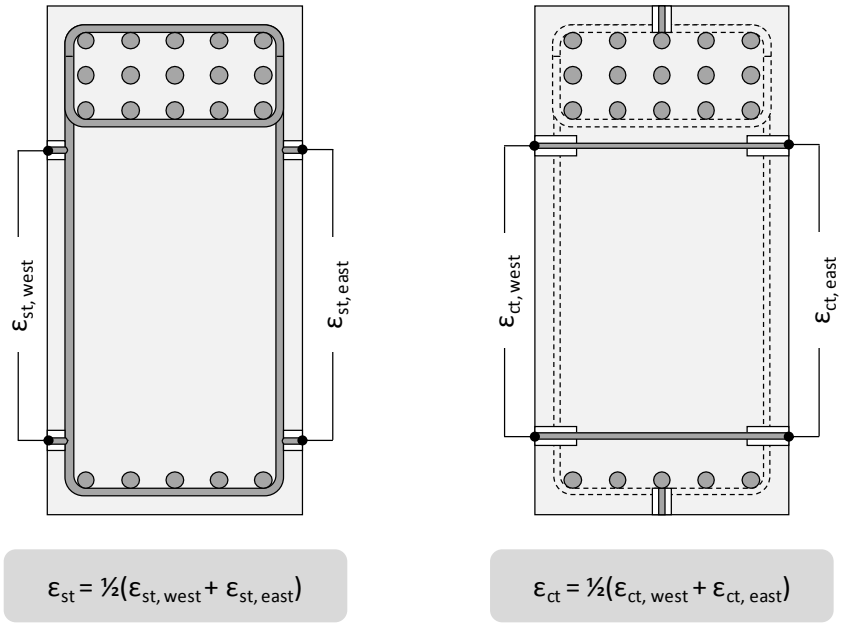

Figure 5-5: Calculation of Average Concrete Expansions and Reinforcement Strains

Expansion histories for the first series reactive specimens are presented in Figure 5-6 (R1) and Figure 5-7 (R2). Reinforcement strains (solid lines) and structural core expansions (dashed lines) are plotted for both directions of the two test regions (deep beam and sectional shear spans) of each specimen. All plots for the first series specimens are held at the same vertical scale to allow a simple visual comparison of the expansion magnitudes. The location of the averaged measurements within each test region is indicated by the small diagram in the upper left hand corner of each expansion plot.

Reinforcement strains in the transverse and longitudinal directions generally grew at the same rate as the corresponding structural core expansions. Furthermore, the magnitude of the strain was typically comparable to the underlying concrete expansion. Slight deviations between the reinforcement strain and core expansions can be primarily attributed to the spatial variation of expansion (referenced above). Due to the

arrangement of the monitoring hardware, the core and reinforcement measurements could not and did not perfectly coincide at the same cross-section of the bent cap specimens. In spite of the minor deviations, the former observations suggest that the bond and anchorage of the reinforcement was not impacted by the ongoing ASR/DEF deterioration. Please recall that design measures (Chapter 3) were taken to ensure that each bar was well-anchored; the performance of lap splices and anchorage were not objectives of the current study.

Relatively low concrete expansions within specimen R1 failed to significantly strain the reinforcement in the transverse direction. The maximum strains (ε_{st}) developed within the sectional shear test region were slightly below the measured yield point of the stirrups. Corresponding expansion (ε_{ct}) in the deep beam test region was subject to more than twice the restraint. The reduction in the reinforcement strains was proportional; less than half of the yield strain was measured within the stirrups.

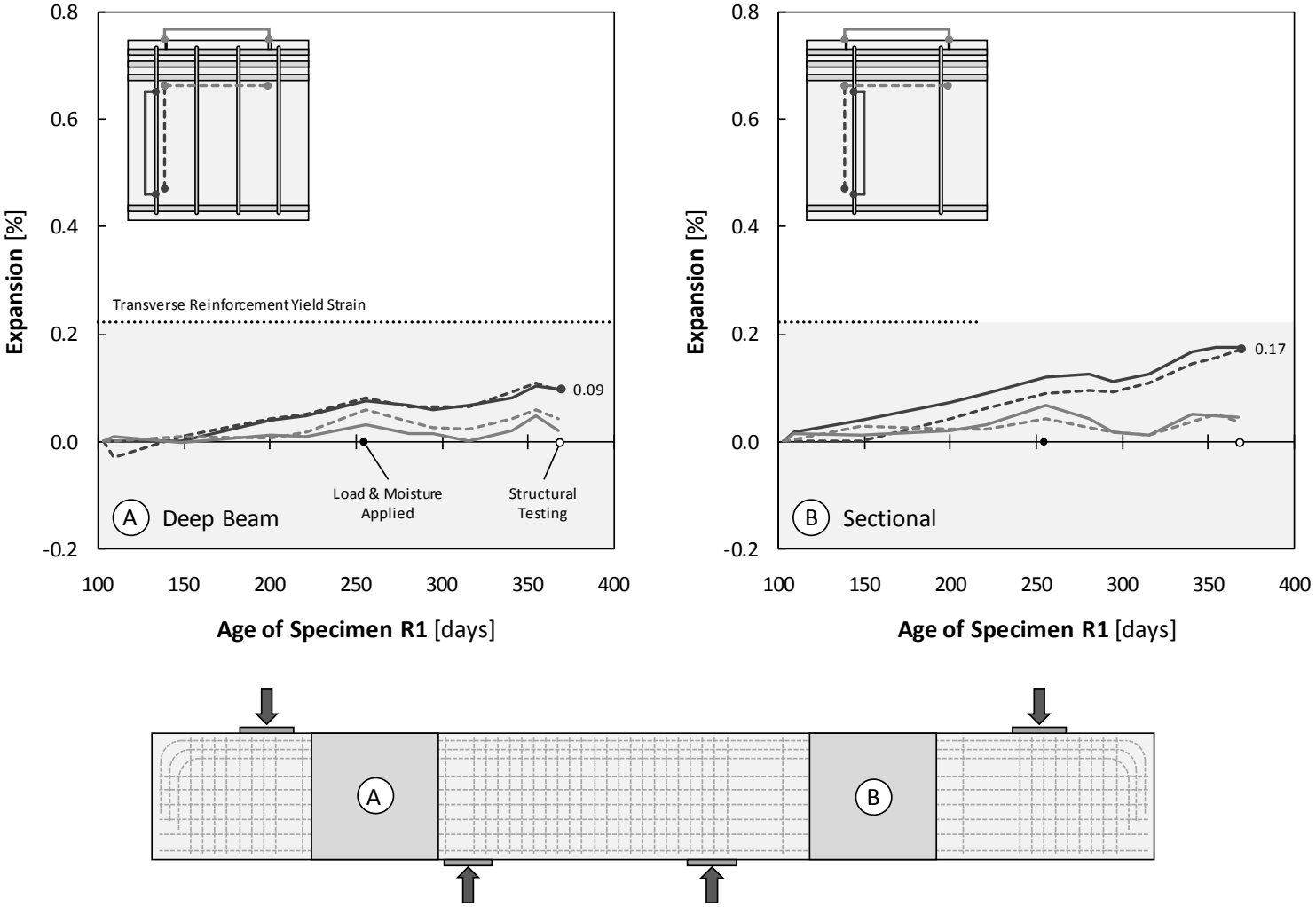

Figure 5-6: Specimen R1 Test Region Expansions (A) Deep Beam (B) Sectional

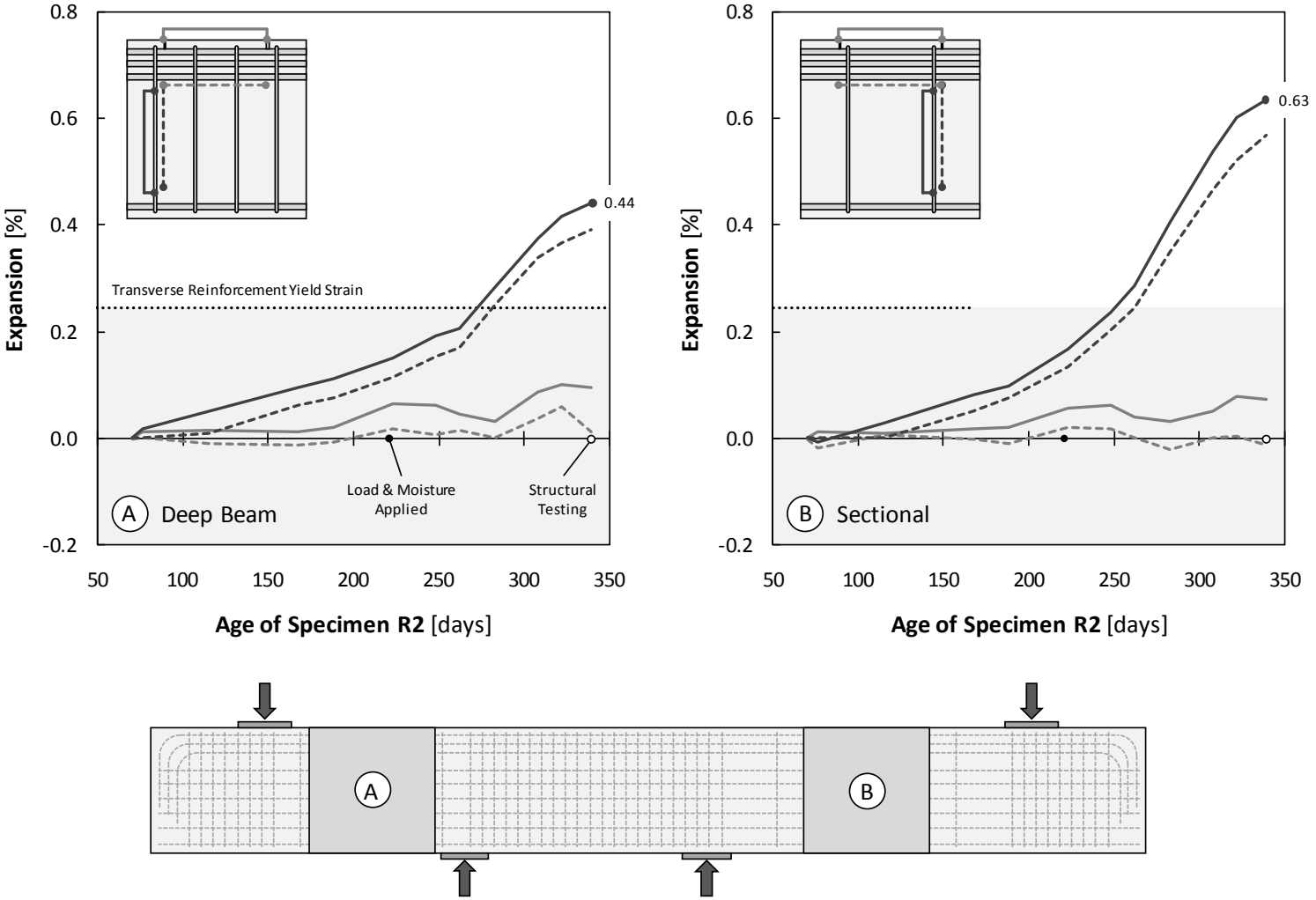

Figure 5-7: Specimen R2 Test Region Expansions (A) Deep Beam (B) Sectional

In contrast, the expansions and reinforcement strains measured within specimen R2 were significantly larger. Yielding of the transverse reinforcement in both test regions occurred within the first two-hundred fifty days. Beyond that point, the expansion and strain growth seemed to accelerate. The confinement potential of the transverse reinforcement had been exhausted; additional growth of the core did not lead to further development of confining pressures. When specimen R2 was transferred to the laboratory floor for shear testing, the transverse strains and expansions were still growing rapidly. The results shown in Figure 5-8 (R3) and Figure 5-9 (R4) suggest that the expansion potential was not fully utilized. Nevertheless, structural testing of the specimen allowed the time-dependent loss of shear strength to be investigated.

Following Phase III of the experimental program (shear testing), the second series specimens (R3, R4, nR2) were left to condition under load and moisture for an extended (and undefined) period of time. All three of the specimens had conditioned a minimum of six hundred days at the time of publication. The development of deterioration within the bent caps was very similar to that of the first series. Slow (nearly absent) growth for the first one hundred fifty days was followed by a period of rapid (constant rate) expansion. The maximum strains encountered within the transverse reinforcement of each specimen approached or exceeded one percent; significant yielding had occurred. All relevant expansion measurements are summarized within Table 5-4, included in Section 5.2.3. Within three hundred fifty days of the concrete placement, the expansion rate dropped rapidly. Currently the second series specimens are in a period of rest, but further expansion is expected to occur. Results presented within Section 5.4 will demonstrate that the damage accumulated to date may be primarily credited to ASR; conclusive signs of DEF-related deterioration have yet to be found.

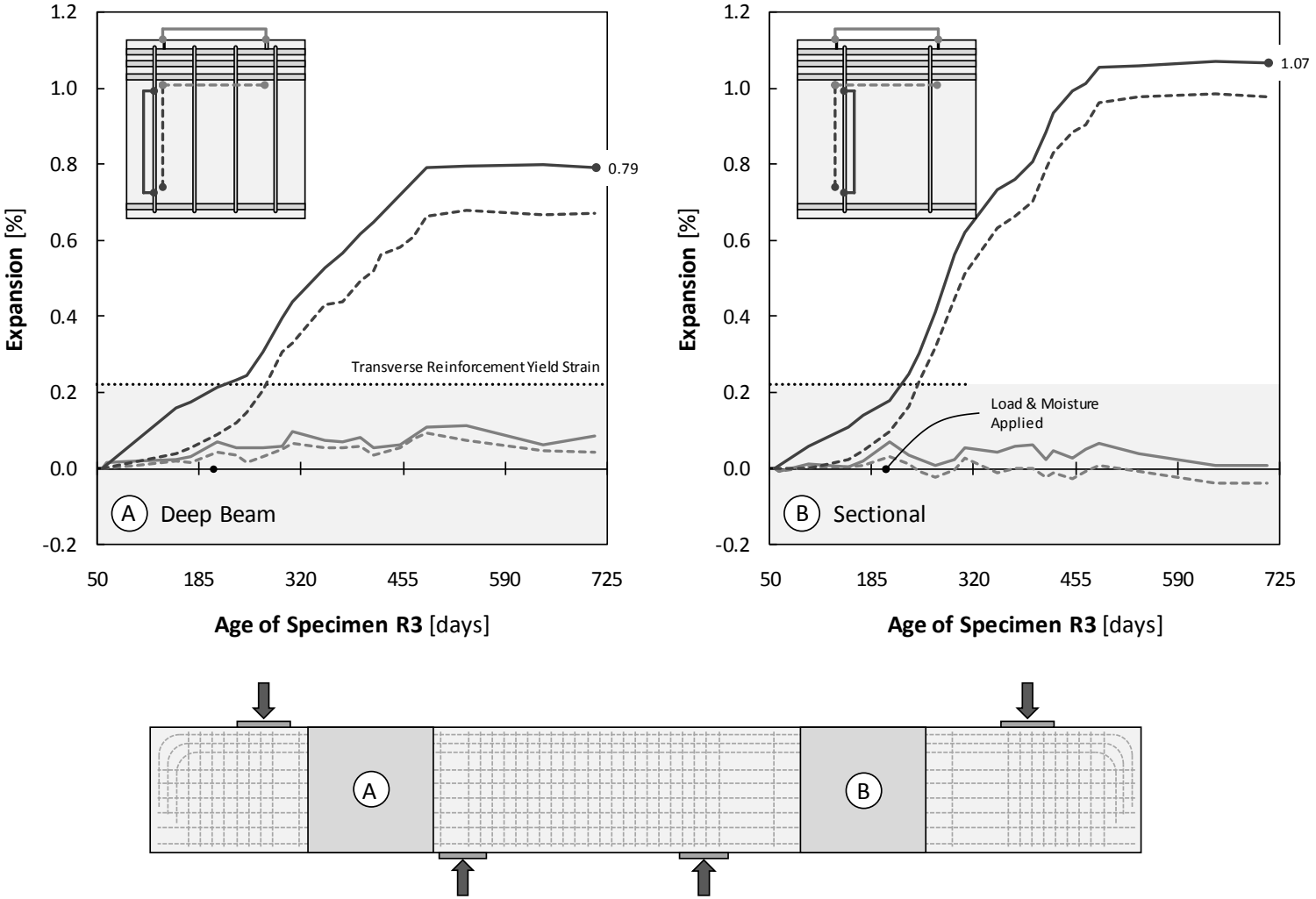

Figure 5-8: Specimen R3 Test Region Expansions (A) Deep Beam (B) Sectional

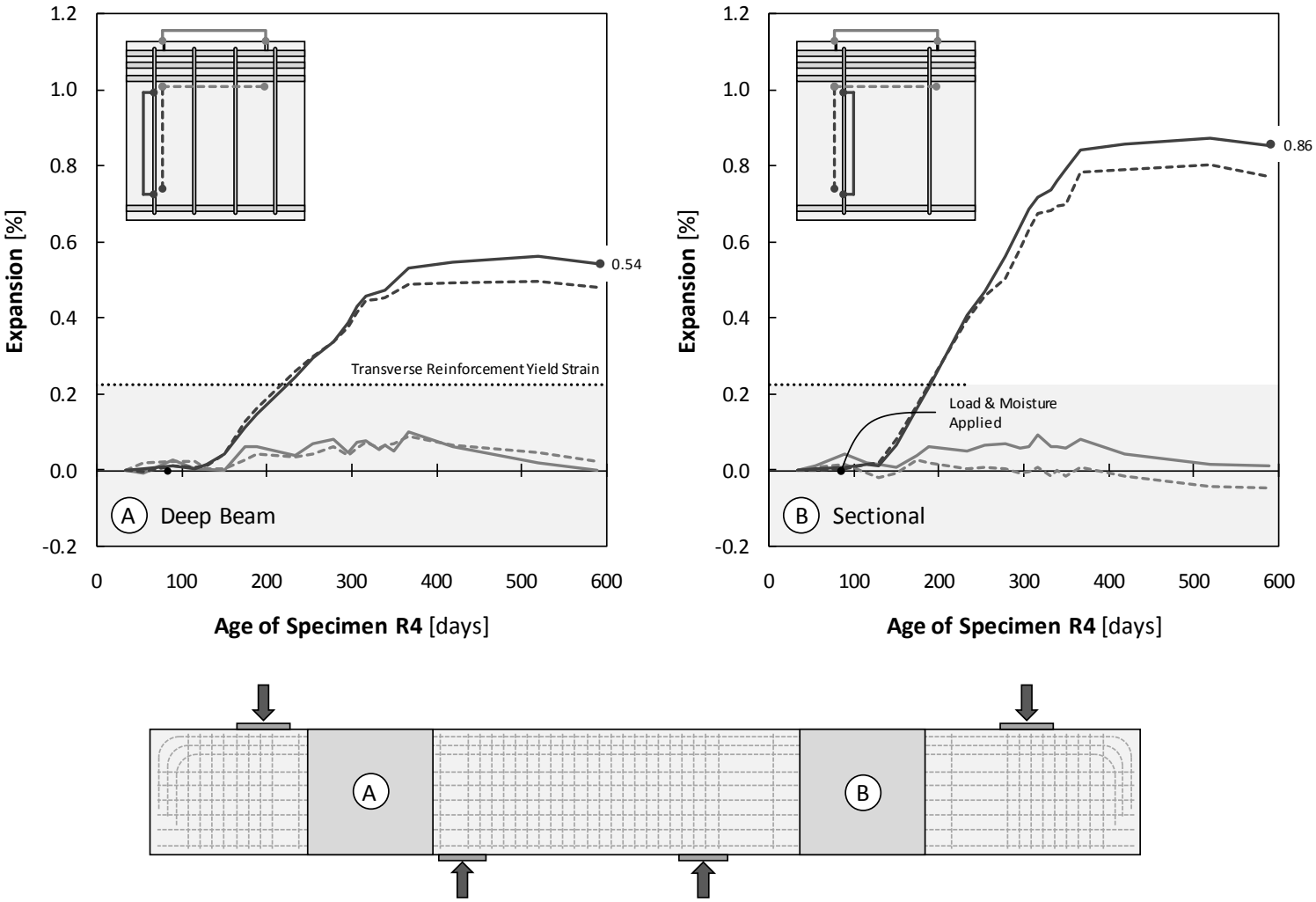

Figure 5-9: Specimen R4 Test Region Expansions (A) Deep Beam (B) Sectional

While not immediately apparent (concrete cracking is typically associated with tension), the deterioration process placed the structural core of each reactive bent into compression. To clarify, the accumulation of damage within the transverse direction of each shear span generated significant tensile strains and stresses in the shear reinforcement. The reinforcement stress was equilibrated by a commensurate amount of compression in the concrete. Traditionally, the performance of a concrete sample under triaxial compression is superior to that of a sample under uniaxial compression. For ASR/DEF-affected concrete, the critical question lies in the ability of the compression to compensate for the microstructural damage done by the expansion. To evaluate the impact of these stresses and further define the state of stress within each test region, it is valuable to calculate the compressive stresses generated within the concrete. Please note that the longitudinal stresses are ignored due to the ambiguity surrounding their role in the restraint of expansion.

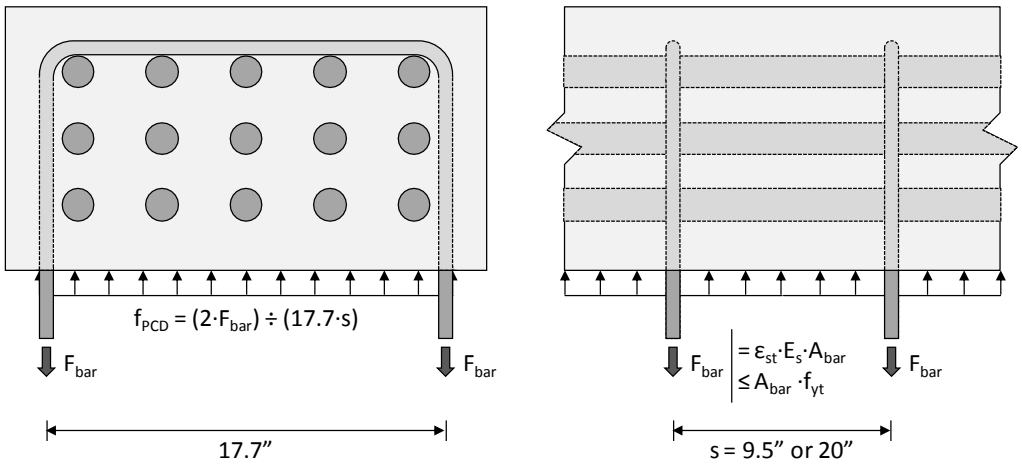

Figure 5-10: Calculation of Stresses Induced by PCD-Related Expansion

The average reinforcement strain ($\varepsilon_{st,avg}$) for a given section of the bent cap is first used to calculate the cumulative force within the two stirrup legs. The compressive stress is then obtained by distributing the concentrated force over the tributary core area serviced by the particular stirrup in question. Please note that the cover concrete is not considered in this calculation. There were a number of observations presented over the course of this chapter which suggest that the structural integrity of the heavily cracked cover concrete is questionable at best. The compressive stresses generated within the structural core are summarized within Table 5-2.

Table 5-2: Summary of Stresses Induced by PCD-Related Expansion

Specimen		Deep Beam			Sectional		
		ε_{st}	ε_{yt}	f_{PCD}	ε_{st}	ε_{yt}	f_{PCD}
		reinforcement strain as reported in Section 5.2.1	yield strain of transverse reinforcement	stress induced by PCD-related expansion	reinforcement strain as reported in Section 5.2.1	yield strain of transverse reinforcement	stress induced by PCD-related expansion
† First Series	R1	0.09 %	0.22 %	96 psi	0.17 %	0.22 %	86 psi
	R2	0.44	0.25	267	0.63	0.25	127
‡ Second Series	R3	0.79	0.22	235	1.07	0.22	112
	R4	0.54	0.22	235	0.86	0.22	112
† as recorded immediately before shear testing ‡ as recorded on July 14, 2009							

With the exception of specimen R1, the confinement potential had been maximized within all of the specimens. The peak stress generated within any of the structural cores was over two hundred pounds per square inch. The resulting stresses were substantial. However, they were not sufficient to restrain the expansive mechanisms of ASR. Pressures upwards of six hundred pounds per square inch would be required to physically restrain the deterioration (Folliard et al. 2008). The influence of these stresses will be considered during the discussion of the shear testing results (Section 5.3).

5.2.2 Observed Cracking Patterns

The development of ASR/DEF-related surface cracking is subjected to a wide variety of boundary conditions (external loading, reinforcement configurations, exposure conditions, etc.). Field-observed patterns of cracking are consequently innumerable and occasionally difficult to distinguish from damage due to overloads, poor serviceability design, or other durability problems. To gain a better understanding for which factors are the most influential on the pattern of cracking, observations made over the course of the study are reviewed here. In particular, a collection of photos and measurements is used to explore the impact of (1) the internal restraint due to reinforcement configuration and (2) stresses generated through the application of external loads.

5.2.2.1 Influence of Reinforcement Details

Results from the first series specimens (R1, R2) are used to explore the effects of reinforcement restraint. These bent caps were placed under a conditioning load relatively late during the exposure period (over 200 days after concrete placement, please refer back to Figure 5-1). As a result, restraint of the early ASR/DEF-related cracking was limited to that of the reinforcement. The following descriptions are based on observations made immediately prior to testing. Please note that the late application of load did not have a noticeable effect on the pre-established cracking.

The surface cracking noted within the first series test regions was particularly fine and very well distributed, as shown in Figure 5-11. Upon first sight, the overall pattern could be easily characterized as map cracking; directionality of the damage was not immediately evident. Closer examination of the crack width summation data (refer to Section 5.4.2.1), however, did reveal the influence of the reinforcement restraint.

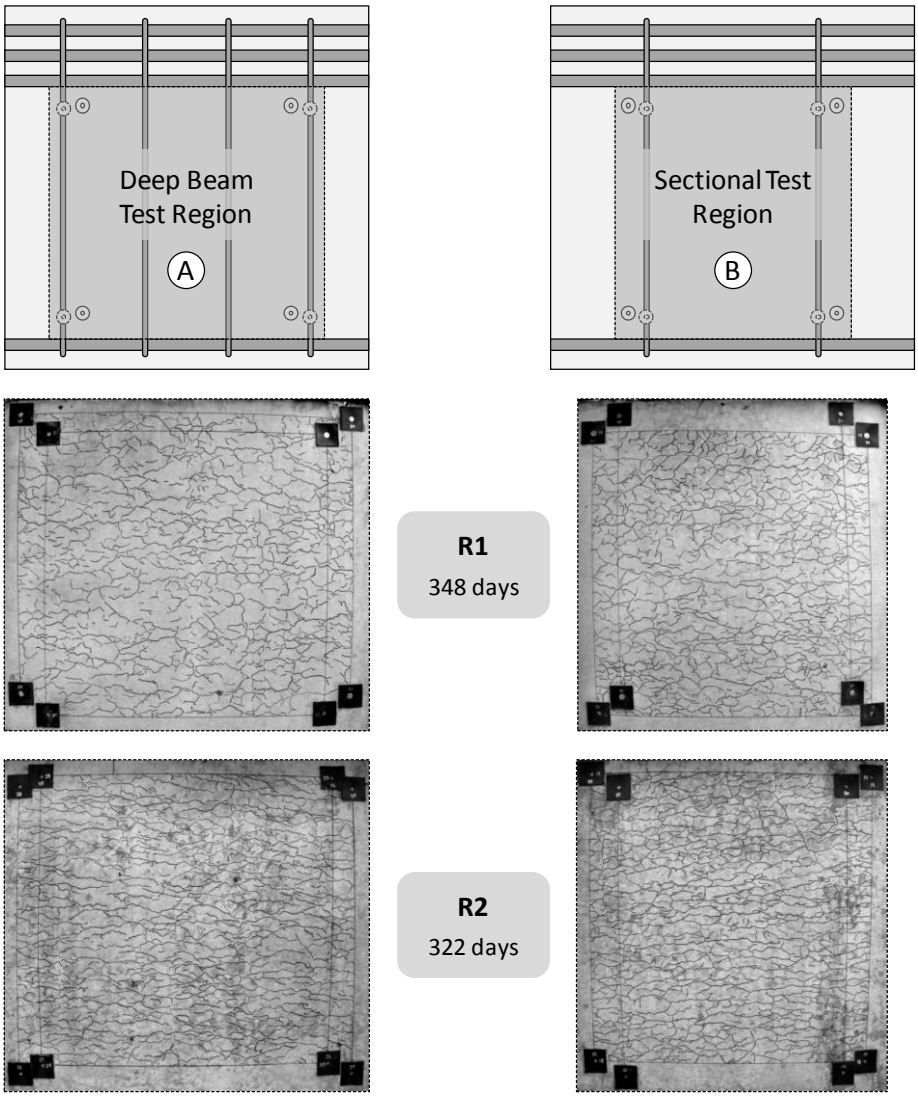

Figure 5-11: ASR/DEF Surface Cracking in First Series Test Regions

To illustrate the abovementioned assertion, cracking within the sectional shear test region of R2 (shown in Figure 5-11B) will be reviewed. The average spacing of the measurable cracks ($\omega_c \geq 0.002$ inches in width) running the length of the bent (i.e. longitudinally) was approximately one inch. The same measure of average spacing grew to nearly four inches for cracks oriented in the perpendicular direction (i.e. transversely). Furthermore, the longitudinal cracks were generally wider than transverse cracks. All of these observations are indicative of the anisotropic expansion reviewed earlier and can be generalized to all of the first series reactive test regions. In-depth consideration of the crack patterns consistently showed that the heavy longitudinal reinforcement dominated the

development of notable surface cracking. While obscured by the map cracking pattern, the primary cracks (the widest and most noticeable) always occurred in the longitudinal direction (due to transverse expansion). Table 5-3 (located at the end of this section) includes a summary of the longitudinal crack widths and corresponding levels of expansion.

The map cracking presented in Figure 5.11 was consistent over nearly all faces of the first series specimens. One exception did exist. Particularly heavy cracking was concentrated at the ends of each bent cap. The damage was easily attributed to the lack of confinement at the ends. Transverse reinforcement was commonly terminated at one foot from each end face. Consequently, deleterious expansions within the end blocks went virtually uncontrolled; a near-free expansion scenario. The first series specimens are shown in Figure 5-12A. At one year of age, each specimen end block exhibited the beginnings of severe deterioration. The maximum crack width for specimen R2 at 344 days was approximately one-eighth of an inch.

Ⓐ First Series Specimens

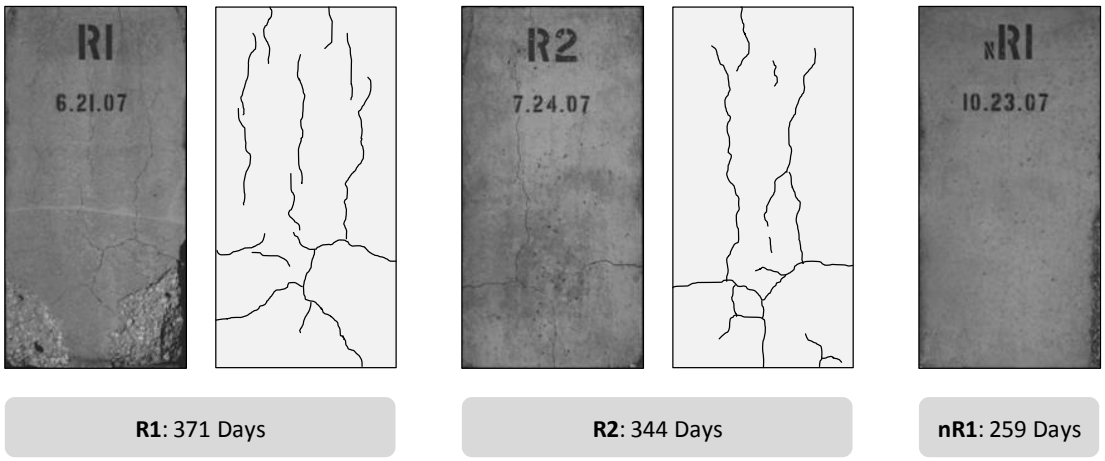

Ⓑ Second Series Specimens

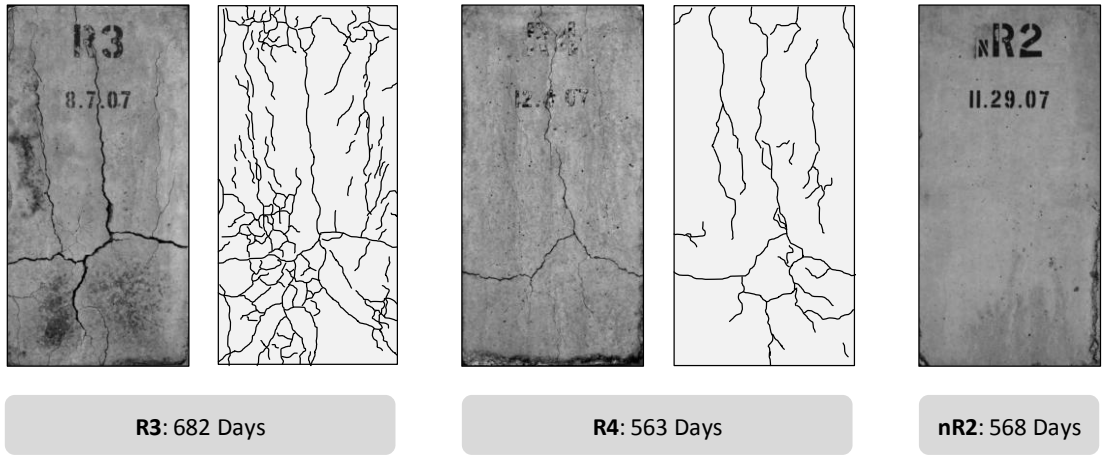

Figure 5-12: End Block Cracking (A) First Series Specimens (B) Second Series Specimens

If specimen R2 had been left to condition an additional year, the end block cracking may have resembled the damage seen in Figure 5-12B. At nearly two years of age, the end blocks of specimen R3 had been subjected to substantial geometric distortion (Figure 5-13). The resulting damage was so severe that cracks as wide as five-eighths of an inch allowed a direct view of the longitudinal reinforcement anchorage. At this time, it is worth reiterating that the condition of the end blocks was in stark contrast to the deterioration found within the test regions of any given specimen. The largest

measureable crack outside of the end blocks of specimen R3 was no more than one sixteenth of an inch wide at the time the photograph in Figure 5-13 was taken.

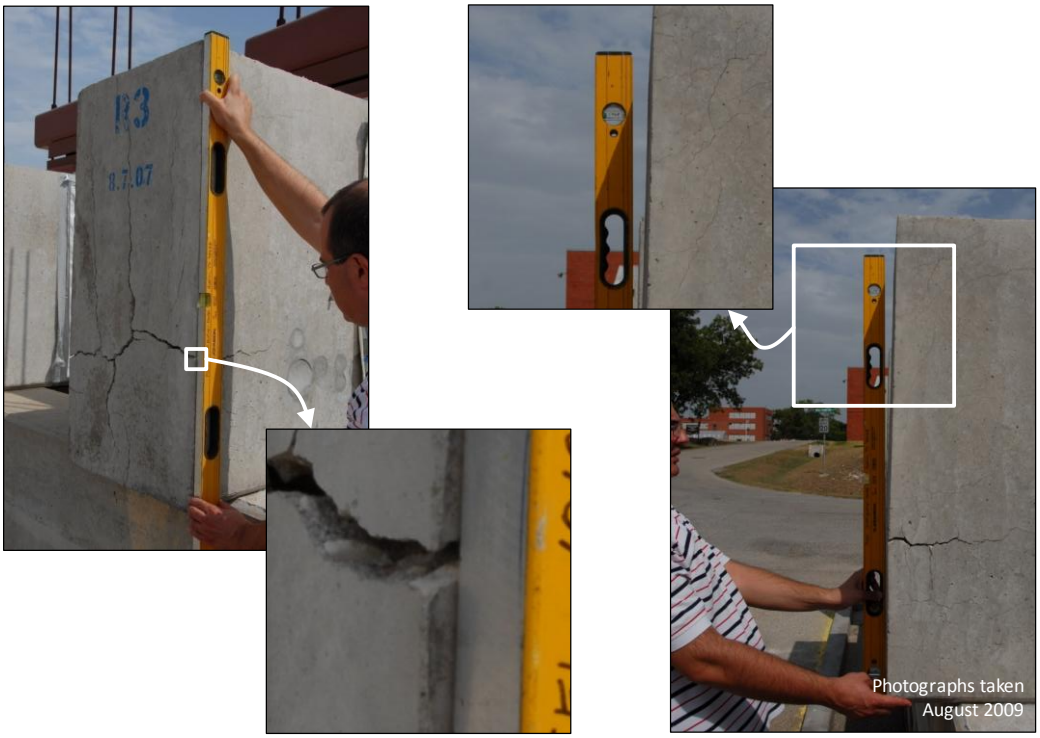

Figure 5-13: Distortion of End Block Geometry Due to Lack of Confinement

While the damage at the ends of each bent cap did not pose a threat to the load-bearing capacity (conservatively designed anchorage), it is does dramatically demonstrate the destructive power of ASR and DEF. Or to put the observation in a different light, the end block damage dramatically highlights the critical role which reinforcement plays in the maintenance of geometric and structural (discussed within Section 5.3) integrity.

5.2.2.2 Influence of External Loading

Deterioration within the test regions of the second series specimens (R3, R4) is now used to explore the influence of external loading. Specimen R4 was placed under a conditioning load within the first one hundred days of exposure. Significant expansion had yet to occur (see Figure 5-9). ASR/DEF-related surface cracking therefore developed under the full influence of the external load; a circumstance which ultimately provided the evidence necessary for the current discussion. Specimen R3 is not unlike the first series specimens described earlier and consequently serves as another point of

comparison. It is important to note that the following discussion is based upon the most recent survey of the second series damage. As implied above, the additional year of conditioning led to substantially greater expansions and damage. The data summarized within Table 5-3 illustrate the consequences of sustained ASR/DEF deterioration.

Before reviewing the surface cracking patterns, the practicality of the current exercise will be considered. Under select circumstances, ASR/DEF-related surface cracking has formed a striking (occasionally deceiving) resemblance to commonly-recognized structural cracking. The researchers of TxDOT Project 0-1857 (Bridges with Premature Concrete Deterioration) discovered numerous longitudinal cracks within the bottom flanges of precast, pretensioned highway girders. While the cracks were initially characterized as splitting damage, material testing was ultimately necessary to expose the contributing role of ASR. High longitudinal compressive stresses had suppressed the development of tell-tale map cracking and forced a tight directionality of the damage. Shortly before the current study began, TxDOT engineers within the Houston District discovered a number of straddle bent caps with diagonal cracking (an example of the damage is shown in Figure 5-14). The discovery was made as engineers within the district were also trying to assess the severity of the ongoing ASR/DEF outbreak. As a result, Houston District engineers began to question the role of PCD: Could dead load stresses have forced the development of the ASR/DEF-related diagonal cracks within these bent caps? It is hoped that the following discussion will answer the former question and allow appropriate repairs to be made.

Figure 5-14: Diagonal Cracking within an Inverted Tee Bent Cap

The surface cracking last documented within specimen R3 was visually indistinguishable from the damage noted in the previous section. When compared to specimen R2, an approximate doubling of the transverse expansion ratio (ε_{ct}) resulted in a commensurate growth of the longitudinal crack widths and a slight decrease in the crack spacing (to less than one inch). In general, increasing expansions within the first three specimens (R1, R2, and R3) led to wider and more narrowly spaced longitudinal cracks. Propagation of the transverse cracking was similar, but generally inconsequential due to relatively small changes in the longitudinal expansions.

The damage documented within the test regions of specimen R4 was of a completely different character. Cracks which generally ran the length of the specimen were exceptionally wide (up to 0.045 inches in width) and spaced from two to four inches apart. Transverse cracks were present, but typically small (about 0.005 inches in width) and widely spaced. The resulting appearance of specimen R4 was generally dominated by the longitudinal cracking. Figure 5-15 illustrates the striking difference between the cracking patterns of specimens R3 and R4. The rendering of each specimen was

assembled from a series of photographs taken immediately after the completion of a watering cycle. As the water evaporated, the crack pattern was highlighted. A simple strut-and-tie model is superimposed on the renderings to indicate the flow of forces within each test region. Please note that while the primary longitudinal cracks are slightly inclined from the load to the support, they do not follow the indicated load paths. Diagonal cracking, as commonly defined for shear behavior, was not observed.

In reference to the Houston District straddle bents, it is unlikely that dead load stresses led to the development of ASR/DEF-related diagonal cracks. Generally, the magnitude of service stress found within a highway structure is not sufficient to force tight directionality of the ASR/DEF-induced cracking; as formerly observed within the context of highly stressed, precast highway girder. Furthermore, ASR/DEF-related map cracking was not observed (even in the slightest form) within the lightly stressed regions of the straddle bent structure. It should be noted that TxDOT has since released funding for a comprehensive study into widespread inverted tee service cracking.

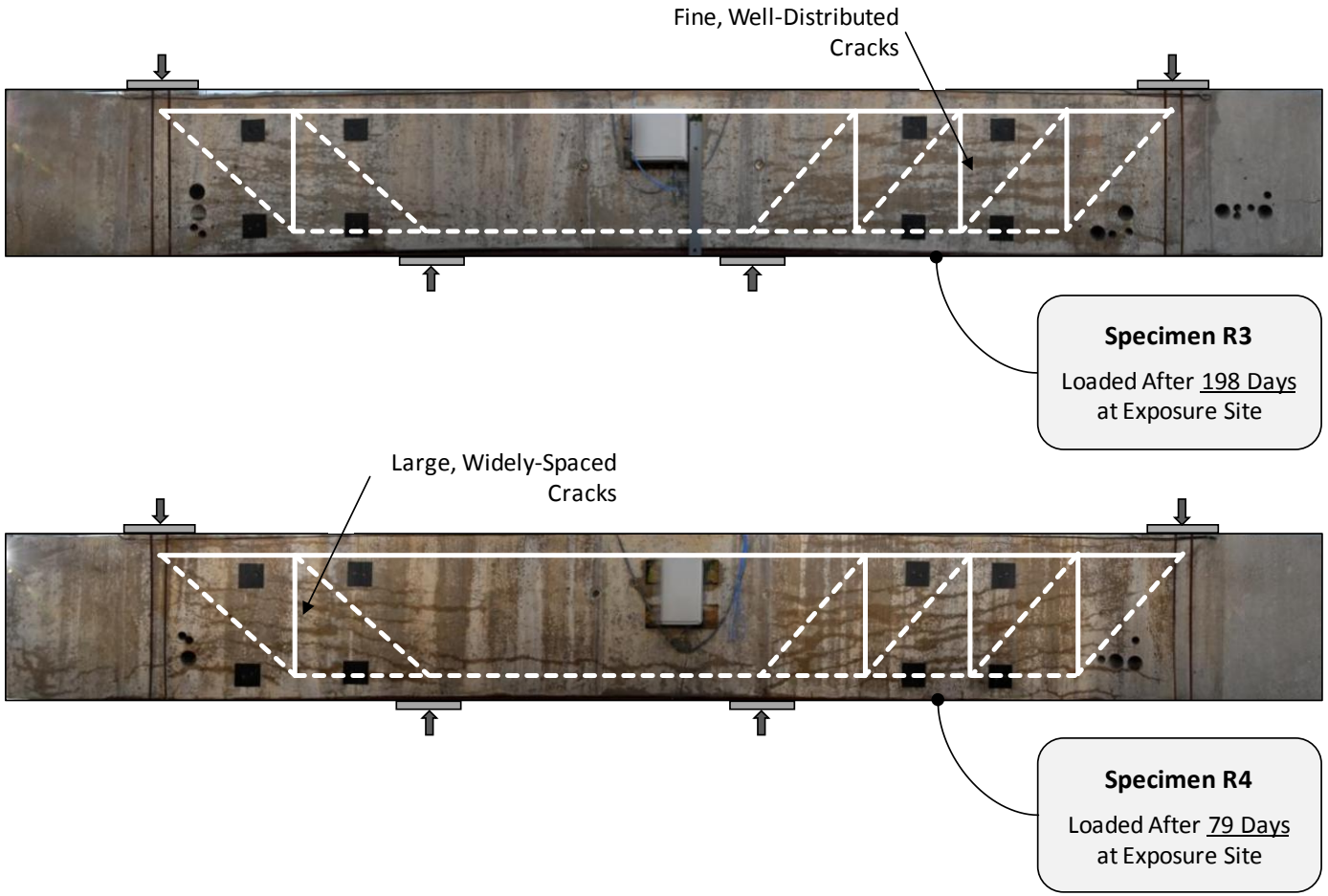

Figure 5-15: ASR/DEF Surface Cracking in Second Series Specimens

While the early application of dead load stresses did not lead to the formation of diagonal cracks, the resulting effect on the ASR/DEF-related surface cracking was noteworthy. The previous comment should not be misinterpreted. Implications of the cracking (observed within the test regions of specimen R4 and characterized in Table 5.3) are unlikely to include any structural effects. As suggested throughout this report, the condition of the cover layer is rarely indicative of the damage incurred by the structural core. A few observations presented within the remainder of this chapter serve as evidence in support of the former statement. In general, the surface cracks are typically arrested once they penetrate the outer edges of the confined concrete core. Commonly observed cracks sub-parallel to the surface of the concrete also result in a virtual delamination of the cover layer; further limiting the impact on the structural performance.

Table 5-3: Characteristics of Cracking Found within First and Second Series Test Regions

Specimen		Deep Beam			Sectional		
		$\varepsilon_{ct,\,max}$	$\omega_{cl,\,average}$	$\omega_{cl,\,max}$	$\varepsilon_{ct,\,max}$	$\omega_{cl,\,average}$	$\omega_{cl,\,max}$
		peak core expansion in transverse direction	average width of longitudinal cracks	maximum width of longitudinal cracks	peak core expansion in transverse direction	average width of longitudinal cracks	maximum width of longitudinal cracks
† First Series	R1	0.17 %	0.004 in	0.007 in	0.16 %	0.003 in	0.013 in
	R2	0.37	0.003	0.010	0.63	0.004	0.010
‡ Second Series	R3	0.86	0.006	0.016	0.94	0.008	0.030
	R4	0.46	0.008	0.025	0.76	0.011	0.045
† as recorded on June 4, 2008 ‡ as recorded on November 7, 2008							

Only one relevant implication was identified during the study of the surface cracking. Implementation of the crack width summation technique (used to estimate in-situ expansions, outlined in Chapter 4) may yield substantially different levels of conservatism when applied to the different cracking patterns. To that end, Section 5.4.2.1 includes a review of the resulting expansion estimates with proper consideration given to the nature of the cracking.

5.2.3 Pre-Test Specimen Condition Inventory

The previous review of concrete expansions, reinforcement strains, and surface cracking patterns effectively characterized the condition of each reactive bent cap specimen. The most recent expansion measurements for the first series specimens are presented within Table 5-4. The values summarize the damage present immediately before the initiation of the shear testing phase. The transverse reinforcement strains and expansions will be used in the next section to investigate the correlation between the level of damage and ultimate shear strength. Collectively the first series specimens represented three levels of deterioration: undamaged ($\varepsilon_{ct,max}$ = 0.0%), mild damage ($\varepsilon_{ct,max}$ = 0.2%), and moderate damage ($\varepsilon_{ct,max}$ = 0.7%).

Table 5-4: Summary of ASR/DEF Expansion within First and Second Series Test Regions

Specimen		Age	Deep Beam				Sectional			
			Reinforcement		Core		Reinforcement		Core	
			$\varepsilon_{st,max}$	$\varepsilon_{sl,max}$	$\varepsilon_{ct,max}$	$\varepsilon_{cl,max}$	$\varepsilon_{st,max}$	$\varepsilon_{sl,max}$	$\varepsilon_{ct,max}$	$\varepsilon_{cl,max}$
† First Series	R1	368 days	0.10 %	0.04 %	0.17 %	0.06 %	0.18 %	0.05 %	0.19 %	0.07 %
	R2	339	0.45	0.09	0.45	0.07	0.68	0.07	0.69	0.02
‡ Second Series	R3	709	0.82	0.08	0.91	0.10	1.18	0.03	1.02	0.05
	R4	590	0.56	0.00	0.51	0.04	0.90	0.05	0.83	0.05

† as recorded immediately before shear testing ‡ as recorded on July 14, 2009

The most recent expansion measurements (available at the time of publication) for the second series specimens are also summarized within Table 5-4. Future testing of these specimens will result in a comprehensive consideration of the time-dependent structural effects of ASR and DEF in both sectional and deep beam shear spans.

5.3 Live Load Performance of ASR/DEF-Affected Bent Cap Specimens

The expansion and cracking caused by ASR/DEF has the potential to cause the significant loss of strength and stiffness in plain concrete materials; a fact which was well documented within Chapter 2. It is not unreasonable to assume that the common engineer would infer an alarming loss of structural capacity from such material testing results. To explore the consequences of such logic, the development of compressive strength for

each of the first series specimens is presented within Figure 5-16. The non-reactive specimen easily attained the specified design strength in under seven days. In contrast, the twenty-eight day strengths for the reactive specimens failed to reach the five ksi target and little strength gain was observed over the remainder of the conditioning period.

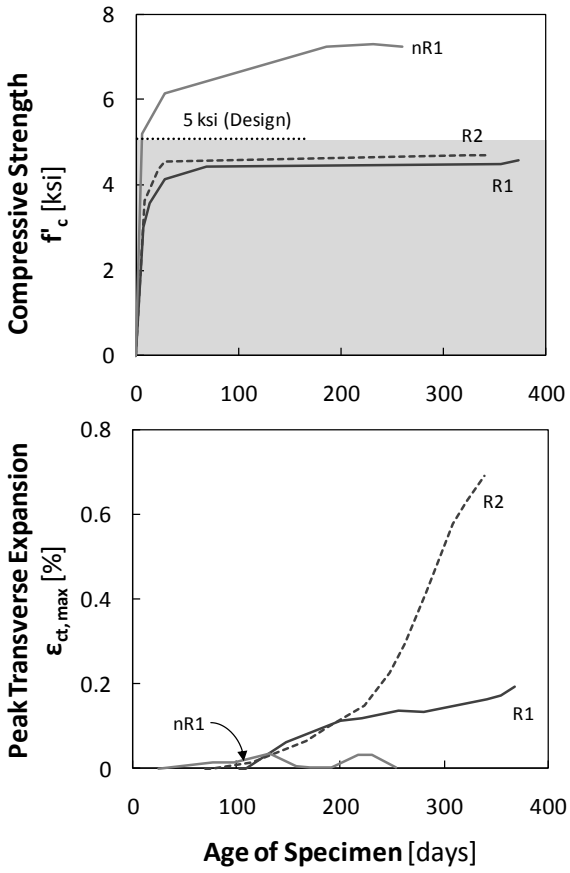

Figure 5-16: Time-Dependent Strength Gain and ASR/DEF Expansion Growth

A preliminary assessment based on these results would likely be negative. The widespread cracking and poor strength gain would place the structural adequacy of these bents into question. While such logic cannot be questioned, a few critical factors are missing from this preliminary assessment. Only the comprehensive consideration of: (1) the concrete expansion and cracking, (2) the poor material performance, (3) the reinforcement tensile strains and (4) consequential concrete compressive stresses will lead to a fair evaluation of the damage. The effect of these four conditions on the live load performance of both sectional (Section 5.3.1) and deep beam (Section 5.3.2) shear spans is explored herein.

5.3.1 Sectional Shear Behavior

Four identical sectional shear spans were tested over the course of the experimental program. The length of each shear span was equal to three times the effective depth (a/d = 3). To ensure a lower bound representation of current design practice, the minimum amount of transverse reinforcement was provided at the maximum allowable spacing. The final shear reinforcement ratio (ρ_v) was 0.15 percent; number five stirrups spaced at twenty inches on center. Heavy longitudinal reinforcement provided the flexural capacity necessary to ensure a shear failure.

Table 5-5: Summary of Deterioration within the First Series Sectional Shear Spans

Specimen		Age	$f'_{c,\,test}$	$\varepsilon_{ct,\,max}$	$\varepsilon_{st,\,max}$	f_{PCD}	$\omega_{cl,\,max}$
		days since concrete placement	concrete strength at time of testing	peak core expansion in transverse direction	peak strain in transverse reinforcement	transverse stress induced by PCD related expansion	maximum width of longitudinal cracks
Reactive	R1	371 days	4.5 ksi	0.19 %	0.18 %	86 psi	0.013 in
	R2	341	4.2	0.69	0.68	127	0.010
Non-Reactive	nR1	259	7.2	0.01	0.00	-	-
	Pilot	32	5.2	-	-	-	-

The level of ASR/DEF deterioration was the primary variable within the current study. As noted within the previous section, measurement of the damage which accumulated within the transverse direction had the most structural relevance. The range of transverse damage encompassed by the first series sectional shear spans is repeated in Table 5-5 for convenience. The non-reactive specimens (nR1 and Pilot) are damage-free and therefore serve as the baseline for the comparison of shear testing results. The moderately-damaged specimen R2, on the other hand, represents the highest level of deterioration tested within the current study. Transverse concrete expansions as high as 0.69 percent yielded the transverse reinforcement and led to the formation of cracks as large as 0.013 inches wide. The following discussion will reveal the impacts of the former deterioration on both the service and ultimate load behavior of sectional shear spans found within reinforced concrete bent caps.

5.3.1.1 Serviceability

As traditionally defined, serviceability relates to the ability to control excessive deflections and undesirable cracking under service loads. Due to the large size and inherent stiffness of the deep concrete members considered here, the magnitudes of the service load deflections are typically small and generally not a relevant concern. For that reason, the discussions herein will be limited to the study of service load cracking. Review of the crack progression and pattern will serve two similar, yet independent functions. First, the nature of the load-induced cracking will provide insights into the structural effects of ASR/DEF deterioration. It should be noted that the cracking pattern of a reinforced concrete member is uniquely tied to its behavior. Secondly, comparison of the cracking within the reactive and non-reactive bent cap specimens will place the performance of the damaged bents within the context of acceptable behavior.

The development of cracking was thoroughly documented during each test. Prior to the application of load, pre-existing cracks (from the application of the conditioning load, not including ASR/DEF damage) were marked and noted. The beam was then loaded to failure over a series of load increments (typically a total of ten). The initiation and growth of cracks were marked and noted at the end of each load increment. Visual examination of the reactive test regions required a fastidious approach; load-induced cracking could easily be overlooked due to the pre-existing damage. A series of photos taken over the course of each shear test collectively summarize the cracking progression for each test region. All documentation relating to this serviceability study can be found in Appendix B. The progression of cracking within both non-reactive (nR1) and reactive (R2) specimens is illustrated within Figure 5-17. A brief description of each test follows below.

The progression of cracking within specimen nR1 (shown in Figure 5-17B) is described first. Shortly after the application of load, pre-existing (from the conditioning phase) flexural cracks began to extend toward the applied load point. The first diagonal crack was noted to form at approximately one-third of the maximum applied shear. It extended over the center third of the beam height at a forty-five degree angle. Further loading led to the distribution of flexural and flexure-shear cracks along the shear span length and depth. A very well-distributed network of cracking was noted immediately before failure.

The response of specimen R2 was markedly different (Figure 5-17A). The application of several load increments did not result in any structural cracking. Furthermore, changes (if any existed) within the ASR/DEF cracking pattern were imperceptible. Periodic

measurement of select cracks did not reveal widening of the existing damage. The development of a relatively short flexure-shear crack at three-quarters of the maximum applied shear was immediately followed by the formation of a diagonal crack through the test region. Impending failure was not made apparent by the cracking pattern. In fact, only two diagonal cracks were present immediately before (at 95% of the maximum applied shear) failure occurred.

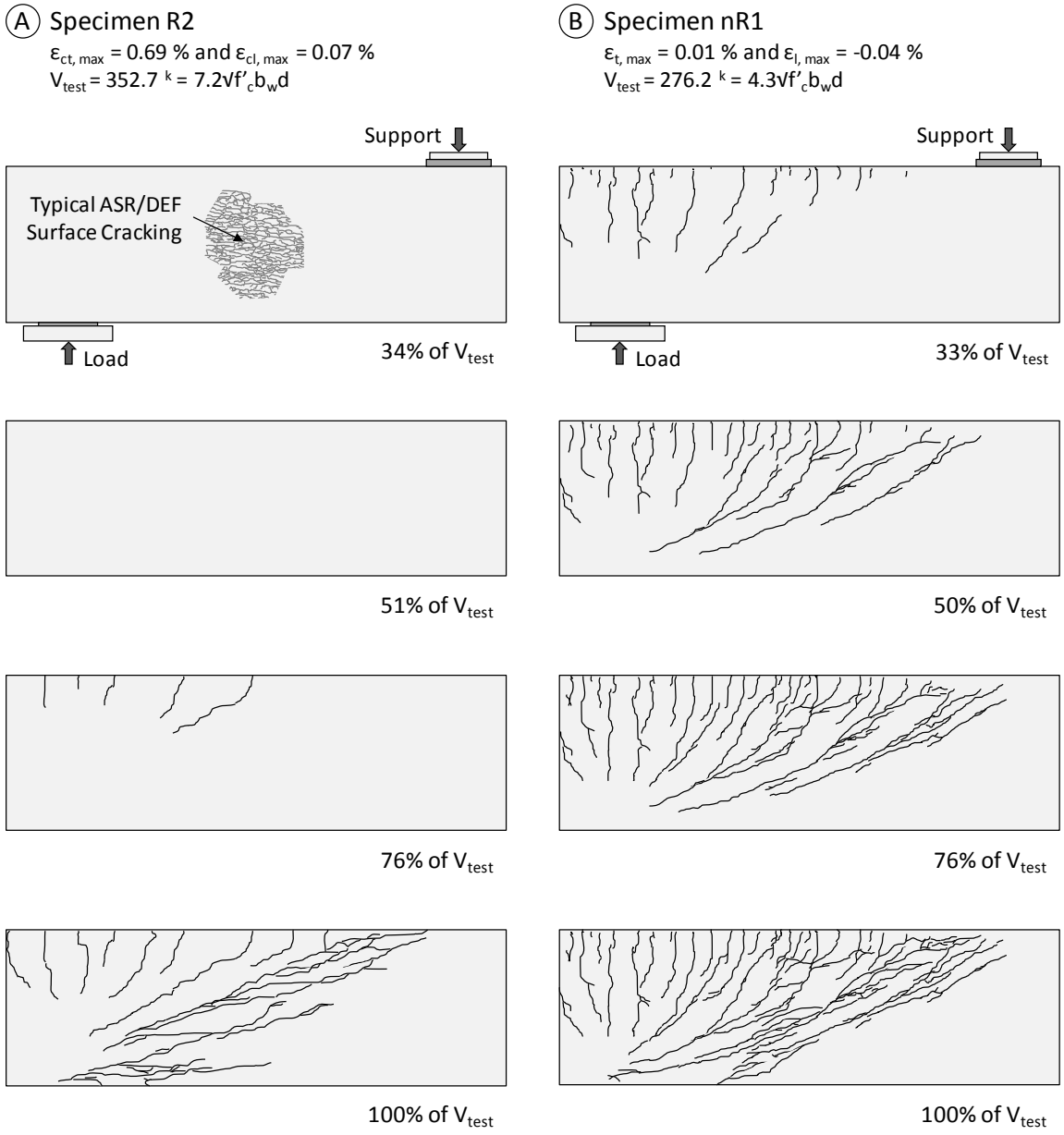

Figure 5-17: Typical Progression of Cracking within Sectional Shear Spans

In general, behavior of the reactive specimens was characterized by the late formation of poorly distributed diagonal cracking. To further investigate the phenomena, the diagonal cracking load of each specimen needed to be conclusively defined. Visual observations from each of the tests were substantiated via an examination of the transverse reinforcement strain histories. As shown in Figure 5-18, a sudden increase in the strain measured within select stirrup legs was indicative of the diagonal crack formation. A summary of all the cracking loads can be found in Figure 5-20.

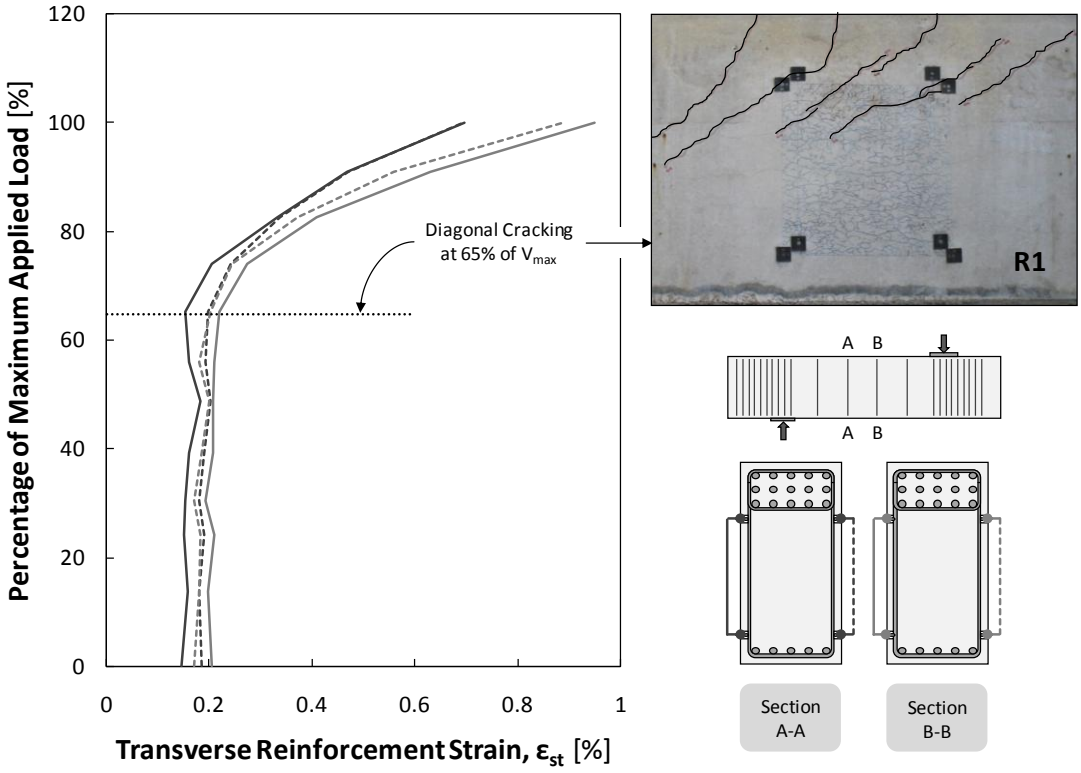

Figure 5-18: Visual and Experimental Determination of Diagonal Cracking Load

Each diagonal cracking load (presented as a percentage of the maximum applied shear) is plotted against the peak transverse concrete expansion in Figure 5-19. Despite the small number of data points, it is clear that higher transverse expansions result in greater suppression of the diagonal cracking. This behavior is most likely attributable to the confining stresses that are generated when the transverse reinforcement is placed into tension. Compression of the concrete would serve to limit the initial and subsequent development of load-induced cracking (analogous to the use of prestressing to limit flexural cracks under service loads). A theoretical limit (observed upper bound) to the observed behavior is also shown in Figure 5-19. As discussed within Section 5.2, the

development of confining stresses is limited by the reinforcement yield strain. Therefore, the maximum suppression of the load-induced cracking would be realized in a test region with yielded transverse reinforcement. It should be noted that the previous statement assumes that strain hardening of the reinforcement will not occur. Maximum ASR expansions reported within the literature (about 1%) correspond to roughly fifty percent of the strain corresponding to the onset of strain hardening.

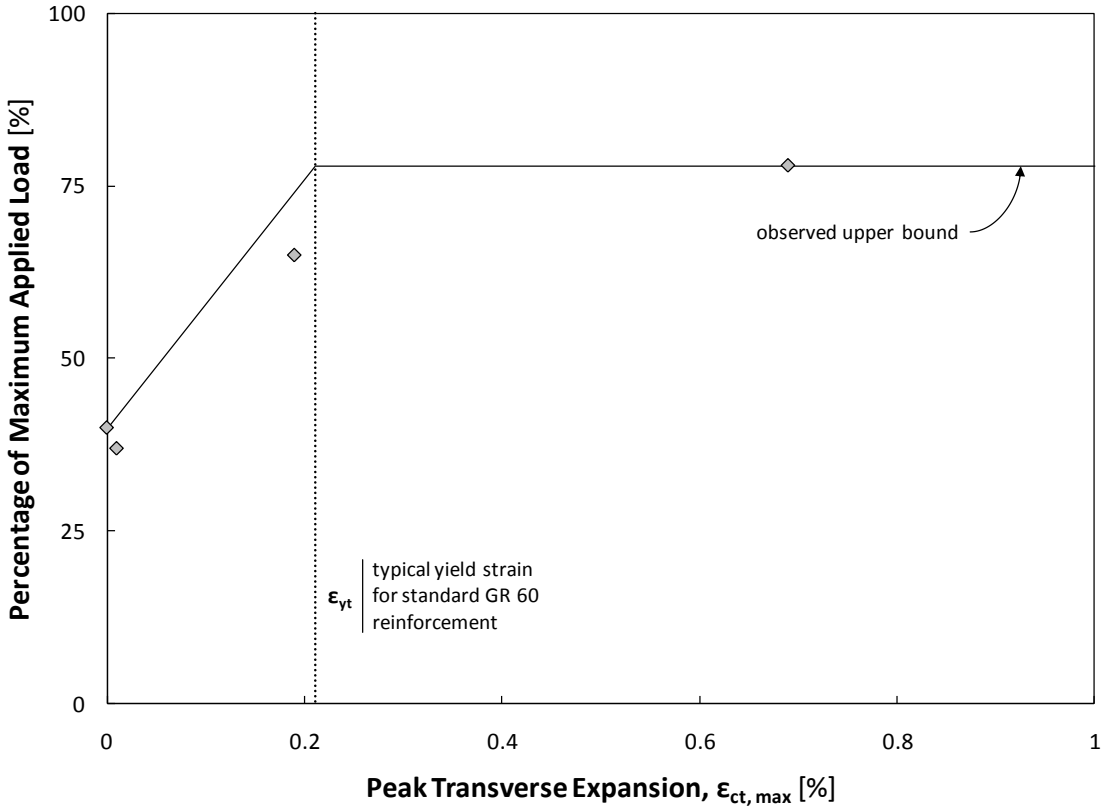

Figure 5-19: ASR/DEF Suppression of Diagonal Cracking in Sectional Shear Spans

While comparison of the reactive and non-reactive bent cap results is valuable, evaluation of the diagonal cracking loads with established code equations will provide a conclusive reference to current practice. Expressions for the estimation of the diagonal cracking load were obtained from the ACI 318-08 Specifications and recommendations made by the researchers of TxDOT Project 0-5253 (*Strength and Serviceability Design of Reinforced Concrete Deep Beams*). Both expressions may be found in Figure 5-20. Equation 11-5 from the ACI 318-08 code takes into account the effect of section size, concrete tensile strength, longitudinal reinforcement ratio, and the shear span-to-depth ratio. The expression recommended by TxDOT Project 0-5253 dismisses the impact of the

longitudinal reinforcement for the sake of practicality. In fact, a lower bound approach ensures that scatter due to extraneous variables is inconsequential. The resulting estimates are summarized within Figure 5-20. Please consider that preventing the initial formation of diagonal cracks (i.e. through the use of conservative/restrictive estimates) may be more desirable than attempting to control the width of cracks formed under service loads (i.e. through the use slightly unconservative/lenient estimates and supplementary reinforcement detailing).

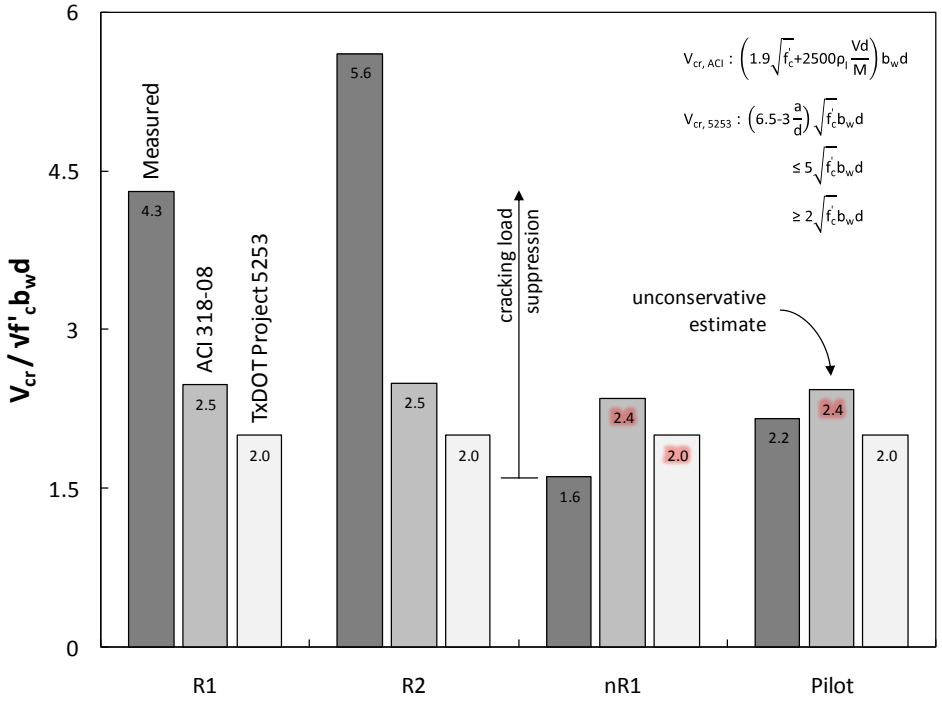

Specimen		$\varepsilon_{ct, max}$	$V_{cr, test}$	ACI 318-08		TxDOT Project 5253	
				$V_{cr, ACI}$	$\frac{V_{cr, test}}{V_{cr, ACI}}$	$V_{cr, 5353}$	$\frac{V_{cr, test}}{V_{cr, 5253}}$
		peak core expansion in transverse direction	experimental cracking load	predicted cracking load	ratio of experimental to predicted cracking load	predicted cracking load	ratio of experimental to predicted cracking load
Reactive	R1	0.19 %	219 kips	126 kips	1.74	101 kips	2.13
	R2	0.69	275	123	2.25	98	2.19
Non-Reactive	nR1	0.01	103	152	0.68	129	0.80
	Pilot	-	118	133	0.89	109	1.10

Figure 5-20: Comparison of Sectional Cracking Loads to Code Predictions

Both expressions provided conservative estimates for the diagonal cracking loads recorded within specimens R1 and R2. To interpret this result in a slightly different manner, the diagonal cracking loads (for R1 and R2) were much higher than typically observed within historical shear tests (which serve as a basis for the code expression development). This observation was earlier attributed to the confining stresses generated during the deterioration processes. Now as a slight diversion from the focus of this study,

each of the empirical methods will be evaluated through a brief comparison of the measured and estimated cracking loads for the undamaged specimens. Neither provision found within ACI 318-08 or TxDOT Project 0-5253 provided conservative estimates for the diagonal cracking observed within specimen nR1. The estimates were thirty to fifty kips higher than the observed cracking load. However, if one temporarily disregards the nR1 estimates, it becomes clear that the conservatism of the TxDOT Project 0-5253 recommendations exceeded that of the ACI 318-08 provisions. It should be noted that the researchers of 0-5253 were most interested in limiting the in-service cracking without substantial additional effort; estimation of diagonal cracking loads was not a primary focus of the study. As a result, the recommendation is well suited for owners with a desire to confidently limit cracking under service loads.

Typically, the formation of diagonal cracks within a bent cap is not desirable. The cracks are not only a sign of poor structural performance; they also compromise the durability and appearance of a structure. In the case of an ASR/DEF-affected bent cap, engineers are faced with a completely different set of concerns. The durability and aesthetics of the structure have already been compromised. Further cracking is not likely to elevate an engineer's concern in that regard. In truth, it is the absence of structural cracking which becomes the most critical concern. No outward indication of poor structural performance is available. Severe overloads could compromise the structural integrity of an ASR/DEF-affected bent cap, but the formation of cracks signaling imminent failure would not occur until the damage was practically irreversible. In other words, the formation of diagonal cracks within an ASR/DEF-affected bent cap is a clear signal that failure is imminent.

5.3.1.2 Ultimate Strength

From the outset, the primary goal of the current study was to determine the impact of ASR/DEF deterioration on the structural safety of reinforced concrete bent caps. As suggested within the introduction to this section (5.3), the severe surface cracking and commonly acknowledged material strength loss due to ASR was alarming to TxDOT personnel. The evaluation and maintenance of several damaged bent cap structures within the state was a current and growing problem. It is hoped that the results presented below may help to assuage the immediate concerns of the responsible parties. With that said, the current study is subject to certain limitations which will be outlined at the end of this discussion. Ongoing ASR/DEF deterioration will continue to present challenges in the future.

Results of the sectional shear tests are presented in Figure 5-21. Expansions characterizing the pre-existing ASR/DEF damage within each test region may be found alongside each of the failure crack patterns. The measured shear capacity is also included for reference. Please note that variation of concrete strength between the specimens required the normalization of the test results for comparison purposes. Here, the measured shear capacity has been normalized by the square root of the compressive strength ($\sqrt{f'_c}$); a direct reflection of the diagonal tension which dominates the behavior sectional shear spans. The following discussion will elaborate on the failure modes of both the non-reactive and reactive specimens.

Imminent failure of the non-reactive specimens was signaled by the distribution of cracking between the load and support. The applied load dropped quickly when a single crack extending between the inside edges of the bearing plates suddenly grew wider. The primary crack for each specimen was characteristic of a sectional shear failure. Inclination of the crack, nearly forty-five degrees near the center of the shear span, became increasingly shallow as the crack approached both the load and support points. Attempts to apply additional load were met by increasing deflections and growth of the failure crack at the compression side of the beam. As indicated by mechanical strain gage measurements, the response of both the transverse and longitudinal reinforcement (only just) remained in the elastic range throughout the tests. The shear capacity was governed by the concrete strength.

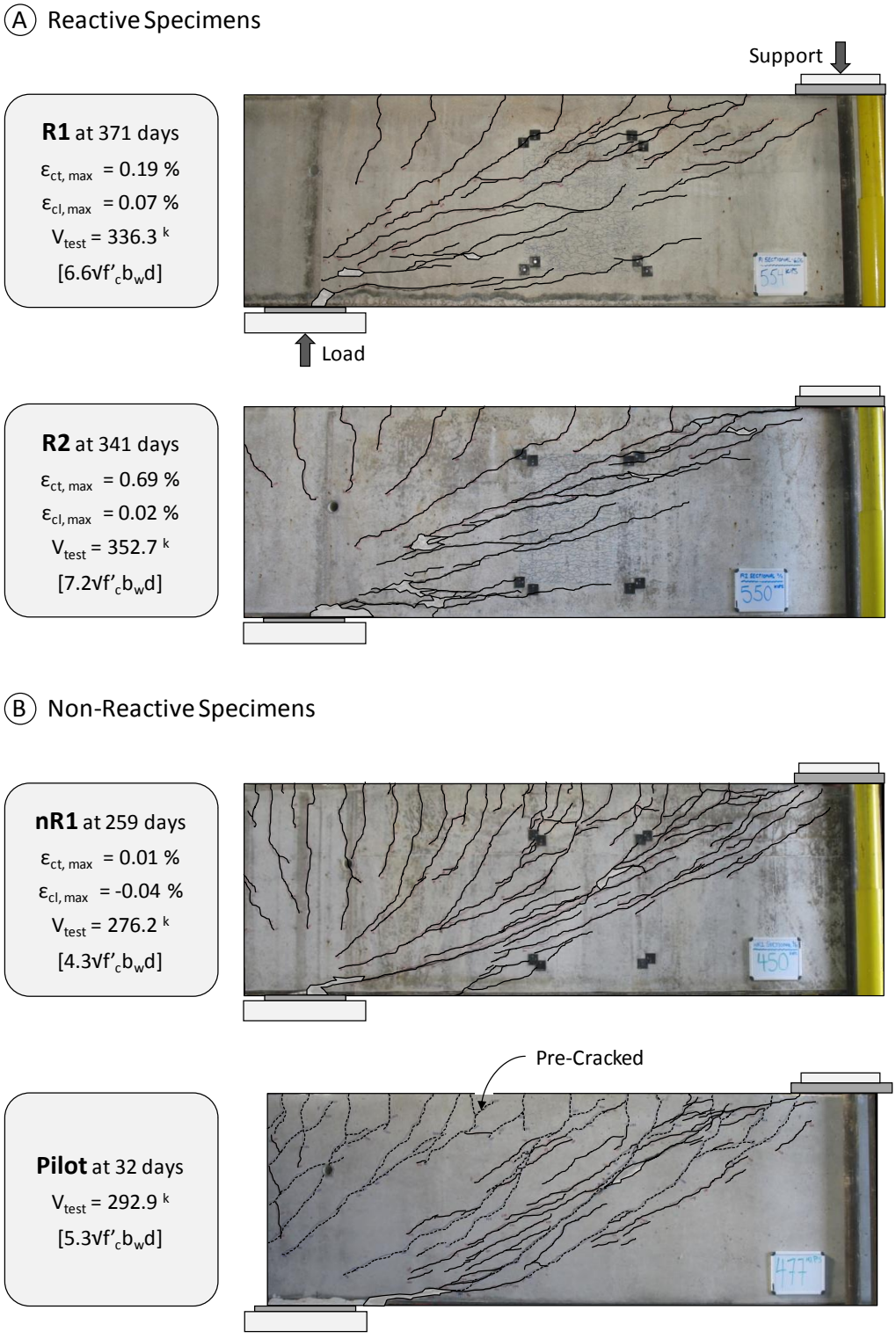

Figure 5-21: First Series Sectional Shear Spans at Failure (A) Reactive (B) Non-Reactive

Failure of the reactive specimens occurred after the formation of relatively few diagonal cracks. Before continuing, it should be noted that the effect was not as severe within specimen R1. Transverse reinforcement strains and the resultant confinement stresses were not as significant as those within specimen R2. Regardless, the distribution of both flexure- and shear-related cracking was particularly poor in both cases; impending failure was not apparent. Shear failure of each reactive test region was sudden and definitive. A substantial drop in the applied load was accompanied by an equally significant increase in the bent cap deflection; exceptionally brittle in nature. While neither specimen was subject to longitudinal yielding, the transverse reinforcement within both specimens was subject to significant strains (up to 1% elongation); fracture of a single stirrup leg occurred within specimen R2.

Figure 5-22: Delamination of Cover Concrete from Compression Face of Specimen

A unique aspect of one particular shear failure should be discussed before the review of the failure modes is dismissed. Following shear failure, specimen R2 was unloaded for further examination of the damage. Particularly wide cracks, emanating from the load point, were noted to have formed parallel to the bottom side of the bent cap specimen. Upon closer examination, it appeared that a substantial portion of the cover concrete had delaminated at failure (shown in Figure 5-22). Very little effort was required to remove the concrete section and expose the layer of compression reinforcement. At this point, it should be emphasized that this behavior was not observed within the non-reactive specimens. The delamination was most likely the result of substantial ASR/DEF-related cracking which had occurred at the interface between the cover concrete and structural

concrete core. The forces encountered during the sectional shear test were sufficient to break the cover loose. This observation simply substantiates earlier comments which suggested that the cover concrete serves very little structural purpose after significant deterioration has occurred.

In spite of the substantial ASR/DEF damage (which included well-established yielding of the transverse reinforcement) incurred by specimens R1 and R2, both sectional shear spans met the benchmarks established by the non-reactive specimens. In other words, the load-carrying capacity was successfully maintained over the range of deterioration generated within the first series specimens. Please refer to Figure 5-23 for a visual comparison of the normalized shear capacities measured within the current study.

To further validate the results, relevant code expressions were used to estimate the sectional shear capacity of each specimen (non-reactive and reactive). Shear provisions within the Interim 2008 AASHTO LRFD Bridge Design Specifications (General Procedure, Article 5.8.3.4.2) and ACI 318-08 Specifications (Section 11.1) served as the basis for these calculations. The two respective design codes collectively include shear strength models based on the modified compression field theory and simplified truss model; the two most common approaches used within practice. Please note that three match-cured cylinders (stored next to each of the specimens) were tested in compression immediately following failure of each corresponding shear span. The compressive strengths obtained from those cylinders served as the basis for the calculation of code capacities. The extraction and use of cores to establish the concrete strength is explored within Section 5.4. Shear capacity estimates from the AASHTO LRFD and ACI 318 specifications are summarized in the table found within Figure 5-23.

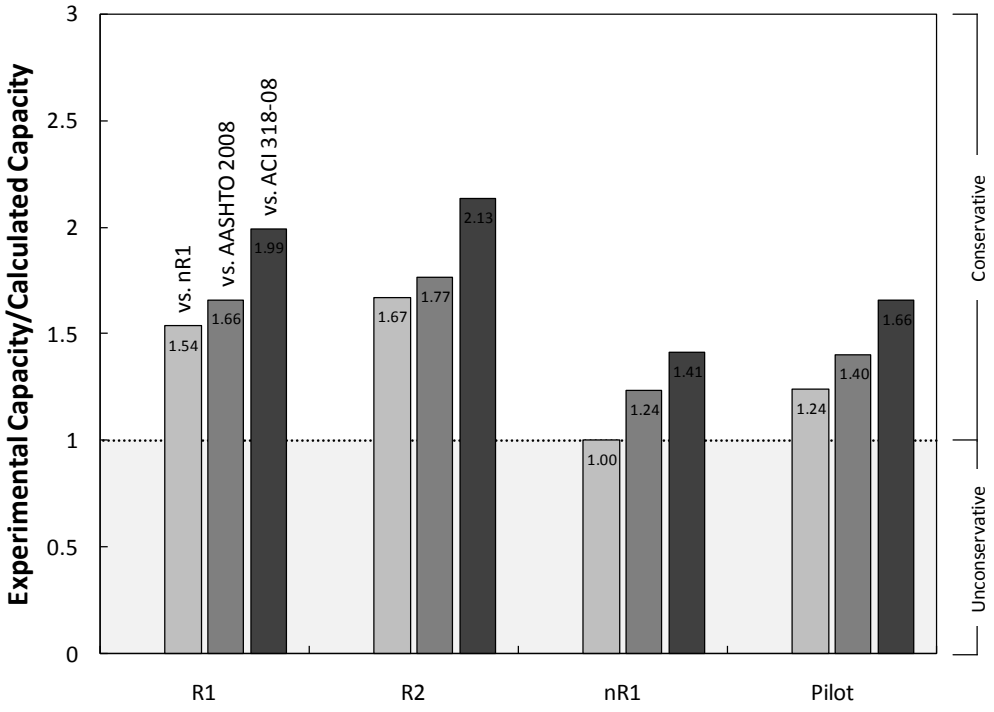

Specimen		$f'_{c,\,test}$	V_{test}	AASHTO 2008		ACI 318-08	
				$V_{n,\,AASHTO}$	$\frac{V_{test}}{V_{n,\,AASHTO}}$	$V_{n,\,ACI}$	$\frac{V_{test}}{V_{n,\,ACI}}$
		concrete strength at time of testing	experimental shear capacity	calculated shear capacity	ratio of experimental to calculated capacity	calculated shear capacity	ratio of experimental to calculated capacity
Reactive	R1	4.5 ksi	336.3 kips	202.6 kips	1.66	168.8 kips	1.99
	R2	4.2	352.7	199.6	1.77	165.2	2.13
Non-Reactive	nR1	7.2	276.2	223.4	1.24	195.4	1.41
	Pilot	5.2	292.9	208.8	1.40	176.6	1.66

Figure 5-23: Comparison of Experimental Capacities to Sectional Shear Predictions

The shear capacity of each specimen was conservatively estimated using the AASHTO LRFD and ACI 318 specifications. Based on these results, it is safe to assume that representative cylinder strengths may be used to predict the shear capacity of damaged bent cap structures. However, to provide further relevance to the field assessment of ASR/DEF-affected bent caps, cores were taken shortly after shear testing. The use of

cores to establish the concrete compressive strength for the purposes of strength prediction is explored within Section 5.4. It must be emphasized that the former results are only applicable to the shear strength of reinforced concrete bent caps subject to the same levels of ASR/DEF deterioration encompassed within these tests. The evaluation of alternate modes of failure (especially those which primarily rely on the tensile strength of concrete; i.e. reinforcement bond and anchorage) is not considered within the current study.

Finally, it must be recognized that the maintenance of structural capacity is due in large part to the confining stresses which are imposed by the transverse reinforcement. Fracture of the reinforcement (as experienced in Japan, refer back to Chapter 2) would lead to the loss of confinement and rapid deterioration of the shear capacity. With that said, it is unclear whether or not the reactive aggregates and concrete mixtures typically used within TxDOT structures are capable of producing the expansions necessary for transverse reinforcement fracture. Determination of the expansion required to fracture a reinforcing bar may be the first step taken to establish the severity of the threat posed by long-term ASR/DEF-related expansion. Continued conditioning and monitoring of the second series specimens will hopefully provide answers to these questions.

5.3.2 Deep Beam Shear Behavior

Repair of the sectional shear failure allowed four deep beam shear spans (located at the opposite end of each bent cap specimen) to be tested. The length of each shear span was equal to 1.85 times the effective depth (a/d = 1.85). To ensure a lower bound representation of current design practice, the minimum amount of transverse reinforcement was again provided at the maximum allowable spacing. The final shear reinforcement ratio (ρ_v) was 0.31 percent; number five stirrups spaced at 9 ½ inches on center. Heavy longitudinal reinforcement placed at the tensile side of the beam provided the flexural capacity necessary to ensure a shear failure. Please refer to Chapter 3 for further detail regarding the design of both the sectional and deep beam shear spans.

As noted in Section 5.2, doubling of the transverse reinforcement within the deep beam test region did not lead to a proportional decrease of the transverse expansion (when compared to that of the corresponding sectional shear test region). As a result, the accumulation of damage within the transverse direction is once again used to define the range of deterioration within the first series deep beam test regions (summarized within Table 5-6). The following text explores the service load and ultimate strength implications of transverse concrete expansions up to 0.45 percent.

Table 5-6: Summary of Deterioration within the First Series Deep Beam Shear Spans

Specimen		Age	$f'_{c,\,test}$	$\varepsilon_{ct,\,max}$	$\varepsilon_{st,\,max}$	f_{PCD}	$\omega_{cl,\,max}$
		days since concrete placement	concrete strength at time of testing	peak core expansion in transverse direction	peak strain in transverse reinforcement	transverse stress induced by PCD related expansion	maximum width of longitudinal cracks
Reactive	R1	375 days	4.6 ksi	0.17 %	0.10 %	96 psi	0.007 in
	R2	345	3.9	0.45	0.45	267	0.010
Non-Reactive	nR1	260	7.3	0.00	0.00	-	-
	Pilot	29	5.1	-	-	-	-

Please note that the previous discussion of sectional shear behavior outlined the thought process underlying the review and analysis of the test results. Certain general statements are therefore omitted from the following discussion for the sake of brevity. All details relating directly to the performance of the deep beam shear spans are reviewed herein.

5.3.2.1 Serviceability

The serviceability of ASR/DEF-affected deep beam shear spans is examined within the limited context of service load cracking. Review of the crack progression and pattern will: (1) allow insights into the structural effects of the deterioration and (2) place the performance of the damaged bents within the context of acceptable behavior. The progression of cracking within both non-reactive (nR1) and reactive (R2) specimens is illustrated within Figure 5-24. A brief description of each respective test follows.

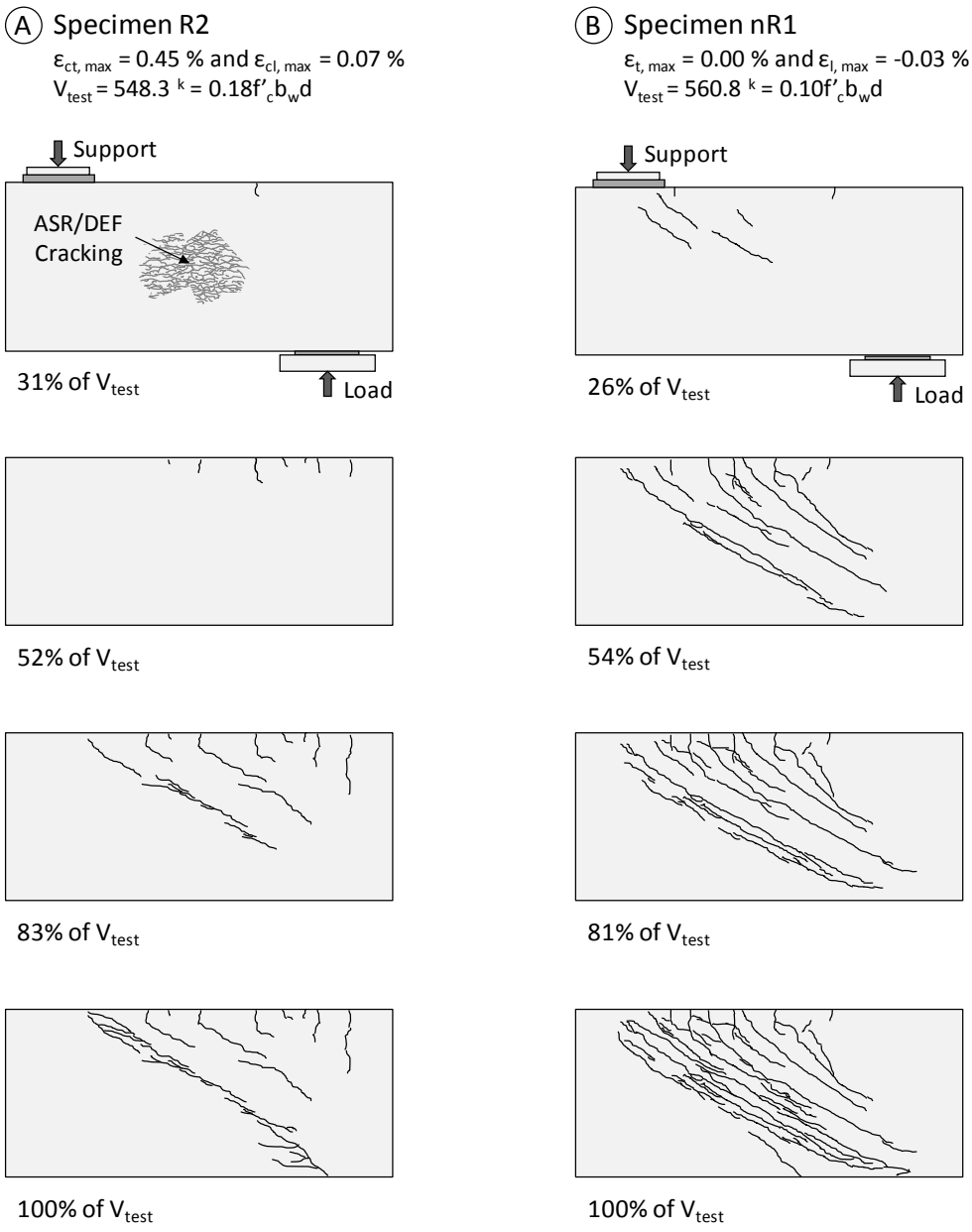

Figure 5-24: Typical Progression of Cracking within Deep Beam Shear Spans

Load-induced cracking of the deep beam shear span (specimen nR1, Figure 5-24B) was initially limited to the extension of flexure-shear cracks formed during the sectional shear test (conducted at the opposite end of the specimen). Continued application of load eventually led to the development of a primary diagonal crack which stretched between the load and support points. Further diagonal cracking generally occurred parallel to the

primary crack at even intervals along the length of the shear span. Impending failure was ultimately made apparent by the development of closely-spaced cracks along the axis of primary load transfer (i.e. the compressive strut).

Sectional shear testing of specimen R2 did not lead to the formation of load-induced cracks within the deep beam shear span. The appearance of the ASR/DEF map cracking within the span was virtually the same as when the bent cap was prepared for testing (Figure 5-24A). The initial development of load-induced cracking was limited to the formation of short flexural cracks (no longer than eight inches) along the length of the shear span. The first significant diagonal crack was noted to penetrate the test region at nearly seventy-five percent of the maximum applied load. As shear failure approached, propagation of flexure-shear cracking was accompanied by the distribution of short cracks within the immediate vicinity of the primary diagonal crack.

Behavior of the reactive specimens was once again characterized by the late formation and poor distribution of diagonal cracking. To place the behavior within the context of the sectional shear span results, the diagonal cracking loads for the deep beam shear spans were defined according to the methods noted within Section 5.3.1.1. Please note that the pre-test cracking within the non-reactive shear spans was limited to short flexure-shear cracks which did not penetrate the test region. Strain measurements could therefore be used to substantiate the observed diagonal cracking loads. Each of the deep beam cracking loads is plotted against the peak transverse concrete expansion in Figure 5-25. The observed trend is practically identical to that observed within the study of sectional shear span results (Figure 5-19). The occurrence of this phenomenon within the deteriorated deep beam shear spans reemphasizes the influence of the confining stresses generated by the strained transverse reinforcement.

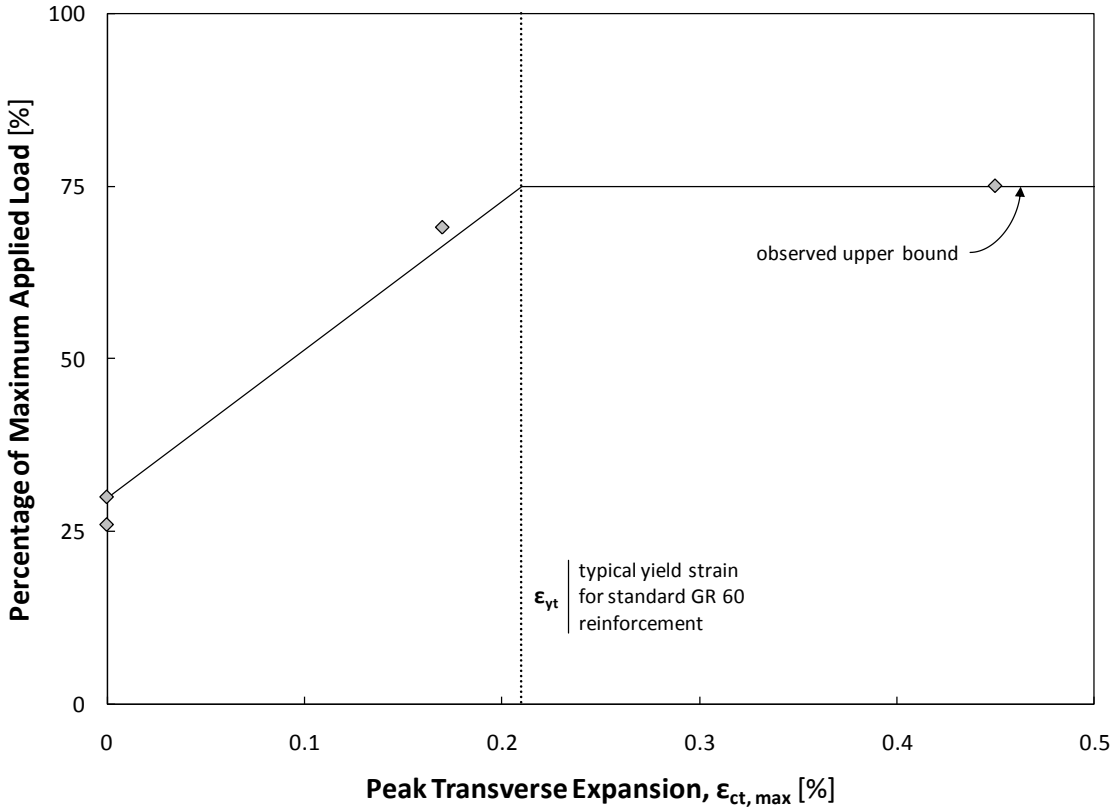

Figure 5-25: ASR/DEF Suppression of Diagonal Cracking in Deep Beam Shear Spans

Serviceability results from the deep beam shear span tests were evaluated with the same expressions used within the sectional shear study. The first diagonal cracking load estimates obtained from the ACI 318-08 Specifications and TxDOT Project 0-5253 recommendations are summarized within Figure 5-26. Of primary interest for the current study is the large disparity between the estimated and observed cracking loads for the reactive deep beam shear spans. Now, this is not meant to be interpreted as a poor performance of the predictive equations. Rather it serves to highlight the extraordinary (in comparison to sound, durable structures) behavior witnessed within the ASR/DEF affected specimens. Finally, performance of the expressions with respect to the non-reactive specimens (nR1 and Pilot) is subject to interpretation. It is worth briefly noting that the TxDOT Project 0-5253 recommendations provided reasonably conservative estimates of the cracking load. Further commentary regarding the estimation of diagonal cracking loads can be found within Section 5.3.1.1.

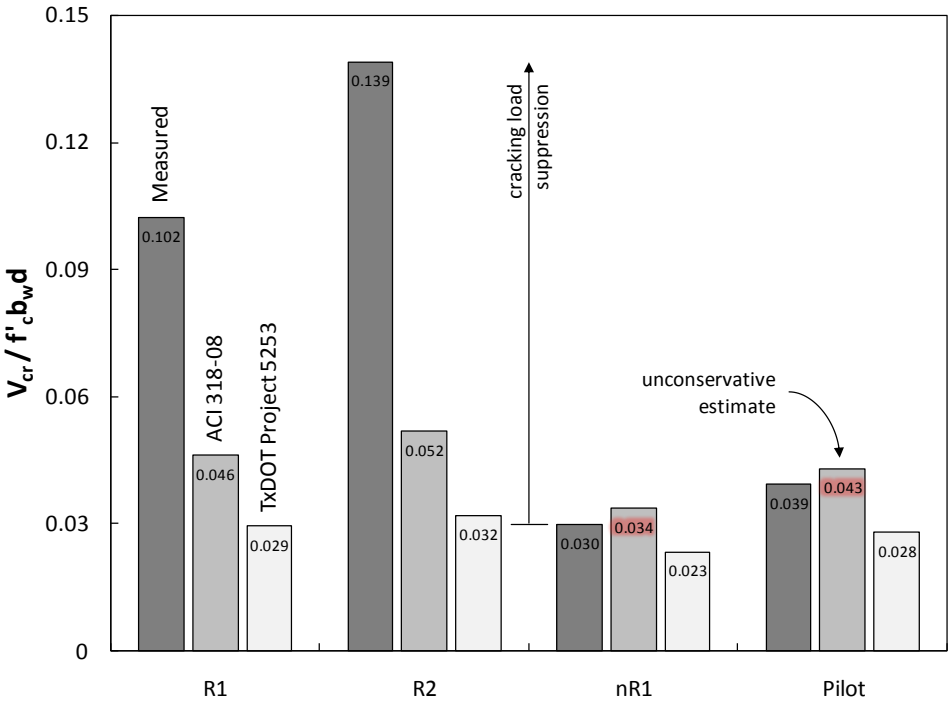

Specimen		$\varepsilon_{ct,\,max}$	$V_{cr,\,test}$	ACI 318-08		TxDOT Project 5253	
				$V_{cr,\,ACI}$	$\frac{V_{cr,\,test}}{V_{cr,\,ACI}}$	$V_{cr,\,5353}$	$\frac{V_{cr,\,test}}{V_{cr,\,5253}}$
		peak core expansion in transverse direction	experimental cracking load	predicted cracking load	ratio of experimental to predicted cracking load	predicted cracking load	ratio of experimental to predicted cracking load
Reactive	R1	0.17 %	356 kips	161 kips	2.21	103 kips	3.50
	R2	0.45	411	153	2.68	95	4.18
Non-Reactive	nR1	0.00	166	186	0.89	130	1.29
	Pilot	-	152	166	0.91	108	1.39

Figure 5-26: Comparison of Deep Beam Cracking Loads to Code Predictions

Please recall that the observed suppression of cracking is not a new discovery. A number of research studies, referenced within Chapter 2, noted a significant delay in the formation of flexure and shear cracks within ASR deteriorated specimens and some even commented on a complete absence of cracking at the nominal capacity; signs of ductility were limited. It should be recognized, however, that few failed to make the connection

between the observed suppression of cracking and the confining stresses imposed by the reinforcement. As noted throughout this chapter, the role of the confining reinforcement is critical to the performance of ASR/DEF-affected structures.

5.3.2.2 Ultimate Strength

Review of the deep beam testing results will fulfill the central purpose of this study: to evaluate the shear strength of ASR/DEF-affected reinforced concrete bent caps. Consideration of ASR/DEF-affected sectional shear behavior and ultimate strength was already considered within Section 5.3.1. Results of the corresponding deep beam shear tests are presented in Figure 5-27. Expansions characterizing the pre-existing damage within each test region may once again be found alongside each of the failure crack patterns. The measured and normalized shear capacities are also included for reference. Please note that the measured shear capacities are normalized by the compressive strength (f'_c); a direct reflection of the compressive strutting which dominates the behavior of deep beam shear spans.

Failure of each non-reactive deep beam shear span was preceded by the propagation of several near-parallel cracks running between the load and support points. Such behavior indicated splitting of the compression strut; underlying reinforcement could no longer maintain equilibrium. Sudden sliding along the primary diagonal crack was accompanied by a sudden drop in the applied load. Further attempts to apply load were met by unimpeded deflection and large relative movement between the two sections of the sheared span. Reinforcement strain measurements did not indicate yielding of the longitudinal reinforcement. Failure of each non-reactive span, however, was tied to yielding of every instrumented stirrup leg within the test region.

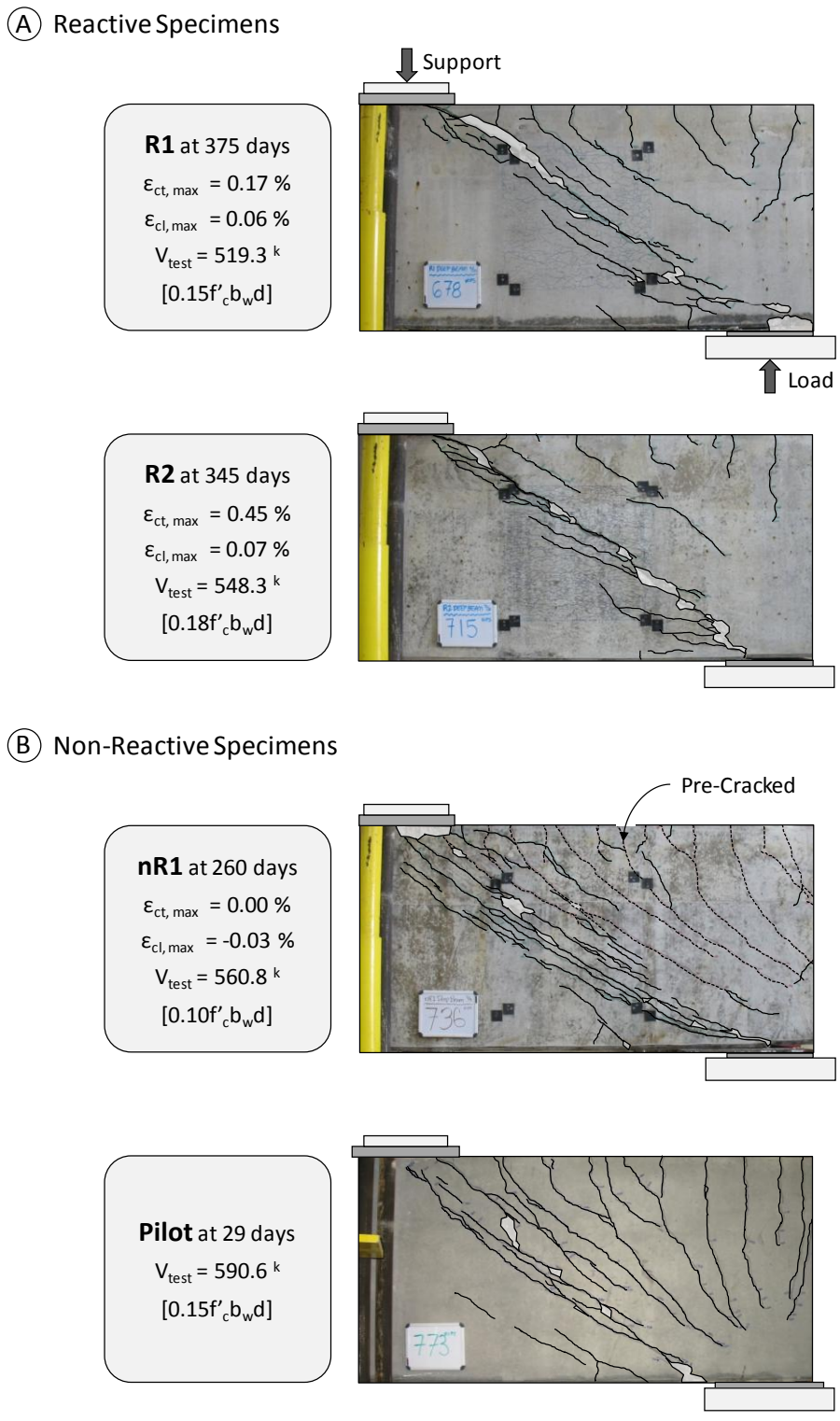

Figure 5-27: First Series Deep Beam Shear Spans at Failure (A) Reactive (B) Non-Reactive

In the case of the reactive specimen, R2, only one diagonal crack was present at ninety percent of the maximum applied load (at $0.9V_{test}$); two diagonal cracks were noted within R1 at a similar fraction of the load. Failure was decidedly more brittle than that which was observed during the ASR/DEF-affected sectional shear tests. Propagation of the primary crack between the support and load point was sudden. Furthermore, the formation of secondary cracks commonly observed before failure did not occur. Measured reinforcement strains generally increased at eighty percent of the maximum load. The final magnitude of each measured strain increase was typically under two tenths of a percent. Ductility of the reinforcement was not exploited.

The load-carrying capacity was not compromised by the wide range of deterioration generated with first series deep beam shear spans. Please refer to Figure 5-29 for a comparison of the normalized shear capacities measured within the test series. Also included are the nominal strength estimates provided by three separate strut-and-tie modeling provisions. Currently enforced modeling procedures within the Interim 2008 AASHTO LRFD Bridge Design Specifications (Article 5.6.3) and ACI 318-08 Specifications (Appendix A) were used in conjunction with design provisions recently recommended by the researchers of TxDOT Project 0-5253. All three methods rely of the same strut-and-tie model for analysis. The single panel model with non-hydrostatic nodes (as recommended within 0-5253) is shown in Figure 5-28. Deviation between the estimates is traceable to the strut and node efficiency factors recommended within each separate document. The researchers of TxDOT Project 0-5253 further recommended expressions to exploit triaxial confinement of the CCC and CCT nodes located at the load and support points, respectively. Those recommendations are taken into account while performing calculations using the TxDOT Project 0-5253 design provisions. Please note that compressive strengths obtained from the match-cured cylinders are used as the basis for all strength estimates provided within Figure 5.29.

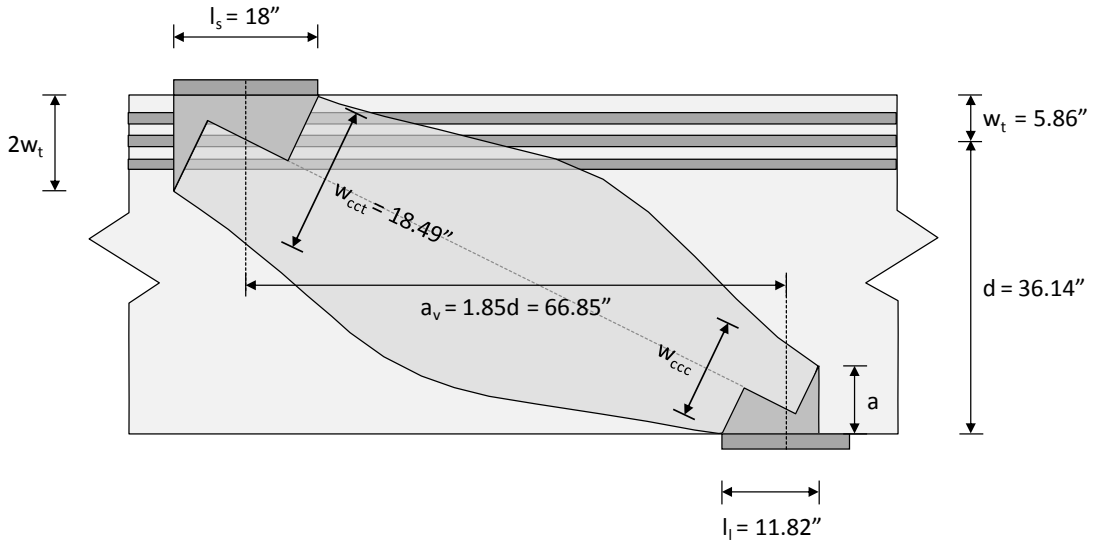

Figure 5-28: Known Strut-and-Tie Model Geometry

The shear capacity of each deep beam shear span was conservatively estimated using all of the aforementioned strut-and-tie modeling procedures. Based on these results, it is once again safe to assume that representative cylinder strengths may be used to predict the shear capacity of damaged bent cap structures. Please note that estimates obtained through the practical implementation of core extraction and testing will be explored within Section 5.4. Before the review of strength prediction is dismissed, it is worth recognizing the accuracy achieved by the recommendations of TxDOT Project 0-5253. The margin of error is about as narrow as can be expected within the context of shear behavior (generally under 30%).

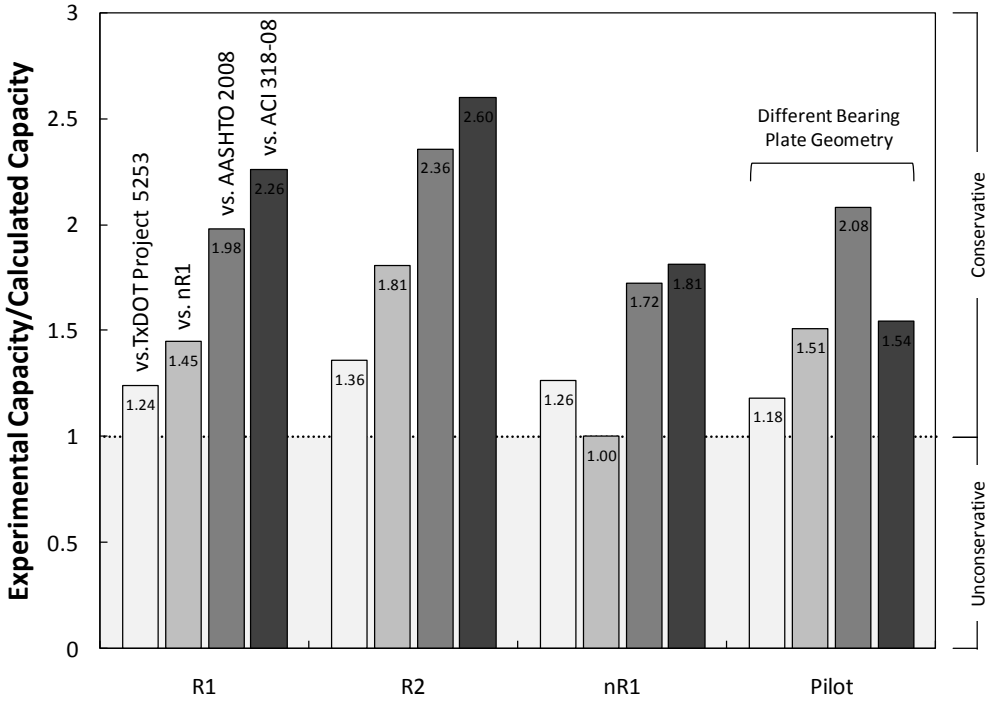

Specimen		$f'_{c,test}$	V_{test}	AASHTO 2008		ACI 318-08		TxDOT Project 5253	
				$V_{n,AASHTO}$	$\frac{V_{test}}{V_{n,AASHTO}}$	$V_{n,ACI}$	$\frac{V_{test}}{V_{n,ACI}}$	$V_{n,5353}$	$\frac{V_{test}}{V_{n,5253}}$
		concrete strength at time of testing	experimental shear capacity	calculated shear capacity	ratio of experimental to calculated capacity	calculated shear capacity	ratio of experimental to calculated capacity	calculated shear capacity	ratio of experimental to calculated capacity
Reactive	R1	4.6 ksi	519.3 kips	262.0 kips	1.98	230.0 kips	2.26	417.9	1.24
	R2	3.9	548.3	232.6	2.36	211.0	2.60	403.5	1.36
Non-Reactive	nR1	7.3	560.8	325.1	1.72	309.4	1.81	443.5	1.26
	Pilot	5.1	590.6	283.5	2.08	382.5	1.54	498.8	1.18

Figure 5-29: Comparison of Experimental Capacities to Strut-and-Tie Predictions

The results of the deep beam shear tests generally reinforced the observations and conclusions drawn during the study of the damaged sectional shear spans. In particular, both test series highlighted the influential nature of the confining stresses generated by the strained transverse reinforcement. During the analysis of serviceability data, it was apparent that the ASR/DEF-related confining stresses suppressed the formation of

structural cracking; a seemingly beneficial result which may be misinterpreted initially. While the formation of diagonal cracking under service loads is typically undesirable, it serves a critical function under higher load levels: to indicate poor structural performance. In the case of the deteriorated specimens, diagonal cracking was not observed until failure was imminent (at 80% of the maximum applied load). The results ultimately suggest that the formation of diagonal cracks within an ASR/DEF-affected bent cap should not be taken lightly; immediate action is necessary in such a circumstance. Analysis of the ultimate strength data revealed an alternate and somewhat positive consequence of the ASR/DEF-related confining stresses. The maintenance of structural capacity over the wide range of deterioration encompassed by the first series specimens was due in large part to the confining stresses imposed by the transverse reinforcement. In contrast to the severe surface cracking observed outside the influence of the transverse reinforcement (i.e. cover concrete layer), the structural core damage was limited to structurally irrelevant micro-cracking. Please recognize that these results are not universally applicable to deteriorated bent structures. Serious implications may exist when structures are subjected to longer periods of exposure and persistent expansion. Loss of confinement through the fracture of highly stressed reinforcement would lead to rapid deterioration of the structural core and an unquestionable loss of structural safety.

5.4 APPLICABILITY OF FORENSIC ANALYSIS TECHNIQUES

Based on the recommendations of current assessment guidelines (reviewed within Chapter 4), a number of forensic techniques were selected to establish the (1) cause, (2) extent, and (3) future potential of ASR/DEF deterioration within the bent cap specimens. Each forensic technique was implemented separately and the results (including first-hand experience) were used to establish the accuracy and utility of each method. Measurements taken over the course of the study served as the basis for comparison. Collective implementation of all the techniques ultimately allowed an examination of the rationale currently underlying assessment guidelines.

Results from the implementation of each forensic technique are presented within this section. First, the findings of a petrographic analysis are used to establish the nature of the deterioration found within the first series specimens. Observations regarding the cause of deterioration, general character of the microstructural cracking, and qualitative severity of the damage are presented (Section 5.4.1). Second, expansion estimates obtained from implementation of the crack width summation and elastic rebound techniques are compared to measured in-situ concrete expansions (Section 5.4.2). Third, the use of core-based material strength measurements (compressive and splitting tensile

strength tests) for the estimation of shear capacity is explored. General comments regarding the conservatism of the resulting estimates are made (Section 5.4.3). Finally, future expansion estimates obtained from a series of laboratory core tests are placed within the context of measured in-situ expansion (Section 5.4.4).

5.4.1 Diagnosis of ASR/DEF Deterioration

A total of six cores, one from each shear span of the first series specimens (R1, R2, and nR1) were submitted to the TxDOT Concrete Laboratory for evaluation. The petrographic analysis served three purposes: (1) to visual document and qualify the contributions of ASR and DEF deterioration, (2) to characterize the crack networks occurring within the cover and structural core concrete layers, and (3) to provide a qualitative comparison of the unique microstructural damage found within each specimen. The documentation associated with each of these tasks is briefly reviewed herein.

After a thorough review of lapped section photographs, scanning electron imagery and spectral analyses of the reaction products, TxDOT personnel concluded that specimens R1 and R2 had "suffered significant distress from alkali-silica reaction." The development of ASR deterioration was attributed to the fine aggregate fraction of the concrete mixture: "the primary ASR aggregate type is an igneous fine aggregate… of the Ryholitic volcanic rock type." One of the images depicting a distressed fine aggregate particle is included in Figure 5-30A. While ettringite formation was noted to line many of the air voids and microstructural cracks, the distinct petrographic features (see Figure 5-30B) of delayed ettringite formation were seldom found. "It is inconclusive whether DEF has contributed to the distress based on the limited amount of true gapping due to paste expansion." No conclusive evidence of ASR or DEF was found during the examination of cores from specimen nR1.

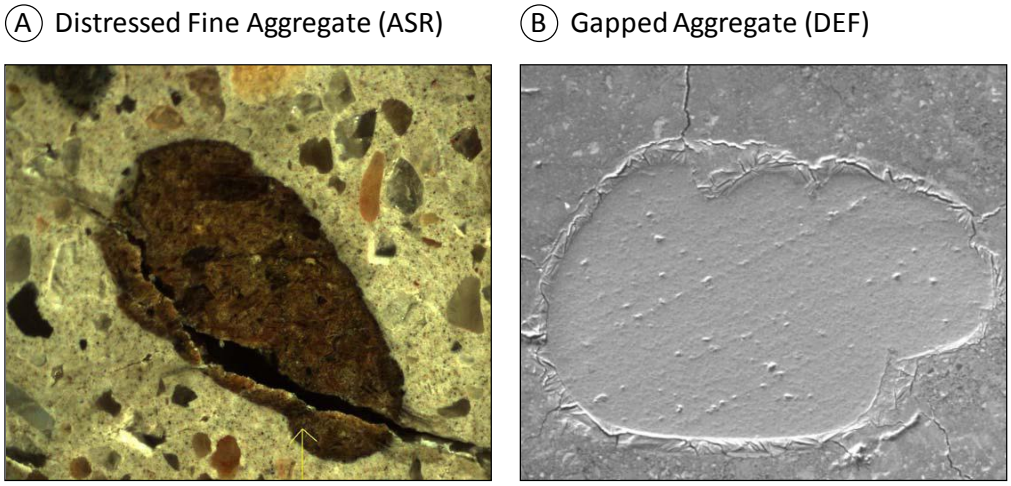

Figure 5-30: Examples of Microstructural Damage within First Series Specimens

Throughout this report, the deterioration of each specimen has been attributed to both ASR and DEF; commonly referred to as ASR/DEF or PCD (premature concrete deterioration). While the chemical processes of each mechanism are unique, the structural effects are very similar. Both are responsible for volumetric expansion and microcracking of the concrete materials. Therefore, the application of the test results (obtained from *ASR-affected* structures) presented within the previous sections should not be limited to structures which are singularly affected by ASR deterioration. Due to the fundamental similarities of the microstructural damage, the structural effects of ASR and DEF are likely to be the same; regardless of their participation (or lack thereof) in premature concrete deterioration. As discussed below, the future development of DEF deterioration within the second series specimens will be used to validate the former assertion.

Due to the distinct similarities between the first and second series, it is safe to assume that (for a given age) the microstructural damage incurred by the second series specimens was relatively similar. Therefore, it is likely the DEF-related expansion has yet to occur within reactive specimens R3 and R4. The expansion of each second series specimen stopped shortly after the petrographic analyses were performed; a signal that ASR-related deterioration has concluded. It should also be noted that "normally expansion due to DEF in field concrete occurs after 2 to 6 years" (Thaulow et al. 1997). Further moisture conditioning of the second series specimens will ensure the sufficient leaching of alkalis necessary to trigger the second round of deterioration.

To further investigate the relationship between the structural core expansions and resultant surface cracking, the general orientation of the microcracking within each core

was documented as a function of the depth into the concrete section (from the surface). Please recall that the cores were extracted horizontally through the width of each test region (perpendicular to the main axis of the bent cap specimen). To illustrate the general crack orientation within each of the reactive cores, TxDOT personnel assembled the diagram shown in Figure 5-31. The most striking feature of the diagram is the distinct transition which occurs within the first two inches of the core length (as measured from the exterior surface). The inner-region of sub-parallel cracking is indicative of the high local stresses imposed by the transverse reinforcement; the direction of least restraint (at least locally) is perpendicular to the bar. Interestingly, the absence of the same sub-parallel cracking within the first two inches of length serves as powerful evidence of the passive role played by the cover concrete. The observation strengthens earlier statements substantiating the use of surface crack width summation. It can be safely assumed that cracking of the inactive cover concrete is a singular manifestation of the structural core expansion.

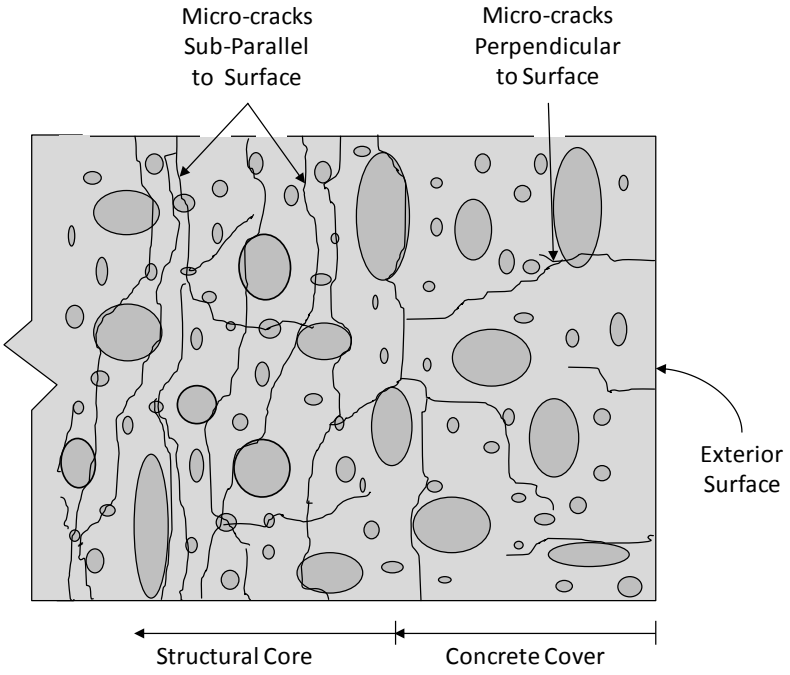

Figure 5-31: General Crack Orientation within Cores from First Series Specimens

Following the review of microstructural damage, TxDOT personnel were asked to qualitatively rank the severity of the deterioration found within each core. This exercise was requested to provide preliminary insight into the applicability of petrographic damage rating techniques (commonly used to infer material strength loss). Please note

that the following commentary is based on a very limited study of the deterioration. Full implementation of the damage rating procedures (including the use of a petrographic feature counting and weighting factors) is necessary to substantiate the comments made here. Based on their visual assessment of the deterioration, TxDOT personnel could not qualitatively distinguish between the damage in cores extracted from specimens R1 and R2. Please recall that the difference between the corresponding transverse expansion measurements was appreciable ($\varepsilon_{ct,\ max}$ = 0.17% for R1 versus $\varepsilon_{ct,\ max}$ = 0.63% for R2). It was therefore surprising that visual disparities could not be recognized. One would expect a *noticeable* increase in the frequency and volume of the reaction products for a near four-fold increase of the expansion. Likely, subjectivity would not play a role in such a simple ranking exercise. Based on these observations, the lack of correlation noted above is likely to extend to traditional implementation of the damage rating index. Ultimately, one should consider the utility of such a technique within the context of a structural assessment. The ability to predict the loss of material strength is nonessential when one has limited knowledge of the reinforcement strains. As demonstrated within Sections 5.2 and 5.3, proper assessment of a structure must consider all critical components, including the reinforcement.

5.4.2 Estimation of Current Expansive Strains

The development/validation of techniques for the estimation of in-situ expansions was deemed necessary within Chapter 4. As rationalized, possession of a sufficiently accurate method would not only allow rapid implementation of the current test results; it would also allow the consulting engineer to confidently explore the consequences of ASR/DEF deterioration in quantifiable structural terms. Two simple techniques based on the measurement of ASR/DEF-related structural phenomena were therefore selected. The accuracy and conservatism of the (1) surface crack width summation and (2) in-situ reinforcement testing are reviewed below.

5.4.2.1 Accuracy of Crack Width Summation

The use of crack width summation was predicated on the theory that ASR/DEF-related surface cracking is the singular manifestation of the structural core expansion (as discussed and substantiated above). Under ideal conditions, the summation of crack widths divided by the length over which they were measured should equate to the total core expansion minus the initial cracking strain of the concrete. Within the current study, the measurement of over 1,700 crack widths resulted in over 150 estimates which span the range of expansion (ε_c = 0.0 $\rightarrow$ 1.0%) observed within this study. The following

discussion examines the influence of the expansion direction (longitudinal versus transverse) and cracking pattern (please see Section 5.2.2.2) on the accuracy and conservatism of the expansion estimates.

Before reviewing the results, it is important to establish a set of reasonable expectations for the comparison of estimated and measured expansions. The formation of ASR/DEF-related surface cracking is subject to a number of factors (i.e. exposure conditions, mixture composition, cover depth, reinforcement configuration, etc.) which could lead to significant variations within the surface cracking pattern and corresponding estimates; even before the subjectivity of the engineer is introduced. With that said, the application of the crack width summation technique is not meant to provide exact estimates of the expansion. Rather it is hoped that the technique will allow an engineer to establish the condition of an affected bent cap in relation to certain structural thresholds (including reinforcement yield and strain hardening). In general, crack width summation will underestimate in-situ expansions; a result of the unmeasured concrete strain which occurs between each pair of cracks. While the underestimation of the concrete strains is an unconservative practice, one should consider that expansions well in excess of the reinforcement yield strain did not prove to be detrimental to the shear capacity. Use of the estimate will ultimately provide valuable, structurally-relevant information with very little effort. The practicing engineer will simply have to be aware of the limitations inherent to the method.

The use of crack width summation for low magnitude expansion estimates is examined first. For the purposes of this discussion, *low magnitude* refers to expansions at or below the nominal yield strain for grade sixty reinforcement (about 0.2%). Results for the selected range are plotted in Figure 5-32. Please note that data falling below the line of *perfect correlation* are unconservative estimates, while the opposite is true for data above the line. While a majority of the data collected from the longitudinal direction indicates an equal tendency for conservative and unconservative estimates, a few data points suggest that substantial over-estimation of the in-situ longitudinal expansion is possible. In reality, it should be recognized that expansions lower than one tenth of a percent are inconsequential in the realm of ASR/DEF deterioration (as observed within the current study). Furthermore, the utility of longitudinal expansion estimates for the evaluation of shear strength is minimal. Primary consideration should be given to the transverse expansion.

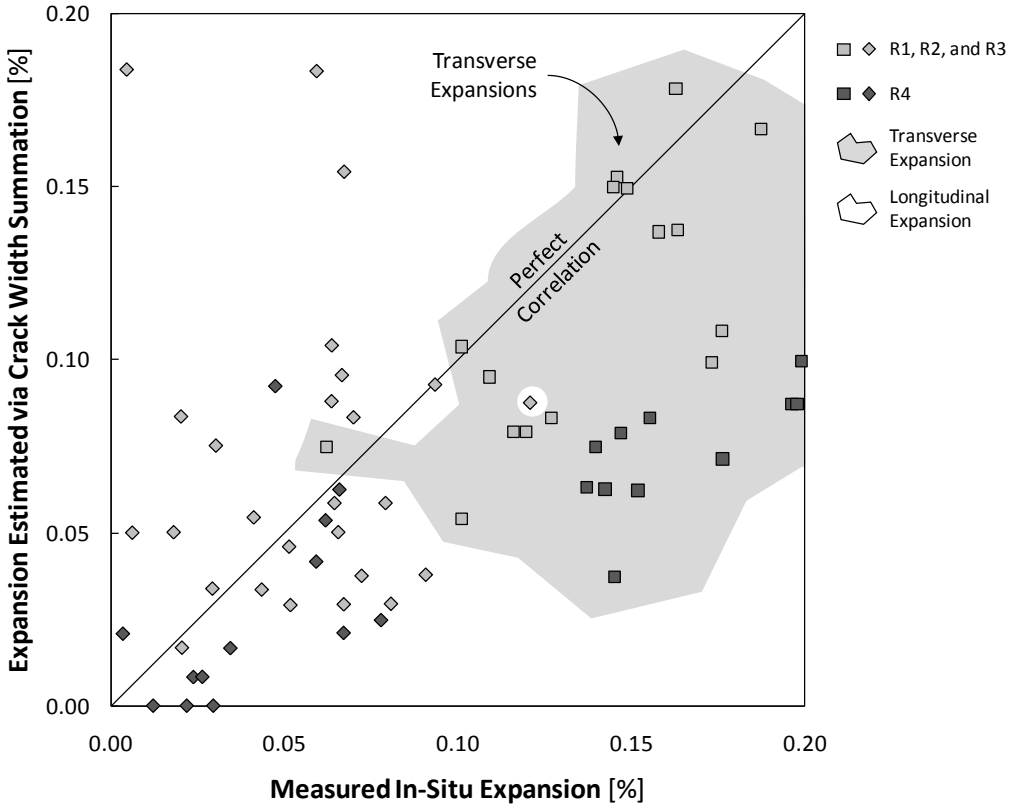

Figure 5-32: Use of Crack Width Summation to Estimate Low Magnitude Expansions

The transverse expansion estimates at low magnitudes are generally unconservative (please refer to the shaded area of data within Figure 5-32). At an expansion equivalent to reinforcement yield, it appears that one can expect estimates to be as low as 0.09 percent or about half of the yield strain. To examine the nature of the expansion estimates for transverse strains further, the results are plotted on a full-range basis (up to 1% expansion). As shown in Figure 5-33, the technique consistently provides low estimates (up to 60% less) over the full-range of measured in-situ expansion. The accuracy does seem to improve at high levels of expansion, but additional data points are necessary to adequately define the variability for extreme levels of expansion.

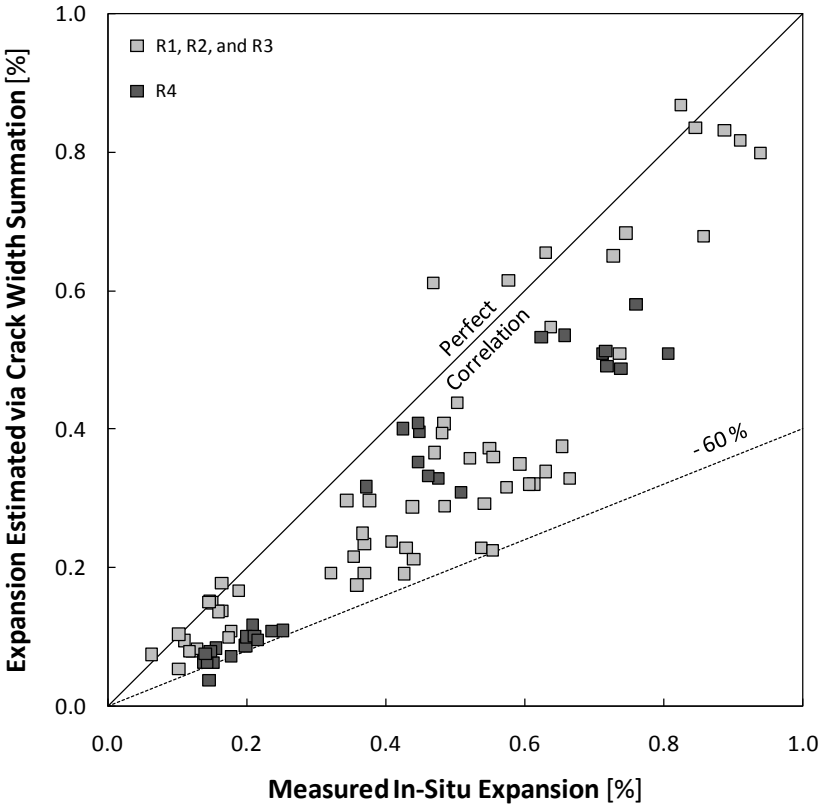

Figure 5-33: Use of Crack Width Summation to Estimate Transverse Expansions

In truth, validation of the technique could benefit from additional testing. The four reactive specimens included within the current study were nearly identical and did not allow a thorough investigation of the influential factors noted above. To illustrate the potential implications of at least one of the factors (external loading), the expansion estimates from specimen R4 have been highlighted within Figure 5-32 and Figure 5-33. Please recall that the early application of external load led to the development of a unique surface cracking pattern (Section 5.2.2.2). In reference to the estimation of transverse expansions, it appears that the wide, poorly-distributed cracks noted within each span of specimen R4 may result in particularly unconservative estimates of low level expansion. Theoretically, the result appears to be valid. Finely-spaced surface cracking (as noted within the other three reactive specimens) would certainly minimize the impact of the concrete strain between each pair of cracks and therefore lead to the more accurate estimate. It is important to recognize that the former statement can be considered speculative at this point in time. Additional testing is recommended to further establish the utility of the crack width summation technique.

5.4.2.2 Accuracy of In-Situ Reinforcement Testing

The concept for in-situ reinforcement testing was predicated on the compatibility which exists between the steel and concrete within a reinforced concrete structure. Excluding any external influences, the strains experienced by any single length of reinforcement should be equivalent to the expansion of the surrounding ASR/DEF-affected concrete. The measurement of the reinforcement strains within an existing structure can only be accomplished through destructive means. In the current study, small segments of the transverse reinforcement were exposed and instrumented with a foil gage. The reinforcement was then cut and subsequent shortening (elastic rebound) of the relieved segment was recorded.

The practicality and limitations of in-situ reinforcement testing were thoroughly examined within Chapter 4. One of the overriding limitations is worth repeating here. Due to the permanent deformations which occur after reinforcement yield (ε_y), expansions in excess of ε_y cannot be estimated through the use of this method. With that said, the method may be used to accurately establish the *occurrence* of reinforcement yield and (potentially) strain hardening. The three scenarios presented below will establish the capabilities of the in-situ reinforcement test. Assuming that *ASR/DEF expansions are…*

- *…less than the reinforcement yield point ($\varepsilon_c < \varepsilon_y$).*

  The reinforcement strain measured during the elastic unloading of the reinforcement should be equivalent to the measured concrete expansion.

- *…greater than the reinforcement yield point ($\varepsilon_y < \varepsilon_c < \varepsilon_{sh}$).*

  The reinforcement strain measured during the elastic unloading should be equivalent to the reinforcement yield strain.

- *…greater than the reinforcement strain hardening point ($\varepsilon_c > \varepsilon_{sh}$).*

  The compressive strain measured during the elastic unloading should be greater than the reinforcement yield strain, but not equal to ε_c.

In general, *elastic* unloading of the reinforcement (as a result of the cut) cannot lead to the full recovery of the *plastic* deformations which may have occurred as a result of expansion.

In-situ reinforcement tests were conducted on transverse reinforcement of each first series specimen (deep beam shear spans only). The six tests reported here cover the range of expansions which will be commonly encountered in practice (i.e. less than reinforcement strain hardening, $\varepsilon_c < \varepsilon_{sh}$). Figure 5-34 includes a comparison of the in-situ structural core expansions and the measured reinforcement strains (i.e. expansion estimates). All structural core expansions used as a basis for comparison were obtained from the mechanical strain gage measurements. Please note that the expansions and estimates are normalized by the transverse reinforcement yield strains corresponding to each specimen. In-situ expansions in excess of the reinforcement yield strain will therefore be indicated by values greater than one.

Results corresponding to the elastic scenario ($\varepsilon_c < \varepsilon_y$) will be reviewed first. The deep beam test region of the non-reactive specimen (nR1) was not subject to any long-term transverse expansion. In fact, the average structural core expansion indicated long-term shrinkage (ε_{ct} = -3% of ε_{yt}). Application of the in-situ reinforcement test was therefore expected to yield little (if any) elastic response from the transverse reinforcement. A single test conducted within the deep beam test region resulted in an expansion estimate equivalent to seven percent of the transverse reinforcement yield strain (ε_{yt}). Due to the lack of expansion within specimen nR1, the test should be interpreted as a measure of the error to be expected from implementation of the technique. This observation will be used to analyze the reactive test region results. The deep beam test region of specimen R1 was subject to structural core expansions ranging from forty-one to seventy-five percent of the reinforcement yield strain (Figure 5-34). Three individual elastic rebound tests were conducted within the corresponding region. Estimated expansions ranged from sixty-six to eighty-six percent of the yield strain; with an average estimate of seventy-three percent. In light of the aforementioned error, the expansion estimates for specimen R1 should be viewed favorably. The estimates do tend toward the higher end of the in-situ expansion range, but a nearly complete overlap of the results is achieved when one considers the potential error.

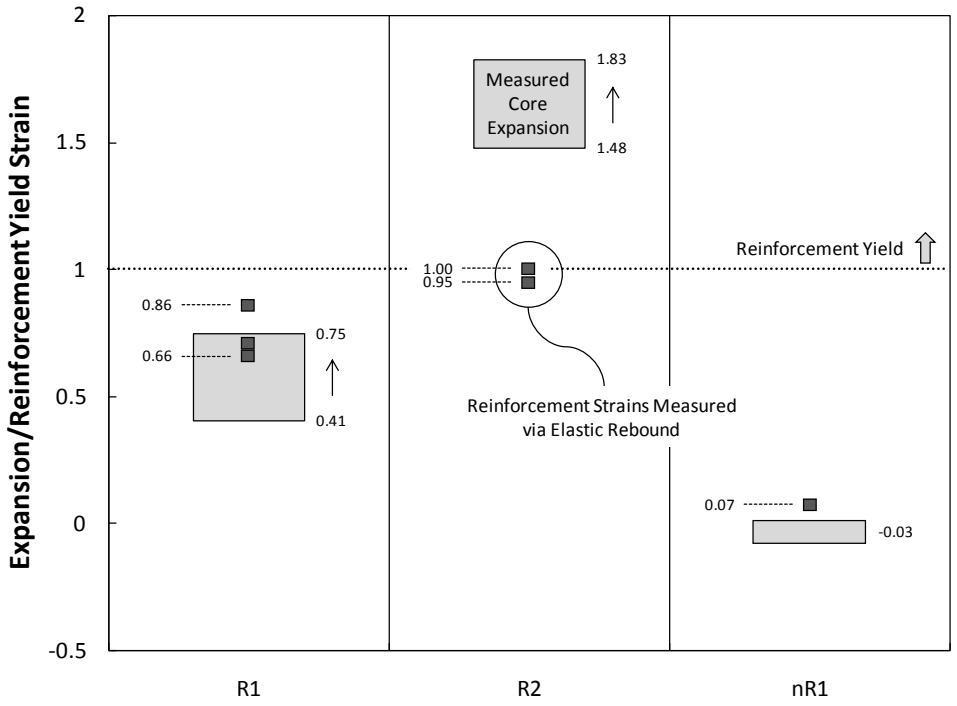

Figure 5-34: Use of Elastic Rebound Testing within the Deep Beam Shear Spans

The performance of the test under the plastic scenario ($\varepsilon_y < \varepsilon_c < \varepsilon_{sh}$) was equally admirable. The deep beam test region of specimen R2 was subject to structural core expansions of nearly double the reinforcement yield strain. Corresponding estimates of the in-situ expansions ranged from ninety-five to one hundred percent (of ε_{yt}). These results fall well within the theoretical limitations and measured accuracy presented above. Although *estimation* of the moderate-level expansions (in excess of reinforcement yield) was not possible, the *occurrence* of reinforcement yielding within the test region was successfully identified.

Implementation of the in-situ reinforcement test demonstrated excellent accuracy over for all three test regions. In fact, at low levels of expansion the method appears to be a great substitution for the crack width summation technique. The latter technique should not be immediately dismissed. Further refinement of crack width summation at moderate expansion levels could lead to a complementary pair of sufficiently-accurate estimation techniques. Such a tool set would be invaluable to consulting engineers attempting to establish the transverse expansion (the most structurally relevant measure of deterioration) within an affected structure.

5.4.3 Determination of In-Situ Concrete Properties

The shear capacity estimates presented within Section 5.3 were based on compressive strengths measured from standard cylinders. The estimates, while valid within the context of the laboratory testing, did not address the needs of practicing engineers. Strength assessment of deteriorated structures in the field will commonly require the extraction and testing of concrete cores. Recognition of this fact led to the material testing program previously outlined in Chapter 4. Concrete properties obtained from both cores and cylinders are compared within this section. Implications for the estimation of shear strength are subsequently reviewed.

Shortly after the conclusion of the shear testing phase, a total of six cores were extracted from each of the first series specimens (R1, R2, and nR1). Four of the cores were typically used to establish the splitting tensile strength, while the remaining samples were tested in compression. The skewed distribution of tests catered to earlier observations regarding the sensitivity of the test methods to ASR/DEF deterioration (please refer to Chapter 2). All of the results presented below are the average values from each series of cores. Variation between samples was minimal and within the acceptable bounds defined by ASTM C42. Individual test results can be found within Appendix C. Please recall that the cores represented the most severe damage found within each test region. This approach ensured that the resulting strength estimates would be conservative in nature.

The compression test results are summarized within Figure 5-35. In general, the strengths obtained from the standard cylinder tests were twenty to thirty percent higher than those obtained from the core tests. Before conclusions were drawn, general inconsistencies between standard cylinder tests and core tests were examined. Historically, concrete material strength loss has been reported as a result of the core extraction process (Bae et al. 2007). To compensate for the effect of the coring operations (and other factors), a factor of 0.85^{-1} is commonly recommended for the modification of the concrete strengths obtained from core tests. In other words, concrete cores can be assumed to have eighty-five percent of the strength measure from standard concrete cylinders (ASTM C42 2004). The concrete strengths obtained through core tests were modified as recommended (Figure 5-35). The adjusted compressive strengths compare reasonably well to the cylinder-based measurements. The slight differences (less than 15%) remaining are most likely attributable to minor inconsistencies between the cylinder and structural core deterioration.

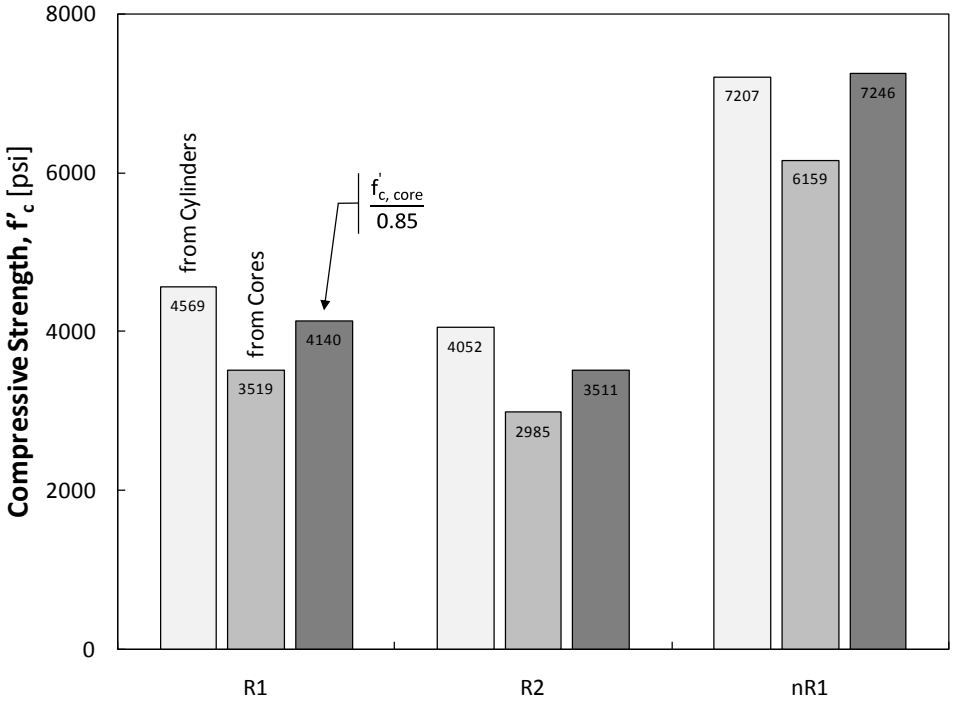

Figure 5-35: Compressive Strength from Standard Cylinders and Cores

The splitting tensile test results are summarized within Figure 5-36. While the tensile strengths obtained from the cylinders were generally greater than those obtained from the cores, the maximum discrepancy observed was only eleven percent. The results display excellent compatibility despite the fact that this comparison (unlike the previous) does not even take into account any extraction-related losses of strength which may have occurred in the cores. Based on the results of both compression and splitting tensile testing, it can be concluded that the cylinders provided an excellent representation of the structural core strength.

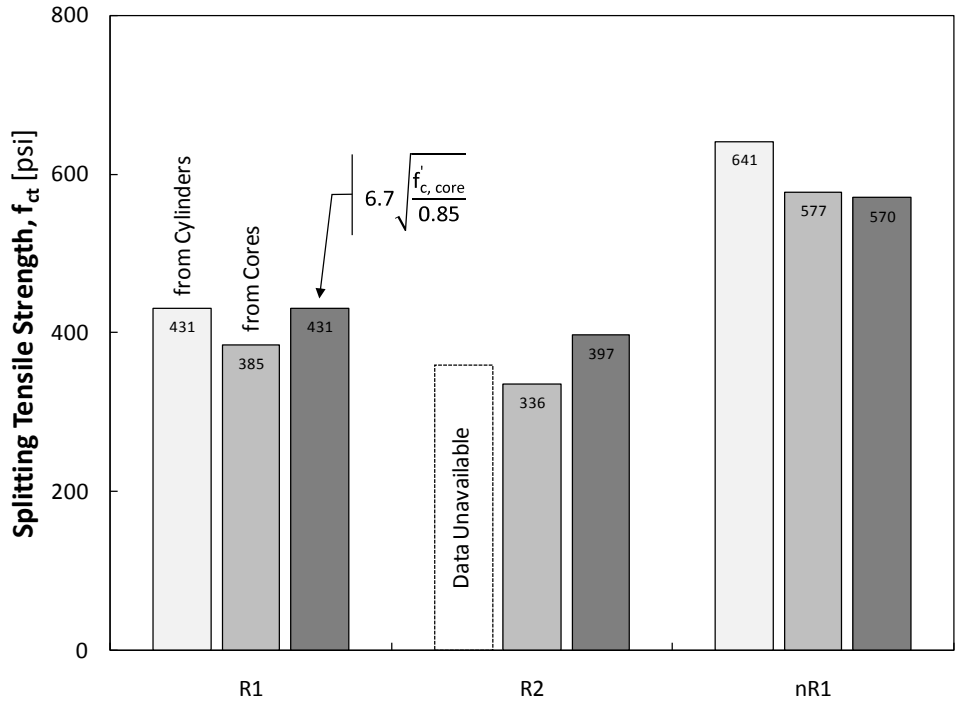

Figure 5-36: Splitting Tensile Strength from Standard Cylinders and Cores

The use of the standard cylinder strengths within Section 5.3 led to the conservative estimation of the bent cap shear capacity for both deep beam and sectional shear spans. Subsequent testing of cores led to consistently lower compressive and splitting tensile strengths than obtained via the standard cylinders. Due to the transitive nature of the comparison, it can be concluded that the use of in-situ material properties would also provide conservative estimates for the shear capacity of ASR/DEF-affected bent cap structures.

Examination of the strength data also allowed the performance of the ASR/DEF-affected concrete to be placed within the context of normal concrete behavior. The relationship between the splitting tensile and compressive strength of a typical concrete cylinder or core can be described by the following expression: $f_{ct} = 6.7\sqrt{f'_c}$ (ACI 318-08). For concrete subject to ASR and/or DEF, it has been suggested that the splitting tensile strength is lost at a faster rate than the compressive strength (please refer to Chapter 2). This implies that the aforementioned relationship is not maintained as expansions grow larger. To examine this claim within the context of the current study, material testing results (unaltered) from the cylinders and cores are plotted within Figure 5-37. Based on the proximity of each result to the predictive equation, it does not appear that ASR/DEF-

related expansion has led to the accelerated loss of concrete tensile strength. To further demonstrate the applicability of the ACI expression, estimates for the concrete tensile strength within the reactive specimens were calculated and included within Figure 5-36. Excellent agreement with the measured strengths was achieved.

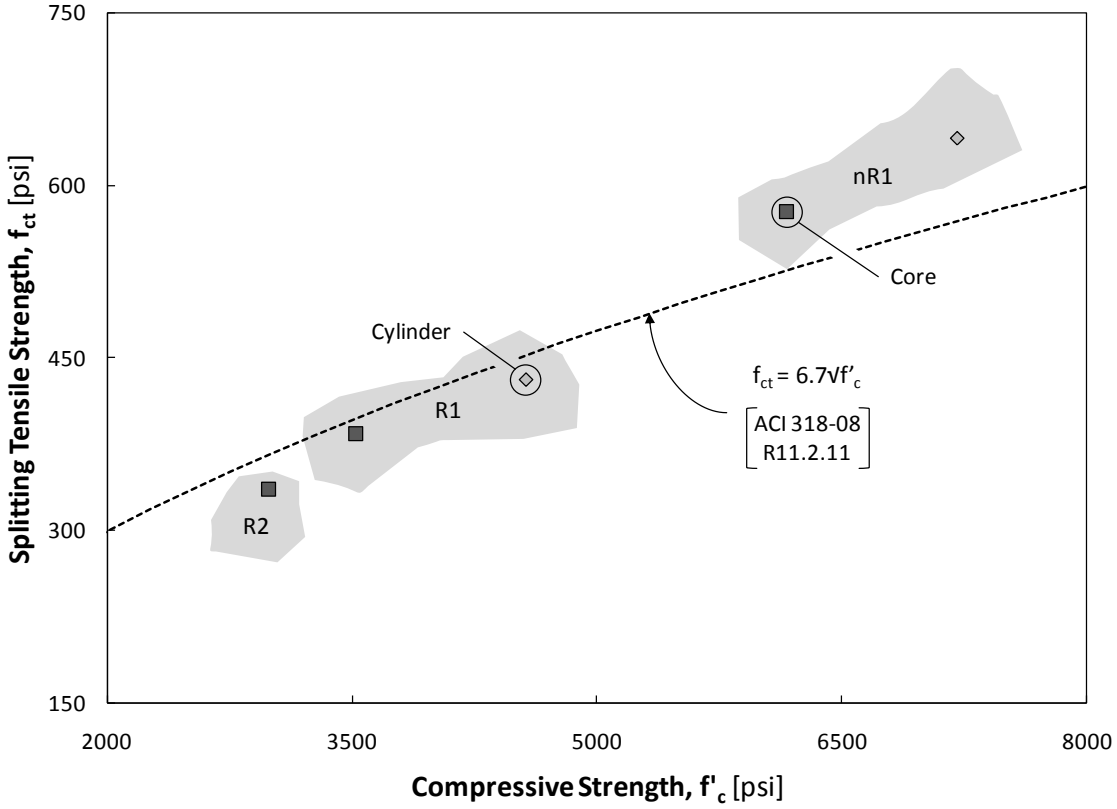

Figure 5-37: Relationship between Splitting Tensile and Compressive Strength

It is important to recognize that the results presented here are characteristic of the concrete mixture used within the current study. Alternate mixture proportions and constituent materials could lead to substantially different performance of the hardened concrete. With that said, it is unlikely that the use of in-situ concrete properties (i.e. obtained from core tests) will ever lead to an unconservative estimate of shear capacity. Extraction of the cores results in the loss of structural context and beneficial confining stresses. Subsequent testing of the unconfined, damaged material will only result in a conservative measure of strength.

5.4.4 Estimation of Future Expansion Potential

The expansion testing of cores from an affected concrete structure is purported (within the literature) to accomplish two goals: (1) to determine if the concrete is susceptible to further ASR and/or DEF deterioration, and (2) to evaluate the magnitude of future expansions. While the aforementioned goals are admirable, the value of the resulting data for the purposes of structural evaluation has yet to be established. Three distinct expansions tests outlined within Folliard's *Protocol for the Diagnosis and Prognosis of Concrete Structures Affected by ASR and/or DEF* (2007) were therefore implemented within the current study. Although a full disclosure of the testing details was made in Chapter 4, select details are repeated here for the reader's convenience.

To provide a fair representation of the damage, nine cores (of various sizes, three per expansion test) were extracted from select locations within each of the second series specimens. The twenty-seven samples were then trimmed and outfitted with gage points. Following an initial set of length measurements, the cores were placed within their respective conditioning environments (detailed below). Periodic length change measurements established the time-dependent expansion history. As an aside, it should be noted that overall implementation of the expansion testing required a significant investment of resources. The investment of man-hours and facilities necessary to conduct such a program may be beyond what is practically accomplishable within an individual assessment budget.

Each of the three expansion tests was conducted to accomplish one (but not both) of the aforementioned goals. To successfully establish the susceptibility to ASR and/or DEF, two tests isolated the development of each mechanism. The concrete samples for Test A (*ASR Expansion Potential*) were subjected to a near-infinite supply of the alkalis necessary for aggregate expansion. The complementary set of concrete samples for Test B (*DEF Expansion Potential*) was soaked in limewater to lower the pH below the threshold necessary for ettringite precipitation. In either case, the conditioning environment represented the ideal conditions necessary for the respective mechanism. As a result, the magnitudes of the core expansions are not likely to be representative of the measured in-situ expansions. A realistic estimate of the future expansion due to either of mechanisms was therefore accomplished with Test C (*PCD Expansion Potential*). The results from all of the tests are summarized within Figure 5-38. Please note that the horizontal and vertical axes are all held to the same scale to expedite comparisons. To ensure a fair evaluation of the expansion testing program, the following analysis of each test method is limited to a review of the performance relative to the intended purpose.

The ability of Tests A and B to establish the *potential* for future deterioration will be reviewed first. At the time of core extraction, examination of the expansion monitoring and petrographic evaluation results revealed that the second series specimens were subject to ongoing ASR deterioration. No conclusive signs of DEF were identified at that point. It was therefore expected that both expansion Tests A and B would yield positive indication of further ASR and DEF expansion (respectively). As shown within Figure 5-38, the expectations held true. Cores taken from specimens R3 and R4 exhibited final ASR and DEF expansions of at least 0.13 percent and as much as 1.06 percent. In reference to the former values, it is important to recognize that the core expansion tests are measures of supplementary expansion (i.e. the expansion which occured in addition to the in-situ expansions noted at the time of core extraction). Core test values should not be expected to correlate with the total in-situ expansions.

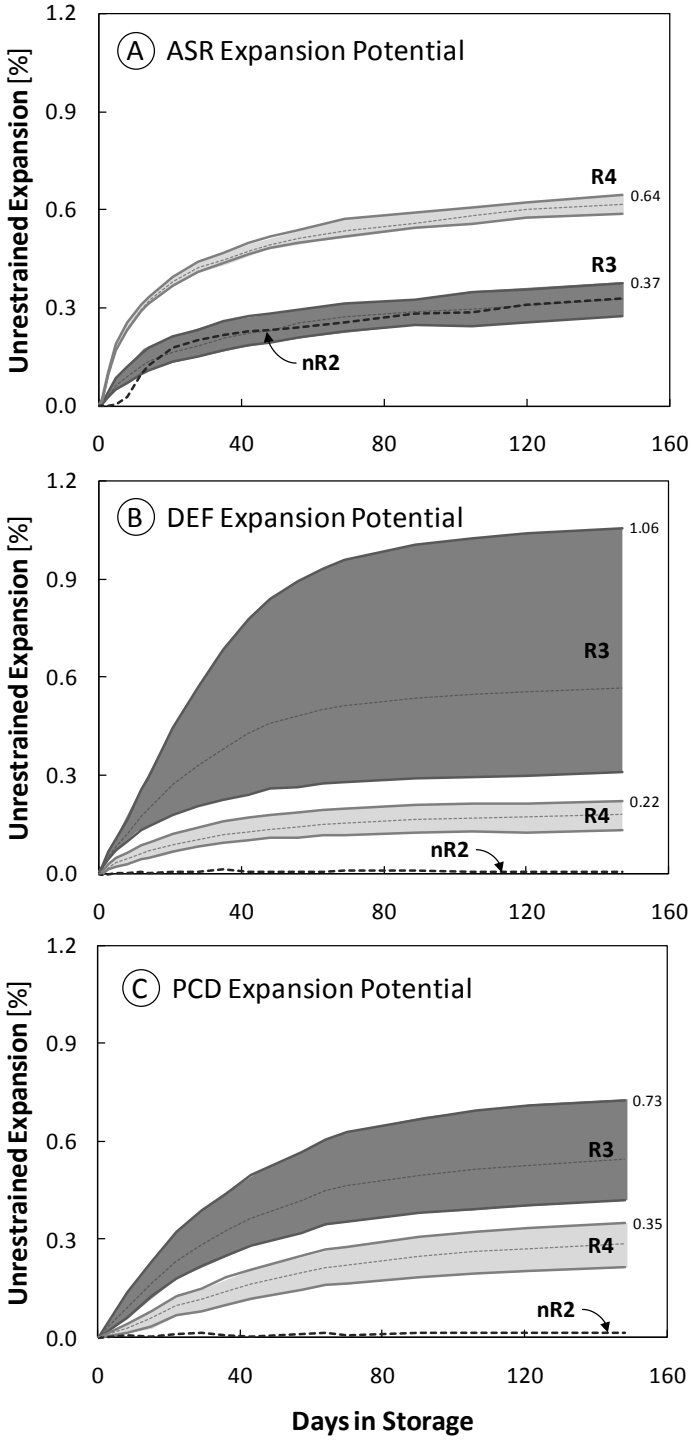

Figure 5-38: Summary of Expansion Testing Conducted on Second Series Specimens

While the tests were successful in indentifying the future expansion potential, the nature and utility of the results need to be further examined. As currently defined, the results of both tests can only be interpreted in a binary manner: the potential for expansion does or does not exist. Such a simple (and unsubstantiated) interpretation could lead to poor diagnoses. Non-reactive specimen nR2 illustrates the former assertion. In spite of never exhibiting any signs of deterioration (before or after core extraction), the result of Test A indicated that specimen nR2 could be subject to future ASR-related expansions as severe as specimen R3 (Figure 5-38A). Without additional information, such a diagnosis for a durable field structure would be extremely misleading. Proper confirmation or denial of such a result would require an additional test (at *additional* cost) to define the availability of alkalis within the structure. By now the substantial costs associated with expansion testing should be apparent. It has been suggested by TxDOT personnel that a reduction of the sampling requirements would be of substantial benefit to the practicality of the approach (Vogel 2008). While the need to reduce the number of specimens is appreciated, results from Test B show that the cost-cutting measure may have negative implications on the conservatism of the method. Final DEF-related expansions measured within samples from specimen R3 ranged widely, from 0.31 to 1.06 percent. Based on the variation obtained within the three samples, it is conceivable that a reduction in the core requirements could lead to the extraction of highly unrepresentative samples; and ultimately result in potential misdiagnosis. The observation substantiates the Protocol's recommendations for sampling, but also eliminates the potential for cost-savings (and enhanced practicality) through reduced sampling requirements.

Ultimately, one has to question the utility of the information gained through Tests A and B. A practicing engineer conducting a structural assessment is unlikely to benefit from the knowledge that ASR- and/or DEF-related expansions are possible in the future. While the potential cause of the deterioration is of critical importance to those coordinating mitigating measures, it is of little consequence to structural engineers. The effects of the deterioration are indistinguishable in structural terms. With that said, a *reasonably* conservative estimate of the future PCD-related expansions would be relatively beneficial. However, neither of the aforementioned tests can serve such a role due to their overly-conservative nature. The ideal storage conditions and lack of structural context will consistently lead to expansion values well-in-excess of those measured within the field.

The final expansion test may provide the most useful information of the core testing program. As noted above, the purpose of Test C (*PCD Expansion Potential*) is to provide realistic estimates of expansion due to either of the premature concrete deterioration

mechanisms. In contrast to Tests A and B, the cores within Test C were subjected to harsh, but not necessarily aggressive, storage conditions (100°F and near 100% relative humidity). The designed balance of specimen size and moisture exposure within the test allows the deterioration to develop in a manner similar to that found within field structures. In other words, controlled leaching leads to the full development of ASR and subsequent initiation of DEF. Final expansion estimates from Test C are summarized within Figure 5-39 (corresponding core histories are included within Figure 5-38). The expansion results from each individual core are plotted against the range of *expansion growth* measured within a given specimen. Please note that the term *expansion growth* refers to the measured change of in-situ deterioration occurring between the core extraction operations and the plateau of expansion noted in Section 5.2.1. The results from Tests A and B are included within the Figure 5-39 to highlight the disparities noted earlier.

Based on evidence obtained during the petrographic analysis (Section 5.4.1), it was assumed that the observed plateau of in-situ expansions coincided with the conclusion of ASR-related deterioration. DEF-related expansions are therefore expected to occur in the future. Consequently, the results from the final expansion test (Test C) should not be expected to coincide with the measured structural core expansion growth. Future development of DEF deterioration within the second series specimens will ultimately allow a more conclusive comparison of the results. For now, a brief review of the results for specimen R3 will illustrate the range of behavior to be expected. In the time between core extraction operations and the expansion plateau, the structural core expansions grew between 0.08 and 0.17 percent (as a result of ASR-related deterioration). Corresponding final expansion estimates provided by Test C ranged from 0.42 to 0.73 percent (as a result of ASR- and DEF-related deterioration). If one temporarily neglects any external effects, future DEF-expansions can be expected to range from 0.25 to 0.65 percent. Such growth could ultimately lead to peak transverse expansions of nearly 1.6 percent. While the former estimate seems reasonable, future DEF-related expansions are likely to fall well below the range of estimates provided above (for reasons which are discussed in further detail below).

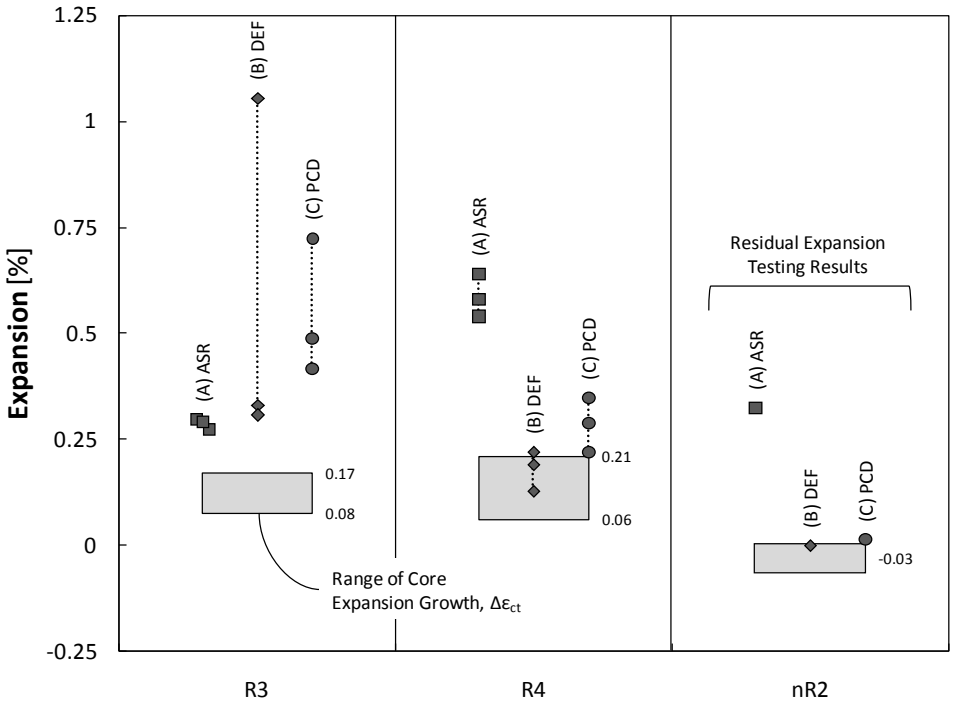

Figure 5-39: Comparison of Residual Expansion Testing and Measured Expansion Growth

As noted within Chapter 4, the fundamental flaw with the expansion testing approach is the "unknown true correlation between *free expansion* of cores and the actual expansion in reinforced concrete members" (Fournier 2004). Attempts to generalize the effects of restraint on the free expansion of ASR/DEF concrete are conducted in vain. An inordinate amount of testing would be required to establish a relationship which accounted for the large variation of concrete materials and mixture proportions encountered within practice. Furthermore, application of the relationship would be limited by the inability to accurately quantify the active restraints and stresses within a field structure. Expansion testing, in particular Test C (PCD Expansion Potential), will only show promise if reasonably conservative estimates of the expansion can be obtained without manipulation of the results. Otherwise, the high costs associated with the method will general prohibit implementation during routine structural assessment of ASR/DEF-affected structures.

5.5 SUMMARY

Results of the three-phase experimental program (Phase I: Specimen Conditioning and Expansion Monitoring, II: Shear Testing, and III: Forensic Analysis) were reviewed

within this chapter. Concurrent analysis of the results from each phase was conducted with one goal in mind: to establish the relationship between measured (or estimated) in-situ damage and the shear capacity of the ASR/DEF-affected bent cap specimens.

Review of the specimen deterioration began with a detailed exploration of the structural concrete core expansions and reinforcement strains. Following a generally short incubation period, the reactive specimens were subject to rapid deterioration which lasted for several months. The resulting structural core expansions were characterized by overwhelming growth in the transverse direction; net long-term expansion within the perpendicular direction was generally not observed. The role of reinforcement restraint was subsequently examined in an effort to explain the anisotropic nature of the expansion. Advanced stages of the deterioration generally subjected the transverse reinforcement to exceedingly high tensile strains (near 1%, well in excess of yield). The longitudinal (flexural) reinforcement strains, however, were consistently low for all stages of deterioration; active restraint of ASR/DEF-related expansion was not apparent. Distinct similarities drawn between the longitudinal response of both reactive and non-reactive specimens ultimately suggested that the flexural reinforcement was not entirely responsible for the anisotropy of the expansions (an observation supported by literature reviewed within Chapter 3). Regardless of the potential causes, transverse expansion was recognized as the most structurally relevant measure of the long-term deterioration for the specimens included within the current study.

Examination of the surface cracking within all four reactive bent cap specimens completed the review of time-dependent deterioration. Comparison of photographs and measurements taken from each specimen helped to clarify the role of externally applied restraint. The first series specimens were placed under conditioning more than two hundred days after the concrete placement. As a result, expansions and cracking developed under the influence of the reinforcement restraint only. The resulting cracks were particularly fine and very well distributed. The overall pattern could have been classified as random *map cracking*, though in-depth consideration of the crack distribution revealed anisotropy consistent with that noted earlier. In comparison, the last reactive specimen to be fabricated was placed under conditioning load within the first one hundred days of exposure; cracking had yet to be observed. The resulting crack pattern was of a completely different nature. Exceptionally wide longitudinal cracks (up to 0.045 inches) were poorly distributed through the depth of the beam. The cracks were slightly inclined due to the presence of the conditioning load, but they in no way resembled the load path which existed between the two opposing bearing plates. Due to limited

penetration of the surface cracks into structural core, it was concluded that the effect of conditioning load on structural performance would be limited.

Prior to the review of shear testing results, the state of deterioration within each bent cap specimen was summarized. Transverse expansions within the first series specimens ranged from 0.0 percent (undamaged) to 0.7 percent (moderate damage) immediately before Phase II shear testing commenced. Deterioration within the second series specimens (untested at the time of publication) also covered a wide range of transverse expansions; from 0.0 percent to 1.0 percent.

Effects of the deterioration (as encompassed by the first series specimens) on service and ultimate load behavior were evaluated through the examination of four sectional (a/d = 3) and four deep beam (a/d = 1.85) shear tests. The following observations and conclusions are applicable to both shear span-to-depth ratios due to similarity of the results. Application of service level loading (generally equivalent to one-third of the maximum applied load, as defined by TxDOT Project 0-5253 researchers) did not lead to the development of shear cracking within the reactive specimens. In fact, first diagonal cracking typically occurred at double the load at which cracking was first observed within the corresponding non-reactive specimens. The uniqueness of the observation was confirmed through the examination of code-based diagonal cracking estimates. Suppression of the cracking was ultimately attributed to the compressive stresses induced by the restraint of the transverse reinforcement. Failure of the reactive shear spans came with little warning. The development of very few diagonal cracks was succeeded by a sudden, decidedly brittle loss of equilibrium. Failure crack patterns presented in this chapter illustrated the severe disparity between the behavior of undamaged and deteriorated shear spans. Despite this observation, the strength of each bent cap specimen was not compromised; regardless of the deterioration severity. Furthermore, the use of both sectional and strut-and-tie models (in combination with material strengths from cores or cylinders) resulted in conservative estimates of the shear capacity in every case.

The sectional and deep beam shear capacities were maintained in spite of peak transverse expansions of up to 0.7 and 0.45 percent, respectively. This fortunate outcome was attributed to the confinement provided by the transverse reinforcement. More specifically, the transverse reinforcement maintained equilibrium of the expansive cross-section and thereby generated compressive stresses which offset the material strength loss due to ASR/DEF. It was previously noted that the importance of the confining reinforcement should not be underestimated. Loss of confinement through fracture of the

highly stressed reinforcement would lead to rapid deterioration of the structural core and an unquestionable loss of structural safety.

Application of the shear testing results depended on the ability to accurately characterize the deterioration within affected field structures. A number of forensic analysis techniques were therefore implemented within the current study. For the sake of brevity, specific results from the techniques will not be summarized here. Rather, the two general approaches to forensic analysis will be reviewed to provide insight into the practicality of the individual methods. The first subset of the techniques singularly characterized the condition/behavior of the deteriorated concrete materials through sample testing (i.e. damage rating index, residual expansion testing). For the purposes of structural assessment, these methods suffered from a lack of structural context. Observed correlation between the individual test results and in-situ behavior was typically limited to a particular material and structure. Practical application of the results would therefore require the development of numerous correlations. The practicality of such methods was further limited by the costs associated with the extensive material testing required. In contrast, alternate methods which relied on the measurement of ASR/DEF-related structural phenomena (i.e. crack width summation, in-situ reinforcement testing) typically resulted in sufficiently accurate estimates of the in-situ deterioration. Implementation of the techniques was limited to relatively simple field work; significant investment in material testing infrastructure was not necessary. Information gathered through these methods was applicable to the behavior of both the reinforcement and deteriorated concrete. As noted multiple times above, knowledge of both the reinforcement and concrete performance are critical to a proper structural assessment.

CHAPTER 6
Field Assessment

6.1 OVERVIEW

Shortly after the conclusion of Phase II (Shear Testing), researchers at Ferguson Structural Engineering Laboratory were given the opportunity to inspect a prematurely damaged bent cap in Houston, Texas. This chapter summarizes the results of the inspection and includes (1) the conditions leading to the deterioration, (2) the visual nature of the field damage, and (3) the general approach to inspection and assessment of the bent cap structure. First-hand experience from the inspection is ultimately used to pass judgment on the assessment rationale developed within Chapter 5.

6.2 PREMATURE DETERIORATION OF US 59 AND I-10 INTERCHANGE

In 1997, the Texas Department of Transportation began reconstruction of the US 59 and I-10 interchange in Houston, Texas. The ambitious project included the replacement of the US 59 mainline structures and several exit ramps to and from I-10. It was, in fact, the largest interchange project to be undertaken near downtown Houston since 1974 (corresponding to the US 59 and I-45 interchange project). Construction lasted about four years and cost nearly one hundred twenty-seven million dollars. The new interchange formally opened in 2001 (Jackson and Slotboom 2008).

One connection ramp is of particular interest within the context of the current study. The ramp from US 59 North to I-10 West is highlighted in the aerial view of the interchange contained within Figure 6-1. It consists of steel trapezoidal box girder pairs supported by a combination of cast-in-place hammerhead piers and straddle bents. The ramp supports one lane of traffic and includes a *stub-out* for further expansion to the Hardy Toll Road freeway extension (yet to be built). It is the longest connection bridge structure within the US 59 and I-10 interchange.

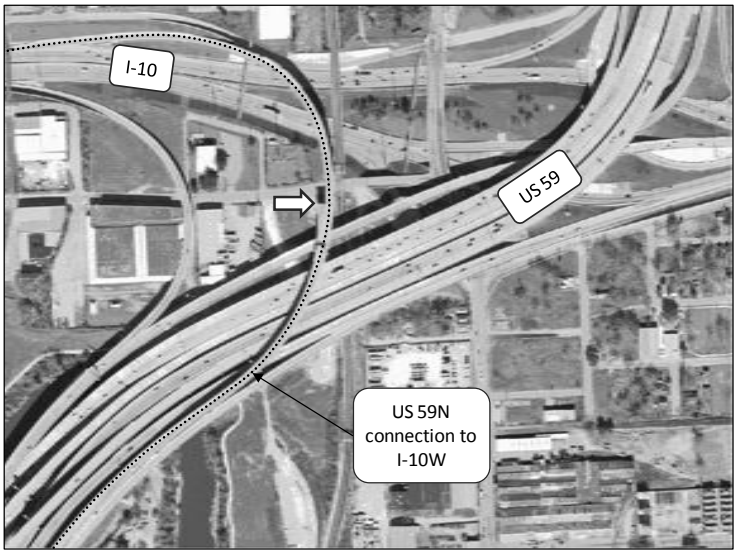

Figure 6-1: US 59N Connection Ramp to I-10W

Within seven years of the interchange opening, substructures of the US 59 North connection ramp to I-10 West displayed visual indications of ASR-related deterioration. During a preliminary visit to the structure in 2008, map cracking and a mottled buff color were clearly noticeable on the exposed sections of the hammerhead piers and straddle bent caps. It is important to note that these observations were made from the ground; affected elements were commonly forty to sixty feet above grade. Examples of the deterioration which appeared on a number of the substructure elements are provided within Figure 6-2.

Figure 6-2: Signs of Deterioration within Connection Ramp Structures

Common signs of deterioration found within each of the crossheads and bent caps led to an examination of the concrete mixture design for those elements. Table 6-1 summarizes the mixture proportions and material sources for the concrete used throughout the connection ramp substructure. Please note that the following information (mixture design, petrography results, etc.) was obtained from the Houston District engineers responsible for the management of the deteriorated structures (Vogel 2008). The total quantity of cementitious material (cement and fly ash) was equivalent to a six and one-half sack concrete mixture. While the proportion of cementitious material is high, it is not indicative of a reactive concrete mixture. Only knowledge of the in-situ concrete alkali content could be used to establish such a condition. In truth, the most concerning aspect of the concrete mixture design lies in the use of recycled fine and coarse aggregates. It is unclear whether standard durability tests (i.e. ASTM C1260, ASTM C1293) were required prior to the use of the recycled aggregates for the interchange project. However, current TxDOT specifications do not allow the use of recycled aggregates for structural applications of any kind; a fact which potentially represents an acknowledgement of poor durability performance in the past.

Table 6-1: Mixture Design for Connection Ramp Structures

	Mix Design	Source
Type I/II Cement	507 lb/yd^3	Sunbelt Cement Inc. Katy, Texas
Type C Fly Ash	106 lb/yd^3	W.A. Parish Power Plant Thompsons, Texas
Water	248 lb/yd^3	Municipal Water Supply
Recycled Fine Aggregate	950 lb/yd^3	DDS Aggregates Inc. Cleveland, Texas
Recycled Coarse Aggregate	1845 lb/yd^3	DDS Aggregates Inc. Cleveland, Texas
Water-to-Cement Ratio	0.40	
Theoretical Unit Weight	135 lb/ft^3	
28-Day Strength Estimate	4050 psi	

Confirmation of the recycled aggregate reactivity came through the petrographic analysis of a single core taken from the crosshead of a pier structure (designated Bent 12). All aspects of the analysis were carried out by the TxDOT Concrete Laboratory. The appearance of the core upon extraction gave an immediate indication of the deterioration

mechanism. White reaction product (Figure 6-3B, a common sign of alkali-silica reaction) was visible in at least one of the air voids present on the fractured surface of the core. Following a complete petrographic examination, the deterioration was attributed to siliceous cemented sandstone particles which commonly exhibited signs of distress (Figure 6-3A). It was further concluded that the reactive aggregate particles were introduced to the mixture through the use of crushed concrete (i.e. recycled) aggregate.

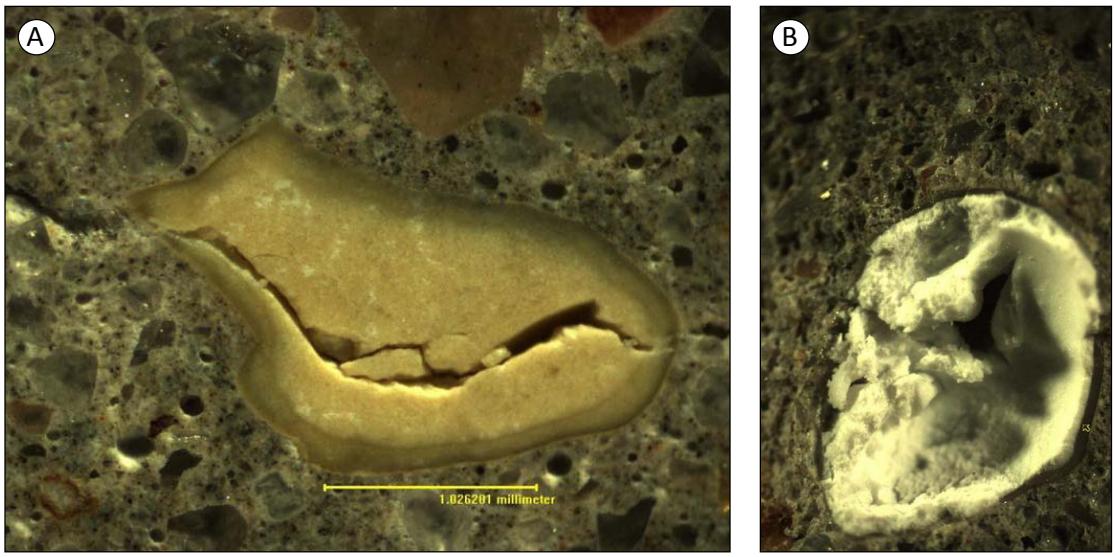

Figure 6-3: Petrographic Evidence of ASR
(A) Distressed Fine Aggregate (B) Gel-Filled Air Void

At the time of the preliminary examination (described above), Houston District engineers were faced with a similar state of deterioration in a number of bent caps throughout the city. Uncertainty regarding the appropriate management strategy for the deteriorating structures undoubtedly supported the need for the current project.

6.3 FIELD INSPECTION OF BENT 15

One particular bent within the US 59 North connection ramp to I-10 West was subject to deterioration which was exceptionally severe in appearance. Bent 15 supported the primary lane of traffic to I-10 West as well as a *stub-out* for future connection to the Hardy Toll Road freeway extension (as described earlier). The location of the bent within the connection ramp bridge is indicated by the arrow in Figure 6-4 (and Figure 6-1). The geometry of the bent structure (including dimensions) can be found within Chapter 3. In

general, the bent cap was six feet deep, six feet wide and spanned a distance of about thirty feet between the inside faces of the two columns.

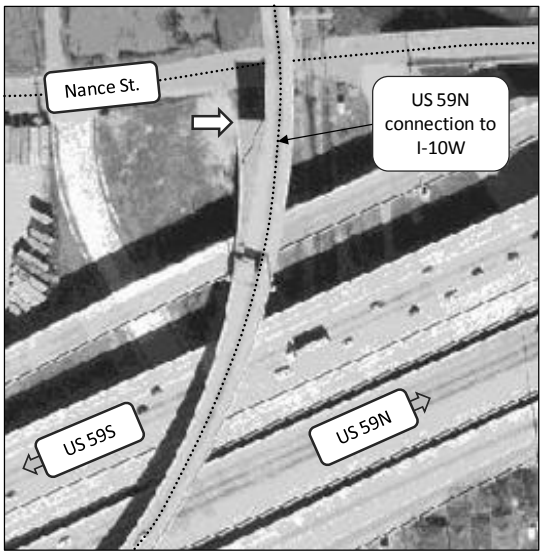

Figure 6-4: Location of Bent 15 within US 59N Connection Ramp to I-10W

The accommodation made for the future connection meant that a relatively long segment of the bent would remain unsheltered until the superstructure was put into place. In light of the aggregate reactivity, the resulting exposure conditions were severe. Run-off from the *stub-out* fell directly onto the top of the bent structure. Furthermore, a drain line from the superstructure was directed through the western end of the bent cap. From the moment the ramp opened, a high-volume, renewable source of moisture was present to fuel any deterioration mechanisms which may have been present. The condition clearly exacerbated the development of expansion within the first few years of construction. To more accurately characterize the deterioration which was present less than twelve years after the start of construction, an aerial lift (i.e. *bucket truck*) was used to conduct a close-up inspection of the Bent 15, as shown in Figure 6-5.

Figure 6-5: Bent 15 Inspection with Aerial Lift

Signs of deterioration noted within the exposed span of the bent cap are shown in Figure 6-6. The western end of the bent cap was subject to particularly heavy cracking which appeared to emanate from the point at which the drain line entered the structure. Cracking at the ends and throughout the bent cap was generally random in nature. Cracks were widely spaced (a general spacing of about four inches was noted) and unaccompanied by the fine cracks noted within the laboratory study. The overall pattern was best classified as map cracking. Alternate signs of deterioration included small areas of concrete subject to spalling and an atypical buff coloring of the concrete which was only found within the exposed sections of the structure.

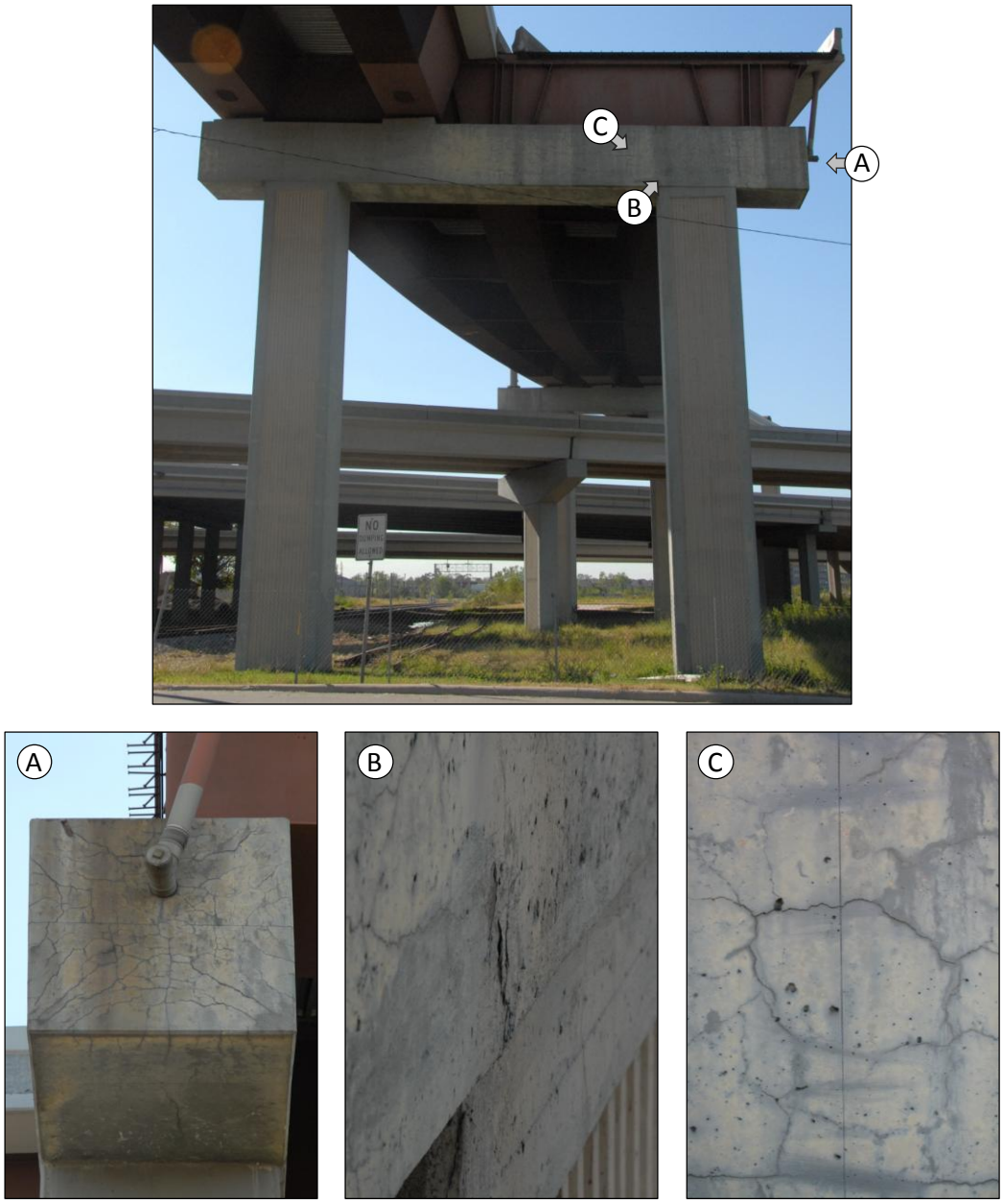

Figure 6-6: Visual Signs of Bent 15 Deterioration

While close-up inspection of the bent cap reinforced the qualitative *severity* of the visible deterioration, structural assessment of the bent cap could only be accomplished through quantitative estimation of the in-situ expansions.

6.4 STRUCTURAL ASSESSMENT OF BENT 15

Preliminary assessment of the structural safety (in regards to shear strength) was accomplished through documentation of the surface cracking and estimation of the ASR-induced expansions. First, a series of photographs were taken along the length of the bent cap to record the surface cracking pattern. The photographs were then digitally stitched together; thereby allowing the cracks to be comprehensively mapped over the entire north elevation of the structure (as shown in Figure 6-8). Second, ASR-induced expansions were estimated through the use of the crack width summation method (introduced and evaluated within Chapters 4 and 5, respectively). Measurement of the crack widths was conducted over a number of prepositioned forty-eight inch gage lengths, as shown within Figure 6-9. These locations were selected to explore the influence of the reinforcement configuration (shown in Figure 6-7) and load position (indicated within Figure 6-8). Please note that all assessment operations were conducted during the aforementioned inspection. No more than three operating hours were logged on the aerial lift in total.

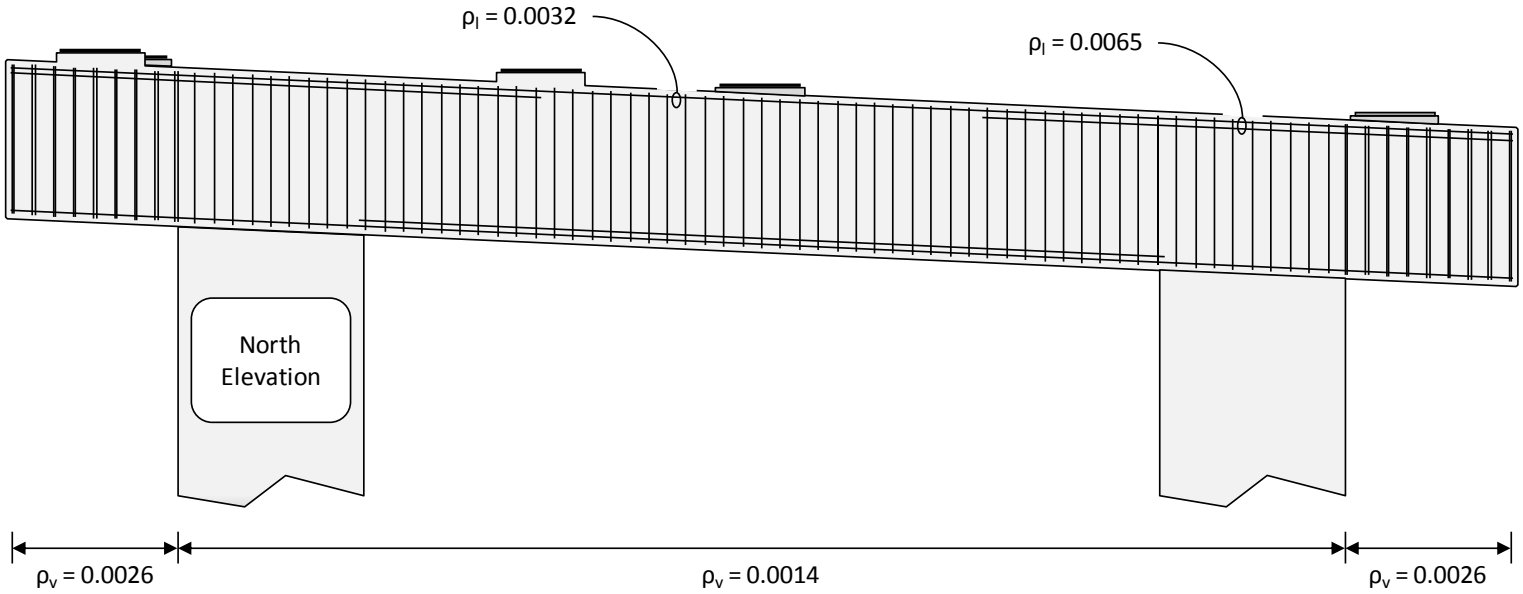

Figure 6-7: Reinforcement Configuration for Bent 15

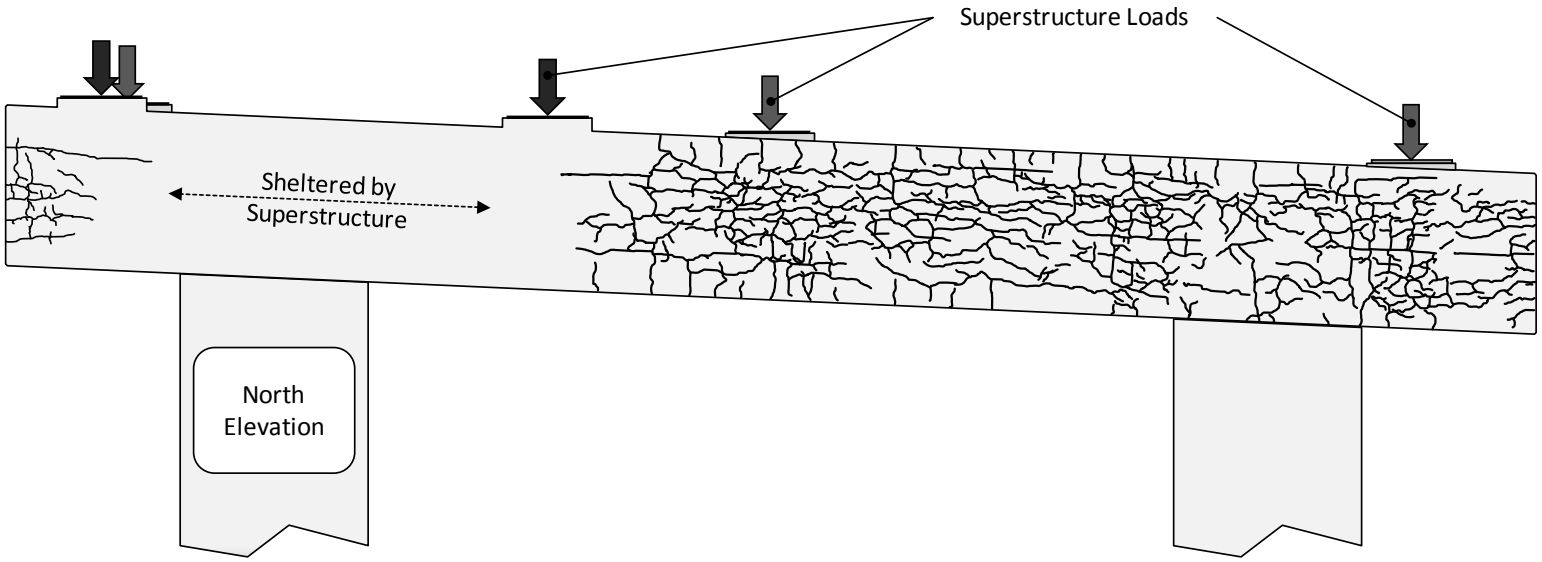

Figure 6-8: Surface Cracking Pattern on Bent 15

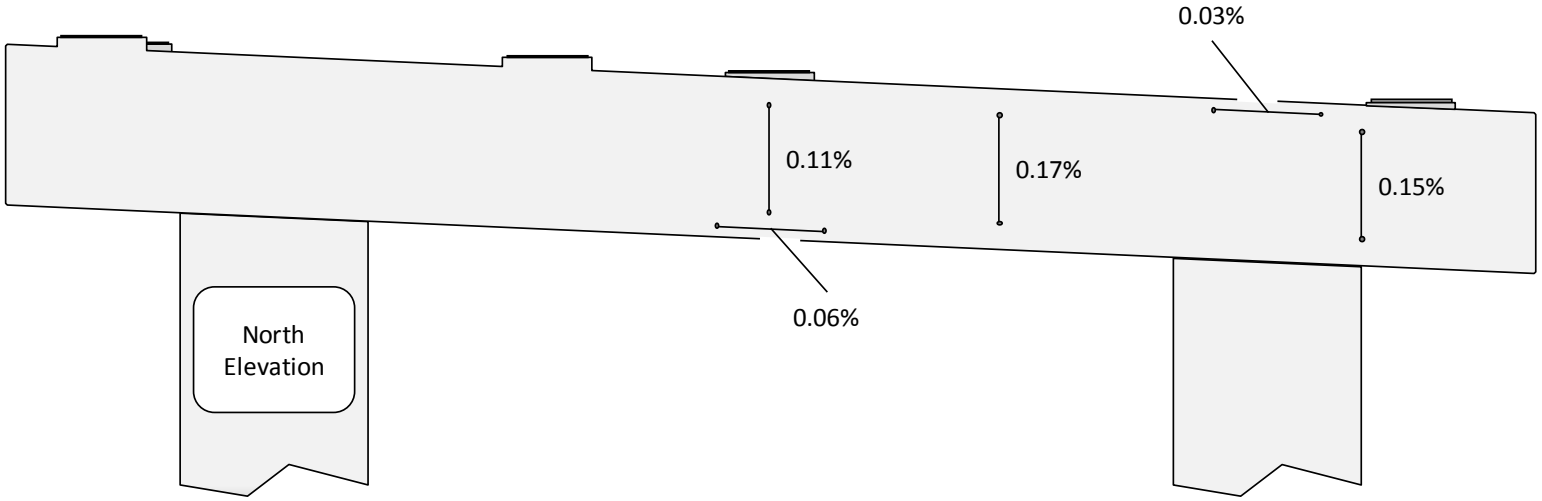

Figure 6-9: Expansion Estimates for Bent 15

As noted during the inspection, the overall appearance of the crack pattern was random in nature. Influence of the superstructure dead load on the surface cracking was not apparent, if present at all. The absence of ASR-induced diagonal cracks only supports the conclusions made within Chapter 5. If such a phenomenon were to be observed, it would have undoubtedly occurred within the exceptionally short, heavily loaded, shear span at the east end of the bent cap (far right in Figure 6-8). Further review of the crack pattern did reveal the anisotropy noted within the laboratory study. Primary cracks (i.e. the widest) ran parallel to the main axis the bent cap and therefore indicated that the predominant expansion was occurring in the transverse direction. The largest longitudinal (due to transverse expansion) and transverse cracks (due to longitudinal expansion) were 0.02 and 0.007 inches in width, respectively.

Implementation of the crack width summation technique confirmed the preliminary indications of anisotropy. Longitudinal expansion estimates conducted at the points of maximum positive and negative moment ranged from 0.03 to 0.06 percent. Corresponding transverse expansion estimates were more than twice as large on average; ranging from 0.11 to 0.17 percent. The general anisotropy of the expansion is illustrated by the expansions summarized within Figure 6-9. The expansion estimates for Bent 15 further illustrate the strong influence of casting direction on the anisotropy of the expansions. In spite of reasonably comparable reinforcement ratios in the longitudinal and transverse directions, expansions were clearly dominated by transverse growth. It can be concluded that successful modeling of ASR deterioration within the laboratory can only be accomplished when the casting direction is given proper consideration.

One peculiarity of the estimates should be reviewed prior to discussion of the structural implications. The estimate of transverse expansion within the heavily reinforced region ($\rho_v = 0.0026$) was equivalent to expansions measured within the lightly reinforced region ($\rho_v = 0.0014$). While expansions within the former region were subject to greater restraint, they were also subject to more severe exposure conditions (external and internal supplies of water). The supposed inconsistency is not unreasonable given the variation of exposure conditions within the bent cap. Such insights are critical to the successful interpretation of (and confidence placed within) crack width summation results.

Up to this point, in-situ expansions have been considered without regard to the error inherent to estimation technique. When one refers back to the results of Chapter 5, it becomes clear that the transverse reinforcement within Bent 15 has most likely yielded (equivalent to an expansion of 0.2%). The crack width summation technique underestimated expansions by up to sixty percent during the experimental program.

Furthermore, the underestimation of the in-situ expansion was most likely enhanced by the presence of paint which obscured the width of the ASR-related surface cracking (Figure 6-10). Sandblasting of the cap surface would have allowed more accurate measurement of the crack widths and estimation of the in-situ expansions.

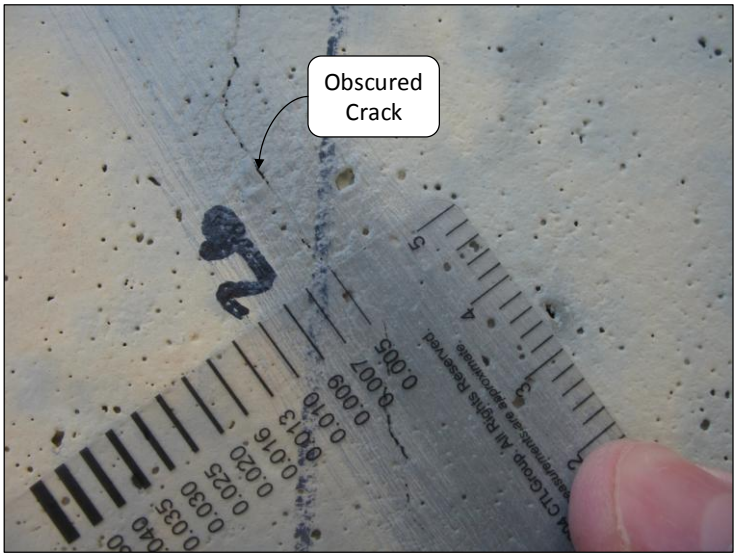

Figure 6-10: Measurement of Crack Obscured by Paint

Despite almost assured yielding of the transverse reinforcement, one can confidently conclude that an appreciable loss of shear strength has not occurred within any of the Bent 15 shear spans. Neither deep beam (a/d < 2) nor sectional (a/d > 2) shear spans within the current study suffered a loss of strength due to reinforcement yielding. It should be noted that current shear testing results would become irrelevant in less than two decades if the current rate of expansion (an estimated 0.2% per decade) is sustained. With that said, the rate of expansion in field structures is highly variable. It is possible that expansions could soon accelerate and rapidly leave Houston District engineers without a set of experimental results to reference for management decisions.

In truth, the loss of shear strength is not expected to occur at expansion levels in excess of those currently encompassed by the first series shear tests. As noted within Chapter 5, the magnitude of the concrete expansion *was not* critical to the loss of shear strength. Confinement of the expansive concrete core ultimately maintained the integrity of the bent caps, irrespective of damage severity. It can therefore be inferred that the loss of confinement (through reinforcement fracture) would lead to the immediate, irreversible loss of member strength. To conclusively establish the potential for strength loss within

the US 59 and I-10 interchange structures, the risk of reinforcement fracture needs to be defined; an issue beyond the scope of the current study.

6.5 SUMMARY

The condition and assessment of an ASR-affected interchange structure was reviewed within this chapter. Results of the assessment were positive; the shear strength of the bent under consideration did not appear to be compromised by transverse expansions at or in excess of the reinforcement yield strain. Overall, inspection and assessment of the damaged field structure had two immediate benefits: (1) implementation of the crack width summation technique demonstrated the utility of the assessment rationale recommended within Chapter 5 and (2) the researchers gained an appreciation for the challenges faced by TxDOT engineers charged with future management of the ASR/DEF-affected inventory.

CHAPTER 7
Summary, Conclusions, and Recommendations

7.1 SUMMARY

Over the last decade, a number of reinforced concrete bent caps within Houston, Texas have exhibited premature concrete damage (cracking, spalling and a loss of material strength) due to alkali-silica reaction and/or delayed ettringite formation. The alarming nature of the severe surface cracking prompted the Houston District of the Texas Department of Transportation to initiate an investigation into the structural implications of ASR and/or DEF deterioration. Specifically, an interagency contract with the University of Texas at Austin charged engineers at Ferguson Structural Engineering Laboratory to (1) establish the time-dependent relationship between in-situ deterioration and nominal shear capacity, and (2) develop practical recommendations for the evaluation of in-service bridge bent caps affected by ASR and/or DEF.

The rising concerns of Houston District engineers were rapidly addressed with a simple, yet carefully crafted, strategy: testing of the most vulnerable shear details found in practice would definitively expose any potential threats to the safety of damaged bent cap structures. Correspondingly, large-scale bent cap specimens, representative of the most severe circumstances of deterioration found in the field, were produced using select concrete materials and unique fabrication techniques. Each specimen required over eight cubic yards of laboratory-batched concrete and weighed over twenty-five thousand pounds when completed. Ultimately, four reactive and two non-reactive shear-critical specimens were produced over the course of a seven month period. The necessity of large-scale testing within the current study cannot be overemphasized. The complexity of ASR/DEF deterioration and poor scaling effects of shear behavior required the use of near full-scale concrete elements.

Experimental testing of the large-scale bent cap specimens was conducted in three phases which collectively addressed the need for information regarding the structural performance and assessment of ASR/DEF-affected bent caps. Following fabrication, a conditioning regime was used to foster the development of realistic ASR/DEF-related damage. The time-dependent deterioration of each bent cap specimen was recorded through the use of unique instrumentation. Monitoring results were subsequently examined to clarify the role of reinforcement and external loading in the deterioration

process (Phase I: Specimen Conditioning and Expansion Monitoring). Upon attainment of the desired levels of deterioration, three of the six bent caps were tested in shear. A total of six shear-critical spans were tested: three deep beam and three sectional shear tests. The most severe deterioration included ASR/DEF-induced expansions well in excess of the reinforcement yield strain. Service and ultimate load effects of the concrete expansion and reinforcement yielding were examined with respect to the damage severity (undamaged, mild and moderate). It was noted that future shear testing of the remaining three specimens (not reported here) would establish the implications of severe deterioration (Phase II: Shear Testing). Implementation of the shear testing results ultimately relied on the ability to estimate the expansions within field structures. A number of forensic analysis techniques were therefore evaluated within the context of the current study. The ability of each method to (efficiently) provide insight into the structural performance of a damaged bent was carefully scrutinized (Phase III: Forensic Analysis). Results from all three phases of the experimental program were collectively used to conduct the preliminary assessment of a damaged bent structure within Houston, Texas.

7.2 CONCLUSIONS AND RECOMMENDATIONS

In light of the potential loss of structural safety, investigation into the strength implications of ASR/DEF-related deterioration was of critical importance. As detailed below, testing of six large-scale shear spans (i.e. first series) did not reveal a loss of shear capacity at low to moderate levels of ASR-induced deterioration. These preliminary results are promising, but future implications may exist at higher levels of premature concrete deterioration. A number of similar observations made, and insights gained, over the course of the three-phase experimental program are summarized here.

7.2.1 Phase I: Development of ASR/DEF Deterioration

1. ***Due to resulting anisotropy, consideration of the casting direction is of critical importance to the realistic modeling of ASR-related deterioration within laboratory specimens.*** Time dependent ASR deterioration within all of the reactive bent cap specimens was dominated by expansion in the transverse direction. Close examination of the expansion histories for both non-reactive and reactive specimens suggested that the reinforcement configuration was not entirely responsible for the behavior. The observation supported a conclusion independently drawn by at least two researchers studying the influence of casting direction. Multon (2005) and Smaoui (2004) indicated that ASR-induced expansion parallel to the casting direction

could be more than twice as large as expansions measured in the perpendicular direction (irrespective of reinforcement effects).

2. ***Higher initial curing temperatures enhanced the severity of the ASR-related expansion measured within a given timeframe.*** Although temperature control is typically advocated for the prevention of DEF-related expansion, current experimental results suggest that a similar approach should be taken to limit the potential magnitude of future ASR-induced expansions. Three of the reactive specimens were subjected to peak curing temperatures which ranged from 163°F to 192°F. Despite equivalent exposure conditions and mixture proportions, the expansion of each specimen was notably different. Closer examination of the data ultimately revealed a remarkable correlation between the structural core expansions (due to ASR, as confirmed by petrographic analysis) and peak curing temperatures measured within each specimen.

3. ***ASR/DEF related expansions could not be restrained by the minimum shear reinforcement required by AASHTO sectional and strut-and-tie design models.*** The most severe deterioration subjected the transverse reinforcement to deformations well in excess of the yield strain. Resulting confinement of nearly 300 psi was well short of the compressive stresses necessary to restrain deterioration. To actively confine the expansions (i.e. generate compressive stresses of 600 psi, as noted by Folliard in 2008) would have required transverse reinforcement (No. 5 stirrups) to be spaced at an impractically small increment of 3 ½ inches.

7.2.2 Phase II: Service and Ultimate Load Behavior

1. ***Compressive stresses imposed upon the structural core (by the shear reinforcement) effectively suppressed the development of shear cracking at meaningful service loads.*** As defined by Birrcher et al. (2008), the service level shear for a bent cap is generally equivalent to one third of the experimental shear capacity. Non-reactive (undamaged) specimens within the current study were typically subject to (minor) diagonal cracking under the aforementioned service level shear (i.e. ⅓ of V_{test}). In contrast, diagonal cracking did not develop within the reactive specimens until the applied shear was approximately ¾ of the experimental shear capacity. While diagonal cracking under service loading is generally undesirable, its formation under overloads is critical to the early detection of poor structural performance. ASR-induced deterioration virtually eliminated such indications; diagonal cracking corresponded to imminent (and irreversible) failure of the bent cap specimen.

2. ***The shear strength of sectional (a/d = 3) and deep beam (a/d = 1.85) shear spans was not compromised by transverse concrete expansions of up to 0.69 and 0.45 percent, respectively.*** The measured shear capacities of four reactive spans (individually subject to low or moderate levels of deterioration) were normalized and compared to test results from a control (non-reactive) specimen. Regardless of the shear span-to-depth ratio or the severity of deterioration, the capacity of the reactive shear span always exceeded that of the corresponding non-reactive shear span. Most importantly, all of the experimental shear capacities exceeded current code estimates provided by ACI 318-08 and Interim 2008 AASHTO LRFD Bridge Design Specifications. Recommended design provisions included within the technical report for TxDOT Project 0-5253 also provided conservative (and slightly more accurate) estimates of the experimental shear capacities.

3. ***Confinement provided by the shear reinforcement played a critical role in the maintenance of structural integrity.*** In contrast to the severe surface cracking observed outside the influence of the transverse reinforcement, the structural core damage was limited to visually indistinguishable microcracking (as indicated through examination of cored samples). Any potential loss of material strength due to this damage was offset by the compressive stresses imposed by the shear reinforcement. It is important to reemphasize that this conclusion is limited to bent structures that are subject to similar levels of deterioration. Serious implications may exist when structures are subjected to longer periods of exposure and persistent expansion (i.e. reinforcement fracture, see Section 7.3).

7.2.3 Phase III: Structural Assessment

1. ***The shear capacity of sectional (a/d > 2) and deep beam (a/d < 2) shear spans may be conservatively estimated using current code provisions in combination with core-based material strengths.*** As noted earlier, conservative shear strength estimates were obtained through the use of cylinder-based material strengths. Corresponding mechanical tests on extracted samples provided material strength values which were consistently lower, but not overly conservative. One can therefore expect to obtain a similar level of conservatism in shear strength estimates obtained through the use of core-based material strengths.

2. ***Within the context of structural assessment, the practicality of a forensic technique can only be judged by its ability to provide an indication of the structural performance as a whole.*** Accordingly, practical techniques which provide

sufficiently accurate estimates of the current concrete expansions and reinforcement strains should be the focus of further study and refinement. The most likely candidates will be those methods based upon the measurement or characterization of ASR/DEF-related structural phenomena (cracking, deformation, etc). Such methods include those implemented within the current study (i.e. crack width summation technique, in-situ reinforcement testing) and alternate methods which may be found during a more-comprehensive literature review of structural assessment techniques (for example, the overcoring method). Implementation of such an assessment methodology will provide the most structurally relevant information at the lowest cost (as discussed within Chapter 5).

3. ***Forensic analysis techniques which solely rely on laboratory testing of concrete samples are inherently limited in their ability to represent in-situ structural behavior.*** From the moment cores are extracted from a structure, all relevant loads, stresses, strains, and other general in-situ conditions are lost. Subsequent interpretation of the tests conducted on the cores is therefore complicated by attempts to relate the laboratory and field conditions. In the case of residual expansion testing, the loss of the confinement and use of ideal exposure conditions leads to ambiguity regarding the utility of the results for structural assessment purposes. Attempts have been made to establish the correlation between the restrained field and unrestrained laboratory expansions, but the results are typically limited to a particular concrete mixture and structural configuration. In general, the implementation of such methods is restricted by a need for the development of correlation over a wide range of concrete materials and mixture proportions; an especially daunting task within the State of Texas. Aside from the impracticalities associated with test interpretation, these methods cannot be recommended due to the high costs associated with the extensive material testing required for successful implementation within the field.

7.3 FUTURE WORK

Although the current study has provided substantial insight into the structural implications of ASR/DEF-induced deterioration, the limited scope of the project leaves a number of items unresolved. Specifically, the long-term consequences of sustained deterioration could not be studied within the three year tenure of the current project. It is consequently hoped that future large-scale testing will advance the state of knowledge regarding the following items.

1. ***In regards to the long-term consequences of ASR/DEF-induced deterioration (not explored here), the potential for and consequences of transverse reinforcement fracture should be established.*** The Japanese discovery of reinforcement fracture illustrated the dire consequences of uncontrolled, persistent expansion (please refer to Chapter 2). Unfortunately, limited details regarding the circumstances leading to reinforcement fracture made it impossible to evaluate the potential for such an outcome within TxDOT-owned infrastructure. Further investigation of the phenomenon is essential to the task of establishing the long-term structural risk imposed by ASR/DEF-related deterioration. Loss of confinement through the fracture of highly stressed reinforcement would most likely lead to rapid deterioration of the structural core and an unquestionable loss of structural safety. Confirmation of the potential would elevate the need to develop mitigation techniques or rapid-replacement strategies.

2. ***The development of reliable, field-proven ASR/DEF mitigation techniques is critical to minimizing future inspection, maintenance and repair costs*.** Results from the current study have placed the risk of ASR/DEF-related shear failure at virtually zero for low to moderate levels of deterioration. However, the risk is undefined for higher levels of deterioration and alternate failure modes; especially those related to anchorage or bond. Frequent inspection and structural assessment must therefore be conducted while the deterioration mechanisms persist within a reinforced concrete bent cap. Although inspection requirements may eventually be relaxed through future structural testing, it would be more effective to halt the deterioration and thereby guarantee long-term structural safety *and* durability. To date, attempts to control the deterioration within the field have been unsuccessful (refer to Chapter 2). Future development of mitigation technology should be approached with a strong appreciation for the scale of commonly-affected structures and the effects of highly variable field exposure conditions.

APPENDIX A
Additional Material Testing Results

Appendix A includes the results of standard material tests which were outlined, but not reported within Chapters 1 through 7. The results are organized in the following fashion:

- *ASTM A 615/A 615M Standard Specification for Deformed and Plain Carbon-Steel Bars for Concrete Reinforcement:* Table A-1
- *ASTM C 1293 Standard Test Method for Determination of Length Change of Concrete due to Alkali-Silica Reaction:* Figure A-1 through Figure A-5

Table A-1: Reinforcement Properties for First and Second Series Specimens

Specimen		Transverse Reinforcement (No. 5)			Longitudinal Reinforcement (No. 11)		
		ε_{yt}	f_{yt}	f_{ut}	ε_{yl}	f_{yl}	f_{ul}
First Series	R1	0.224%	65 ksi	100 ksi	0.221%	64 ksi	109 ksi
	R2	0.245	71	116	0.228	66	105
	nR1	0.221	62	99	0.238	69	104
Second Series	R3	0.221	64	103	0.228	66	105
	R4	0.224	65	103	0.238	69	106
	nR2	0.224	65	103	0.238	69	106

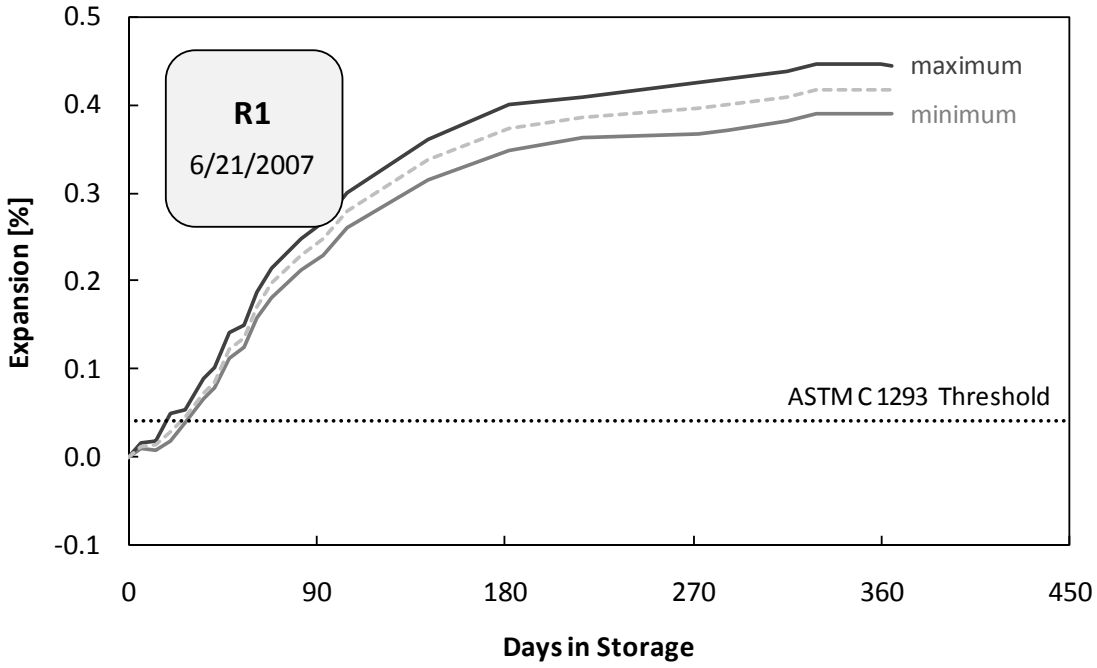

Figure A-1: Free Expansion of ASTM C 1293 Prisms – Specimen R1

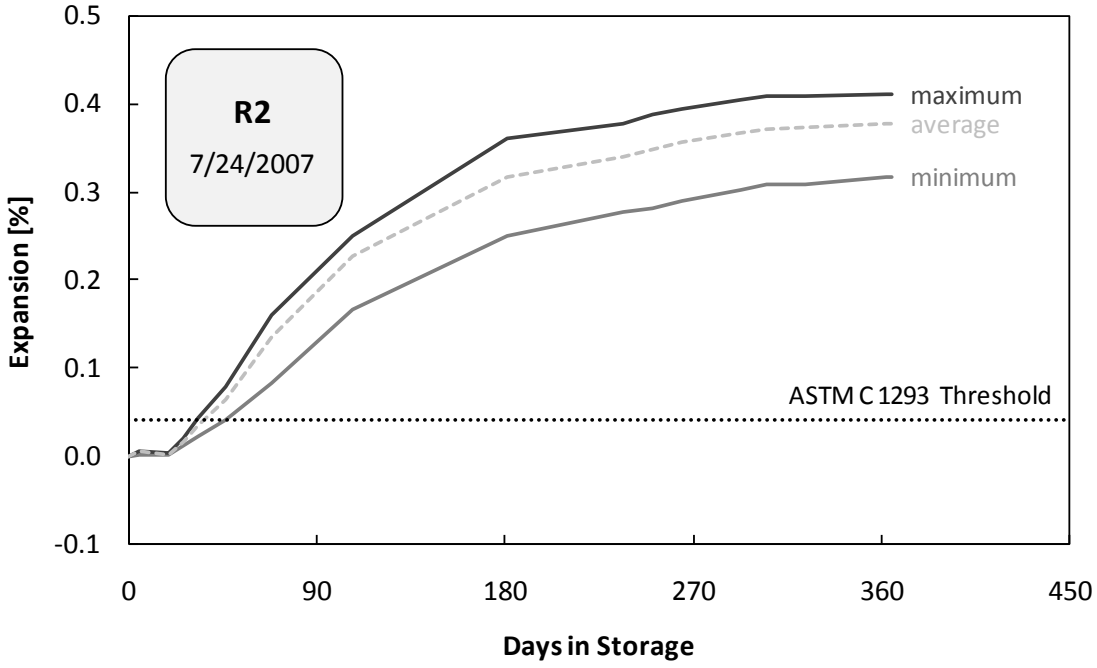

Figure A-2: Free Expansion of ASTM C 1293 Prisms – Specimen R2

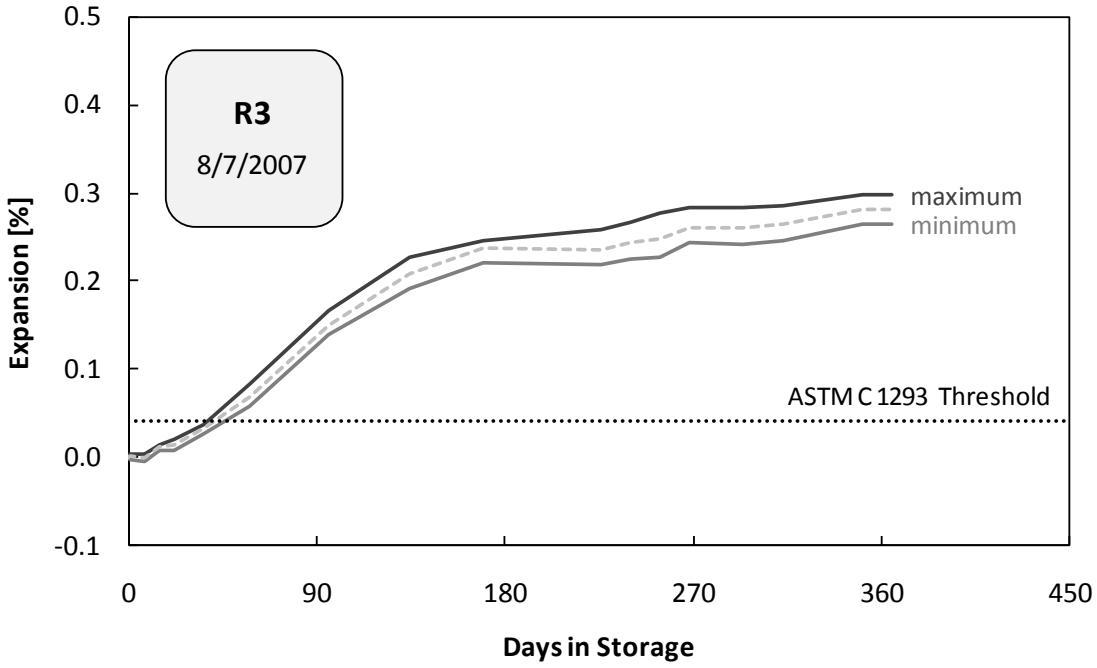

Figure A-3: Free Expansion of ASTM C 1293 Prisms – Specimen R3

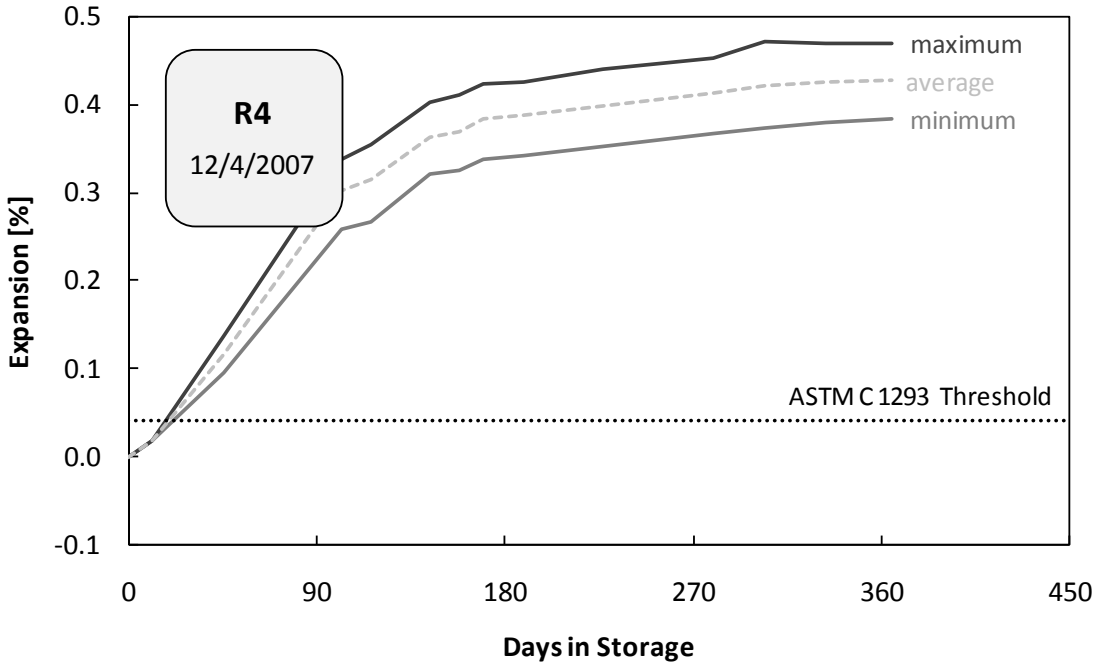

Figure A-4: Free Expansion of ASTM C 1293 Prisms – Specimen R4

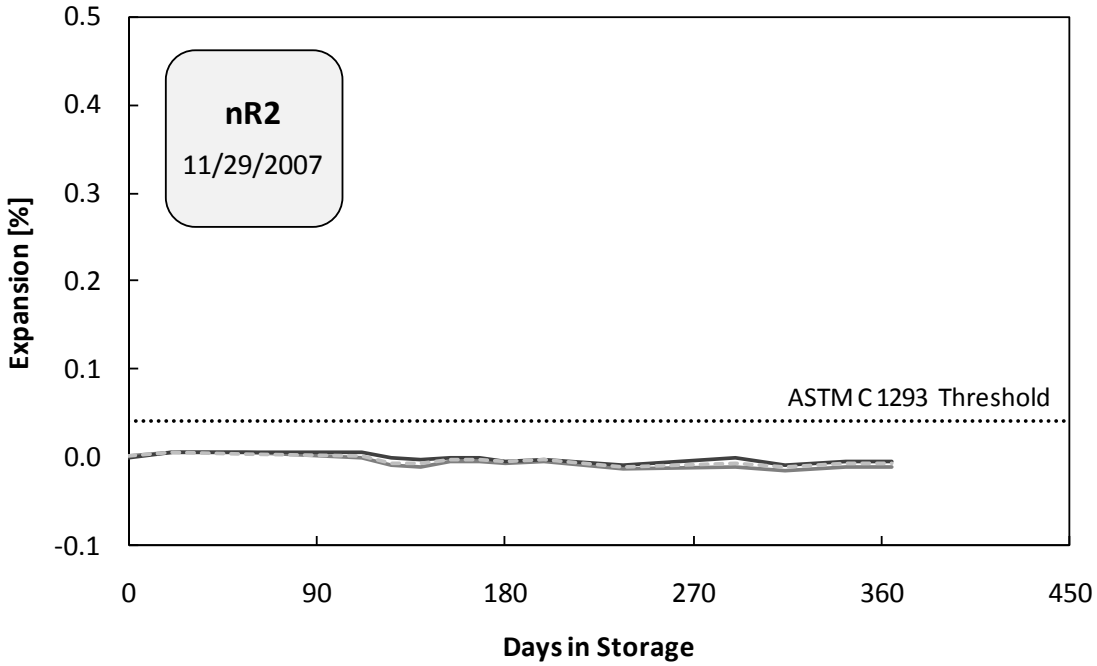

Figure A-5: Free Expansion of ASTM C 1293 Prisms – Specimen nR2

APPENDIX B
Shear Test Photographs

Appendix B includes photographs which document the progression of cracking during the deep beam and sectional shear tests. The photographs are grouped in the following manner:

- *Deep Beam Shear Tests:* Figure B-1 (Non-Reactive) and Figure B-2 (Reactive)
- *Sectional Shear Tests:* Figure B-3 (Non-Reactive) and Figure B-4 (Reactive)

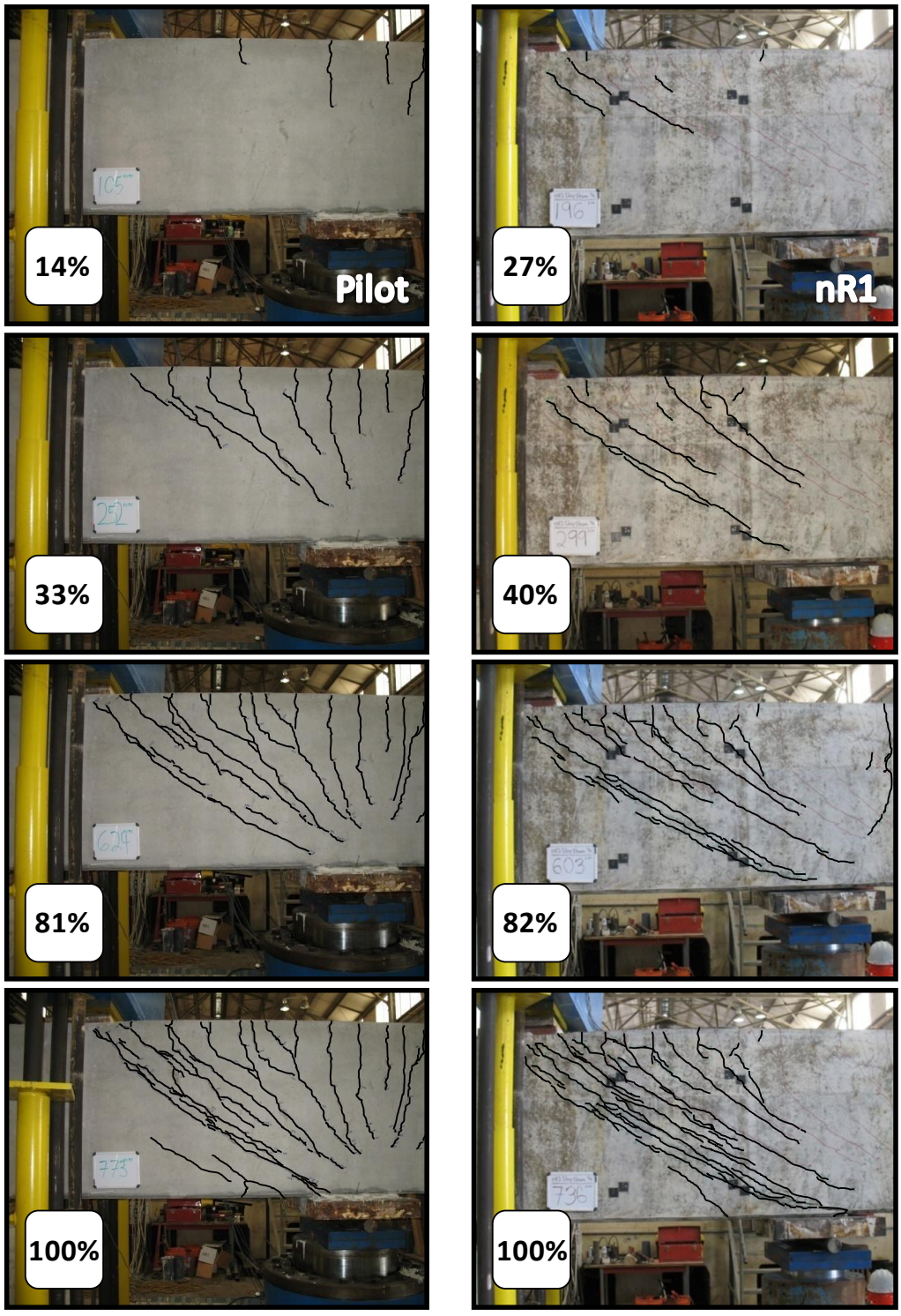

Figure B-1: Deep Beam Shear Tests within Non-Reactive Specimens

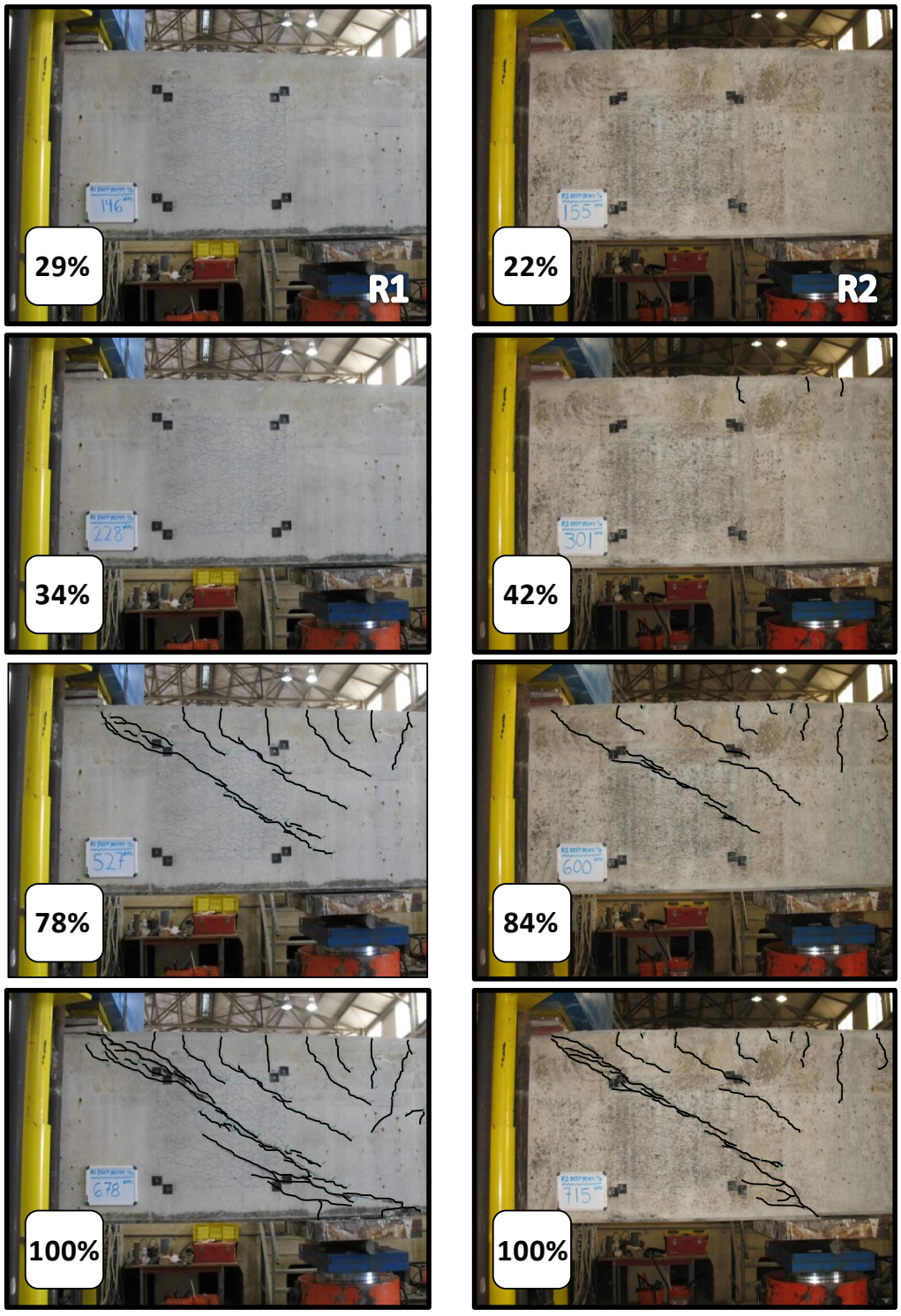

Figure B-2: Deep Beam Shear Tests within Reactive Specimens

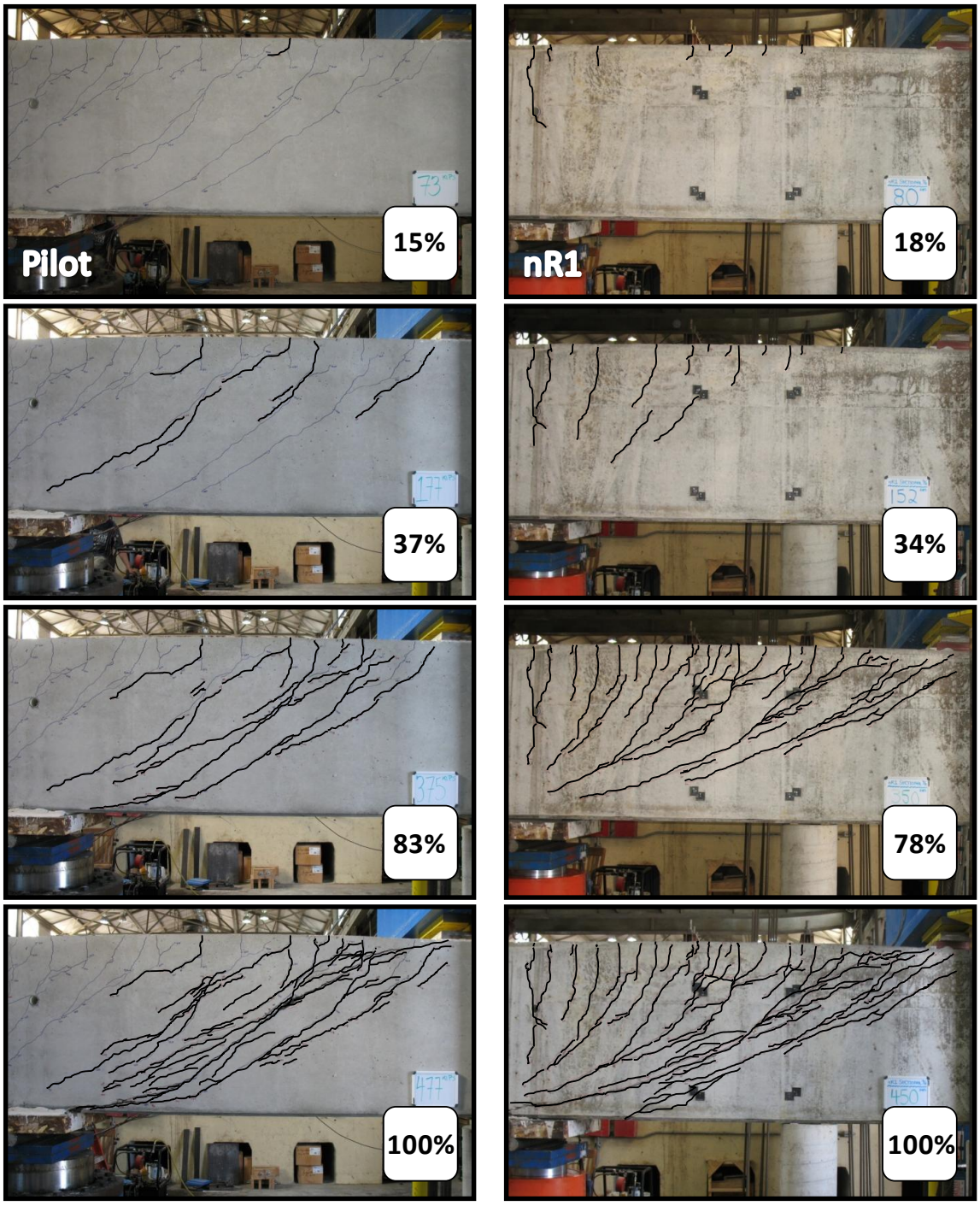

Figure B-3: Sectional Shear Tests within Non-Reactive Specimens

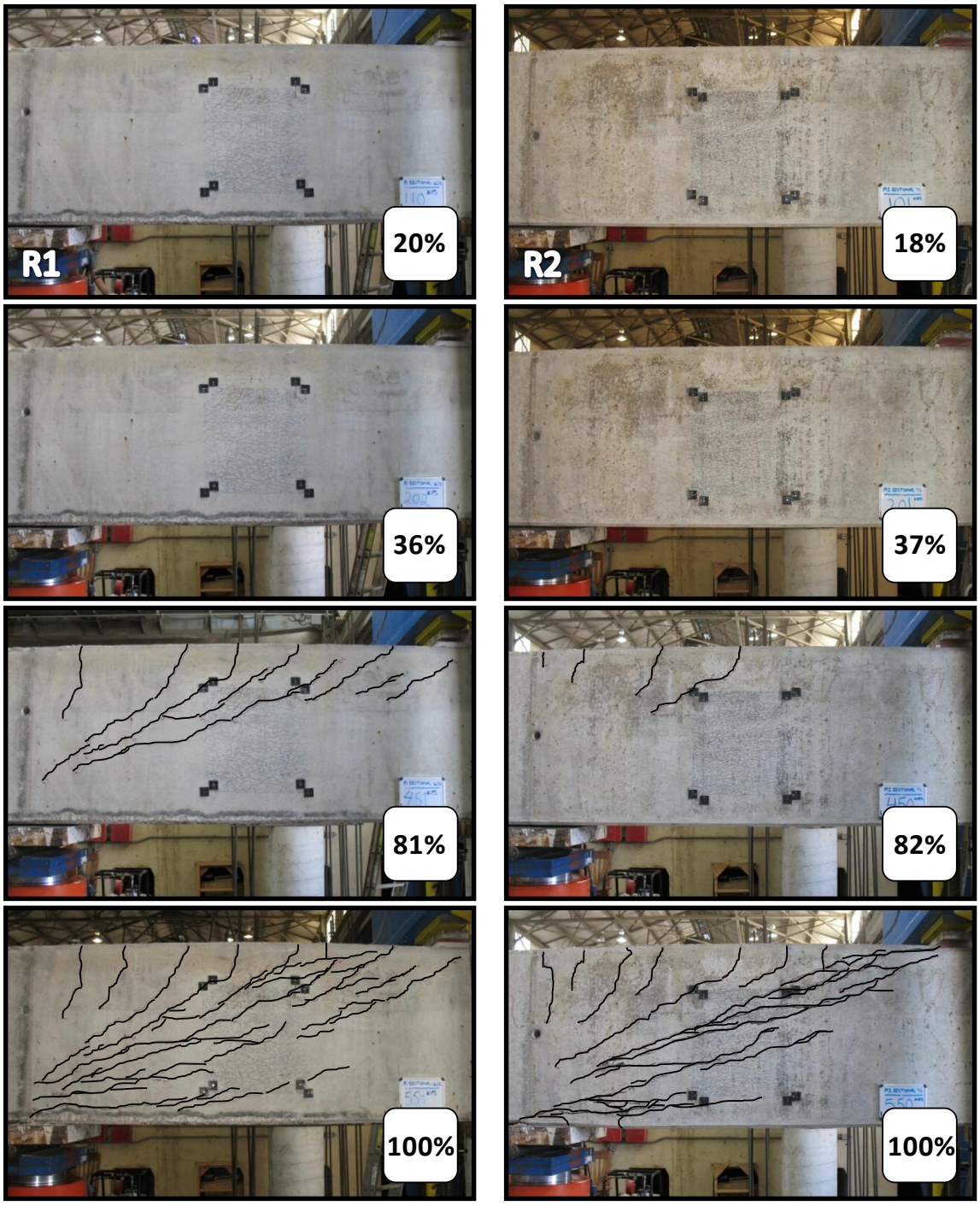

Figure B-4: Sectional Shear Tests within Reactive Specimens

APPENDIX C
Forensic Analysis Details

Appendix C includes additional information relevant to the forensic analysis conducted during Phase III of the current study. The information is organized in the following fashion:

- *Illustrated Layout of Forensic Tests per Specimen:* Figure C-1 through Figure C-6.
- *Mechanical Testing Results from First Series Cores:* Table C-1 and Table C-2.
- *Physical Dimensions of Residual Expansion Cores:* Table C-3 through Table C-5.

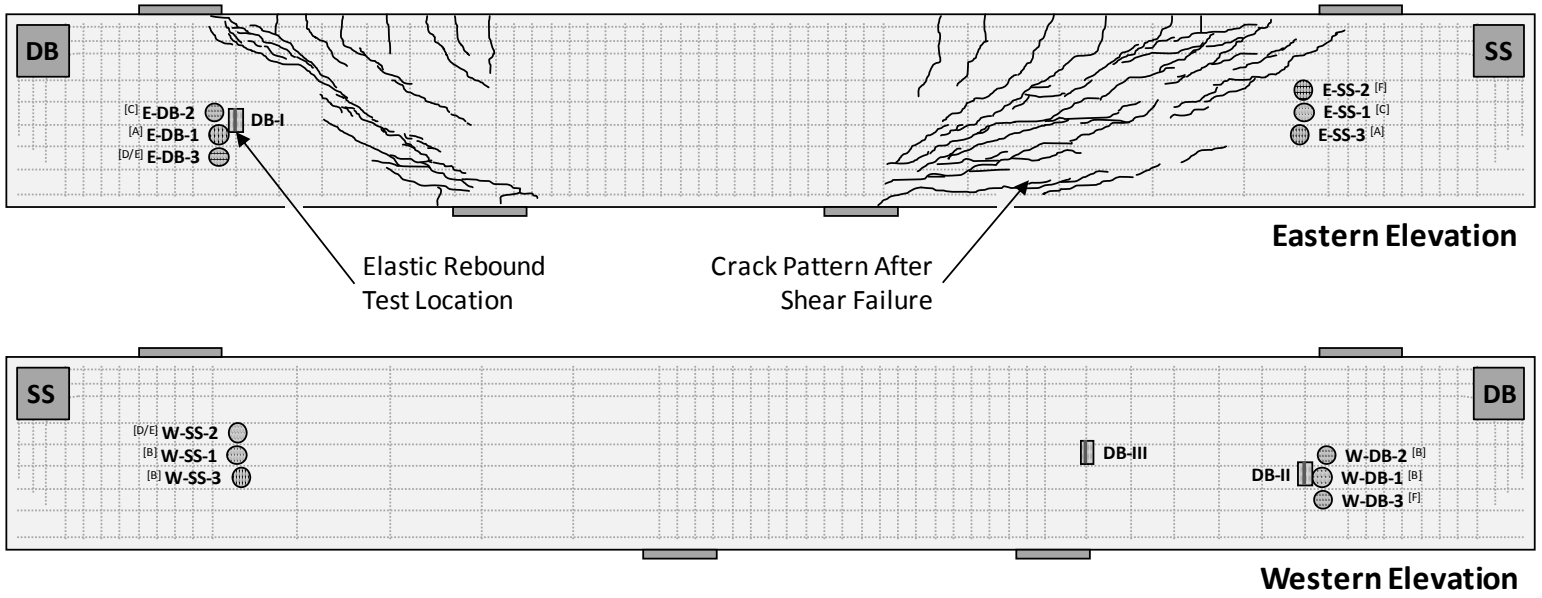

R1	**Concrete Placement:** 6.21.2007 [0 days] **Core Extraction:** 7.31.2008 [406 days]	**Material Testing:** A. Compressive Strength B. Splitting Tensile Strength C. Petrographic Examination D. ASR Expansion Potential E. DEF Expansion Potential F. PCD Expansion Potential G. Water-Soluble Alkali Content

Figure C-1: First Series – Layout of Forensic Tests for Specimen R1

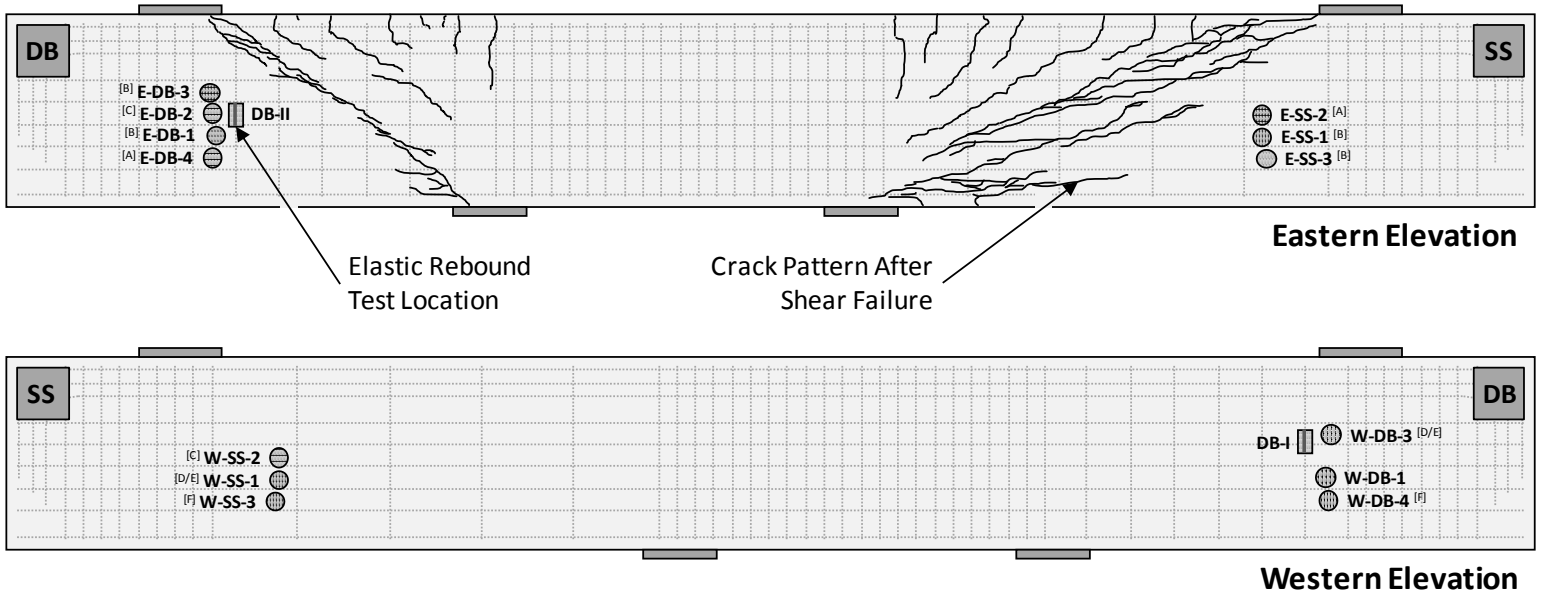

R2	**Concrete Placement:** 7.24.2007 [0 days] **Core Extraction:** 8.4.2008 [377 days]	**Material Testing:** A. Compressive Strength B. Splitting Tensile Strength C. Petrographic Examination D. ASR Expansion Potential E. DEF Expansion Potential F. PCD Expansion Potential G. Water-Soluble Alkali Content

Figure C-2: First Series – Layout of Forensic Tests for Specimen R2

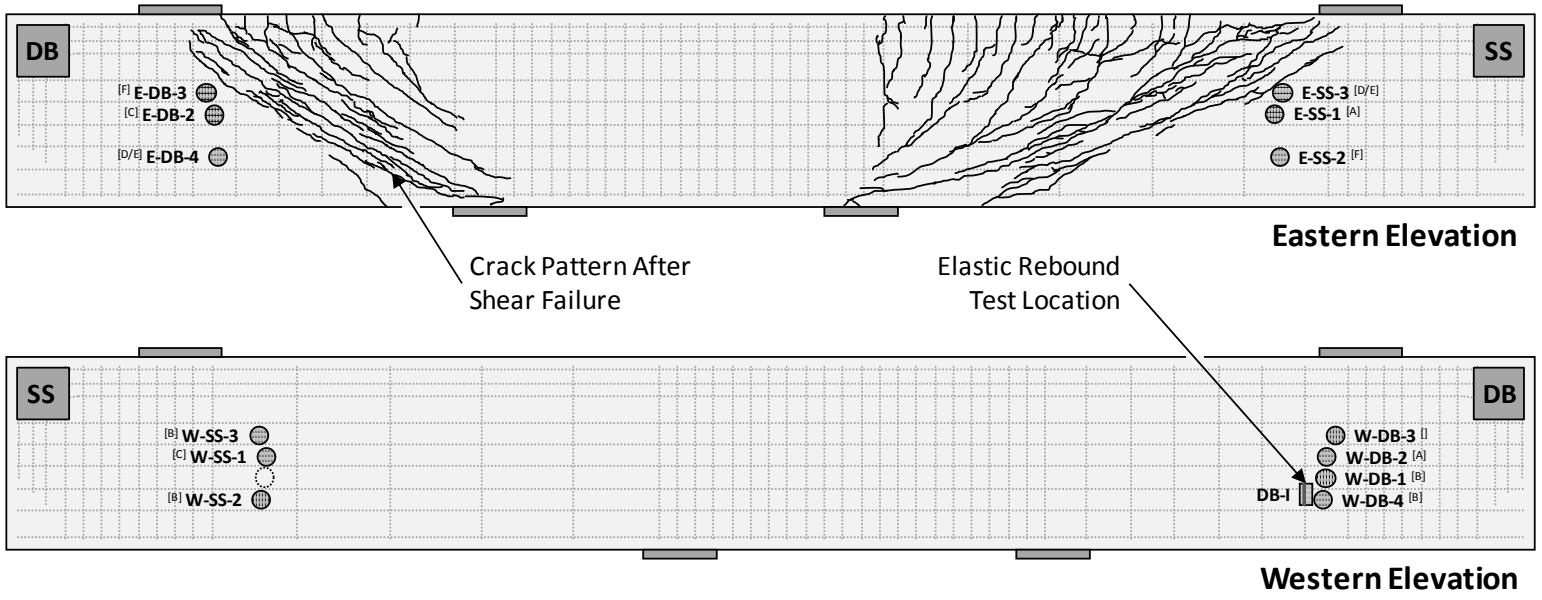

nR1	**Concrete Placement:** 10.23.2007 [0 days] **Core Extraction:** 8.1.2008 [283 days]	**Material Testing:** A. Compressive Strength B. Splitting Tensile Strength C. Petrographic Examination D. ASR Expansion Potential E. DEF Expansion Potential F. PCD Expansion Potential G. Water-Soluble Alkali Content

Figure C-3: First Series – Layout of Forensic Tests for Specimen nR1

R3	**Concrete Placement:** 8.7.2007 [0 days] **Core Extraction:** 9.20.2008 [410 days]	**Material Testing:** A. Compressive Strength B. Splitting Tensile Strength C. Petrographic Examination D. ASR Expansion Potential E. DEF Expansion Potential F. PCD Expansion Potential G. Water-Soluble Alkali Content

Figure C-4: Second Series – Layout of Forensic Tests for Specimen R3

R4	**Concrete Placement:** 12.4.2007 [0 days] **Core Extraction:** 9.25.2008 [296 days]	**Material Testing:** A. Compressive Strength B. Splitting Tensile Strength C. Petrographic Examination D. ASR Expansion Potential E. DEF Expansion Potential F. PCD Expansion Potential G. Water-Soluble Alkali Content

Figure C-5: Second Series – Layout of Forensic Tests for Specimen R4

nR2	**Concrete Placement:** 11.29.2007 [0 days] **Core Extraction:** 9.20.2008 [304 days]	**Material Testing:** A. Compressive Strength B. Splitting Tensile Strength C. Petrographic Examination D. ASR Expansion Potential E. DEF Expansion Potential F. PCD Expansion Potential G. Water-Soluble Alkali Content

Figure C-6: Second Series – Layout of Forensic Tests for Specimen nR2

Table C-1: First Series – Compressive Strength of Cores

Specimen	Core	Age	Length	Diameter	f'_c
R1	E-DB-1	419 days	7.5 in	3.8 in	3497 psi
	E-SS-3	419	7.6	3.8	3541
R2	E-DB-4	386	7.5	3.7	3187
	E-SS-2	386	7.5	3.7	2782
nR1	W-DB-2	295	7.5	3.70	5875
	E-SS-1	295	7.5	3.7	6443

Table C-2: First Series – Splitting Tensile Strength of Cores

Specimen	Core	Age	Length	Diameter	f_{ct}
R1	W-DB-1	419 days	7.6 in	3.8 in	375 psi
	W-DB-2	419	7.6	3.8	381
	W-SS-1	419	7.5	3.8	375
	W-SS-3	419	7.3	3.8	407
R2	E-DB-1	386	7.5	3.7	345
	E-DB-3	386	7.6	3.7	339
	E-SS-1	386	7.5	3.7	339
	E-SS-3	386	7.5	3.7	321
nR1	W-DB-1	295	7.5	3.7	669
	W-DB-4	295	7.5	3.7	668
	W-SS-2	295	7.5	3.7	620
	W-SS-3	295	7.5	3.7	651

Table C-3: Cores Extracted for ASR Expansion Potential (Protocol Test A)

Specimen	Core	Age (Start of Test)	Length	Diameter	Notes
R1	E-DB-3	476	8.0 in	3.8 in	Halved Core†
	W-SS-2	476	8.0	3.8	Halved Core
R2	W-DB-3	443	8.0	3.7	Halved Core
	W-SS-1	443	8.0	3.7	Halved Core
nR1	E-DB-4	352	8.0	3.7	Halved Core
	E-SS-3	352	8.0	3.7	Halved Core
R3	G-4	429	11.1	1.7	Repaired‡
	M-2	429	11.0	1.7	-
	B-2	429	11.0	1.7	-
R4	G-4	310	11.0	1.7	-
	M-3	310	11.1	1.7	-
	B-3	310	11.0	1.7	-
nR2	G-3	315	11.0	1.7	-
	M-3	315	11.0	1.7	-
	B-3	315	11.0	1.7	Repaired

† Core was halved lengthwise to obtain proper surface area-to-volume ratio for residual expansion testing.
‡ Transverse fracture in core was repaired using a ceramic repair epoxy.

Table C-4: Cores Extracted for DEF Expansion Potential (Protocol Test B)

Specimen	Core	Age (Start of Test)	Length	Diameter	Notes
R1	E-DB-3	449	8.0 in	3.8 in	Halved Core[†]
	W-SS-2	449	8.0	3.8	Halved Core
R2	W-DB-3	416	8.0	3.7	Halved Core
	W-SS-1	416	8.0	3.7	Halved Core
nR1	E-DB-4	325	8.0	3.7	Halved Core
	E-SS-3	325	8.0	3.7	Halved Core
R3	G-3	429	8.8	1.7	-
	M-1	429	8.8	1.7	-
	B-1	429	8.8	1.7	-
R4	G-3	310	8.8	1.7	-
	M-2	310	8.8	1.7	-
	B-4	310	8.8	1.7	-
nR2	G-4	315	8.8	1.7	-
	M-2	315	8.8	1.7	-
	B-5	315	8.8	1.7	-

[†] Core was halved lengthwise to obtain proper surface area-to-volume ratio for residual expansion testing.

Table C-5: Cores Extracted for PCD Expansion Potential (Protocol Test C)

Specimen	Core	Age (Start of Test)	Length	Diameter	Notes
R1	E-SS-2	464	8.0 in	3.8 in	-
	W-DB-3	464	8.0	3.8	-
R2	W-SS-3	431	8.0	3.7	-
	W-DB-4	431	8.0	3.7	-
nR1	E-SS-2	340	8.0	3.7	-
	E-DB-3	340	8.0	3.7	-
R3	G-1	429	8.9	3.7	-
	M-3	429	8.9	3.7	-
	B-4	429	8.9	3.7	-
R4	G-2	310	8.9	3.7	-
	M-1	310	8.8	3.7	-
	B-2	310	8.9	3.7	-
nR2	G-1	315	8.8	3.7	-
	M-1	315	8.8	3.7	-
	B-2	315	8.8	3.7	-

References

1. *AASHTO LRFD Bridge Design Specifications, 4th Edition, 2008 Interim Revisions*. Washington, D.C.: American Association of State Highway and Transportation Officials, 2007.

2. ACI-ASCE Joint Committee 426-1973. *The Shear Strength of Reinforced Concrete Members*. Farmington Hills: American Concrete Institute, 1973.

3. ACI Committee 318-2008. *Building Code Requirements for Reinforced Concrete (ACI 318-08)*. Farmington Hills: American Concrete Institute, 2008.

4. Ahmed, T; Burley, E.; Rigden, S. and Abu-Tair, A.I. "The Effect of Alkali Reactivity on the Mechanical Properties of Concrete." *Construction and Building Materials* Vol. 14 (2003): 123-144.

5. Ahmed, T.; Burley, E. and Rigden, S. "The Static and Fatigue Strength of Reinforced Concrete Beams Affected by Akali-Silica Reaction." *ACI Materials Journal* Vol. 95 No. 4 (1998): 376-388.

6. *ASTM A 615/A 615M Standard Specification for Deformed and Plain Carbon-Steel Bars for Concrete Reinforcement*. West Conshohocken: American Society for Testing and Materials, 2008.

7. *ASTM A 370 Standard Test Methods and Definitions for Mechanical Testing of Steel Products*. West Conshohocken: American Society for Testing and Materials, 2008.

8. *ASTM C 157/C 157M Standard Test Method for Length Change of Hardened Hydraulic-Cement Mortar and Concrete*. West Conshohocken: American Society for Testing and Materials, 2008.

9. *ASTM C 192/C 192M Standard Practice for Making and Curing Concrete Test Specimens in the Laboratory*. West Conshohocken: American Society for Testing and Materials, 2007.

10. *ASTM C 39/C 39M Standard Test Method for Compressive Strength of Cylindrical Concrete Specimens*. West Conshohocken: American Society for Testing and Materials, 2005.

11. *ASTM C 42/C 42M Standard Test Method for Obtaining and Testing Drilled Cores and Sawed Beams of Concrete*. West Conshohocken: American Society for Testing and Materials, 2004.

12. *ASTM C 496/C 496M Standard Test Method for Splitting Tensile Strength of Cylindrical Concrete Specimens*. West Conshohocken: American Society for Testing and Materials, 2004.

13. *ASTM C 1293 Standard Test Method for Determination of Length Change of Concrete due to Alkali-Silica Reaction*. West Conshohocken: American Society for Testing and Materials, 2008.

14. Bae, S.; Bayrak, O.; Jirsa J.O. and Klingner, R.E. *Anchor Bolt Behavior in ASR/ DEF-Damaged Drilled Shafts*. Austin: Ferguson Structural Engineering Laboratory, University of Texas at Austin, 2007. TxDOT IAC 88-5DDIA004.

15. Bauer, S.; Cornell, B.; Figurski, D.; Ley, T.; Miralles, J. and Folliard, K.J. *Alkali-Silica Reaction and Delayed Ettringite Formation in Concrete: A Literature Review*. Austin: Center for Transportation Research, University of Texas at Austin, 2001. TxDOT Report 0-4085-1.

16. Berube, M.A.; Smaoui, N.; Fournier, B.; Bissonnette, B. and Durand, B. "Evaluation of the Expansion Attained to Date by Concrete Affected by Alkali-Silica Reaction. Part III: Application to Existing Structures." *Canadian Journal of Civil Engineeing* Vol. 32 No. 3 (2005): 463-479.

17. Bindrich, B.V. "The Effects of Alkali-Silica Reaction and Delayed-Ettringite Formation on the Structural Performance of the Dapped End Region of Prestressed Concrete Trapezoidal Box Beams." MS Thesis. University of Texas at Austin, 2009.

18. Birrcher, D.; Tuchscherer, R.; Huizinga, M.; Bayrak, O.; Wood, S. and Jirsa, J.O. *Strength and Serviceability Design of Reinforced Concrete Deep Beams*. Austin: Center for Transportation Research, University of Texas at Austin, 2008. TxDOT Report 0-5253-1.

19. Blight, G.E.; Alexander, M.G. and Lampacher, B.J. "Structural Repair of Reinforced Concrete Portal Frame." *Magazine of Concrete Research* Vol. 45 No. 163 (1993): 97-101.

20. Blight, G.E.; Alexander, M.G.; Ralph, T.K. and Lewis, B.A. "Effect of Alkali-Aggregate Reaction on the Perfomance of a Reinforced Concrete Structure over a Six-Year Period." *Magazine of Concrete Research* Vol. 41 No. 147 (1989): 69-77.

21. Blight, G.E.; Alexander, M.G.; Schutte, W.K. and Ralph, T.K. "The Effect of Alkali-Aggregate Reaction on the Strength and Deformation of a Reinforced Concrete Structure." *Proceedings of the Sixth International Conference on Alkali-Aggregate Reaction*. Copenhagen. 1983. 401-410.

22. Blight, G.E. and Ballim, Y. "Properties of AAR-Affected Concrete Studied over 20 Years." *Proceedings of the Eleventh International Conference of Alkali-Aggregate Reaction*. Quebec. 2000. 1109-1118.

23. Blight, G.E. and Lampacher, B.J. "Repair of Reinforced Concrete Portal Frame Damaged by Alkali-Silica Reaction: Strains After 5-1/2 Years." *Magazine of Concrete Research* Vol. 50 No. 4 (1998): 293-296.

24. Boenig, A. "Bridges with Premature Concrete Deterioration: Field Observations and Large-Scale Testing." MS Thesis. University of Texas at Austin, 2000.

25. Chana, P.S. and Korobokis, G.A. *Structural Performance of Reinforced Concrete Affected by Alkali-Silica Reaction: Phase I*. Crowthorne: Transport and Road Research Laboratory, Department of Transport, 1991. Contractor Report 267.

26. Clark, L.A. *Critical Review of the Structural Implications of the Alkali-Silica Reaction in Concrete*. Crowthorne: Transport and Road Research Laboratory, Department of Transport, 1989. Contractor Report 169.

27. Clayton, N.; Currie, R.J. and Moss, R.M. "The Effects of Alkali-Silica Reaction on the Strength of Prestressed Concrete Beams." *The Structural Engineer* Vol. 68 No. 15 (1990): 287-292.

28. Courtier, R H. "The Assessment of ASR-Affected Structures." *Cement and Concrete Composites* Vol. 12 (1990): 191-201.

29. Danay, A. "Structural Mechanics Methodology in Diagonosing and Assessing Long-Term Effects of Alkali-Aggregate Reactivity in Reinforced Concrete Structures." *ACI Materials Journal* Vol. 91 No. 1 (1994): 54-62.

30. Eskridge, A.E.; Klahorst, J.T.; Klingner, R.E. and Kreger, M.E. *Mitigation Techniques for In-Service Structures with Premature Concrete Deterioration: Project Summary Report*. Austin: Center for Transportation Research, University of Texas at Austin, 2005. TxDOT Report 0-4069-S.

31. Fan, S. and Hanson, J.M. "Effect of Alkali-Silica Reaction Expansion and Cracking on Structural Behavior of Reinforced Concrete Beams." *ACI Structural Journal* Vol. 95 No. 5 (1998): 498-505.

32. Farny, J.A. and Kerkhoff, B. *Diagnosis and Control of Alkali-Aggregate Reactions in Concrete*. Skokie: Portland Cement Association, 2007.

33. Ferguson, P.M; Breen, J.E. and Jirsa, J.O. *Reinforced Concrete Fundamentals*. 5th ed. New York: John Wiley & Sons, 1988.

34. Figg, J. "ASR - Inside Phenomena and Outside Effects (Crack Origin and Pattern)." *Proceedings of the 7th International Conference on Alkali-Aggregate Reaction*. Ottawa. Far Ridge: Noyes, 1986. 152-155.

35. Folliard, K.J.; Burgher, F.; Ley, T.; Thibonnier, A. and Thomas, M.D.A. *Extending Service Life of Large or Unusual Structures Affected by Premature Concrete Deterioration*. Austin: Research and Technology Implementation, Texas Department of Transportation, 2008. TxDOT Report 0-5218-S.

36. Folliard, K.J.; Barborak, R.; Drimalas, T.; Du, L.; Garber, S.; Ideker, J.; Ley, T.; Williams, S.; Juenger, M.; Thomas, M.D.A. and Fournier, B. *Preventing Alkali-Silica Reaction and Delayed Ettringite Formation in New Concrete: Project Summary Report*. Austin: Center for Transportation Research, University of Texas at Austin, 2006. TxDOT Report 0-4085-S.

37. Folliard, K.J.; Barborak, R.; Drimalas, T.; Du, L.; Garber, S.; Ideker, J.; Ley, T.; Williams, S.; Juenger, M.; Fournier, B. and Thomas, M.D.A. *Preventing ASR/DEF in New Concrete: Final Report*. Austin: Center for Transportation Research, University of Texas at Austin, 2006. TxDOT Report 0-4085-5.

38. Folliard, K.J.; Thomas, M.D.A. and Fournier, B. *Protocol for the Diagnosis and Prognosis of Concrete Structures Affected by Alkali-Silica Reaction and/or Delayed Ettringite Formation*. Austin: Concrete Durability Center, University of Texas at Austin, 2007.

39. Fournier, B.; Berube, M.A.; Thomas, M.D.A.; Smaoui, N. and Folliard, K.J. *Evaluation and Management of Concrete Structures Affected by Alkali-Silica Reaction: A Review.* Ottawa: CANMET Materials Technology Laboratory, Natural Resources Canada, 2004. Report Number MTL 2004-11.

40. Frank, K.H. Personal Communication, 2007.

41. Hime, W.G. "Delayed Ettringite Formation - A Concern for Precast Concrete?" *Journal of the Precast/Prestressed Concrete Institute* Vol. 41 No. 4 (1996): 26-30.

42. Hobbs, D.W. *Alkali-Silica Reaction in Concrete*. London: Thomas Telford, 1988.

43. Imai, H.; Yamasaki, T.; Maehara, H. and Miyagawa, T. "The Deterioration by Alkali-Silica Reaction of Hanshin Expressway Concrete Structures - Investigation and Repair." *Proceedings of the Sixth International Conference on Alkali-Aggregate Reaction*. Copenhagen. 1983. 131-135.

44. Institution of Structural Engineers. *Structural Effects of Alkali-Silica Reaction*. London: SETO, 1992.

45. Jackson, R. and Slotboom, E. "US 59 and I-10 Interchange Construction." *Texas Freeway*. 21 Dec. 2001. <http://www.texasfreeway.com/Houston/construction/us59/construction_us59_i10.shtml>.

46. Jones, A.E.K. and Clark, L.A. "The Practicalities and Theory of Using Crack Width Summation to Estimate ASR Expansion." *Proceedings of the Institution of Civil Engineers: Structures and Buildings* Vol. 104 No. 2 (1994): 183-192.

47. Klingner, R.E. and Fowler, T.J. *Bridges with Premature Concrete Deterioration: Project Summary Report*. Austin: Center for Transportation Research, University of Texas at Austin, 2003. TxDOT Report 0-1857-S.

48. Kojima, T.; Hayashi, H.; Kawamura, M. and Kuzume, K. "Maintenance of Highway Structures Affected by Alkali-Silica Reaction." *Proceedings of the Eleventh International Conference on Alkali-Aggregate Reaction*. Quebec. 2000. 1159-1166.

49. Larkin, T.J. and Bomar, G.W. *Climatic Atlas of Texas*. Austin: Texas Department of Water Resources, 1983. LP 192.

50. Lawrence, B.L.; Moody, E.D.; Guillemette, R.N. and Carrasquillo, R.L. "Evaluation and Mitigating Measures for Premature Concrete Distress in Texas Department of Transportation Concrete Elements." *Cement, Concrete, and Aggregates* Vol. 21 No. 1 (1999): 73-81.

51. MacGregor, J.G. and Wight, J.K. *Reinforced Concrete Mechanics and Design*. 4th ed. Upper Saddle River: Pearson Prentice Hall, 2005.

52. McLeish, A. *Structural Implications of the Alkali-Silica Reaction in Concrete*. Crowthorne: Transport and Road Research Laboratory, 1990. Contractor Report 177.

53. Memberg, L.S.; Klingner, R.E. and Fowler, T.J. *Bridges with Premature Concrete Deterioration: Damage Indices, Strand-Pullout Tests, and Field Observations*. Austin: Center for Transportation Research, University of Texas at Austin, 2002. TxDOT Report 0-1857-4.

54. Mikata, Y.; Maeda, S.; Hatano, Y. and Inoue, S. "Effect of Fractured Anchorage of Shear Reinforcements on Loading of PC Beams." *Proceedings of the Thirteenth International Conference on Alkali-Aggregate Reaction*. Trondheim. 2008.

55. Miyagawa, T.; Seto, K.; Sasaki, K.; Mikata, Y.; Kuzume, K. and Minami, T. "Fracture of Reinforcing Steels in Concrete Structures Damaged by Alkali-Silica Reaction - Field Survey, Mechanism, and Maintenance." *Journal of Advanced Concrete Technology* Vol. 4 No. 3 (2006): 339-355.

56. Multon, S. and Toutlemonde, F. "Effect of Applied Stresses on Alkali-Silica Reaction-Induced Expansions." *Cement and Concrete Research* Vol. 36 (2006): 912-920.

57. Ng, K.E. and Clark, L.A. "Punching Tests on Slabs with Alkali-Silica Reaction." *The Structural Engineer* Vol. 70 No. 14 (1992): 245-252.

58. Pruski, K. "Water-Proofing Specification." Message to John Vogel and Jon Kilgore. 5 May 2005. E-mail.

59. Rigden, S.R.; Majlesi, Y. and Burley, E. “Investigation of Factors Influencing the Expansive Behavior, Compressive Strength and Modulus of Rupture of Alkali-Silica Reactive Concrete Using Laboratory Mixes.” *Magazine of Concrete Research* Vol. 47 No. 170 (1995): 11-21.

60. Smaoui, N.; Berube, M.A.; Fournier, B.; Bissonnette, B. and Durand, B. “Evaluation of the Expansion Attained to Date by Concrete Affected by Alkali-Silica Reaction. Part I: Experimental Study.” *Canadian Journal of Civil Engineering* Vol. 31 No. 5 (2004): 826-845.

61. Smaoui, N.; Berube, M.A.; Fournier, B. and Bissonnette, B. “Influence of Specimen Geometry, Orientation of Casting Plane, and Mode of Concrete Consolidation on Expansion due to ASR.” *Cement, Concrete, and Aggregates* Vol. 26 No. 2 (2004): 58-70.

62. Smaoui, N.; Bissonnette, B.; Berube, M.A.; Fournier, B. and Durand, B. “Mechanical Properties of ASR-Affected Concrete Containing Fine or Coarse Reactive Aggregates.” *Journal of ASTM International* Vol. 3 No. 3 (2006): 1-16.

63. Smaoui, N.; Fournier, B.; Berube, M.A.; Bissonnette, B. and Durand, B. “Evaluation of the Expansion Attained to Date by Concrete Affected by Alkali-Silica Reaction. Part II: Application to Non-Reinforced Concrete Specimens Exposed Outside.” *Canadian Journal of Civil Engineering* Vol. 31 No. 6 (2004): 997-1011.

64. Stanton, T.E. “Expansion of Concrete through Reaction between Cement and Aggregate.” *Proceedings of the American Society of Civil Engineers* Vol. 66 (1940): 1781-1811.

65. Stark, D. “Alkali-Silica Reactions in Concrete.” *Significance of Tests and Properties of Concrete and Concrete-Making Materials*. West Conshohocken: American Society for Testing and Materials, 2006. 401-409. STP 169D.

66. Swamy, R.N. and Al-Asali, M.M. “Engineering Properties of Concrete Affected by Alkali-Silica Reaction.” *ACI Materials Journal* Vol. 85 No. 5 (1988): 367-364.

67. Thaulow, N.; Johansen, V. and Jakobsen, U.H. “What Causes Delayed Ettringite Formation?” *Mechanisms of Chemical Degradation of Cement-Based Systems*. Proceedings of the Material Research Society’s Symposium on Mechanisms of Chemical Degradation of Cement-Based Systems. London: Taylor and Francis, 1997. 219-226.

68. Thomas, M.D.A.; Folliard, K.J.; Drimalas, T. and Ramlochan, T. “Diagnosing Delayed Ettringite Formation in Concrete Structures.” *Cement and Concrete Research* 38 (2008): 841-847.

69. *TxDOT Bridge Design Manual*. Austin: Texas Department of Transportation, 2001.

70. *TxDOT Bridge Standards*. Texas Department of Transportation, 18 Aug. 2009. <http://www.txdot.gov/insdtdot/orgchart/cmd/cserve/standard/bridge-e.htm>.

71. *TxDOT LRFD Bridge Design Manual*. Austin: Texas Department of Transportation, 2009.

72. Vogel, J. Personal Communication, 2008.

73. Vogel, J. "RE: Evaluation Protocol" Message to Oguzhan Bayrak and Dean Deschenes. 15 Aug. 2008. E-mail.

74. Vogel, J. "RE: Ballpark Bent and Others." Message to Dean Deschenes. 10 Oct. 2008. E-mail.

75. Vogel, J. "Petrography for Connection L Bent Caps" Message to Oguzhan Bayrak. 9 Dec. 2008. E-mail.

76. Walker, H.N.; Lane, D.S. and Stutzman, P.E. *Petrographic Methods of Examining Hardened Concrete: A Petrographic Manual*. McLean: Federal Highway Administration, 2004. FHWA-HRT-04-150.

77. West, G. *Alkali-Aggregate Reaction in Concrete Roads and Bridges*. London: Thomas Telford, 1996.